THE HONG KONG POLYTECHNIC UNIVERSITY

DEPARTMENT OF CIVIL AND STRUCTURAL ENGINEERING

THREE DIMENSIONAL SLOPE STABILITY ANALYSIS AND FAILURE MECHANISM

By

Wen-Bing WEI

BEng, MSc

Supervisor: Dr. Y. M. Cheng

A Thesis Submitted in Partial Fulfilment of the Requirements

for the Degree of Doctor of Philosophy

July 2008

CERTIFICATE OF ORIGINALITY

I hereby declare that this thesis is my own work and that, to the best of my knowledge and belief, it reproduces no material previously published or written, nor material that has been accepted for the award of any other degree of diploma, except where due acknowledgement has been made in the text.

Signed:

Name: Wen-Bing WEI

Abstract of thesis entitled

THREE DIMENSIONAL SLOPE STABILITY ANALYSIS AND FAILURE MECHANISM

submitted by **Wen-Bing Wei**

for the degree of Doctor of Philosophy

at The Hong Kong Polytechnic University in July 2008

For slope stability problem, two-dimensional analysis is commonly used for simplicity, though all slope failures are three-dimensional (3D) in nature. There are only limited applications of 3D analysis due to the various limitations of three-dimensional slope stability methods. Recently, there are various important progresses for 3D analysis. 3D limit equilibrium method (LEM) for general asymmetrical problem together with innovative optimization method for locating the general critical 3D failure surface has recently been developed. In addition, 3D strength reduction method (SRM) can now be conducted within a tolerable duration. Until now, there is still a lack of detailed investigation of 3D slope stability failure mechanism and the application of 3D LEM and SRM under different 3D conditions. This study aims to conduct an extensive three-dimensional slope stability analysis and to investigate the failure mechanism under different situations. The 3D effect considered in this study includes the important factors such as slope geometry, boundary conditions, water, soil nail and pile.

Both the LEM and SRM are conducted in this study, and some interesting differences between these two methods are discovered. It is concluded that both methods have their own merits and limitations, and a good understanding of these methods are required before a good solution can be obtained. The suitability of these two methods under different conditions is investigated and precautions when these methods are applied are suggested.

In this study, some results which appear to be different from common understanding are obtained. Some of the results are also different from published studies, and careful investigations have revealed that the present detailed studies have provided a better and more reasonable understanding about the failure and stabilization mechanism. For example, for a simple slope extending to infinity, the critical slip surface is still basically two-dimensional until the external loading is large to induce a three-dimensional failure. The failure mechanisms due to the self weight of soil and external loads are actually different. The discretization domain required for SRM analysis is found to decrease with the increase of external loads which is also out of expectation. The distribution of tension force in soil nail is found to be influenced by the state of the slope (service state, limit state) and the failure modes (external failure, internal failure). In general, the line of the maximum tension may not correspond to the critical slip surface as commonly believed, except when the failure mode is an internal tensile failure. For slope supported with one row of piles, the slip surface is divided into two parts when the pile spacing is very small, and these two parts gradually become connected to form a clear single slip surface mechanism with the increase of pile spacing. The point of maximum shear force in the pile which is commonly used to determine the location of the slip surface in traditional design is found to be not a valid assumption, and this is important for design of slopes reinforced with piles. Some engineers have questioned the disturbance of the seepage pattern due to the presence of soil nails and piles. Such blocking effect is however found to be negligible.

With the detailed study on 3D failure and stabilization mechanism, a clearer and better understanding of three-dimensional slope failure has been achieved in the present study.

LIST OF PUBLICATIONS

Wei, W. B., Cheng, Y. M., and Li, L. (2008). Three-dimensional slope failure analysis by the strength reduction and limit equilibrium methods. Computers and Geotechnics, In Press.

Wei, W. B. and Cheng, Y. M. (2008). Soil nailed slope by the strength reduction and limit equilibrium methods, submitted to International Journal for Numerical and Analytical Method in Geomechanics.

Wei, W. B. and Cheng, Y. M. (2008). Strength reduction analysis for slope reinforced with one row of piles, submitted to Journal of Geotechnical and Geoenvironmental Engineering.

Wei, W. B. and Cheng, Y. M. (2008). Stability analysis of slope with water flow by strength reduction method, submitted to Soils and Foundations.

Cheng, Y. M., Lansivaara, T., and **Wei, W. B**. (2008). Reply to Comments on "Two-dimensional slope stability analysis by limit equilibrium and strength reduction methods". Computers and Geotechnics, Vol. 35, No.2, 309-311

Cheng, Y. M., Lansivaara, T., and **Wei, W. B.** (2007). Two-dimensional slope stability analysis by limit equilibrium and strength reduction methods. Computers and Geotechnics, Vol. 34, No.3, 137-150

Wei, W. B. and Cheng, Y. M. (2007). Strength reduction method for three dimensional slope stability analysis. 60th Canadian Geotechnical Conference and 8th Joint CGS/IAH-CNC Groundwater Conference (Ottawa, Ontario, Canada, October 21-24, 2007), 815-820

Cheng, Y. M., **Wei, W. B.**, and Lansivaara T. (2006). Factors of safety by limit equilibrium and strength reduction methods. Numerical Methods in Geotechnical Engineering – Schweiger (ed.), Sixth European Conference on Numerical Methods in Geotechnical Engineering (Graz, Austria, 6-8 September 2006), 485-490

ACKNOWLEDGEMENTS

I would like to express my great gratitude and sincere thanks to my supervisor, Dr. Y. M. Cheng, for his continued inspiration, support and invaluable guidance during my study. Without his endless efforts and experienced guidance, it would not have been possible to complete this work. I also appreciate his caring about my life.

Financial support for this research work from The Hong Kong Polytechnic University is greatly acknowledged. Also, administrative and technical supports from the staff of the Department of Civil and Structural Engineering are deeply appreciated.

I am very thankful to Professor J. A. Wang of University of Science and Technology Beijing who introduced me to the world of geotechnical engineering. Many thanks are due to Professor H. G. Ji and Professor Z. H. Chen of University of Science and Technology Beijing for their useful suggestions and discussions. Thanks are also extended to my friends Dr. Z. Fang, Dr. L. J. Su, Dr. W. H. Zhou and Dr. H. H. Zhu for their fruitful discussions.

I would also like to express my sincere gratitude to the members of my oral examination committee, Professor M. W. Xie, Dr. J. Yang and Professor J. H. Yin for reviewing the manuscript and offering valuable comments and suggestions.

I deeply appreciate my parents and my brother for their constant support and endless encouragement. Finally, I wish to express my special thanks to my wife, Lan-Juan Xiao, for her support and understanding.

TABLE OF CONTENTS

LIST OF TABLES

LIST OF FIGURES

CHAPTER 1: INTRODUCTION

1.1 Background and motivation

Due to the rapid increase in population and huge demand for infra-structures, many buildings and highways are constructed adjacent to natural slopes and many cut slopes are formed for various purposes in Hong Kong and other developed cities. Landslides have been a major cause of disasters resulting in considerable loss of human lives and property damages in hilly terrain. Slope stability problem is, therefore, one of the most commonly occurred geotechnical problems in Hong Kong and many other developed cities. Usually, slope failure occurs as a result of triggering mechanisms, in which water is a main factor for slope geo-disasters. The infiltration of water into soil increases pore water pressure and decreases the shear strength of the soil structure, which will then leads to slope instability.

In order to increase the safety factor to the required level, the use of reinforcement is now commonly adopted for slope stabilization. For ease of construction and some other potential benefits, soil nailing has been proven to be a practical technique for stabilization of slopes (Bruce and Jewell, 1986). Passive soil nailing is one of the most widely used slope stabilization measures in Hong Kong over the last two decades. It is currently the predominant method for upgrading the stability of existing soil cut slopes. Installing piles into the slope to improve the stability has also been successful and is also demonstrated to be an effective approach (Ito and Matsui, 1975; Reese et al., 1992).

For slope stability analysis, two-dimensional (2D) plane strain approach is usually employed for simplicity, and the most extensively used method is the limit equilibrium method (LEM) which is well known to be a statically indeterminate problem, and assumptions on the internal force distribution are required for the solution of the factor of safety (Bishop, 1955; Morgenstern and Price, 1965; Spencer, 1967; Janbu, 1973). The calculus of variation approach by Baker and Garber (1978) does not require the assumption on the internal force distribution, but it is not easy to be used in practice. Besides, limit analysis has also been used for simple problems (Chen 1975), but its applications in complicated real problems are still limited, and this method is seldom adopted for routine analyses and designs. In recent years, there is a great development of the shear strength reduction method (SRM) for slope stability analysis (Zienkiewicz et al., 1975; Ugai and Leshchinsky, 1995; Dawson et al., 1999; Griffiths and Lane, 1999). This technique is also adopted in several well-known commercial geotechnical finite element programs. The SRM does not require inter-slice force assumption, and the main advantage is that it can automatically determine the slip surface and is suitable to many complicated conditions.

Two-dimensional analyses, though helpful for designing most of the slopes, are not applicable to many situations in which three-dimensional (3D) effect is obvious. The common approaches for three-dimensional slope stability analysis are still the LEM, which are usually the direct extensions of the various two-dimensional methods. Most of these methods are based on the assumption that the failure mass is symmetrical with a known sliding direction, so a true asymmetric slope failure cannot be modelled directly by the classical three-dimensional methods. The lack of suitable method for locating the critical general 3D failure surface is another major limitation of the 3D LEM. There are also several three-dimensional limit analysis models (Giger and Krizek,

1975; Michalowski, 1989; Chen et al., 2001a; Farzaneh and Askari, 2003) in literature. The construction of the three-dimensional failure mechanism for limit analysis is difficult for a complicated slope, and this approach is seldom adopted except for simple slopes. By contrast, the SRM appears to be simple for extension to three-dimensional analysis, since this method can be employed within a single framework for both two- and three-dimensional slopes. Some special limitations of the SRM are discovered in this study and will be illustrated later.

All slope failures are three-dimensional in nature, especially for some natural slopes or slopes with transverse loads or concentrated loads. There is however only limited application of 3D analysis due to the various limitations of the three-dimensional slope stability methods mentioned previously. Recently, there are various important progresses for 3D analysis. Huang and Tsai (2000) have proposed the first method for 3D asymmetrical slope stability analysis where the sliding direction enters into the direct determination of the factor of safety (FOS), but the sliding direction will be different for different soil columns. Cheng and Yip (2007) have developed a new asymmetric 3D analysis model under which there is only one sliding direction for the whole failure mass, and this assumption has overcome the convergence problem under transverse load in the Huang and Tsai formulation (2000). Cheng et al. (2005) have proposed the use of 3D NURBS surface and the simulated annealing method to locate the critical general failure surface. In addition, with the development of computer hardware and software, 3D SRM can now be conducted within a tolerable time span and may become a prospective approach for complicated 3D slope analysis.

Due to the improvement of 3D LEM and 3D SRM mentioned above, it can be anticipated that the three-dimensional slope stability analysis will be more popular in

the future if the techniques are mature. Up to present, there is still a lack of detailed investigation of 3D methods and their application under different 3D conditions.

In view of the above, this study aims to conduct an extensive three-dimensional slope stability analysis and to investigate the failure mechanism under different situations. The 3D effect considered in this study lies on two aspects. Firstly, for slopes with no reinforcement, the 3D analysis should be conducted in the following situations: the slope geometry is irregular, the soil properties are not homogeneous, the slope is subject to concentrated load, or the boundary conditions cannot be ignored. Secondly, for slopes with reinforcement, even though the slope geometry and boundary conditions have no obvious 3D effect, if the reinforcement is not continuous along the slope, 3D analysis should also be conducted. For example, if the reinforcement is geotextile, it is reasonable to conduct 2D analysis. If the reinforcement is soil nail or pile, 3D analysis should be preferred for better modelling of the nail/pile-soil interaction.

In this study, both the limit equilibrium and strength reduction methods are used. The strength reduction analysis is conducted for all the cases involved in this thesis, since SRM is powerful in automatically detecting the failure surface without any optimization search technique which is usually required in the LEM analysis, and it is also powerful in modelling the interaction between soil and reinforcement. Some of the results are also compared with the limit equilibrium analysis, and these useful comparisons have revealed the merits and limitations of the LEM and SRM which are important for the proper analysis of slope stability problem. Slopes with and without reinforcement are both considered, and useful and important results are obtained. Besides, the slope with water flow is also investigated. Some interesting and useful findings are obtained from

this analysis, and different failure modes are found for slopes with and without reinforcement.

1.2 Objective

The main objectives of this research are as follows:

(a) Study the stability and failure mechanism of non-reinforced slopes with obvious 3D effects in geometry or boundary conditions, such as locally loaded slopes.

(b) Study the stability and failure mechanism of soil nailed slopes without obvious 3D effects in slope geometry.

(c) Study the stability and failure mechanism of soil nailed slopes with obvious 3D effects in slope geometry.

(d) Study the stability and failure mechanism of pile supported slopes.

(e) Study the stability and failure mechanism of slopes with water flow.

(f) Investigate the suitability of 3D LEM and 3D SRM approaches under different conditions, and provide suggestions and precautions in employing these methods.

1.3 Organization of thesis

This thesis consists of nine chapters which are organised as follows:

Chapter 1 is the current chapter which briefly introduces the background and objectives of this research.

Chapter 2 reviews previous investigations concerning the present research in four aspects: 2D and 3D slope stability analysis methods which includes limit equilibrium methods, variational calculus methods, limit analysis methods, strength reduction methods; stability analysis of soil nailing slope; stability analysis of slopes reinforced with piles; stability analysis of slopes with water flow.

Chapter 3 gives an extensive comparison on the factors of safety and the locations of critical failure surfaces obtained by the limit equilibrium method and strength reduction method for various 2D slopes. The advantages and limitations of the strength reduction and limit equilibrium methods are illustrated and some useful and surprising results are also found.

Chapter 4 analyzes several typical non-reinforced slopes with obvious 3D effects by 3D strength reduction method and 3D limit equilibrium method. The suitability of these two methods under different conditions is investigated and precautions for these methods are suggested. Some surprising results are also found and are explained.

Chapter 5 presents a detailed strength reduction study of nailed slope under different conditions. A more realistic 3D analysis is carried out to consider the interaction between soil and nail, while the slope geometry has no apparent 3D effect. The results are also compared with those obtain by the LEM.

Chapter 6 is devoted to investigation of some soil nailed slopes with obvious 3D effects in geometry and boundary conditions (locally loaded slope, idealized curvature slope, and intersected slope).

Chapter 7 conducts 3D SRM analysis for the slope reinforced with one row of piles and the failure mode is determined with respect to different pile spacing. The upper and lower bounds of the factor of safety, and the optimal pile location are also discussed.

Chapter 8 employs the strength reduction method on slope stability analysis with water flow. Several 2D and 3D slope models with and without reinforcement are investigated and discussed.

Chapter 9 summarizes the major findings from this research and suggests some areas which require further study.

CHAPTER 2: LITERATURE REVIEW

The review of previous investigations relevant to the present research is described in this chapter, and it is mainly divided into four parts. The first part is an introduction to the slope stability analysis methods. The second part presents the stability analysis of soil nailed slope. The third part is devoted to the stability analysis of slopes reinforced with piles. The fourth part presents the stability analysis of slopes with water flow.

2.1 Slope stability analysis methods

Slope stability can be analyzed by a number of methods which include limit equilibrium method, variational calculus method, limit analysis method, strength reduction method, rigid element method and others. For slope stability analysis, two-dimensional (2D) plane strain analysis is commonly used for simplicity. All slope failures are however three-dimensional (3D) in nature, particularly for non-homogeneous slopes with transverse loads or concentrated loads. In this section, both the 2D and 3D slope stability methods are briefly summarized.

2.1.1 Limit equilibrium method

For two-dimensional slope stability analysis, the limit equilibrium method (LEM) is the most widely used approach (Bishop, 1955; Lowe and Karafiath, 1960; Morgenstern and Price, 1965; Spencer, 1967; Janbu, 1973). The various 2D limit equilibrium methods are well reviewed and summarized by Fredlund and Krahn (1984), Morgenstern (1992), Duncan (1996), and Cheng and Zhu (2004). Most of the limit equilibrium methods are based on the techniques of slices, and assumptions on the interslice forces distribution

are required for the solution of the factor of safety (FOS). In the traditional LEM analysis, the assumptions are usually focused on the inclination or the location of the interslice forces. There is another type of assumption which is focused on the distribution of the base normal forces on the slip surface, and this approach has been adopted by Bell (1968), Leshchinsky and Huang (1992a, 1992b). The assumption on the base normal stress distribution along the slip surface has received little attention for a long time, but it is reconsidered by Zhu and Lee (2002) to arrive at three equilibrium equations. Incorporation of these equations can lead to a single cubic function with respect to the factor of safety, and this function can be solved explicitly. Subsequently, Zhu et al. (2003) proposed a generalized framework including nearly all of the existing limit equilibrium methods of slices with general failure surfaces. Different assumptions about the interslice forces can be converted into a unified form of expression of the normal stress distribution along the failure surface.

The development of various three-dimensional slope stability methods are basically the extensions of the corresponding 2D analysis. Cavounidis (1987) has demonstrated that the factor of safety of a 3D slope should normally be greater than that for a corresponding two-dimensional slope. 3D problem has one major factor not found in the corresponding 2D analysis: sliding direction. The common 3D methods include those by Baligh and Azzouz (1975), Hovland (1977), Chen and Chameau (1982), Azzouz and Baligh (1983), Hungr (1987), Gens et al. (1988), Zhang (1988), Ugai (1988), Lam and Fredlund (1993), Huang and Tsai (2000, 2002), Chang (2002), Chen et al. (2003a), Loehr et al. (2004), and Cheng and Yip (2007). Most of these methods are based on the assumption that the failure mass is symmetrical with a known sliding direction (usually zero sliding direction), so an asymmetric slope failure cannot be modeled directly by the classical three-dimensional methods. Jiang and Yamagami (1999) have proposed the

concept of axes rotation and minimum factor of safety to determine the sliding direction, but this approach is time consuming in the geometry calculation. Huang and Tsai (2000) have proposed the first method for 3D asymmetrical slope stability analysis where the sliding direction enters into the direct determination of the FOS, but the sliding direction will be different for different soil columns. Cheng and Yip (2007) have developed a new asymmetric 3D analysis model under which there is only one sliding direction for the whole failure mass, and this simplification has overcome the convergence problem under transverse load in the Huang and Tsai formulation (2000, 2002). In this method, the critical general 3D failure surface is located by 3D NURBS surface and the simulated annealing method proposed by Cheng et al. (2005). In recent years, the 3D limit equilibrium methods are incorporated with the geographic information system (GIS) spatial analysis function (Xie et al., 2003, 2004a, 2004b, 2006a, 2006b). This formulation can make use of the spatial functions of GIS for processing complex spatial data, and render the 3D slope stability problem easier to be analyzed.

Most of the existing 3D limit equilibrium methods seldom satisfy all the six equilibrium conditions. By introducing the normal force assumption, which is successfully used in 2D slope limit equilibrium analysis (Zhu and Lee, 2002; Zhu et al., 2003), Zhu and Qian (2007) have derived a rigorous 3D limit equilibrium solution which satisfies six equilibrium conditions. The normal stress distribution over the 3D slip surface is specified by a function with five parameters. The six equilibrium equations are then reduced to a sixth-order algebraic equation in terms of the 3D factor of safety. A similar rigorous limit equilibrium method for the three-dimensional stability analysis of slope is also proposed by Zheng (2007) based on the adjustment of the normal stresses on the slip surface. The distinct advantage of these two rigorous methods is that it does not

require the complicated inter-column force assumptions. In order to render the solution statically determinate, five parameters are introduced to represent the base normal pressure on the slip surface, and whether the general 3D normal stress distribution for different complicated conditions can be perfectly described or adjusted by only five parameters may need some further study.

2.1.2 Variational calculus method

The variational calculus method was first used in 2D slope stability analysis by Baker and Garber (1978). This approach was subsequently employed by Jong (1980) for vertical cut analysis in cohesive frictionless soil. This method does not require the assumption on the internal force distribution, but it is not easy to be used in practical analysis. Cheng et al. (2008) have developed the numerical algorithm based on the extremum principle by Pan, and the formulation which relies on the use of modern heuristic optimization method can be viewed as an equivalent form of the variational method in a discretized form but is applicable for complicated real problem.

The variational calculus approach has been employed in 3D slope stability analysis by Leshchinsky et al. (1985), Ugai (1985), Leshchinsky and Baker (1986), Baker and Leshchinsky (1987), and Leshchinsky and Huang (1992b). In such approaches, the minimum factor of safety and the associated failure surface can be obtained at the same time. However, these methods are limited to homogeneous and symmetrical problems, and further study is required on the application in practical problems with complicated geometric and loading conditions.

2.1.3 Limit analysis method

The limit analysis method includes upper bound approach and lower bound approach, and the general analysis process is the construction of a statically admissible stress field for the lower bound analysis or a kinematically admissible velocity field for an upper bound analysis. Optimization analysis of the objective function will then be conducted. The lower bound approach has been used in 2D slope stability analysis by Chen (1975), Bottero et al. (1980), Zhang (1999), Kim et al. (2002), and Loukidis et al. (2003), while the application of this approach in 3D slope stability analysis has been conducted by Lyamin (1999), Lyamin and Sloan (2002a). In most of these methods, the finite element discretization and linear programming technique are usually used to obtain the lower bound solution. Due to the inability of the linear programming technique for complicated problems with multi local minima, some researchers are using various advanced optimization method in order to obtain a better solution. Stress fields employed in the lower bound solutions are usually assumed without an apparent relation to the actual stress fields, and it is usually not easy to obtain the lower bound solutions for a practical slope problem. The lower bound approach is hence seldom adopted as compared with the upper bound approach in slope stability analysis.

The upper bound approach was first used in 2D slope stability analysis by Drucker and Prager (1952) to determine the critical height of a slope. Subsequently, Chen and Giger (1971), Chen (1975), Karal (1977a, 1977b), and Izbicki (1981) also applied and extended the upper bound approaches in 2D slope analysis. Michalowski (1995) proposed an upper bound approach based on a translational failure mechanism. The vertical slice techniques, which are often used in traditional limit equilibrium approaches, are employed, and the force equilibrium is satisfied for all individual slices. Two extreme kinematical solutions which neglect the interslice strength or fully utilize

the interslice strength of the soil are then obtained. The traditional limit equilibrium solutions of slices with a proper implicit assumption of failure mechanism can fall into the range of these two extremes. Donald and Chen (1997) presented an upper bound method on the basis of a multi-wedge failure mechanism, and the sliding body was divided into a small number of discrete blocks. This approach was subsequently employed by Wang (2001) and Wang et al. (2001) to examine the influence of a non-associated flow rule on the safety factor. Some researchers have tried to use the finite element method to obtain the upper bound solution for structures and geotechnical problems (Anderheggen and Knopfel, 1972; Bottero et al., 1980; Sloan, 1988, 1989; Sloan and Kleeman, 1995; Kim et al., 2002; Loukidis et al., 2003). A new upper bound formulation using the rigid finite element method was presented by Chen (2004) and Chen et al. (2003b, 2004, 2005a). The kinematically admissible velocity fields are constructed by rigid elements, and this formulation render the limit analysis of slope stability suitable to be conducted for different complex conditions, such as slopes with complex geometries, soil profiles, groundwater conditions, and complicated loadings.

The application of the upper bound approach in 3D slope stability analysis was first conducted by Giger and Krizek (1975, 1976), who analyzed the stability of a vertical cut with a variable corner angle for cases with and without concentrated surcharge loading. Michalowski (1989) presented an upper bound formulation for three-dimensional analysis of locally loaded slopes. The through-toe and above-toe failure mechanisms are considered, with energy dissipated along planar velocity discontinuities. Since this method is limited to slopes with homogeneous soil, Farzaneh and Askari (2003) improved and extended this method to non-homogeneous 3D slopes. Chen et al. (2001a, 2001b) proposed another 3D upper bound approach which is extended from the corresponding 2D approaches by Donald and Chen (1997). In most of the 3D upper

bound methods, the column techniques which are usually used in 3D LEM are employed to construct the kinematically admissible velocity field. The vertical columns are used by Michalowski (1989) and Farzaneh and Askari (2003), while the non-vertical columns are used by Chen et al. (2001a, 2001b). The finite element method has also been also used by some researchers to obtain 3D upper bound solution. Lyamin and Sloan (2002b) proposed a new upper bound scheme using linear finite elements and non-linear programming, and this approach is shown to be efficient for large scale three-dimensional stability problems. Chen et al. (2005b) presented a three-dimensional upper bound approach on the basis of the rigid finite element method, and a special sequential quadratic programming algorithm is employed to obtain the optimal solution.

2.1.4 Strength reduction method

In recent decades, there are great developments of the SRM for slope stability analysis. The general procedure of SRM analysis is the reduction of the strength parameters by the factor of safety while the body forces due to weight of soil and other external loads are applied until the system cannot maintain a stable condition. This procedure can determine the safety factor within a single framework for both two- and three-dimensional slopes. The main advantages of SRM are as follows: (1) the critical failure surface is found automatically from the application of gravity loads and/or the reduction of shear strength; (2) it requires no assumption on the interslice shear force distribution; and (3) it is applicable to many complex conditions and can give information such as stresses, movements, and pore water pressures. One of the main disadvantages of the SRM is the long solution time required to develop the computer model and to perform the analysis. With the development of computer hardware and software, 2D SRM can now be performed within a reasonable time span suitable for routine analysis and design, and 3D SRM can also be conducted within a tolerable time span. This technique

is also adopted in several well-known commercial geotechnical finite element or finite difference programs. In strength reduction analysis, the convergence criterion is the most critical factor for the assessment of the factor of safety. Depending on the choice of the program, different criteria for the ultimate state have been used in practice: (1) maximum number of iteration is reached; (2) formation of a continuous failure mechanism; (3) sudden change in the displacement for some selected points. For simple problems, there are no major differences between these criteria, while major differences may be obtained by different convergence criteria for some special cases.

The strength reduction method was early used in 2D slope stability analysis by Zienkiewicz et al. (1975). Good agreement with slip circle solutions is obtained from an idealized homogeneous embankment analysis. It is interesting to find that the associated and non-associated assumptions have little influence on the results from a composite embankment analysis.

Naylor (1982) applied the SRM to 2D problem and the failure was determined by the development of very large displacements of protruding points on the failure mass. Donald and Giam (1988) conducted SRM analysis in which the nodal displacement was also used to assess the ultimate failure state. Donald and Giam (1988) states that it is preferable to plot displacement curves for a number of nodes within the potential failure region, and the nodes located in the toe region should be used if the failure zone is unknown. The precision of the factor safety is found to be influenced by several factors, such as the selection of constitutive model of soil, the location of the node selected for plotting the displacement curve, tolerance for nonlinear analysis, the type of element and the size of the discretized mesh.

Brinkgreve and Bakker (1991) conducted SRM analysis for a river embankment in the tidal zone and for a building trench supported by sheet-pile wall. An arc-length control technique was used for the nonlinear equation solver to overcome the snap-through problem associated with the ultimate limit state which will be followed by an "apparent" negative stiffness matrix beyond the ultimate limit state. This technique makes the analyzing robust as failure needs not be related with a non-converging iterative procedure. Song (1997) also applied the arc-length control technique in the SRM analysis, and good performance was obtained for two examples. A dam is considered in the first example, and the factor of safety obtained by SRM agrees well with the result obtained by the LEM. A road embankment reinforced with geotextiles is studied in the second example, and it demonstrates the wide applicability of the SRM. The arc-length control technique is now incorporated in the commercial finite element software PLAXIS to obtain reliable collapse loads for load controlled calculations.

Matsui and San (1992) conducted SRM analysis in which the slope failure was defined according to the shear strain failure criterion, and the hyperbolic nonlinear elastic soil model was used for practical purpose. Ugai and Leshchinsky (1995) conducted 3D SRM analysis for vertical cuts, which included a pseudo-static seismic force component. Both the factors of safety and their corresponding slip surfaces determined by the SRM demonstrate good agreement with the results from the LEM.

Griffiths and Lane (1999) conducted a detailed description of the SRM analysis and carried out an extensive comparison against limit equilibrium solutions for several typical slope examples. The failure is defined by the algorithm that convergence is not achieved within a user-specified maximum number of iterations, and this implies that no stable stress distribution, which satisfies both the Mohr-Coulomb failure criterion and

the global equilibrium, can be found. The nodal displacement has a drastic increase at the failure state. It is stated that the finite element method accompanied with an elastic-perfectly plastic (Mohr-Coulomb) stress-strain relation can be a reliable and powerful approach for calculating the factor of safety of slopes. It is also suggested that the SRM should be a more powerful alternative to the traditional LEM.

Dawson et al. (1999) conducted an extensive simulation for a homogeneous embankment with respect to a wide range of slope angles, soil friction angles and pore pressure coefficients to assess the accuracy of the strength reduction technique. Factors of safety were calculated using the finite difference software FLAC. The failure is also defined by the non-convergence criterion, which is represented by the nodal unbalanced force in FLAC. It is found that there is no ambiguity to determine the critical safety factor, since the unbalanced force has a drastic change at the failure state, and this phenomenon is due to the use of an elastic-perfectly plastic constitutive model, which has a sharp transition from elastic to plastic behavior. Dawson et al. (1999) also points out that if a model which shows smooth transition from elastic behaviour to plastic behaviour is used (such as the hyperbolic constitutive model which was used by Matsui and San 1992), determination of the failure state will be more difficult and will be more sensitive to the tolerance in the nonlinear analysis. When the numerical mesh is fine enough, the safety factors obtained by SRM are usually found to differ within a few percent from the upper bound limit analysis results.

Zheng et al. (2005) also conducted an extensive SRM analysis and its application in the slope, tunnel, and ultimate bearing capacity of foundations using program ANSYS. Different soil models are considered for SRM analysis, and the results are compared with limit equilibrium methods (Spencer approach) with good agreement.

Griffiths and Marquez (2007) conducted strength reduction analysis for several 3D slope examples. Both vertical and inclined boundaries were considered in the analysis to investigate the constraint effect of slopes with finite length. Non-symmetric slopes with weak soil surrounded by stronger soil were also analyzed. Besides, one example analyzed by Baligh and Azzouz (1975) and two examples analyzed by Zhang (1988) were also discussed.

Deng et al. (2007) have applied strength reduction method in assessing three-dimensional stability of a pre-existing landslide with multiple sliding directions. Shukha and Baker (2008) have employed the strength reduction approach to solve pseudo-static stability problems in a frictional-cohesive material. Gurocak et al. (2008) have applied strength reduction method in rock slope stability analysis using two-dimensional finite element program Phase2 and the Hoek-Brown constitutive model.

2.2 Stability analysis of soil nailed slope

Soil nailing is a useful, economic technique for the construction of new steep cuts or the strengthening of existing slopes. The essential concept of soil nailing is reinforcing the slope with closely spaced inclusions to increase the stability. When the soil movement is induced by excavation for cut slopes or by natural environment changes for existing slopes, the resistant tension force is generated in the soil nail and is transferred into the soil by the friction mobilized at the soil-nail interface.

Bruce and Jewell (1986) summarized the main characteristics and evolution history of soil nailing technique, and revealed the potential benefits of soil nailing system. The cost of soil nailing was found to be 10% to 30% less than that of the anchored diaphragm or Berlin wall. The idea of the soil nailing technique stems from the mining

engineering, in which the fully bonded steel inclusions combined with shotcrete are used to provide immediate and effective support for rock tunneling system. It is demonstrated that this technique can be employed in less competent materials. The application of soil nailing in soils is successful in France, Germany and America in the 1970's, and this technique is employed for stabilizing excavations and slopes. Soil nailing technique has been used in Hong Kong as a permanent slope stabilizing method since the late 1980's.

In this section, the literature about soil nailing technique and its application is surveyed and the review includes four parts. The first part discusses the three kinds of nail resistance. The second part describes various failure modes of soil nailed slope. The third part presents different design methods of soil nailed slope. The fourth part is devoted to full scale and small scale tests of soil nailed slope.

2.2.1 Soil nail resistance

Soil nails have tensile resistance, shear resistance, and bending resistance. It is accepted by many researchers that the axial tensile resistant force of the nail is the main component in maintaining stability of a soil nailed slope, and the contribution from the bending stiffness is very small unless the nails are installed nearly perpendicular to the failure surface. If the nail is installed nearly horizontally, the effect of nail bending will be very small. If the nail is installed at large angle below the horizontal direction and the orientation is almost normal to the slip surface, more bending moment of the nail will be mobilized, however, the bending stiffness still has only a modest improvement to the slope stability compared with the contribution from the tensile resistance (Jewell and Pedley, 1992). It is stated by Byrne et al. (1998) that the contribution to slope stability by nail bending resistance is nearly one order of magnitude less than the contribution by

the tension resistance. In addition, the bending resistance is not fully mobilized until displacements are an order of magnitude larger than those required to generate maximum tension resistance. Pedley and his colleagues (Pedley, 1990; Pedley et al., 1990a, 1990b) maintain that the favorable effects from bending resistance will be the post failure condition, therefore, the potential benefit of nail bending stiffness should be neglected and not considered in design. There are however some different views on the influence of the bending stiffness of the nail. Schlosser (1991) states that the effect of the bending resistance can be either favorable or unfavorable which depends on the behaviour of the soil nailing system, therefore, the bending and shear resistances have to be taken into account in the design of soil nailing slopes. Juran et al. (1990, 1992) assert that the nail bending stiffness has a considerable influence on the failure mechanism and the mobilization of the bending stiffness may result in a remarkable decrease of the slope stability.

Although there are some controversy on the influence of shear resistance and bending resistance for soil nail, it is generally accepted that the principal resistance remains the tensile force developed in the nails. Tensile force is generated in the soil nails primarily as a result of the cohesive and frictional interaction between the nail and the soil. Therefore, the nail-soil interface resistance (pullout resistance) becomes a chief parameter which controls the design and stability evaluation of soil nailed slope. The soil-nail pullout resistance is influenced by many factors, such as the normal stress acting on the nail surface, the shear strength of the soil, the roughness of the nail surface, the nail diameter, soil dilatancy and nail installing methods. Many researchers have investigated the soil nail pullout resistance by analytical or empirical methods and field or laboratory testing (Schlosser and Guilloux, 1981; Cartier and Gigan, 1983; Jewell, 1990; Luo et al., 2000, 2002; Chu, 2003; Hong et al., 2003; Junaideen et al.,

2004; Chu and Yin, 2005; Chai and Hayashi, 2005; Su, 2006; Pradhan et al., 2006; Su et al., 2007; Li et al., 2008). In these investigations, one of the major concerns is whether the pullout resistance is dependent on the depth or not (or overburden pressure). Schlosser and Guilloux (1981) maintain that the pull-out resistance is independent of the depth since the increase of the effective vertical stress offsets the decrease of the apparent friction coefficient. Jewell (1990) suggests an equation in which the pullout resistance is related to the depth. Su (2006) states that the pullout resistance is greatly influenced by the dilatancy of the soil, and the peak pullout shear resistance is not directly related to the overburden pressure.

2.2.2 Failure modes of soil nailed slope

There are three failure modes for reinforced slopes which are shown in Figure 2.1 (Elias et al., 2001): internal failure where the slip surface passes through the reinforcing inclusions; external failure where the slip surface passes behind and below the strengthened soil mass; compound failure where the slip surface passes behind and through the strengthened soil mass.

External failures include sliding failure, bearing failure, overturning failure and external overall failure. The primary reasons for these failures are the insufficient length of nails or the presence of weak soil at the slope base. In the stability analysis for slope with external failure modes, the soil nailed slope mass is usually treated as a block. The equilibrium of this block is established to compute the factor of safety by considering the resistant forces exerting on the slip surface (Lazarte et al., 2003).

Internal failures, which are shown in Figure 2.2 (Byrne et al., 1998), include face failure, pullout failure and tensile failure of nail tendon. The strength of the facing

system in Figure 2.2(a) is not high, but the tensile strength of the nail is strong which prevents the slope from nail tensile failure, and the nail length is very long which prevents the slope from pullout failure. The facing failure is thus the most probable collapse mode, and the active zone which is located between the facing and the failure surface, slips off the front of the soil nail. The nail length in Figure 2.2(b) is limited, but both the strength of the facing system and the nail are high, which prevent the slope from facing failure and nail tensile failure. Pullout failure therefore occurs and the nail slides out from the resistant zone, which is behind the failure surface. The tension strength of the nail in Figure 2.2(c) is modest, but the facing system is strong and the nail length is very long. The most likely failure mode for this case is hence the nail tensile failure.

2.2.3 Design methods of soil nailed slope

The existing design approaches for soil nailed slope can be generally categorized into two major types (ASCE 1997): limit equilibrium design methods which are essentially based on the widely used solutions of modified slope stability analyses and are employed to assess the overall stability of the soil nailing system by considering the contribution of the nails; working stress design methods which are used to calculate the mobilized nail forces at the service state and assess the local stability at each level of nails.

Limit equilibrium methods have been developed by several investigators and these methods include the Davis method (Shen et al., 1981a, 1981b), the German method (Stocker et al., 1979; Stocker and Riedinger, 1990), and the French method (Schlosser, 1982, 1991). For the Davis method, only tensile resistance and pullout capacity of the nail is considered and a parabolic sliding surface passing through the toe of the slope is

assumed. The tensile forces mobilized in the nails are divided into tangential and normal components along the potential slip surface and are added to the resistant forces to determine the safety factor of the slope. For the German method, a bi-linear sliding surface is usually assumed. Gassler (1988) extended this method, in which the slip circle failure surface (rotation mechanism) is also considered, and it is found that this is a relevant failure mode for practical design. Gassler (1988) also states that the rotation of two rigid bodies may occur when very large surcharge loading is applied on the slope crest. For the French method, two essential soil-nail interaction mechanisms are considered, which include the soil-nail interface friction and the passive normal pressure between the soil and the nail. This method takes into account the tensile resistance, shearing resistance and bending stiffness of the nails. Four failure criteria are taken into account: shear strength of the soil along the slip surface, strength of the nail, pullout strength between soil and nail, lateral earth pressure on the nail.

In recent years, there is some development on the limit equilibrium method for soil nail design. Sabahit et al. (1995) presented a design approach for soil nailed slopes in combination with the modified Janbu's generalized limit equilibrium method of slices. The inclinations of nails and distribution of nail forces are regarded as main design parameters and are used to obtain the minimum total nail force required to achieve a desired value of safety factor. Sheahan and Ho (2003) proposed a trial wedge approach to analyze the stability of soil nailing slopes. This method aims to provide a relatively simple and inexpensive procedure for preliminary or complementary design of soil nailed slope. Yuan et al. (2003) presented a limit equilibrium approach and it was employed for reliability analysis of soil nailed slope. In this approach, the inter-slice forces are calculated by recursion and the force equilibrium of the last boundary slice is

satisfied by iteration. Patra and Basudhar (2005) developed a generalized method for optimal design of soil nailing slopes.

Working stress design methods can be generally categorized into three major types (ASCE, 1997): empirical design earth pressure diagrams, kinematical limit analysis, and finite element/finite difference analysis.

Empirical design earth pressure diagrams are slightly modified from the earth pressure design diagram proposed by Terzaghi and Peck (1967) for the design of braced excavation, and are used to compute nail forces (Juran and Elias, 1987). This method can only be employed for slopes with simple geometry and is not suitable to evaluate the influence of various design parameters such as the inclination of the facing, rigidity and inclination of the nails, surcharge loading, and heterogeneity of soil property.

Kinematical limit analysis for soil nailed slope design was proposed by Juran et al. (1990). The upper bound limit analysis solution is employed in this design approach. The constructed kinematically admissible failure mechanism is based on the perceived failure mode in model tests. The local stability at the level of each nail can be assessed and the nail forces can be calculated by this method. The major design parameters (inclination and bending stiffness of nails, embankment slope, facing inclination, and soil shear strength property) are taken into account in the formulation of this approach to evaluate the slope stability. The influence of these parameters on the magnitude and location of the maximum nail forces can also be assessed. In this method, the internal failure criteria include the pullout failure, tensile failure and bending failure.

The two-dimensional finite element or finite difference method for the analysis of nailed slope has been used by Shen et al. (1981b), Juran et al. (1985), Plumelle et al. (1990), Thompson and Miller (1990), Choukier (1996), Unterreiner et al. (1997), Murthy et al. (2002), Babu et al. (2002), and Cheuk et al. (2005). Although two-dimensional analysis provides valuable insight into the behaviours of nailed slope, the effect of soil-nail interaction is not adequately considered. Some researchers adopt three-dimensional finite element method to soil nailed slope analysis (Tabrizi et al., 1995; Smith and Su, 1997; Briaud and Lim, 1997; Zhang et al., 1999; Yang and Drumm, 2000). These researchers focus mainly on the deformation, soil-nail interaction, and comparison of the finite element predictions with observed behaviour of nailing slope, while the factor of safety is seldom considered.

2.2.4 Full scale and small scale test of soil nailing slope

Some full scale and small scale model tests have been conducted to investigate the behaviour of soil nailing system. Full scale test can provide the best representation of the real behaviour of soil-nailed system, but it is very expensive and time consuming to conduct these tests. There are thus only several full scale tests reported in the literature. The first full scale test was the German research and development project "Bodenvernagelung" which took place from 1975 until 1980 (Gassler and Gudehus, 1981; Gassler, 1992; Gassler, 1993). Seven fully instrumented field tests on nailed walls were involved in this project, and the whole research scheme included the following aspects: study the failure mechanisms of the nailed walls by theoretical analysis; investigate the performance of nailed walls at limit equilibrium state by model tests; develop drilling and construction technology in soils by implementation of seven full scale nailed walls; perceive the behavior of nailed walls during the building process, under service loading and at limit state by instrumentation in the tests.

The second large full scale test was the French National Project "Clouterre" carried out from 1986 to 1990 (Plumelle et al., 1990; Schlosser et al., 1992; Clouterre, 1993). Three well instrumented experimental soil nailed walls were involved in this project. The failure mode of the first testing wall was tensile failure of nail induced by partial saturation of the soil from the top of the wall. The failure of the second testing nailed wall was caused by increasing the height of the excavation. The collapse of the third testing nailed wall arose from progressive shortening of the lengths of the nails. Recently, a full scale test on a well instrumented soil-nailed loose fill slope was conducted in Hong Kong (Li, 2003; Li et al., 2008). External concrete blocks are added on the slope crest to induce the failure for wet and dry condition. It is found that soil nailing combined with a surface grillage is a prospective approach to improve the stability of loose fill slopes.

Though small scale or reduced scale test is not a prototype test, this experiment can still provide good insight into the soil nailing behaviour and is much easier to be conducted than full scale test. Stocker et al. (1979) reported some small scale tests, which were carried out to investigate the bearing performance and failure mechanisms of nailed retaining structures, and these tests were part of the German project "Bodenvernagelung". Juran et al. (1984) carried out some small scale model tests to examine the performance of nailed soil and reinforced earth retaining structures, and to study the nail tensile failure mechanism. Kitamura et al. (1988) conducted vertical loading tests for nailed slope models to investigate the influence of the steel bar reinforcement in a sandy slope. Hayashi et al. (1992) carried out a series of model tests to evaluate the function of steel bar reinforcement in a cut-off slope with a thin deposit layer. Kim et al. (1995) conducted small scale model tests to study the influence of external loading on the failure mechanism of soil nailed slopes. Kim et al. (1996)

performed model tests to examine the failure mechanism of soil nailed wall, and the results show that bilinear or log-spiral lines can be good characterization for the slip surface of soil nailed wall. Raju et al. (1997) conducted a series of model tests to investigate the performance of a nailed wall controlled by its self weight.

2.3 Stability analysis of slopes reinforced with piles

Installation of piles to improve slopes stability has been demonstrated to be an effective method (D'Appolonia et al., 1967; De Beer and Wallays, 1970; Ito and Matsui, 1975; Fukuoka, 1977; Wang et al., 1979; Ito et al., 1981, 1982; Reese et al., 1992). A number of approaches have been employed to evaluate the performance and design of the piles which are used as reinforcement in slopes, and these methods are summarized as follows.

Ito and Matsui (1975) proposed a theoretical formulation to analyze the growth mechanism of lateral force exerting on stabilizing piles in a row, and the influence of pile spacing was considered. An accurate estimation about the lateral force is very important in the design of the reinforcing piles, and the magnitude of the force is related to the movement of the soil surround the pile. The formulation presented by Ito and Matsui (1975) estimates a value of the lateral force in the initial state of landslide movement, and this value is less than the force in the ultimate limit state of landslide movement. Two kinds of formulation were derived on the basis of the theories of plastic deformation and plastic flow. The expression by the latter theory assumes a visco-plastic flow occurring around the piles, and this formulation is suitable for very soft soil. The expression by the former theory is applicable for common soils, and some of the assumptions used in this formulation by Ito and Matsui (1975) are: when the soil layer deforms, two sliding surfaces occur on the two sides of the pile which have an

angle of ($\pi/4+\phi'/2$) with the axis normal to the pile row plane; the soil is in a state of plastic equilibrium only in the soil body around the pile where the Mohr-Coulomb yield criterion applies; the soil layer is in a plane-strain condition in the direction of depth; the frictional forces on the sliding surfaces of the two sides of the pile are neglected when the stress distribution in the soil body around pile is considered; the piles are rigid. Ito et al. (1981, 1982) subsequently developed a design methodology for a pile reinforced slope based on the above approach. Hassiotis et al. (1997) also presented an approach for the design of slopes strengthened by a single row of piles in which the plastic state theory developed by Ito and Matsui (1975) was also used to estimate the pressure acting on the piles.

The boundary element method (Poulos, 1973; Poulos and Davis, 1980; Lee et al., 1991; Chen and Poulos, 1997) has also been employed to assess the passive pile response considering the soil moving through the pile. On the basis of this method, Lee et al. (1995) and Poulos (1995) have developed an approach for the design of piles to reinforce slopes. The design procedure by Poulos (1995) is as follows: (1) calculating the total shear force required to improve the slope stability to a desired standard; (2) assessing the maximum shear force that each pile can offer to prevent potentially unstable soil mass from sliding by pile-soil interaction analysis using boundary element method; and (3) determining the type and number of piles, and the optimal pile position.

Chow (1996) presented a numerical method for the analysis of pile stabilized slope. In this method, the piles are simulated by beam finite elements and the soil is simulated by a hybrid approach, in which the subgrade reaction modulus is used to model the soil response, and the elastic theory is used to model the interaction between the pile and the soil.

Yamagami et al. (2000) presented a limit equilibrium design method for slopes reinforced with a row of piles. In this method, two individual failure surfaces are assumed on the upper part and lower part of the pile. Based on the presumed slip surface, the forces exerting on the stabilizing piles can be evaluated according to the prescribed safety factor.

The kinematic approach of limit analysis was employed by Ausilio et al. (2001) to conduct stability analyzing for soil slopes strengthened with piles. The formulation was derived based on the force required for improving the slope stability to a prescribed standard, and the optimal pile position was assessed. It is shown that the optimum pile location is usually near to the slope toe, and the critical slip surface for slope reinforced with pile is deeper than an unreinforced slope.

A new subgrade reaction formulation was developed by Cai and Ugai (2003) to evaluate the response of flexible piles in landslides, and the dimensionless design charts were presented on the basis of this new formulation. The influence of the linear movement of the sliding layer was taken into account in this formulation.

The finite element and finite difference method have also been employed in piled slope analysis by some researchers. Cai and Ugai (2000) have conducted stability analysis for slope reinforced with piles by three-dimensional finite element method using shear strength reduction technique, and the influence of the pile spacing, pile head conditions, bending stiffness, and pile locations on the slope stability were considered. Won et al. (2005) have analyzed the same slope model as Cai and Ugai (2000) by three-dimensional finite difference code FLAC3D, and the shear strength reduction technique was also used to obtain the factor of safety. Both the finite element results by Cai and

Ugai (2000) and finite difference results by Won et al. (2005) were compared with those obtained by limit equilibrium method, where the reaction force of the piles was determined by equation from Ito and Matsui (1975). The factors of safety by the SRM are slightly larger than those by the limit equilibrium method, but the slip surface by the SRM is much deeper which is determined by the maximum point of shear force in the pile. The finite deference method has also been used by Ng and Zhang (2001), Ng et al. (2001) and Zhang et al. (2004) for laterally loaded sleeved piles on slope stability. A series of 3D analyses were conducted to study the behavior of laterally loaded piles and the effects of unsleeved and sleeved piles on the stability of a cut slope, and the SRM was used in evaluating the slope stability. Chen and Martin (2002) have used finite difference program FLAC to investigate the arching effect and mobilization mechanism of the resistant force in passive pile groups when lateral soil movement is induced. Martin and Chen (2005) have also used this program to assess the behavior of piles installed in an embankment slope with a translational failure mode. Pan et al. (2002) and Miao et al. (2006) have used finite element program ABAQUS to investigate the passive pile behavior.

2.4 Stability analysis of slopes with water flow

Water-induced slope failure is a common geotechnical problem. The stability of the slope is reduced because of the seepage force. For slope stability analysis with water flow, the widely used method is still the limit equilibrium method. The inclusion of seepage forces in the limit equilibrium method has some confusion in the past. In the traditional limit equilibrium method, the boundary water forces with total weights are usually used and the water pressures enter into the base normal/shear force calculation but not along the sides between slices. Turnbull and Hvorslev (1967) viewed that the traditional method yields unreasonable results for high value of pore-pressure and

suggested only the effective stress should be resolved in a direction normal to the slip surface. Greenwood (1983, 1985) and King (1989) introduced some effective-stress methods of slices which including interslice water forces. Actually all these methods do not have great difference since we can use either boundary water forces with total weights or seepage forces with submerged weights and these two methods should give the same answer theoretically. The uses of the boundary forces and total weights are usually more convenient and are widely accepted and employed in practice.

For slope stability analysis with water flow, the pore water pressure should be properly determined. In limit equilibrium method, the piezometric line is most commonly used for determining the pore-water pressure distribution. The vertical length from the slice base mid-point up to the piezometric line is calculated, and this length times the unit weight of water will give the pore-water pressure at the slice base. In a slope with water flowing from upper part to lower part, the conventional assumption about the piezometric surface is usually not accurate. In some commercial software, such as SLOPE/W (2004), a correction factor is introduced to more correctly determine the pore-water pressure. Another method, which is also employed in some commercial software is the integration of the limit equilibrium method with the finite element program and to adopt the pore pressure from the flow-net. This integrated procedure has been employed in slope stability analysis with seepage flow by Ng and Shi (1998), Gasmo et al. (2000), Tsaparas et al. (2002), Kim et al. (2004), and Rahardjo et al. (2007).

Limit analysis method was used by Kim et al. (1999) for the analysis of slope subjected to pore water pressures. Both the statically admissible stress fields for the lower bound solution and kinematically admissible failure mechanisms for the upper bound solution

were constructed by three-noded linear triangular finite elements. The influence of the water pressure were taken into account and combined into the finite element analysis.

Another approach, which is called finite element stress method, was proposed by Fredlund et al. (1999). In this method, a finite element stress analysis is combined with a limit equilibrium analysis. The stress distribution in the slope can first be computed by finite element analysis. The stress distribution from the finite element analysis is then introduced into the LEM analysis for calculating the normal stress and mobilized shear stress along any given failure surface. The factor of safety can be determined as the ratio of the summation of the available resistant shear force to the summation of the mobilized shear force along the selected slip surface. If this approach is applied for slope analysis with water flow, couple finite element analysis should be conducted to obtain the effective stress distribution. Cho and Lee (2001) employed this method to calculate the safety factor for an unsaturated slope suffering from rainfall infiltration.

Strength reduction method can also be used in slope stability analysis with water flow. The pore-pressure can be computed by the seepage or consolidation analysis, the effective stress is then used to conduct shear strength reduction analysis. This process can easily be completed in a single finite element or finite difference software, and it does not require coupling of finite element analysis and limit equilibrium analysis. This approach has been employed by Cai et al. (1999), Cai and Ugai (2004) on slope stability analysis under rainfall.

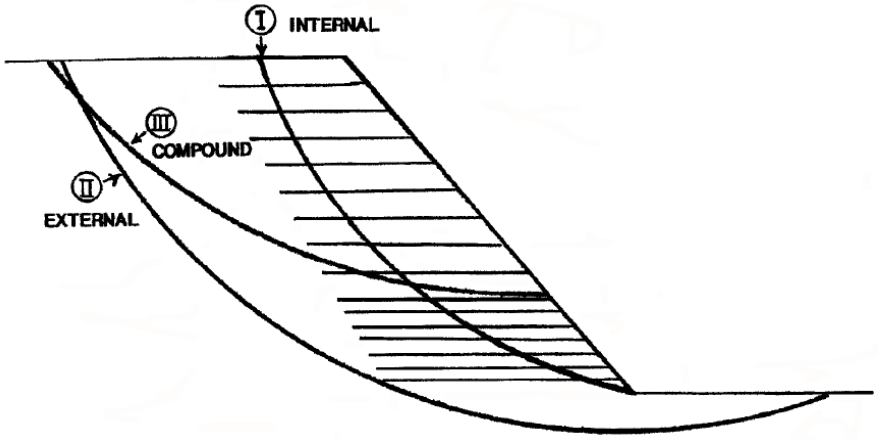

Figure 2.1 Failure modes for reinforced soil slopes (after Elias et al., 2001)

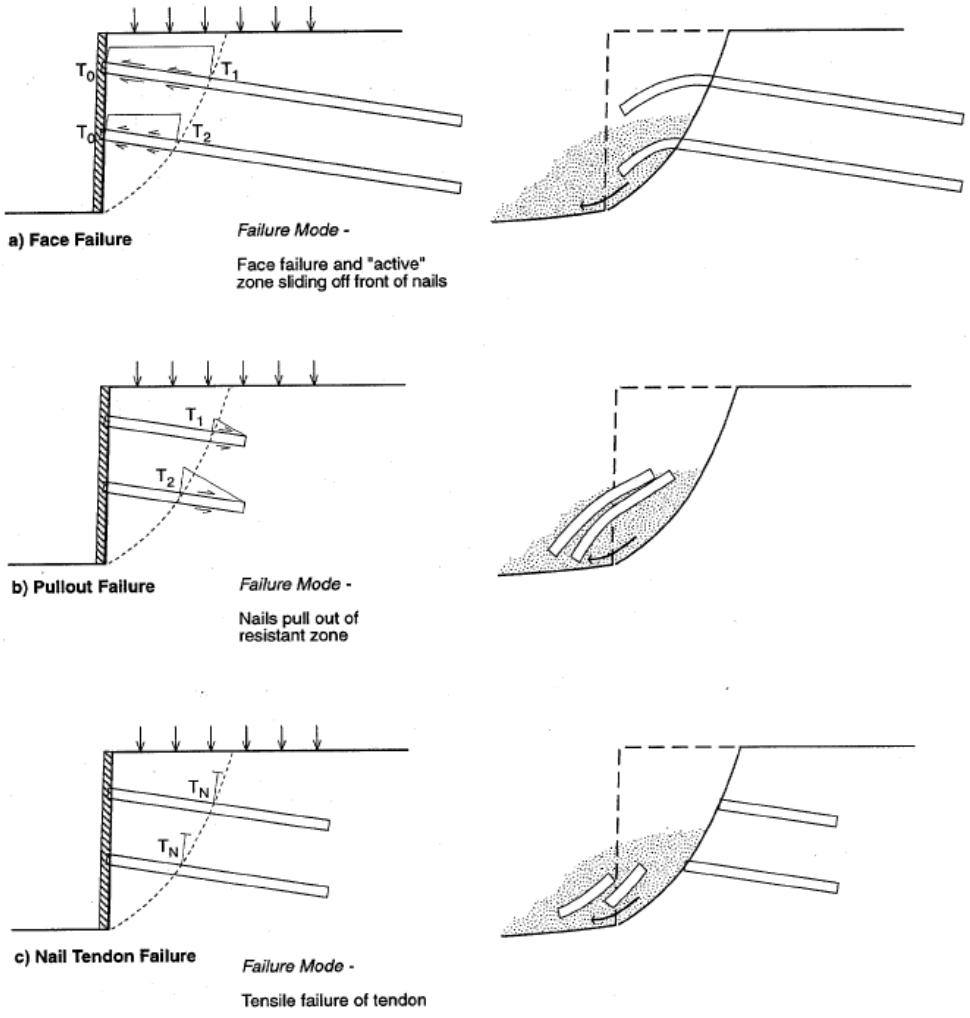

Figure 2.2 Potential soil nail wall internal failure modes (after Byrne et al., 1998)

CHAPTER 3: TWO-DIMENSIONAL SLOPE STABILITY ANALYSIS BY LIMIT EQUILIBRIUM AND STRENGTH REDUCTION METHODS

3.1 Introduction

In this chapter, the factors of safety and the locations of critical failure surfaces obtained by the limit equilibrium method and strength reduction method are compared for various 2D slopes. The study in this chapter will provide a good investigation on the two most important slope stability methods, and the advantages and limitations of these two methods are investigated under different conditions. For SRM analysis, the FOS of a slope is defined as the reduction factor by which the original soil shear strength parameters should be reduced to make the slope to reach the critical failure state. This definition is the same as the one employed in the limit equilibrium method. Thus the reduced shear strength parameters c'_f and ϕ'_f are given as follows:

$$c'_f = c' / \text{FOS} \tag{3.1}$$

$$\phi'_f = \arctan(\tan\phi' / \text{FOS}) \tag{3.2}$$

There is another definition of the FOS for SRM in which the load or gravity is increased by a certain factor to bring the slope to the critical failure state, and this definition is different from that in the traditional LEM. In the present study, the first definition is used in all the SRM analysis, and since this definition is the same as the one used in LEM, the comparison of the FOS between SRM and LEM will be reasonable.

Many researchers have compared the results between the SRM and LEM and have found that generally the two methods will give similar FOS. Most of the studies are, however, limited to homogenous soil slopes and the geometry of the problems is relatively regular with no special features (e.g. the presence of a thin layer of soft material or special geometry). Furthermore, there are only limited studies which compare the critical failure surfaces from the LEM and SRM as the FOS appears to be the primary quantity of interest. In this chapter, the two methods are compared under different conditions and both the FOS and the locations of the critical failure surfaces are considered in the comparisons. In the present study, both a non-associated flow rule (SRM1 and soil dilation angle=0) and an associated flow rule (SRM2 and soil dilation angle=friction angle) are applied for Mohr-Coulomb model in the SRM analyses. To define the critical failure surface from the SRM, both the maximum shear strain rate (the rate of variation of the shear strain at the failure state) and the maximum shear strain increment (the accumulated total shear strain at the failure state) definition can be used. It has been found that these two definitions will give similar locations of the critical failure surface under most cases for different computer programs. The failure surface may also be defined by displacement distribution, but this criterion is usually not very clear as compared with the shear strain criterion.

In the present study, the limit equilibrium method is considered using the Morgenstern-Price method with f(x)=1.0 (equivalent to Spencer method). Krahn (2003) and Abramson et al. (2002) have pointed out that f(x) may be critical for some special cases, but this is generally not the case unless the problem is highly complicated. Besides Spencer's method, the Generalized Limit Equilibrium (GLE) method (Abramson et al. 2002) has also been tried and the results are also similar to those by the Morgenstern-Price method. The differences of the FOS and the critical failure surfaces from f(x)=1.0

and f(x)=sin(x) are also found to be small for both the Morgenstern-Price method and the GLE method in the present study. Hence, the discussions in this chapter are not sensitive to the specific form of LEM. The software Slope2000 by Cheng is used for the LEM analysis.

In performing the SRM analysis, many soil parameters and boundary conditions are required to be defined which are absent in the corresponding LEM analysis. The importance of the various parameters and the applicability of the SRM under several special cases are considered in the following sections. For SRM analysis, except for some special cases which are analyzed by other software, all the examples shown in this chapter are analyzed by commercial software FLAC3D.

3.2 Stability analysis for a simple and homogeneous soil slope

Firstly, a homogeneous soil slope with a slope height equal to 6m and slope angle equal to 45° (Figure 3.1) is considered. For the three cases in which the friction angle is 0, since the critical slip surface is a deep-seated surface with a large horizontal extent, the models are larger than the one as shown in Figure 3.1 and have a width of 40m and a height of 16m. In the parametric study, different shear strength properties are used and the LEM, SRM1 and SRM2 analyses are carried out. The cohesive strength c' of the soil varies from 2 kPa, 5 kPa and 10-20 kPa while the friction angle ϕ' varies from 5°, 15°, 25° and 35° - 45°. The density, elastic modulus and Poisson ratio (ν) of the soil are kept at 20 kN/m^3, 14MPa and 0.3 respectively in all the analysis. As shown in Figure 3.1, the size of the domain for the SRM analyses is 20m in width and 10m in height and there are 3520 zones and 7302 grid points in the mesh for analysis. Based on limited mesh refinement studies, it was found that the discretization as shown in Figure 3.1 is

sufficiently good so that the results of analyses are practically insensitive to a further reduction in the element size. For the LEM, the Morgenstern-Price method, which satisfies both moment and force equilibrium, is adopted and the critical failure surface is evaluated by the modified simulated annealing technique as proposed by Cheng (2003). The tolerance for locating the critical failure surface by the simulated annealing method is 0.0001 which is sufficiently accurate for the present study.

From Table 3.1 and Figures 3.2 to 3.5, it is found that the FOS and critical failure surfaces determined by the SRM and LEM are very similar under different combinations of soil parameters for most cases except when ϕ'=0. When the friction angle is greater than 0, most of the FOS obtained by the SRM differ by less than 7.4 % with respect to the LEM results except for case 16 (c'=20kPa, ϕ'=5°) where the difference is up to 13.2 %. When the friction angle is very small or zero, there are relatively major differences between the SRM and LEM for both the FOS and the critical slip surface (Table 3.1 and Figure 3.5). Based on Table 3.1 and Figures 3.2 to 3.5, some conclusions can be made as follows:

(1) Most of the FOS obtained from the SRM are slightly larger than those obtained from the LEM with only few exceptions.

(2) The FOS from an associated flow rule (SRM2) are slightly greater than those from a non-associated flow (SRM1), and this difference increases with increasing friction angle. These results are reasonable and are expected. The differences between the two set of results are, however, small because the problem has a low level of 'kinematic constraint'.

(3) When the cohesive strength of the soil is small, the differences in FOS between the LEM and SRM (SRM1 and SRM2) are greatest for higher friction angles. When the cohesion of the soil is large, the differences in FOS are greatest for lower friction angles. This result is somewhat different from that of Dawson et al. (2000), who concluded that the differences are greatest for higher friction angles when the results between SRM and limit analysis are compared.

(4) The failure surfaces from the LEM, SRM1 and SRM2 are similar in most cases. In particular, the critical failure surfaces obtained by SRM2 appear to be closer to those from LEM than those obtained from SRM1. The critical failure surfaces from SRM1, SRM2 and LEM are practically the same when the cohesive strength is small (it is difficult to differentiate clearly in Figures 3.2, 3.3a, 3.3b, 3.4a, 3.4b), but noticeable differences in the critical failure surfaces are found when the cohesive strength is high (Figures 3.3d, 3.4d, 3.5a, 3.5b).

(5) The right end of the failure surface moves closer to the crest of the slope as the friction angle of the soil is increased (which is a well known result). This behaviour is more obvious for those failure surfaces obtained from SRM1. For example, for the five cases where the cohesion of the soil is 2kPa (Figure 3.2), when the friction angle is 5, 15 and 25 degrees, the right end-point of the failure surface derived from SRM1 is located to the right of the right end-point of the critical failure surface obtained from the LEM. When the friction angle is 35°, the right end-point of the failure surface obtained by the SRM1 and LEM are nearly at the same location. When the friction angle is 45°, the distance of the right end-point derived from SRM1 is located to the left of the right end-point derived from LEM.

(6) For SRM analyses, when the friction angle of soil is small, the differences between the slip surfaces for SRM1 and SRM2 are greatest for smaller cohesion (Figure 3.3). When the friction angle is large, the differences between the slip surface for SRM1 and SRM2 are greatest for higher cohesion (Figure 3.4).

(7) It can also be deduced from Figures 3.2 to 3.5 that the potential failure volume of the slope becomes smaller with increasing friction angle but increases with increasing cohesion. This is also well known behaviour, as when the cohesive strength is high the critical failure surface will be deeper.

Although there are some minor differences in the results between the SRM and LEM in this example, the results from these two methods are generally in good agreement which suggests that the use of either the LEM or SRM is satisfactory in general. However, an interesting case is constructed in the next section where a limitation of the SRM is demonstrated.

3.3 Stability analysis of a slope with a soft band

A special problem with a soft band has been constructed as it appears that similar problems have seldom been considered previously. The geometry of the slope is shown in Figure 3.6 and the soil properties are shown in Table 3.2 (In practice the elastic modulus should not be the same for different soil. The elastic modulus used in this section for different soil layer is assumed to be 14MPa for simplicity; and it will be shown in the later sections that the influence of the elastic modulus on the SRM analysis is very small, so the use of the elastic parameters should not have great effect on the result). It is noted that c' is zero and ϕ' is small for soil layer 2 which has a thickness of just 0.5m. The critical failure surface is obviously controlled by this soft band, and slope

failures in similar conditions have actually occurred in Hong Kong (for example, the Fei Tsui Road slope failure in Hong Kong).

In order to consider the size effect (boundary effect) in the SRM, three different numerical models are developed to perform the SRM using Mohr-Coulomb analysis and the widths of the domains are 28m, 20m and 12m, respectively (Figure 3.7). In these three SRM models, various mesh sizes were tried until the results were insensitive to the number of elements used for the analysis. For example, when the domain size is 28m, the FOS was found to be 1.37 (Table 3.3a) with 12000 elements, 1.61 with 6000 elements and 1.77 with 3000 elements using SRM1 analysis and the program Phase2.

Since the FOS for this special problem have great differences from those found using the LEM, several well known commercial programs (Flac3D, Flac2D, Phase2, Plaxis) are tried and very surprising results are obtained. For these four commercial programs, Flac3D and Flac2D are finite difference codes, while Phase2 and Plaxis are finite element codes, but the definition of SRM in these codes is practically the same. The ultimate limit state is determined by non-convergence criterion in all these codes, and an arc-length control technique is used in Plaxis to determine the ultimate limit state. The locations of the critical failure surfaces from SRM for solution domain width of 12m, 20m and 28m are virtually the same. The local failures from the SRM, as shown in Figure 3.8b, range from x=5m to x=8m and the failure surfaces are virtually the same for the three different solution domains. The majorities of the critical failure surfaces lie within layer 2, which has low shear strength, and are far from the right boundary. It is surprising to find that different programs produce drastically different results (Table 3.3a) for the FOS even though the locations of the critical failure surface from these programs are very similar. For the cases as shown in Figure 3.1, and other cases in a

latter part of this chapter, the results are practically insensitive to the domain size, while the cases shown in Figure 3.6 are very sensitive to the size of domain for the programs Flac3D (SRM1 and SRM2) and Phase2 (SRM2). Results from the Plaxis program appear to not be sensitive to the domain size but are quite sensitive to the dilation angle (which is different from the previous example). The SRM1 results from program Phase2 are also not sensitive to the domain size for SRM1, but results from SRM2 behave differently. The FOS from Flac3D appear to be overestimated when the soil parameters for the soft band are low, but the results from this program are not sensitive to the dilation angle which is similar to all the other examples in the present study. For SRM1, the results from Phase2 and Plaxis appear to be more reasonable as the results are not sensitive to the domain sizes, while for SRM2, results from Plaxis may be better. It is also surprising to find that Flac2D cannot give any result for this problem, even after many different trials, but the program worked properly for all the other examples in this study.

There is another interesting and important issue when SRM is adopted for the present problems. For the problem with a 12m domain, Phase2 cannot provide a result with the default settings and these settings (including the tolerance and number of iterations allowed) are varied until convergence is achieved. The results of analysis for a 12m domain with Phase2 are shown in Tables 3.4 and 3.5. It is observed that the number of elements used for the analysis has a very significant effect on the factor of safety, which is not observed for the cases in Table 3.1. The tolerance used in the nonlinear equation solution also has a major impact on the results for this case. This is less obvious for other cases considered in the present study.

Besides the special results shown above, the FOS from the 28m domain analysis appears to be large for Flac3D and Phase2 when the strength parameters for the soil layer 2 are low. In fact, it is not easy to define an appropriate factor of safety from SRM analysis for this problem. If the cohesive strength of the top soil is reduced to zero, the factor of safety can be estimated as 0.57 from the relation $\tan\phi'/\tan\theta$, where θ is the slope angle. It can be seen that for the LEM, the cohesive strength 20 kPa for soil 1 helps to bring the factor of safety to 0.927 and a high factor of safety for this problem is not reasonable. Without the results from the LEM for comparison, it may be unconservative to adopt the values of 1.64 (1.61) from the SRM based on Flac3D.

When the soil properties of the soft band are changed to c'=10 kPa and ϕ'=0, the results of analyses are as shown in Table 3.3b. It is found that the critical failure will extend to a much greater distance so that a 28m wide domain is necessary. The FOS from the different programs are virtually the same, which is drastically different from the results in Table 3.3a (the same meshes were used for Table 3.3a and Table 3.3b).

If the soil properties of soils 2 and 3 are interchanged so that the third layer of soil is the weak soil, the FOS from SRM2 are 1.33 by FLAC3D for all three different domain sizes. The corresponding factor of safety from the LEM is 1.29 from the Morgenstern-Price analysis. The locations of the critical failure surface from the SRM and LEM for this case are also very close, except for the initial portion, as shown in Figure 3.9a and 3.9b. It appears that the presence of a soft band with frictional material, instead of major differences in the soil parameters is the actual cause for the difficulties in the SRM analysis. Great care is required in the implementation of a robust nonlinear equation solver for the SRM.

The problems as shown in Table 3.3a may reflect the limitations of commercial programs rather than the limitations of the SRM, but they illustrate that it is not easy to compute a reliable FOS for this type of problem using the SRM. The results are highly sensitive to different nonlinear solution algorithms which are not clearly explained in the commercial programs. Great care, effort and time are required to achieve a reasonable result from SRM for this special problem and comparisons with the LEM are necessary. It is not easy to define a proper factor of safety from the SRM alone for the present problem as the results are highly sensitive to the size of domain and the flow rule. In this respect, the LEM appears to be a better approach for this type of problem.

3.4 Local minimum in LEM

For the LEM, it is well known that many local minima may exist besides the global minimum. This makes it difficult to locate the critical failure surface by classical optimization methods. Comparisons of the LEM and SRM with respect to local minima have seldom been considered in the past, but this is actually a very important issue which is illustrated by the following examples. In the SRM, there is no local minimum as the formation of the shear band will attract strain localization in the solution process. To investigate this issue, an 11m height slope as shown in Figure 3.10 is considered. The slope angle for the lower part of the slope is 45° while the slope angle for the upper part of the slope is 26.7°. The cohesion and friction angle of the soil are 10 kPa and 30°, respectively, and the density of the soil is 20 kN/m^3.

The failure mechanism by the SRM is shown in Figure 3.11 and the FOS is 1.47 for both non-associated flow and associated flow. The right end-point of the failure surface is located to the right of the crest of the slope. The results derived from the LEM are presented in Figure 3.12 (number of slices is 50). The global minimum factor of safety

is 1.383 but a local minimum FOS of 1.3848 is also found. The location of the failure surface for the local minimum 1.3848 is very close to that from the SRM, and the failure surface for the global minimum from the LEM is not the critical failure surface from the SRM. Since the FOS for the two critical failure surfaces from the LEM are so close, both failure surfaces are probable failure surfaces and should be considered in slope stabilization. For the SRM, there is only one unique failure surface from the analysis and another possible failure mechanism cannot be easily determined. Thus, the SRM analysis may yield a local failure surface of less importance while a more severe global failure surface remains undetected, as illustrated in the next example. This is clearly a major drawback of the SRM as compared with the LEM.

Another interesting case which is worth discussion is constructed. Figure 3.13 shows a relatively simple slope with a total height of 55m in a uniform soil. The soil parameters are c'=5 kPa and ϕ'=30° while the unit weight is 20 kN/m^3. The global minimum and local minima are determined in accordance with the procedures of Cheng (2003) and different boundaries for the left and right exit ends are specified in the study. Using the LEM, the global minimum FOS is obtained as 1.33 (Figure 3.13a) but several local minima are found with factors of safety in the range 1.38 to 1.42 as shown in Figures 3.13b-3.13e. From the SRM, only the factor of safety 1.327 is found which is similar to the global minimum shown in Figure 3.13a. If slope stabilization is only carried out for this failure surface, the possible failure surfaces shown by Figures 3.13d and 3.13e will not be considered. Baker and Leshchinsky (2001) have proposed the concept of the "safety map", which enables the global minimum and local minima from the LEM to be visualized easily, but it appears that construction of such a map using the SRM is impossible. In this respect, the LEM is a better tool for slope stability analysis. It is possible that the use of the SRM may miss the location of the next critical failure

surface (with a very small difference in the FOS but a major difference in the location of the critical failure surface) so that the slope stabilization measures may not be adequate. This interesting case has illustrated a major limitation of the SRM for the design of slope stabilization works.

3.5 Influence of elastic modulus for SRM analysis

In order to investigate the influence of the soil elastic modulus in slope stability analysis when the SRM is used, the four different models shown in Figures 3.14-3.17 are considered. In all these models, the strength parameters are the same for every soil so that there is actually only one soil in the LEM analysis. For the SRM analyses, different elastic moduli are used for different soils and the results of the analyses, shown in Tables 3.6-3.9, indicate that they are relatively insensitive to the elastic modulus of soil. When the elastic moduli of soils 1 and 2 are interchanged, there is only a minor change in the factor of safety. In fact, the effect of flow rule is slightly more important than the elastic moduli in the present example. In general, the differences in both the FOS and the locations of the critical failure surfaces are small between the LEM and SRM. For case 2 in Table 3.9, the difference in the FOS between the LEM and SRM is significant but the locations of the critical failure surfaces from the two methods (Figure 3.18) are close to each other.

3.6 Discussion and Conclusion

In the present study, a number of interesting features of the SRM were highlighted which are important for a proper analysis of a slope. While most research has concentrated on the FOS between the LEM and SRM, the present works have compared the locations of the critical failure surfaces from these two methods. In a simple and homogenous soil slope, the differences in the FOS and locations of the critical failure

surfaces from the SRM and LEM are small and both methods are satisfactory for engineering use. It is found that when the cohesion of the soil is small, the difference in FOS from the two methods is greatest for higher friction angles. When the cohesion of the soil is large, the difference in FOS is greatest for lower friction angles. With regard to the flow rule, the FOS and locations of the critical failure surface are not greatly affected by the choice of the dilation angle (which is important for the adoption of the SRM in slope stability analysis). When an associated flow rule is assumed, the critical slip surfaces from SRM2 appear to be closer to those from the LEM than those from SRM1.

For the SRM, the effects of the dilation angle, the tolerance for nonlinear equation analysis, the soil moduli and the domain size (boundary effects) are usually small but still noticeable. In most cases, these factors cause differences of just a few percent and are not critical for engineering use of the SRM. Since the use of different LEM methods will also give differences in the factor of safety of several percent, the LEM and SRM can be viewed as similar in performance for normal cases.

Drastically different results are determined from different computer programs for the problem with a soft band. For this special case, the factor of safety is very sensitive to the size of the elements, the tolerance of the analysis and the number of iteration allowed. It is strongly suggested that the LEM be used to check the results from the SRM. This is because the SRM is highly sensitive to the nonlinear solution algorithms and flow rule for this special type of problem. Even though results from the program Plaxis (and some results from the program Phase2) are insensitive to the domain size, they are very sensitive to the flow rule which is a result not found in all the other

examples. The SRM has to be used with great care for problems with a soft band of this nature.

The two examples with local minima for the LEM illustrate another limitation of the SRM in engineering use. With the SRM, there is strain localization during the solution and the formation of local minima is unlikely. In the LEM, the presence of local minima is a common phenomenon, and this is a major difference between the two methods. Thus, it is suggested that the LEM should be preformed in conjunction with the SRM as a routine check.

Through the present study, two limitations of the SRM have been established: (1) it is sensitive to nonlinear solution algorithms/flow rule for some special cases and (2) it is unable to determine other failure surfaces which may be only slightly less critical than the SRM solution but still require treatment for good engineering practice. If the SRM is used for routine analysis and design of slope stabilization measures, these two major limitations have to be overcome and it is suggested that the LEM should be carried out as a cross reference. If there are great differences between the results from the SRM and LEM, great care and engineering judgment should be exercised in assessing a proper solution. There is one practical problem in applying the SRM to a slope with a soft band. When the soft band is very thin, the number of elements required to achieve a good solution is extremely large so that very significant computer memory and time are required. Cheng (2003) has tried a slope with a 1mm soft band and has effectively obtained the global minimum factor of safety by the simulated annealing method. If the SRM is used for a problem with a 1mm thick soft band, it is extremely difficult to define a mesh with a good aspect ratio unless the number of elements is huge. For the SRM with a 500 mm thick soft band, about one hour of CPU time for a small problem

(several thousand elements) and several hours for a large problem (over ten thousand elements) were required for the Phase2 program, while the program Flac3D required 1-3 days (for small to large meshes). If a problem with a 1mm thick soft band is to be modeled with the SRM, the computer time and memory required will be huge and the method is not applicable for this special case. The LEM is perhaps better than the SRM for these cases.

For the SRM, there are further limitations which are worth observing. Shukha and Baker (2003) have found that there are minor but noticeable differences in the factors of safety from Flac using square elements and distorted elements. The use of distorted elements are however unavoidable in many cases. Furthermore, when both the soil parameters c' and ϕ' are very small, it is well known that there are numerical problems with the SRM. The failure surface in this case will be deep and wide and a large domain is required for analysis. It has been found that the solution time is extremely long and a well-defined critical failure surface is not well established from the SRM. For the LEM, there is no major difficulty in estimating a factor of safety and the critical failure surface under these circumstances.

The advantage of the SRM is the automatic location of the critical failure surface without the need for a trial and error search. With the use of modern global optimization techniques, the location of critical failure surfaces by a simulated annealing method, a genetic algorithm or other methods is now possible and trial and error search with the LEM is no longer required. While the LEM suffers from the limitation of an interslice shear force assumption, the SRM suffers from being sensitive to the nonlinear solution algorithm/flow rule for some special cases.

Griffith and Lane (1999) have suggested that a non-associated flow rule should be adopted for slope stability analysis. As the effect of flow rule on the SRM is not negligible in some cases, such as those involving a soft band, the flow rule is indeed an issue for a proper slope stability analysis. It can be concluded that both the LEM and SRM have their own merits and limitations, and the use of the SRM is not really superior to the use of the LEM in routine analysis and design. Both methods should be viewed as providing an estimation of the factor of safety and the probable failure mechanism, but engineers should also appreciate the limitations of each method when assessing the results of their analyses.

Table 3.1 Factors of safety by LEM and SRM

case	c' (kPa)	ϕ' (°)	FOS (LEM)	FOS (SRM1, non-associated)	FOS (SRM2, associated)	FOS difference with LEM (SRM1, %)	FOS difference with LEM (SRM2, %)	FOS difference between SRM1 and SRM2 (%)
1	2	5	0.25	0.25	0.26	0	4.0	4.0
2	2	15	0.50	0.51	0.52	2	4.0	2.0
3	2	25	0.74	0.77	0.78	4.0	5.4	1.3
4	2	35	1.01	1.07	1.07	5.9	5.9	0
5	2	45	1.35	1.42	1.44	5.2	6.7	1.4
6	5	5	0.41	0.43	0.43	4.9	4.9	0
7	5	15	0.70	0.73	0.73	4.3	4.3	0
8	5	25	0.98	1.03	1.03	5.1	5.1	0
9	5	35	1.28	1.34	1.35	4.7	5.5	0.7
10	5	45	1.65	1.68	1.74	1.8	5.5	3.6
11	10	5	0.65	0.69	0.69	6.2	6.2	0
12	10	15	0.98	1.04	1.04	6.1	6.1	0
13	10	25	1.30	1.36	1.37	4.6	5.4	0.7
14	10	35	1.63	1.69	1.71	3.7	4.9	1.2
15	10	45	2.04	2.05	2.15	0.5	5.4	4.9
16	20	5	1.06	1.20	1.20	13.2	13.2	0
17	20	15	1.48	1.59	1.59	7.4	7.4	0
18	20	25	1.85	1.95	1.96	5.4	5.9	0.5
19	20	35	2.24	2.28	2.35	1.8	4.9	3.1
20	20	45	2.69	2.67	2.83	0.7	5.2	6.0
21	5	0	0.20		0.23		15	
22	10	0	0.40		0.45		12.5	
23	20	0	0.80		0.91		13.8	

Table 3.2 Soil properties for Figure 3.6

Soil name	Cohesion (kPa)	Friction angle (degree)	Density (kN/m^3)	Elastic modulus (MPa)	Poisson ratio
Soil1	20	35	19	14	0.3
Soil2	0	25	19	14	0.3
Soil3	10	35	19	14	0.3

Table 3.3a FOS by SRM from different programs when c'=0 and ϕ'=25° for soft band. The values in each cell are based on SRM1 and SRM2 respectively. (min. FOS=0.927 from Morgenstern-Price analysis)

Program/FOS	12m domain	20m domain	28m domain
Flac3D	1.03/1.03	1.30/1.28	1.64/1.61
Phase2	0.77/0.85	0.84/1.06	0.87/1.37
Plaxis	0.82/0.94	0.85/0.97	0.86/0.97
Flac2D	No solution	No solution	No solution

Table 3.3b FOS by SRM from different programs when ϕ'=0 and c'=10 kPa for soft band. The values in each cell are based on SRM1 and SRM2 respectively. (min. FOS=1.03 from the Morgenstern-Price analysis)

Program/FOS	28m domain
Flac3D	1.06/1.06
Phase2	0.99/1.0
Plaxis	1.0/1.03
Flac2D	No solution

Table 3.4 FOS with non-associated flow rule for 12m domain

Element number	Tolerance (stress analysis)	Maximum number of iterations	FOS
1500	0.001	100	0.80
2000	0.001	100	No result
2000	0.003	100	No result
2000	0.004	100	No result
2000	0.005	100	No result
2000	0.008	100	0.81
2000	0.01	100	0.82
2000	0.001	500	0.74
2000	0.003	500	0.77
2000	0.004	500	0.77
2000	0.005	500	0.79
3000	0.001	100	No result
3000	0.003	100	0.79
3000	0.004	100	0.8
3000	0.005	100	0.8
3000	0.01	100	0.84
3000	0.001	500	0.77

Table 3.5 FOS with associated flow rule for 12m domain

Element number	Tolerance (stress analysis)	Maximum number of iterations	FOS
1000	0.001	100	1.03
1200	0.001	100	1.0
1500	0.001	100	No result
1500	0.003	100	No result
1500	0.004	100	1
1500	0.005	100	1.39
1500	0.01	100	2.09
1500	0.001	500	0.86
1500	0.003	500	0.98
3000	0.001	100	No result
3000	0.003	100	No result
3000	0.004	100	No result
3000	0.005	100	No result
3000	0.01	100	No result
3000	0.001	500	0.85
3000	0.003	500	0.89
3000	0.004	500	0.9
3000	0.005	500	1.5
3000	0.01	500	2.09

Table 3.6 Comparison of factor of safety for Figure 3.14

case	c' (kPa)	ϕ' (°)	Density (kN/m^3)	Poisson ratio	Elastic modulus of soil1 (kN/m^2)	Elastic modulus of soil2 (kN/m^2)	FOS (LEM)	FOS (SRM1)	FOS (SRM2)
1	10	15	20	0.3	1.4e5	1.4e2	0.9826	0.954	0.983
2	10	15	20	0.3	1.4e2	1.4e5	0.9826	0.966	0.989
3	10	25	20	0.3	1.4e5	1.4e2	1.2951	1.235	1.297
4	10	25	20	0.3	1.4e2	1.4e5	1.2951	1.259	1.320

Table 3.7 Comparison of factor of safety for Figure 3.15

case	c' (kPa)	ϕ' (°)	Density (kN/m^3)	Poisson ratio	Elastic modulus of soil1 (kN/m^2)	Elastic modulus of soil2 (kN/m^2)	FOS (LEM)	FOS (SRM1)	FOS (SRM2)
1	10	15	20	0.3	1.4e5	1.4e2	0.982	0.964	0.985
2	10	15	20	0.3	1.4e2	1.4e5	0.982	0.963	0.976
3	10	25	20	0.3	1.4e5	1.4e2	1.295	1.288	1.304
4	10	25	20	0.3	1.4e2	1.4e5	1.295	1.282	1.273

Table 3.8 Comparison of factor of safety for Figure 3.16

case	c' (kPa)	ϕ' (°)	Density (kN/m^3)	Poisson ratio	Elastic modulus of soil1 (kN/m^2)	Elastic modulus of soil2 (kN/m^2)	FOS (LEM)	FOS (SRM1)	FOS (SRM2)
1	10	15	20	0.3	1.4e5	1.4e2	0.9826	0.951	0.980
2	10	15	20	0.3	1.4e2	1.4e5	0.9826	0.975	0.980
3	10	25	20	0.3	1.4e5	1.4e2	1.2951	1.240	1.292
4	10	25	20	0.3	1.4e2	1.4e5	1.2951	1.240	1.275

Table 3.9 Comparison of factor of safety for Figure 3.17

case	c' (kPa)	ϕ' (°)	Density (kN/m^3)	ν	Elastic modulus of soil1 (kN/m^2)	Elastic modulus of soil2 (kN/m^2)	Elastic modulus of soil3 (kN/m^2)	FOS (LEM)	FOS (SRM1)	FOS (SRM2)
1	10	15	20	0.3	1.4e5	1.4e2	1.4e5	0.940	0.932	0.951
2	10	15	20	0.3	1.4e2	1.4e5	1.4e2	0.940	0.903	0.947
3	10	25	20	0.3	1.4e5	1.4e2	1.4e5	1.261	1.210	1.275
4	10	25	20	0.3	1.4e2	1.4e5	1.4e2	1.261	1.211	1.268

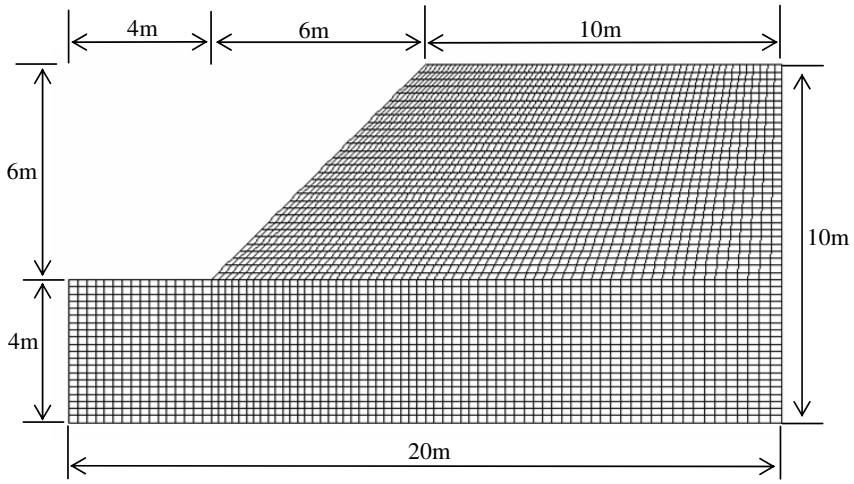

Figure 3.1 Discretization of a simple slope model

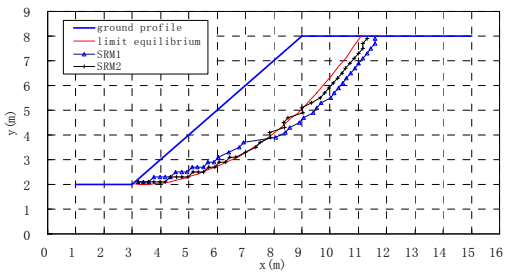

(a) c'=2kPa, ϕ'=5°

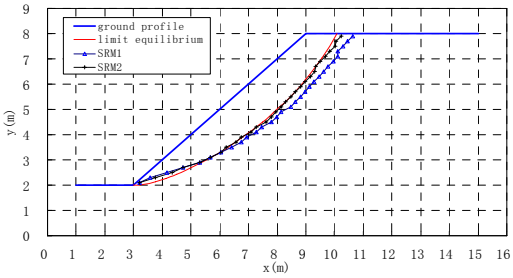

(b) c'=2kPa, ϕ'=15°

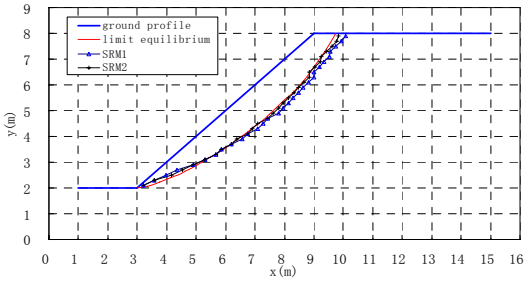

(c) c'=2kPa, ϕ'=25°

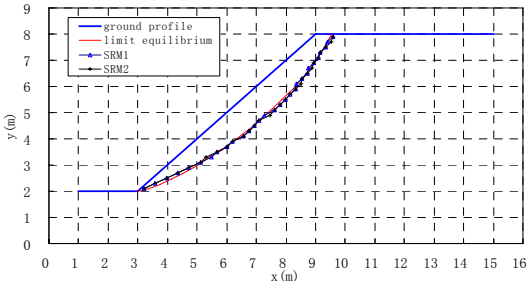

(d) c'=2kPa, ϕ'=35°

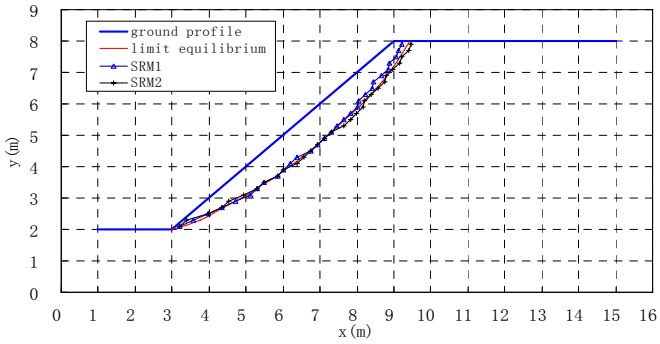

(e) c'=2kPa, ϕ'=45°

Figure 3.2 Slip surface comparison with increasing friction angle (c'=2kPa)

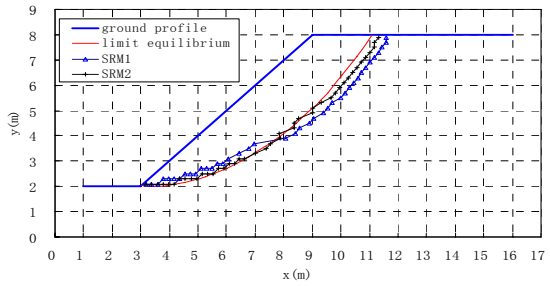

(a) c'=2kPa, ϕ'=5°

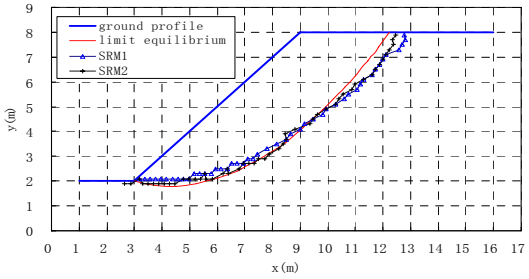

(b) c'=5kPa, ϕ'=5°

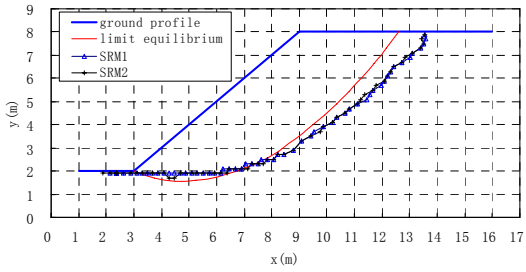

(c) c'=10kPa, ϕ'=5°

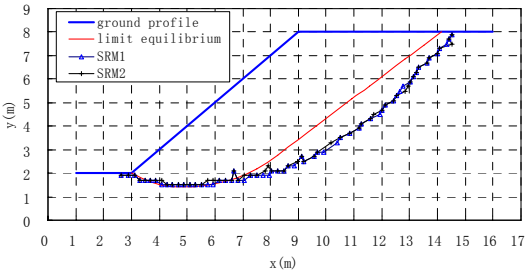

(d) c'=20kPa, ϕ'=5°

Figure 3.3 Slip surface comparison with increasing cohesion (ϕ'=5°)

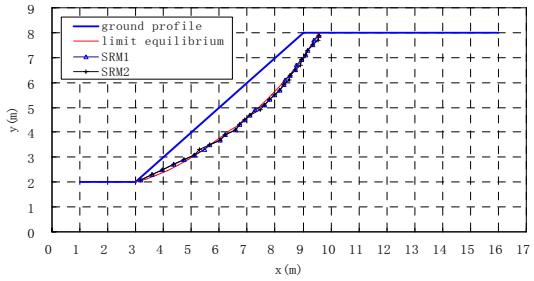

(a) c'=2kPa, ϕ'=35°

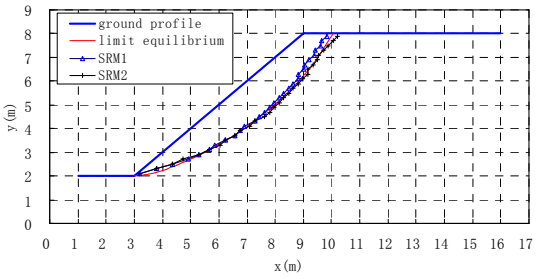

(b) c'=5kPa, ϕ'=35°

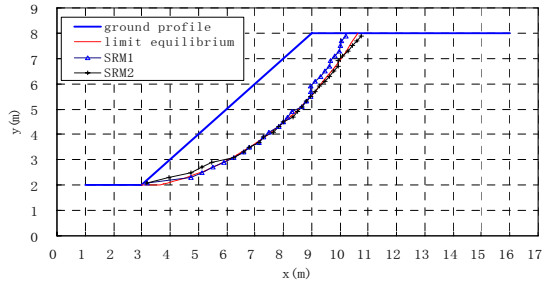

(a) c'=10kPa, ϕ'=35°

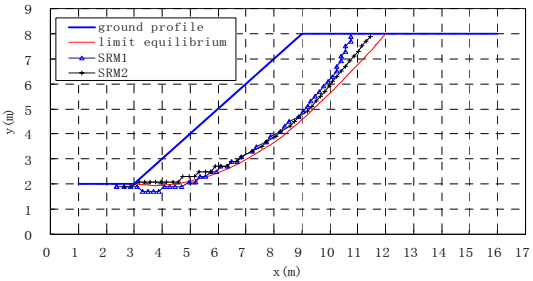

(b) c'=20kPa, ϕ'=35°

Figure 3.4 Slip surface comparison with increasing cohesion (ϕ'=35°)

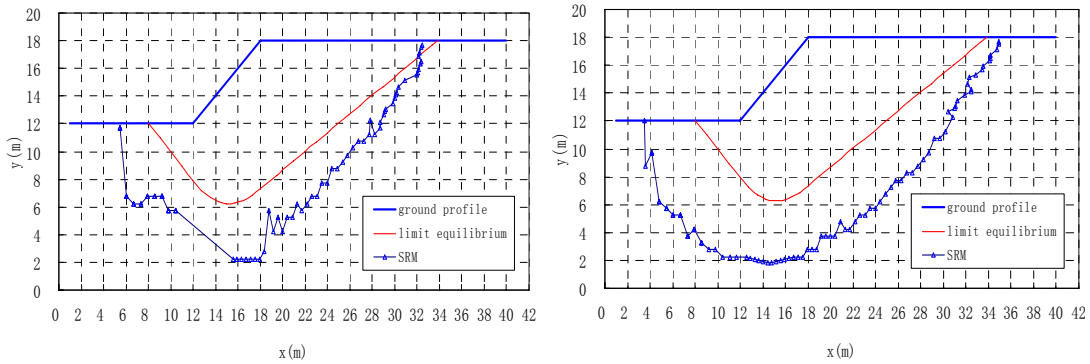

(a) c'=5kPa, ϕ'=0 (b) c'=20kPa, ϕ'=0

Figure 3.5 Slip surface comparison with increasing cohesion (ϕ'=0)

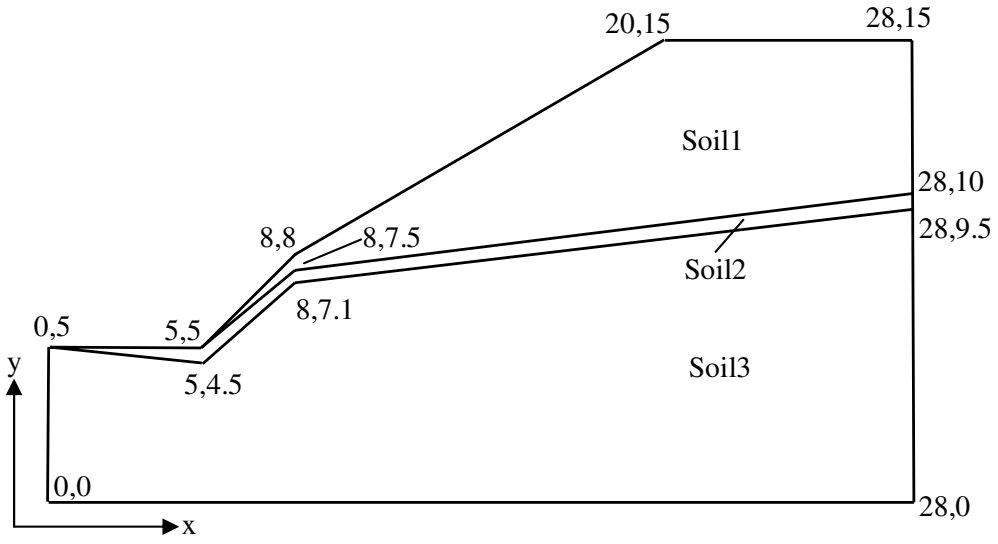

Figure 3.6 A slope with a thin soft band

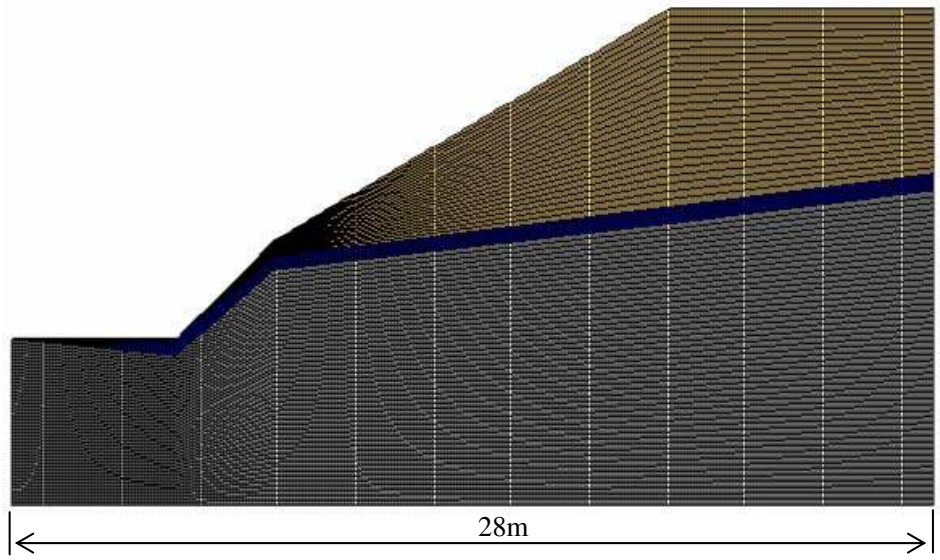

(a) numerical simulation model 1

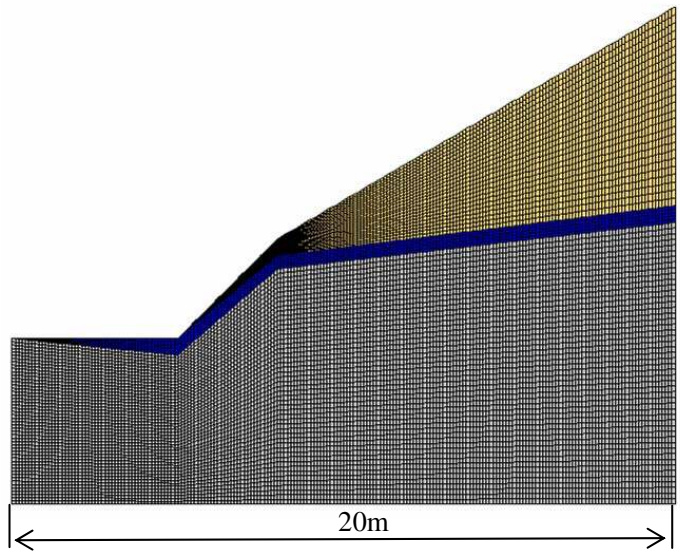

(b) numerical simulation model 2

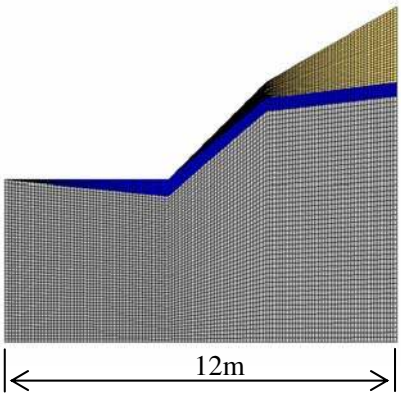

(c) numerical simulation model 3

Figure 3.7 Mesh plot of the three numerical models with a soft band

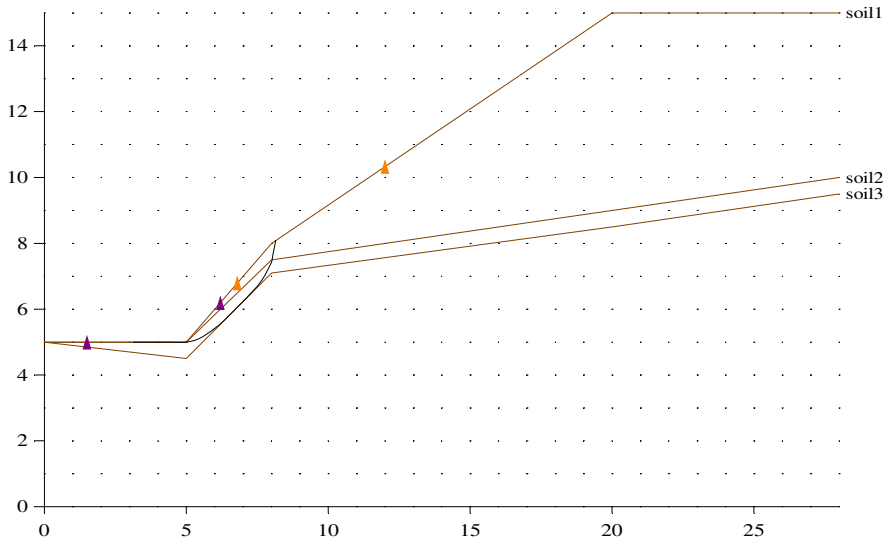

(a) Critical solution from LEM when soft band is frictional material (FOS=0.927)

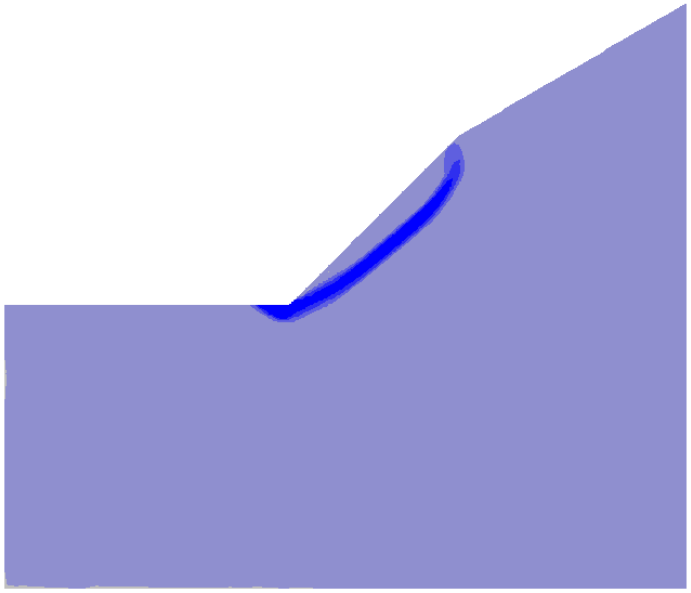

(b) Critical solution from SRM for 12m width domain

Figure 3.8 Critical failure surfaces from LEM and SRM for frictional soft band problem

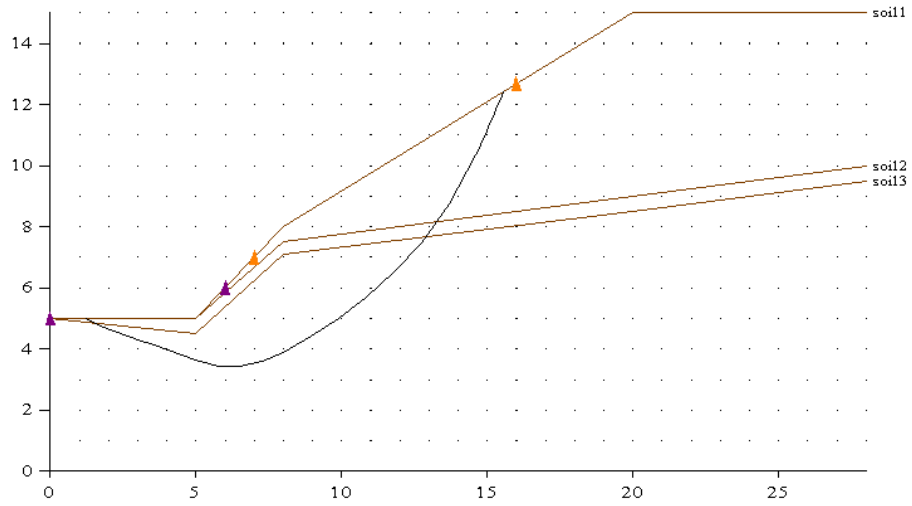

(a) Critical failure surface from LEM when the bottom soil layer is weak (FOS=1.29)

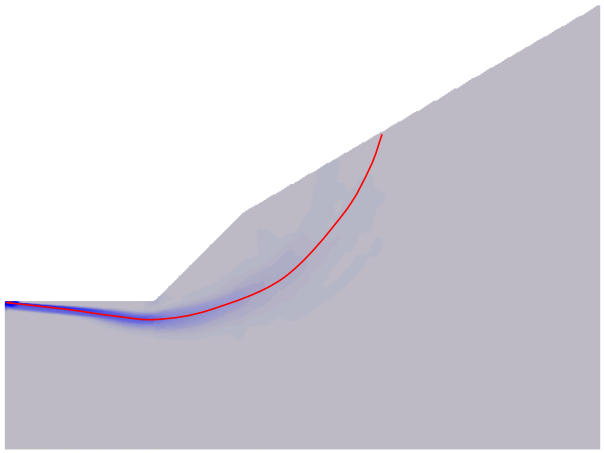

(b) Critical failure surface from SRM2 and 20m domain (FOS=1.33)

Figure 3.9 Critical solutions from LEM and SRM when the bottom soil layer is weak

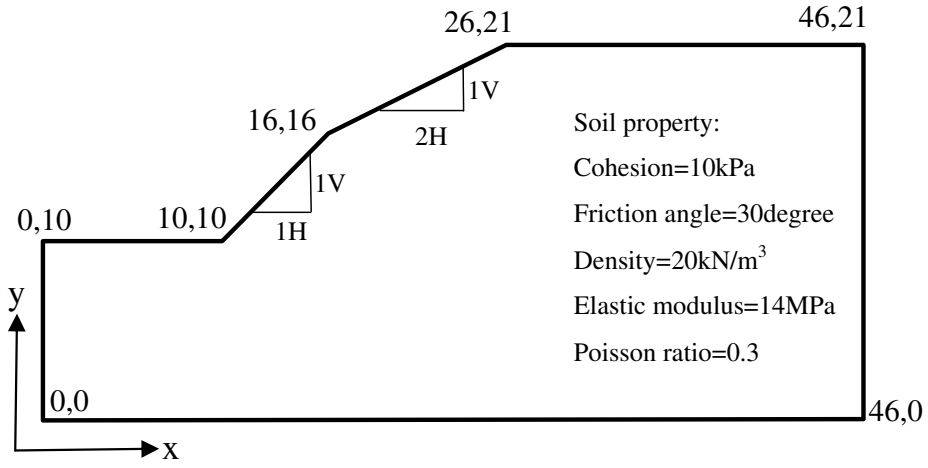

Figure 3.10 Slope geometry and soil property under study

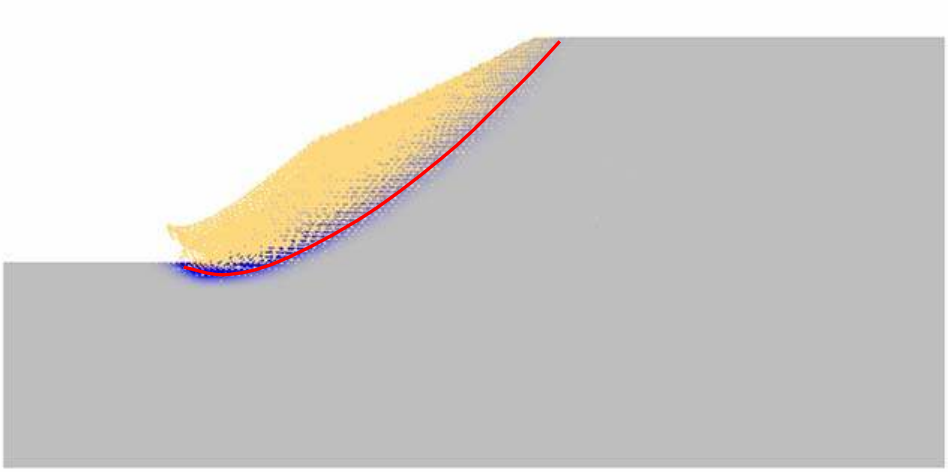

Figure 3.11 Result derived by SRM

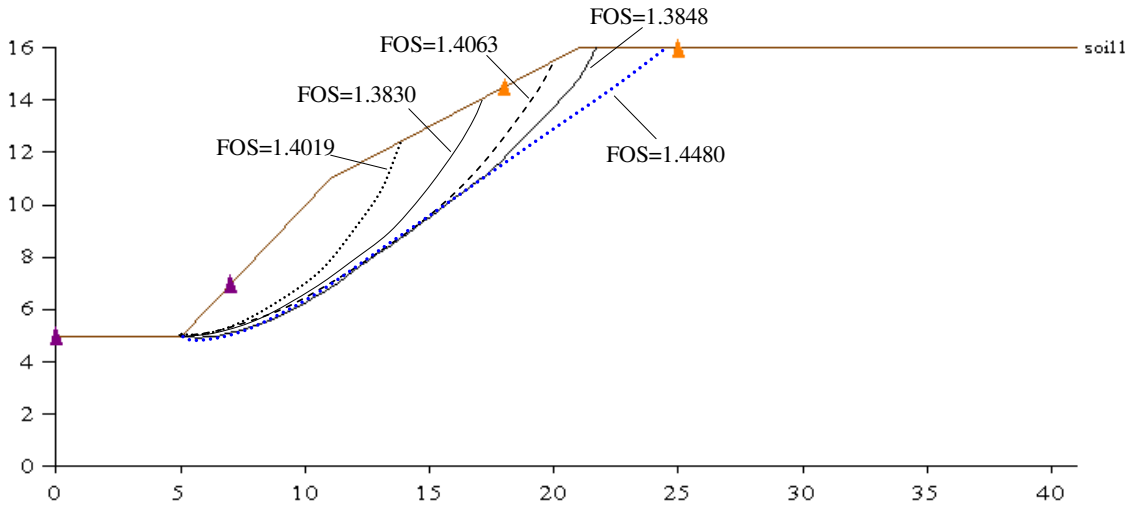

Figure 3.12 Global and local minima by LEM

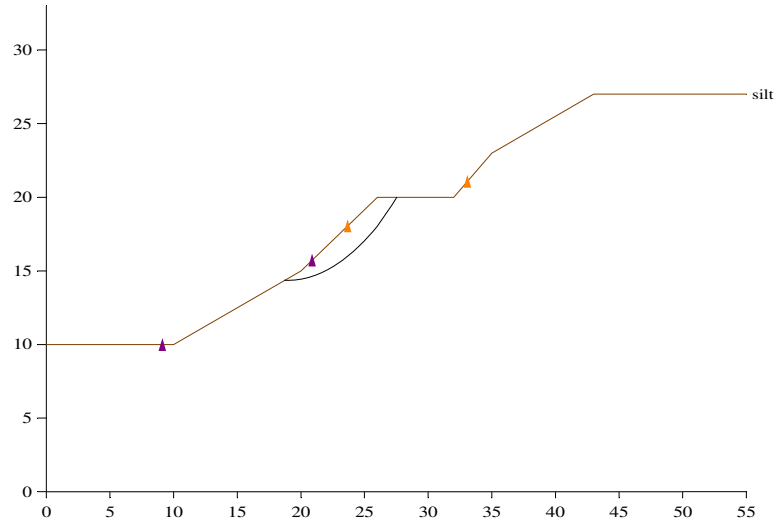

(a) FOS=1.33 (global minimum)

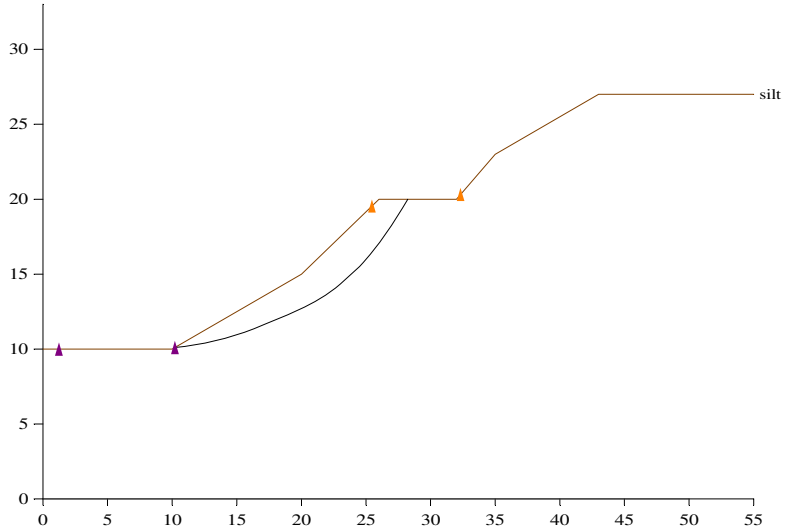

(b) FOS=1.375 (local minimum)

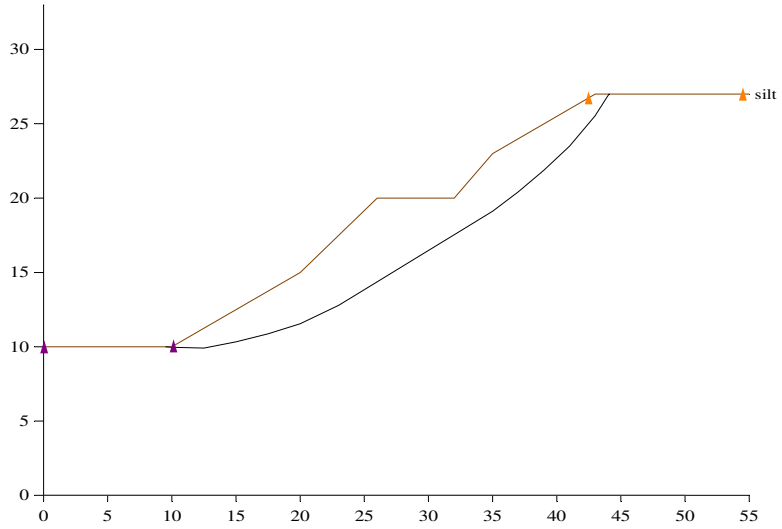

(c) FOS=1.415 (local minimum)

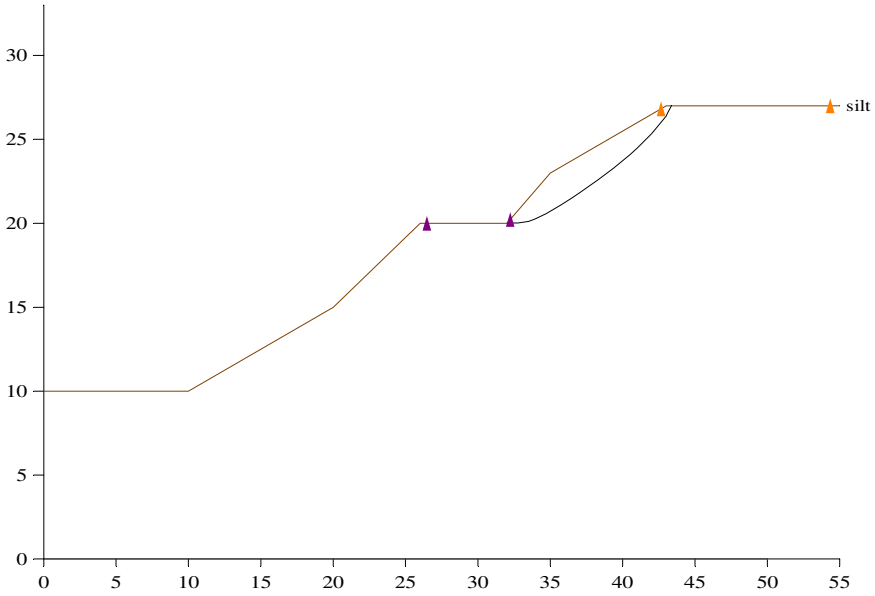

(d) FOS=1.40 (local minimum)

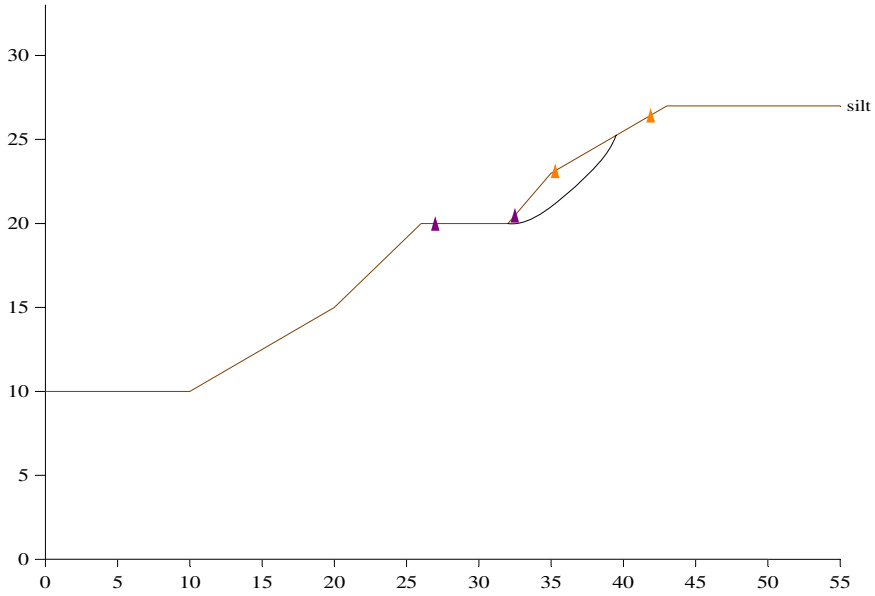

(e) FOS=1.383 (local minimum)

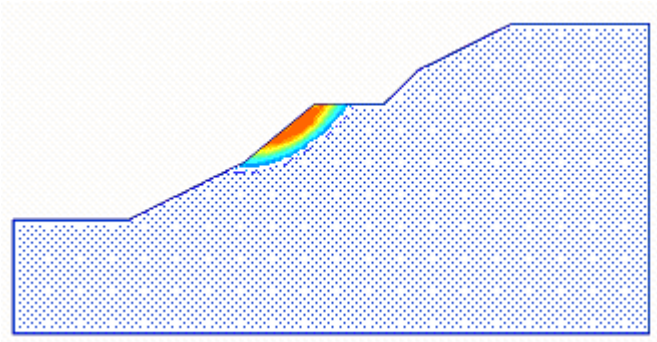

(f) FOS=1.327 from SRM

Figure 3.13 Local minima from LEM and critical solution from SRM for a simple slope

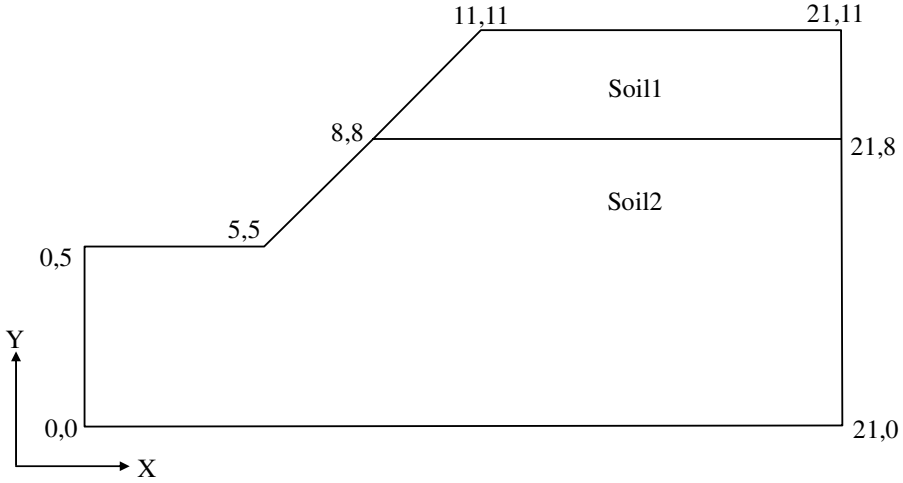

Figure 3.14 Slope geometry with two soils and a horizontal boundary

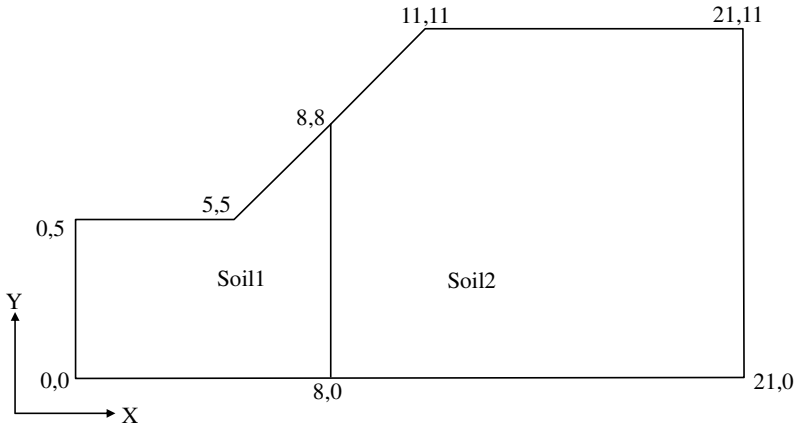

Figure 3.15 Slope geometry with two soils and a vertical boundary

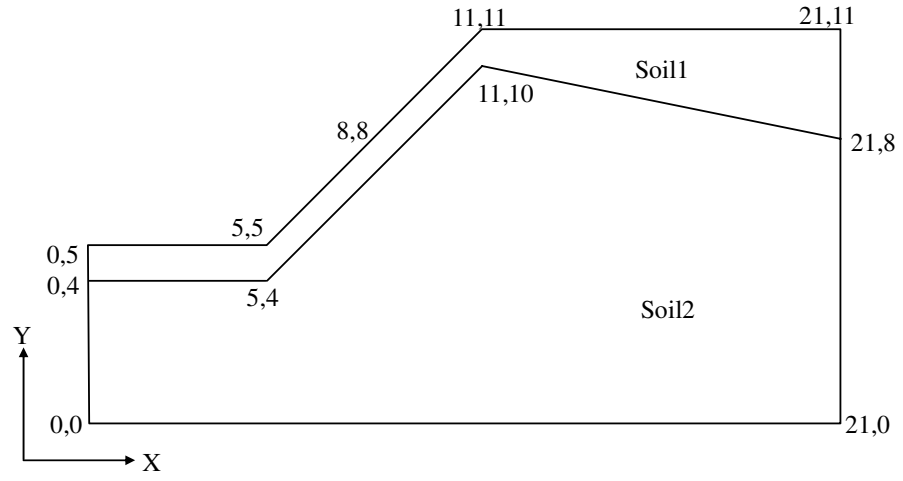

Figure 3.16 Slope geometry with two soils and an inclined boundary

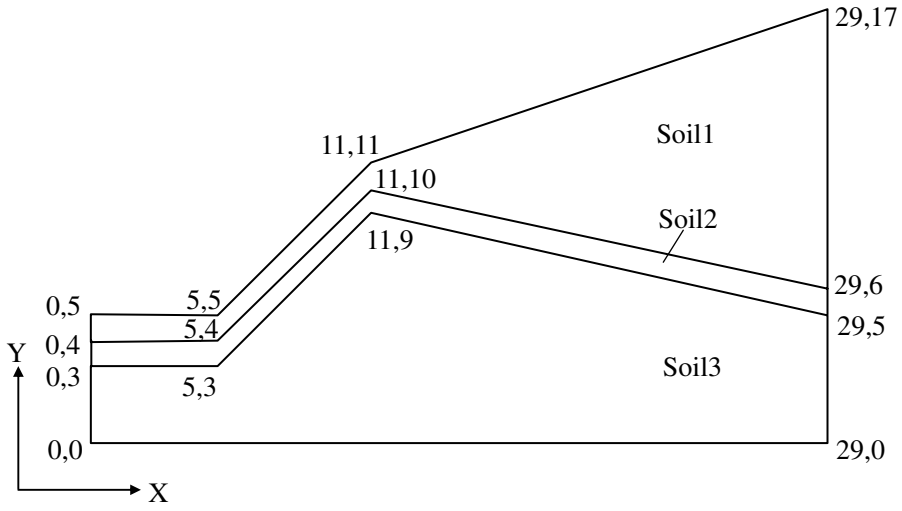

Figure 3.17 Slope geometry with three soils and an inclined boundary

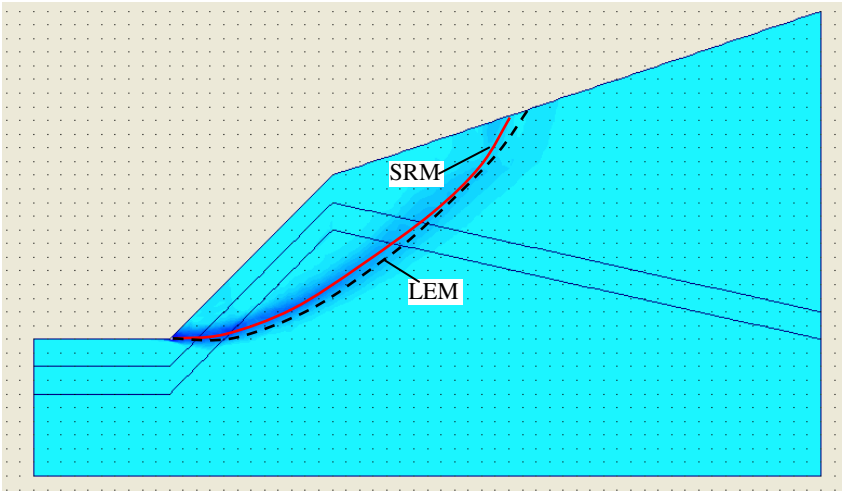

Figure 3.18 Critical slip surface of case 2 in Figure 3.17 based on SRM and LEM

CHAPTER 4: THREE-DIMENSIONAL SLOPE FAILURE ANALYSIS BY THE STRENGTH REDUCTION AND LIMIT EQUILIBRIUM METHODS

4.1 Introduction

So far, there have only been limited investigations of 3D SRM and 3D LEM methods, and there is also a lack of comparison between these two methods. In this chapter, an extensive study on 3D slope failure based on these two methods is conducted for several typical non-reinforced slopes with obvious 3D effects, and some interesting and useful findings not present in the corresponding two-dimensional analysis are obtained. The suitability of these two methods under different conditions is investigated and precautions to apply these methods are suggested. The 3D LEM formulation adopted in the present study is based on that by Cheng et al. (2005) and Cheng and Yip (2007), while the associated flow rule is used for all the SRM studies in this chapter.

4.2 Stability analysis for a vertical cut

Consider the vertical cut slope shown in Figure 4.1. The height of the slope is 5 m while the cohesive strength (c'), friction angle (ϕ') and unit weight of the soil are 24.5 kPa, 20° and 17.64 kN/m^3 respectively. The FOS determined by the 3D SRM using FLAC3D is 1.51 while the critical failure surface is shown in Figure 4.1. It appears that the slip surface is composed of two parts. The first failure mode is a 2D failure along the x-direction while the other failure mode is a 2D failure along the y-direction. The two parts are perpendicular and intersect with each other. To obtain more insight into the failure mode, another model which is unconstrained on only one vertical plane is

developed and the FOS determined by the SRM is 1.55 (Figure 4.2). It can be seen that the FOS for a vertical cut that is unconstrained on two vertical planes is only slightly smaller than that for the vertical cut that is unconstrained on only one vertical plane. The FOS is practically the same in these two cases, which means that the three-dimensional effect is small in this example.

The sliding angle in Figure 4.1 determined by the SRM is equal to 0° or 90°. It is suspected that the sliding direction should be at a direction of 45° in the x-y plane for this vertical cut, so wedge failures as shown in Figures 4.3 and 4.4 are considered in the analysis. Two different sliding directions are proposed for the vertical cut that is unconstrained on two vertical planes. Firstly, a wedge block that fails along a direction of 45° in the x-y plane is considered (Figure 4.3). Secondly, the wedge is supposed to fail along zero degree direction (Figure 4.4). In Figure 4.3, the weight of the three-dimensional sliding wedge block ABCD can be expressed as

$$\mathrm{W} = \frac{\gamma h^3 \cot^2 \theta}{3} \tag{4.1}$$

where γ is the density of the soil, h is the height of the vertical cut, θ is the dip angle of the sliding plane, and W is the weight of the wedge block. The FOS can be expressed as

$$\mathrm{FOS} = \frac{W \cos\theta \tan\phi' + c' h^2 \cot\theta \sqrt{\cot^2\theta + 1}}{W \sin\theta} \tag{4.2}$$

Introducing eq. (4.1) into (4.2) gives the FOS equal to:

$$\mathrm{FOS} = \frac{\gamma h \tan\phi' \cos 2\theta + \gamma h \tan\phi' + 6c'}{\gamma h \sin 2\theta} \tag{4.3}$$

The minimum value of FOS can be obtained by differentiating eq.(4.3), which gives:

$$\gamma h \tan\phi' + \gamma h \tan\phi' \cos 2\theta + 6c' \cos 2\theta = 0 \tag{4.4}$$

From eq.(4.4), we can get

$$\cos 2\theta = -\frac{\gamma h \tan \phi'}{\gamma h \tan \phi' + 6c'} \tag{4.5}$$

Put γ=17.64 kN/m^3, h=5m, ϕ'=20° and c'=24.5 kPa into eqs. (4.5) and (4.3), gives θ= 50.16° while the minimum FOS is 2.0 which is much greater than 1.51 or 1.55 for the 3D SRM.

In Figure 4.4, the sliding angle is supposed to be zero, so it can be simplified to a two-dimensional sliding wedge block. The weight of the two-dimensional sliding wedge block OEF can be expressed as

$$\mathrm{W} = \frac{\gamma h^2 \cot \theta}{2} \tag{4.6}$$

Then the FOS can be expressed as

$$\mathrm{FOS} = \frac{W \cos\theta \tan\phi' + c'h/\sin\theta}{W \sin\theta} \tag{4.7}$$

Introducing eq.(4.6) into (4.7),

$$\mathrm{FOS} = \frac{\gamma h \tan\phi' \cos 2\theta + \gamma h \tan\phi' + 4c'}{\gamma h \sin 2\theta} \tag{4.8}$$

Differentiating eq.(4.8) and setting it equal to zero gives

$$\gamma \mathrm{h} \tan\phi' + \gamma h \tan\phi' \cos 2\theta + 4c' \cos 2\theta = 0 \tag{4.9}$$

From eq. (4.9), we can get

$$\cos 2\theta = -\frac{\gamma h \tan\phi'}{\gamma h \tan\phi' + 4c'} \tag{4.10}$$

Put γ=17.64 kN/m^3, h=5m, ϕ'=20° and c'=24.5kPa into eqs. (4.10) and (4.8), a minimum FOS 1.43 is obtained at θ=52.14°, which is very close to the value of 1.5 determined by the 3D SRM. While the real failure mechanism may not be a wedge failure mechanism, the FOS obtained from the wedge failure mechanism which neglects the inter-column shear forces will provide an estimate of the factor of safety.

From the above analysis, it can be seen that it is actually more difficult for the vertical cut to slide along a 45 degree direction, and this can also be seen from the relationship between the FOS and dip angle of the sliding plane shown in Figure 4.5. Hence, the critical failure surface obtained by the 3D SRM, which is composed of two parts along the x and y directions, should be the reasonable failure mode. As a further check, the vertically cut slope is also analyzed by the 3D LEM method in the program Slope3D by Cheng et al. (2005) and Cheng and Yip (2007), and a FOS 1.47 with a 14° sliding direction is obtained from the optimization analysis by the 3D Janbu method, giving results that are also close to those obtained by the SRM. Though the sliding angle from the LEM is not zero as it is in the SRM, this result is closer to zero than 45°.

Although the FOS for the vertical cut that is unconstrained on two adjoining vertical planes is nearly the same as the one for the vertical cut that is unconstrained on only one vertical plane, there are significant differences when there is local loading on the top of the slope and this issue will be examined in detail in the later section about the effect of curvature on slope stability.

From Figure 4.1, it can also be seen that the shear strain at the top of the vertical cut is larger at the location where the two slip surfaces from the x and y directions intersect. At the slope toe, the shear strain is also larger near the intersection of the two unconstrained planes, and becomes smaller at increasing distances away from the intersection. To consider the boundary effect, a very large model is developed (Figure 4.6). The FOS for this model is 1.56, which is nearly the same as that for the small model (1.51), and the small difference is due to the element size effect. The slip surface is still composed of two parts, but in contrast to the small model, the slip surface does not extend to the solution boundary in the large model. This shows that even though the

FOS for the vertical cut with two unconstrained planes is nearly the same as that with one unconstrained plane, it is still slightly weaker near to the intersection of the two slip surfaces.

In the previous SRM analysis, the finite difference method in the Flac3D software is used. In addition, the finite element program Midas is also used for the 3D SRM in the present study. In the finite element code, the non-convergence criterion occurs when convergence is not achieved after a specified number of iterations. It has been demonstrated in chapter 3 that the choice of the tolerance in the solution to the nonlinear equations and the number of iterations allowed (in the 2D SRM) can be critical in the analysis. There are no simple guidelines for choosing optimum values for general cases, though the default setting in commercial programs appears to be reasonable except for isolated cases. As shown in Table 4.1, when the convergence criterion and the maximum number of iterations vary, the FOS for the vertically cut slope varies from 0.9375 to 2.3125. Since the range of the solution is very large, it will not be easy to choose the proper convergence criterion and the maximum number of iterations in the 3D SRM analysis. It has been shown that the reliance on the computer program default setting may not be adequate for the 2D SRM, and this is also becomes a critical issue for the 3D SRM. Great care and judgment, as well as some trial and error, may be required before a reasonable result can be obtained, which is a major disadvantage in the application of the 3D SRM to routine analysis and design. It is also suggested that results from the 3D LEM are determined for comparison with the results from the 3D SRM.

For the case in Figure 4.1, the displacement criterion (Naylor, 1982; Donald and Giam, 1988; Griffiths and Lane, 1999) has also been tried in which the slope failure is

determined by a sudden change in the displacement instead of relying on the computer program default. The displacement at the corner of the slope crest is shown in Figure 4.7, when the strength reduction factor increases from 1.4 to 1.5 the displacement changes suddenly, so we can assume that the FOS is around 1.5. This result agrees well with the results from the finite difference and limit equilibrium methods. From Figure 4.8, it can be seen that when the strength reduction factor increases from 1.4 to 1.5, the shear strain also changes suddenly. Some other examples have also been tried, and it is found that this criterion appears to be a more consistent criterion than the computer program's default when the results are compared with the 3D LEM. It is, however, not easy to define a precise factor of safety to better than a few percent accuracy from the criterion of a sudden change in the displacement.

4.3 Stability analysis for a vertical cut with a weak layer

The second example, which has also been analyzed by Huang and Tsai (2000), is a vertically cut slope with a 0.5 m thick planar weak layer (Figure 4.9). The FOS obtained by the 3D SRM model as shown in Figure 4.10a is 0.58 and the slip surface is along the weak layer (Figure 4.10c). Since the slope fails along the weak layer (c'=0, ϕ'=10°) and the weak layer is inclined at a 35° angle, the FOS can be obtained by a simple computation as tan10°/tan35°=0.2518. The FOS obtained by 3D Janbu is 0.2539, which agrees well with the expected result from basic soil mechanics. The FOS obtained by the 3D SRM is 0.58, which is much larger than the reasonable value of 0.25, and the model in Figure 4.10a has been carefully checked. When the vertically cut slope is about to fail, a large shear strain will be mobilized at the slope toe. As shown in Figure 4.10c, shear strain is localized along the soft band while the bottom part is still stable. The restraint by the bottom elements on the inclined elements along the soft band will tend to make failure more difficult and hence a higher FOS will be obtained. Actually,

the requirement of continuity from the finite difference or finite element methods is the major cause for this problem if there is major variation of shear strain across a thin soft band. This phenomenon can be further illustrated by the model shown in Figure 4.11. If the element size at the slope toe is very small, a FOS of 0.40 is obtained for this case. This result is better than the first model, but it is still much larger than the expected value. A third model as shown in Figure 4.12 is developed, and the weak layer is raised slightly (by 0.12 m) while the thickness is still 0.5 m. The soft band is still modeled by 4 layers of inclined elements, and only the top layer of elements is not connected to the bottom which may generate the resistance to failure. Even though this model is practically the same as the previous model, a continuous shear band can now formed easily in the top layer of the soft band elements, and a FOS 0.25 is obtained which is the expected value. The generation of a highly localized shear failure zone similar to that of a soft band needs great care in the 3D SRM mesh design. For highly complicated 3D problems, it is not easy to generate a good mesh automatically without any trial and error.

In this soft band example, the cohesion of the soft band is zero. In order to investigate the results when the friction angle of the soft band is very small, another model is developed in which cohesion is equal to 10 kPa and the friction angle is zero. The factors of safety obtained by the first model (Figure 4.10a), the second model (Figure 4.11a) and the third model (Figure 4.12a) are 0.75, 0.56 and 0.47 respectively. The FOS for this problem is given by eq. (4.8) as 0.4826. The third numerical model gives a FOS 0.47 which is very close to the LEM result of 0.4826. The first model is poor as the FOS obtained by this model is much larger than the expected value. The FOS obtained by the second model is larger than the expected value, but the situation is better than that in the previous example where the cohesion strength is 0, so it seems that when the friction is

zero for the soft band, the influence of the mesh design is slightly smaller than that in the previous case.

4.4 Stability analysis for a slope with transverse earthquake load

Cheng and Yip (2007) have proposed a new 3D asymmetrical LEM formulation. Under this new formulation, it is found that when a transverse earthquake load is present, Huang and Tsai's method (2000, 2002) has difficulty in converging because the sliding direction varies between columns. On the other hand, Cheng and Yip's method adopts a single sliding direction and does not encounter such convergence problems. Cheng and Yip (2007) have considered an earthquake coefficient of up to 0.5, but a higher earthquake coefficient which may not be realistic will also be studied in this section. The slope model under consideration is shown in Figure 4.13. The slope height is 6 m, the slope angle is 45°, the soil unit weight is 20.0 kN/m^3, the cohesion is 5 kPa and the friction angle is 35°.

The results of the transverse earthquake load analyses are shown in Tables 4.2 and 4.3. In Table 4.2, the earthquake coefficient in the y-direction (transverse) is 0.5, while the earthquake coefficient load in the x-direction varies from 0.1 to 1.0. Although the FOS obtained by the SRM are larger than those by the LEM, the differences are not great. With an increase in the earthquake load in the x-direction, the FOS becomes smaller, and this is also a very reasonable result. For the SRM analysis, the average of the sliding direction is used in Tables 4.2 and 4.3. Although with increasing earthquake load in the x-direction the sliding angle obtained by the SRM also gets smaller, the angle is smaller than that obtained by the LEM. This difference may be caused by the different mechanisms in the LEM and SRM. In LEM analysis, the sliding mass is assumed to be a rigid block and it moves in the same direction at initiation of slope

failure. In the SRM analysis, the stress-strain relation is used and the velocity and displacement for each element of the sliding mass are different.

In Table 4.3, the earthquake load in the x-direction is 30% of the soil weight, while the earthquake load in the y-direction varies from 1% to 200%. When the earthquake load in the y-direction varies from 1% to 200%, the two results obtained by the SRM and LEM agree well even though the earthquake load is very large and the FOS gets smaller with the increase in earthquake load. It is also reasonable that the FOS gets smaller slowly but the sliding direction gets larger drastically as the earthquake load increases in the y-direction.

4.5 Failure mode due to self weight for a simple infinite slope

Consider a simple slope with a height 6 m and slope angle 45°. The unit weight, friction angle and cohesion of the soil are equal to 20.0 kN/m^3, 10° and 15 kPa. For a slope with regular geometry and uniform soil properties, the failure mechanism from the 3D SRM is practically a 2D failure as shown in Figure 4.14a, which is as expected for an infinite slope. The minimum 2D and 3D factors of safety based on a spherical search for the Spencer method are 1.07 and 1.12, respectively. The distinct 3D failure mode is actually the limitation of the spherical failure surface for the present problem, and this can be illustrated by the adoption of an ellipsoidal or NURBS search (able to model an almost 2D failure). This search gives a more realistic failure mechanism, close to a 2D failure, with a minimum factor of safety very close to 1.07. It is hence important to choose a proper failure shape for locating the critical 3D failure surface in the 3D LEM.

To investigate the importance of heterogeneity, it is introduced into this simple slope with the SRM analysis by defining a Weibull distribution (1951) for the cohesive strength given by eq.(4.11):

$$\varphi(c') = \frac{m}{c_0}\left(\frac{c'}{c_0}\right)^{m-1} e^{-\left(\frac{c'}{c_0}\right)^m} \tag{4.11}$$

where c_0 is a scale parameter and is related to the average value of the soil cohesive strength. The parameter m defines the shape of the density function which controls the degree of material homogeneity, and is referred as the homogeneity index. If m is larger, it means the soil parameters are more homogenous, while if m gets smaller, it means the soil parameters are more heterogeneous. The average value of the cohesive strength is equal to $c_0\Gamma(1+1/m)$. The results for different m values are shown in Figure 4.14, where the average value of cohesion is 15 kPa for both Figures 4.14b and 4.14c. It can be seen that the introduction of strength heterogeneity into the SRM analysis cannot generate a distinct 3D failure mechanism. For this case, heterogeneity by Weibull distribution is not sufficient to generate a distinct 3D failure. If an extreme heterogeneity is introduced by 3D shape soft band, a 3D failure mode may occur easily.

4.6 Stability analysis for a locally loaded slope

To generate a distinct 3D failure due to the self weight of soil, a much greater spatial difference in the soil parameters is required for the simple slope in Figure 4.14. On the other hand, if the failure is induced by external load, a distinct 3D failure will be easily formed. Consider the slope with a rectangular area of vertical loading as shown in Figure 4.15. The loading width B is 2 m while the edge of the loading is 1 m away from the crest of the slope. The slope geometry and the soil properties are shown in Figure 4.15. Results of the analysis are shown in Table 4.4, for a loading q of 100 kPa and where the ratio of the loading length L to loading width B varies from 0 to 10. In the 3D

SRM analysis, when the loading length is 2 m, 4 m, 8 m or 12 m (or L/B=1, 2, 4 and 6), the length of model chosen is 20 m. When the loading length is 16 m or 20 m (viz. L/B=8 and 10), the model length is chosen to be 30 m and the results obtained by the 3D SRM and LEM agree well with the expected pattern of decreasing FOS with increasing loading length. The slip surfaces obtained by the SRM are shown in Figure 4.16. When L/B=1, the slip surface is basically a two-dimensional failure similar to that in Figure 4.14a. Although greater shear strain is mobilized around the loading, the loading is not large enough to mobilize the shear strain to form a 3D slip surface. That means, the effect of the self weight of soil controls the failure so that a 2D slip surface will be obtained. If L/B is increased so that the external load becomes more significant, then the failure will be controlled by the external load. When L/B=2, a nearly three-dimensional slip surface is formed by the SRM. When L/B≥4, a very clear 3D failure can be mobilized. If L is very long, a 2D failure will appear again. In conclusion, when L is very small (close to B), the small external load is shared by a much greater soil mass so that the effect of the external load is small and not effective in generating a 3D failure mode. When L is very large, the problem is clearly a 2D problem, while for the intermediate cases, the external load can generate a distinct 3D failure. If the external load is very high, then a small L can also generate a distinct 3D failure mode for a simple slope. Since the self weight is not effective in generating a true 3D failure in the SRM for a simple slope, the magnitude of the external load superimposed onto the self weight becomes critical in determining the actual failure mode.

To investigate the boundary effect, different model lengths have been tried for L/B=1 and L/B=4 and the results are shown in Table 4.5. For L/B=1, when the model length varies from 10 m to 30 m, the FOS increases from 1.62 to 1.74. For L/B=4, when the model length varies from 10 m to 20 m, the FOS increases from 1.27 to 1.41 and

remains constant with further increase in the model length. It can be seen that for L/B=4, a 20 m model length is good enough while for L/B=1, when the model length increases from 20 m to 30 m, the FOS still increases slightly. This seems to be contrary to what one would intuitively expect in numerical analysis. If the differences in the failure mechanism for these two cases are considered, the results can be explained easily.

For L/B=4, the failure mechanism is a distinct 3D surface. In Figure 4.17, it can be seen that when the model length is 14 m, the slip surface is basically 2D as the boundary is close to the external load which inhibits the development of a distinct 3D failure. When the model length increases to 20 m, the boundary effect disappears and a clear 3D slip surface is formed so that the FOS will remain constant with any further increase in the model length. That means, a finite boundary is sufficient for a true 3D analysis.

For failure controlled by the self weight instead of the external load, the situation will be different. For L/B=1, the true slip surface is 2D because the applied load is small compared with the self weight of the soil, and the FOS for the 2D failure is smaller than for a 3D failure. When there is a small applied load, either a distinct 3D failure mechanism will operate, or an approximately 2D failure with the applied load shared among the whole failure mass will be formed. The actual failure mechanism will be controlled by the mechanism with a smaller FOS, and an approximately 2D failure is still possible for a slope with a small patchy load. When the boundary effect is considered, the failure mechanism is an important factor. The failure mechanism is controlled by both the loaded length and the loading intensity. As shown in Figure 4.18, for L/B=4, when the loading is 20 kPa, the true slip surface is still a 2D failure. When the loading increases to 100 kPa, a distinct three-dimensional slip surface is formed; and

when the loading further increases to 300 kPa, the 3D slip surface is more distinct with a smaller sliding mass volume with increasing external load. The failure mechanism hence varies with the loading length and loading intensity. For a locally loaded slope, the critical failure may range from 2D to 3D, which is not known before the analysis. Based on various trials on many examples, the following procedure is proposed for the assessment of a locally loaded slope which is applicable for both the SRM and the LEM analyses.

If the slope is short in length, the entire slope should be modeled according to its true boundary conditions irrespective of its failure mechanism. If the real slope is very long, the analysis can be conducted as follows.

(1) A certain model length is chosen by experience or by intuition. SRM analysis is then conducted. If the failure mode is 3D, this will be the solution to the problem. If the failure mode is 2D, we should go to the next step for a more detailed analysis (based on the studies as shown above).

(2) Conduct SRM analysis with a longer model length. If the failure mode changes from 2D to 3D, this will be the solution of the problem. If the failure mode is still 2D, we should compare the current FOS value with the one from step 1 above. If the increase in the FOS is very small, we can take this result as the solution of the problem, otherwise, further increase the model length and repeat step 2 until a final judgment can be made.

Finally, there is one important point that must be noted. If the slope is very long and the local loading is small so that the critical failure mode is 2D, when the model length increases to infinity, the FOS will, theoretically, converge to that of a 2D slope without

external load in the SRM. This result would tend to over-estimate slope safety as the mobilized shear strain around the local loading is slightly greater than the remaining soil mass even though a distinct 3D failure mode is not formed. A similar situation will also occur in the 3D LEM as the load is shared by a large volume of soil mass, but a distinct 3D failure can usually be formed more easily by the 3D LEM as compared with the SRM. In this case, a comparison with the 3D LEM is suggested as a check to the SRM result. In addition, to decide the length of the model for analysis with 3D SRM, the boundary effect should be removed and a procedure to determine the appropriate model length is recommended in the above. From the results as shown in this chapter, 2.5L seems to be acceptable for common situations, so this model length can be chosen in the first stage of SRM simulation.

4.7 Curvature effect on the slope stability

In this section, the influence of the curvature on the slope stability is investigated. Firstly, several idealized concave and convex slope models are developed. The slope height is 10m and slope angle is 45° with properties of density=19.5kN/m^3, c'=10kPa and ϕ'=36°. In this analysis, two different groups of slope models are developed. In the first group, no external loading is applied on the slope. In the second group, there is a 4m width 100 kPa external loading applied on the crest of slope. In each group, five models are developed (two concave models with 17m and 35m radius at the slope middle height, two convex models with 17m and 35m radius at the slope middle height and one plane model with no curvature). The typical slope section is shown in Figure 4.19. The typical geometry of the convex and concave slopes is shown in Figure 4.20. Since the strength reduction analysis is time consuming in 3D analysis, if the model size is very large as shown in Figure 4.20, it will take a long time for the analysis, and this

problem is particularly serious for soil nailed slope which will be analyzed in next chapters. To take advantage of symmetry in the present problem to reduce the size of the problem, only a slice mode is adopted in the 3D analysis which is adequate for the present problem. The slice model has a thickness of 1.5m at the middle of the slope, and the typical models are shown in Figure 4.21.

The variation of the safety factors with different curvatures are shown in Tables 4.6 to 4.7. For concave slope, the effect of the curvature is obvious and the FOS increases with the decrease of radius. For convex slope, it appears that the curvature does not have any major effect on the factor of safety, as the FOS is very close to that for a plane problem.

The slip surfaces for different curvature with no loading is applied are shown in Figure 4.22. For slope with loading on the top, the slip surface is influenced by the loading location which is a typically local failure, so the slip surface is not compared for slope with local loading. The slip surfaces for different curvature are nearly the same. This means that the curvature has no major effect on the location of the slip surface under normal curvature (there are some minor effect for extreme curvature).

In the above, several idealized concave and convex slopes are investigated. In practice, the curvature of the slope is usually not idealized as shown in the previous paragraphs (Figure 4.20), and intersected slope is a popular alternative for construction. Two different intersected slope models are thus developed for this study. For the concave slope model, the intersection angle is 135° and for the convex slope the intersection angle is 145°. The slope height is 6 m and the slope angle is 45°.

Firstly, no loading is applied on the slope, and the FOS and slip surface for different curvature are shown in Figure 4.23. The FOS for convex slope is nearly the same as that for a plane slope, but the FOS for concave slope is larger and this result is similar with the previous cases that the curvature does not have any effect on the factor of safety for convex slope. For idealized curved slope shown in the previous paragraphs, the curvature has no effect on the location of slip surface, but for intersected slope, the slip surface is shallower at the intersection area for concave slope and it is deeper at the intersection area for convex slope.

Secondly, rectangular shape vertical loading is applied on the top of the slope. The loading length is 4m and the loading width B is 2m, while the edge of the loading is 1m away from the crest of the slope. The FOS and slip surface for different curvature are shown in Figure 4.24. The FOS for convex slope is also nearly the same as no curvature slope, but the FOS for the concave slope is larger.

In view of the above analysis, it appears that curvature does not has any noticeable effect on the factor of safety for convex slope, but most engineers view that convex slope is less safe. In order to get more insight into this issue, the vertical cut slope (Figure 4.1), which is actually a steeper intersected slope (slope angle is 90°) and the convexity is more obvious (the intersected angle is 90°), is analyzed again in the presence of external loadings. Firstly, 50kPa loading is applied fully along the edge of the crest and the result is shown in Figure 4.25. The FOS is still nearly the same as that for a plane slope. Secondly, 3m long and 3m wide 50kPa loading is applied on the convex corner and the result is compared with a plane slope (shown in Figure 4.26). The FOS is now much smaller for convex slope. This means that if a slope is steep, the

curvature effect will be obvious when local loading is applied on slope top for a convex slope.

4.8 Discussion and conclusion

The results from the 3D LEM and SRM agree reasonably well for normal situations where there is no special geological feature with very high or very low shear strength parameters. In general, the factors of safety obtained by the SRM are slightly higher than those from the LEM, which is a result similar to the corresponding 2D analysis in chapter 3.

There are many results in this study which appear to be unexpected, and a detailed investigation to confirm their validity has been carried out. For the vertical cut with two unconstrained vertical planes intersecting at 90°, the slip surface is found to be composed of two 2D failure modes. It is actually easier to fail along the x-direction or y-direction by a 2D failure mode rather than by a 3D failure mode along the diagonal, as in Figure 4.3. Although the FOS for the vertical cut with two unconstrained planes is nearly the same as the one for the vertical cut with only one unconstrained plane, there are great differences in the capacity to resist external loading which are shown in Figure 4.26.

Based on the present study, it is found that the non-convergence criterion in commercial SRM programs should be assessed carefully, and engineers should not rely completely on the default setting in the computer programs. In this chapter, it is also found that a sudden change of the displacement may sometimes be a better criterion than the default setting in the computer programs for some cases. However, it is difficult to determine a precise factor of safety according to the classical concept with this criterion. Without

comparisons with the LEM, it is not always easy to accept the results from the SRM, as the results from the SRM may be sensitive to the default settings of the analysis. In fact, some very poor results have been obtained from commercial programs using the default settings. In this respect, it seems that the 3D SRM is adequate for normal problems but care and judgment are required for those special cases, and more research to establish a more robust criterion for the ultimate limit state under general condition is required. It is suspected that a more fundamental change in the convergence criterion and nonlinear solution method may be required for those special cases if "human judgment" is not required for the assessment. On the other hand, 3D LEM is relatively insensitive to the tolerance and the column division which is an advantage over the SRM.

With recent development in the heuristic global optimization methods and the domain transformation by Cheng et al. (2007) and Cheng (2007), the presence of a soft band is not a problem in the LEM. From the SRM analysis of the vertically cut slope with a soft band, the shear strain in the soft band may be difficult to mobilize if the mesh of the model is not developed properly. For problems with a soft band or major differences in the soil parameters between soil layers, the numerical model and results should be checked carefully, and a comparison with the LEM is suggested.

For an infinite slope with local loading, whether the critical failure surface is 2D or 3D depends on the magnitude of the external load. It is also interesting to find that the suitable domain size for analysis is largely controlled by the failure mechanism instead of the length of the external load. As the failure mechanism may be greatly affected by the boundary effect, for a proper SRM or LEM analysis, the engineers may either adopt a large domain size at the expense of computer time, or pursue a trial and error analysis as discussed previously to determine the proper domain size.

The basic knowledge in finite element mesh design for non-linear problem will apply to the 3D SRM, and the importance of the aspect ratio is well covered by Shukha and Baker (2003). In the present study, the shapes of the elements in SRM are generally good so that the aspect ratio is not the reason for some of the poor results. For the vertical cut slope with weak layer as shown in Figure 4.9, the strange FOS is due to layout of the mesh instead of the aspect ratio, and more attention to the mesh design is required for the complicated problem using the SRM analysis.

For concave slope, the effect of the curvature is obvious and the FOS will increase with the decrease of radius. For convex slope, it appears that the curvature does not have any noticeable effect on the factor of safety for normal situations, and the FOS is nearly the same as a plane slope. When local loading is applied on the top of convex slope and if the slope is steep, the effect of curvature will be obvious and the FOS of convex slope will get smaller. For the idealized curvature slope, the slip surface for different curvature is nearly the same. For intersected slope, the slip surface is shallower at the intersection area for concave slope, and it is deeper at the intersection area for convex slope.

Table 4.1 The dependence of FOS on convergence criterion and iteration number

Convergence criterion	Iteration number	Factor of safety
stress tolerance=0.03	50	1.0375
stress tolerance=0.03	100	1.0375
stress tolerance=0.03	600	1.0875
stress tolerance=0.01	50	0.9375
displacement tolerance=0.001	1000	1.2875
displacement tolerance=0.005	1000	1.3875
displacement tolerance=0.01	1000	2.3125
displacement tolerance=0.03	1000	2.3125
displacement tolerance=0.03	50	2.3125

Table 4.2 Comparison of SRM and LEM results with various earthquake loads in the x-direction

Earthquake load		SRM		LEM	
Q_x	Q_y	FOS	Sliding direction(degree)	FOS	Sliding direction(degree)
10	50	1.0	27.6	0.90	42.5
30	50	0.8	21.3	0.69	37.9
50	50	0.64	15.8	0.54	32.4
80	50	0.47	9.4	0.37	27.1
100	50	0.38	6.0	0.28	24.4

Note: Q_x and Q_y are the earthquake loads (in % of soil weight) in the x- and y-directions respectively

Table 4.3 Comparison of SRM and LEM results with various earthquake loads in the y-direction

Earthquake load		SRM		LEM	
Q_x	Q_y	FOS	Sliding direction(degree)	FOS	Sliding direction(degree)
30	1	0.90	0.1	0.81	0.8
30	10	0.89	2.0	0.81	8.1
30	30	0.86	12.8	0.77	24.7
30	50	0.80	21.3	0.69	37.9
30	100	0.62	29.2	0.52	56
30	200	0.42	29.0	0.33	70.7

Table 4.4 Safety factors under the local loading of 100kPa

L/B	0	1	2	4	6	8	10
FOS(SRM)	1.82	1.71	1.60	1.41	1.33	1.30	1.26
FOS(LEM)	1.66	1.55	1.47	1.30	1.16	1.13	1.11

Table 4.5 Safety factors with different model lengths, obtained by the SRM

Model length(m)	10	14	20	30
L/B=1	1.62	1.68	1.71	1.74
L/B=4	1.27	1.37	1.41	1.41

Table 4.6 Variation of FOS respect to curvature (no load)

Radius of curvature (m)	17	35	∞ (plane)
Concave(SRM)	1.68	1.57	1.48
Convex(SRM)	1.49	1.48	1.48

Table 4.7 Variation of FOS respect to curvature (with 4m width load 100kPa)

Radius of curvature (m)	17	35	∞ (plane)
Concave(SRM)	1.31	1.24	1.16
Convex(SRM)	1.20	1.17	1.16

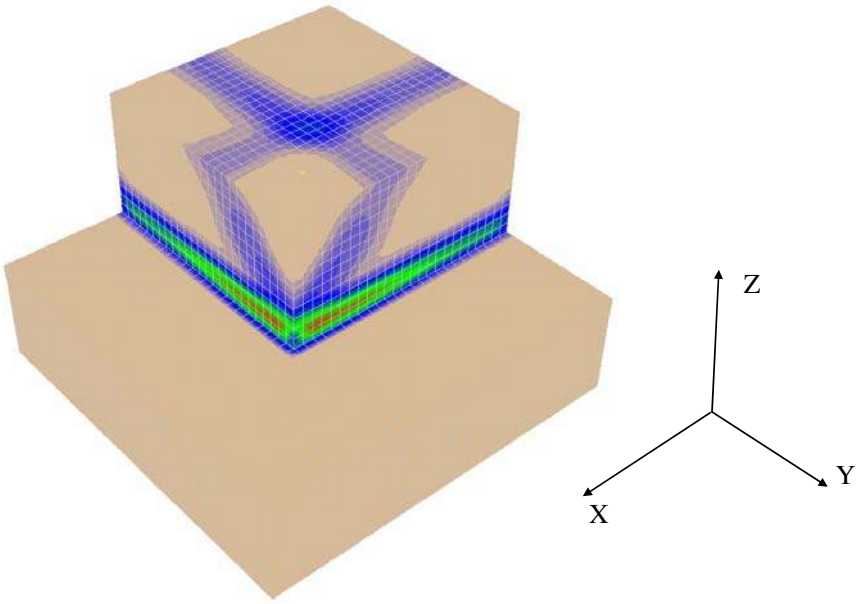

Figure 4.1 Slip surface of a vertical cut with two unconstrained vertical planes (FOS=1.51)

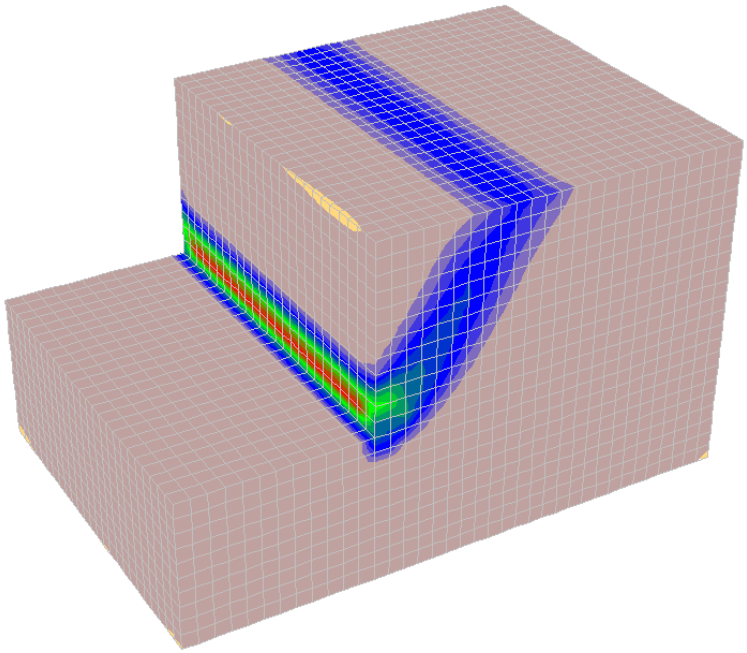

Figure 4.2 Slip surface of a vertical slope with only one unconstrained vertical plane (FOS=1.55)

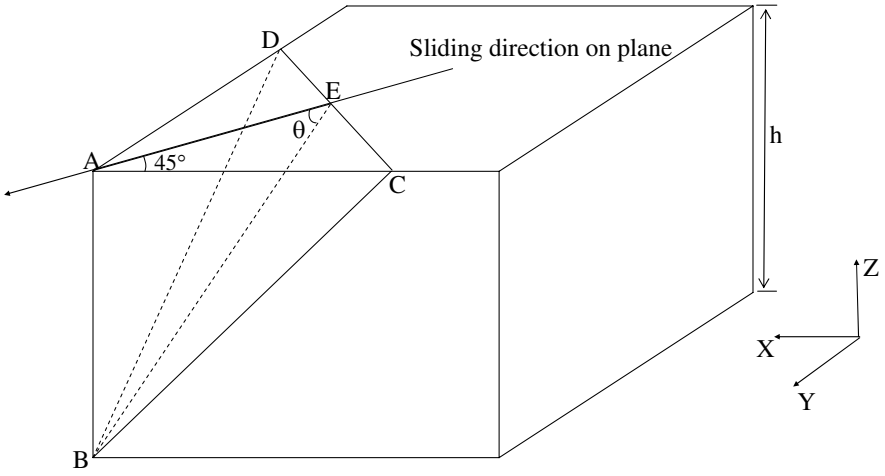

Figure 4.3 The geometry of the three-dimensional wedge block

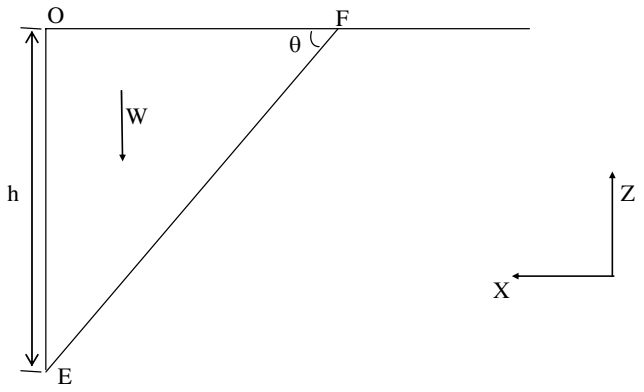

Figure 4.4 The geometry of the two-dimensional wedge block

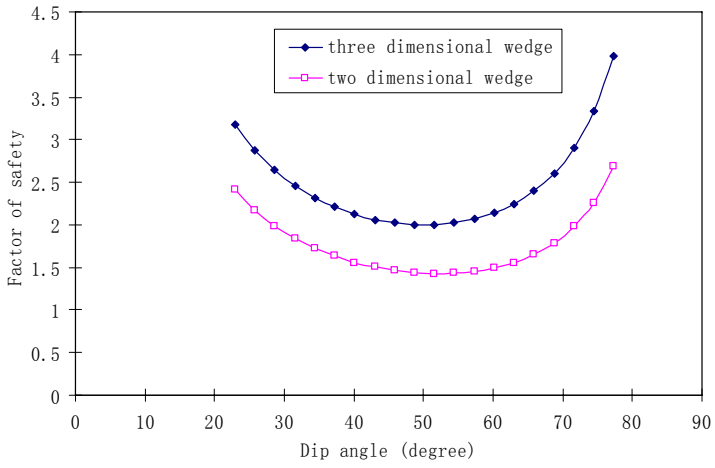

Figure 4.5 Variation of FOS with respect to the dip angle of the sliding plane

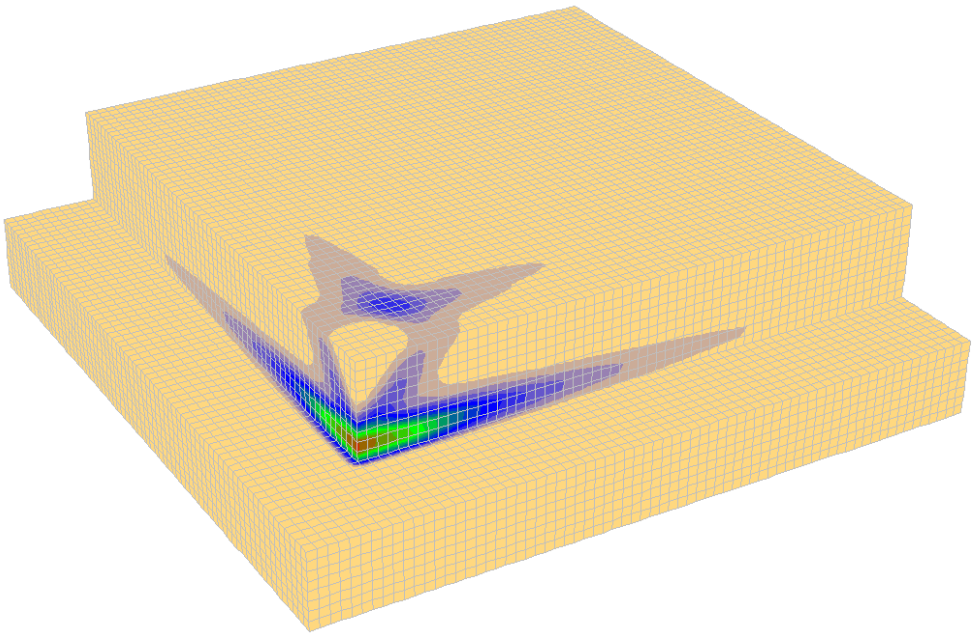

Figure 4.6 A large model for a vertical cut (FOS=1.56)

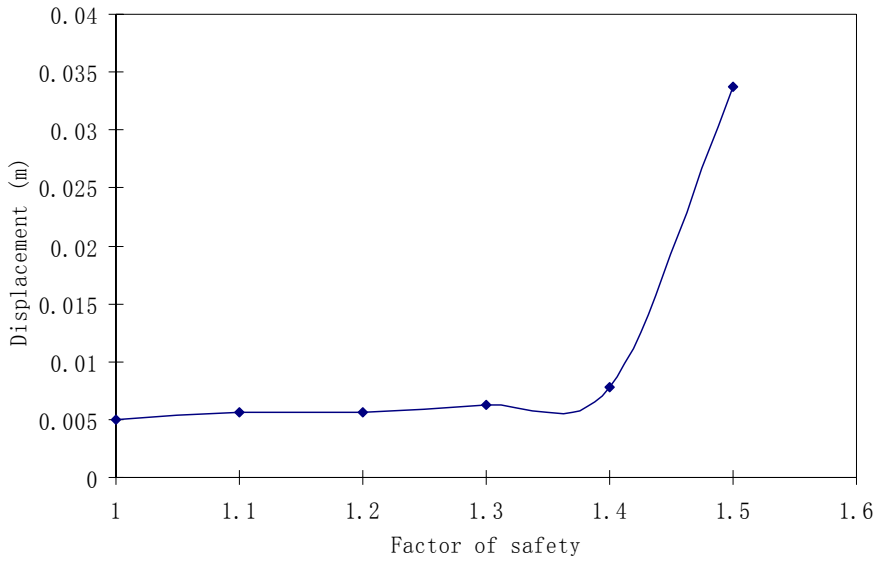

Figure 4.7 Displacement versus factor of safety

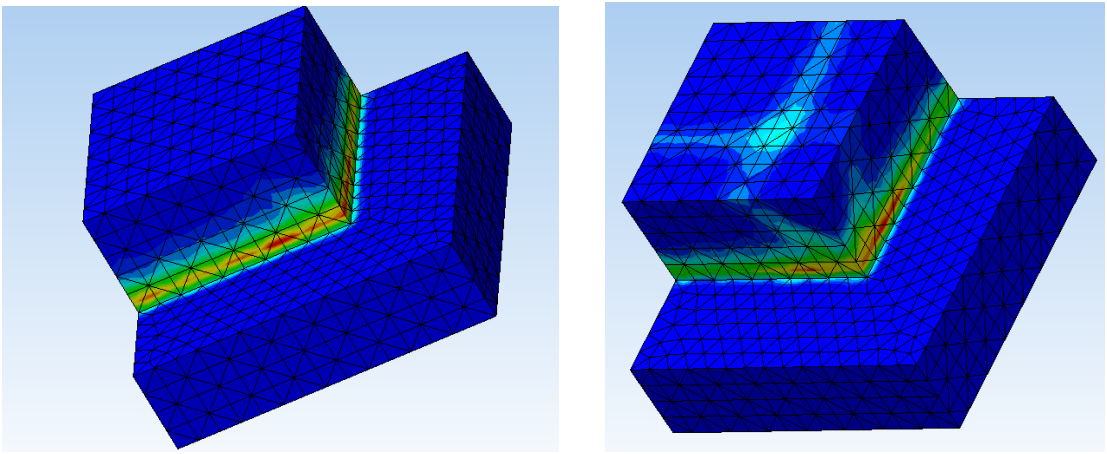

(a) FOS = 1.4 (b) FOS = 1.5

Figure 4.8 Non-linear analysis results using different strength reduction factors

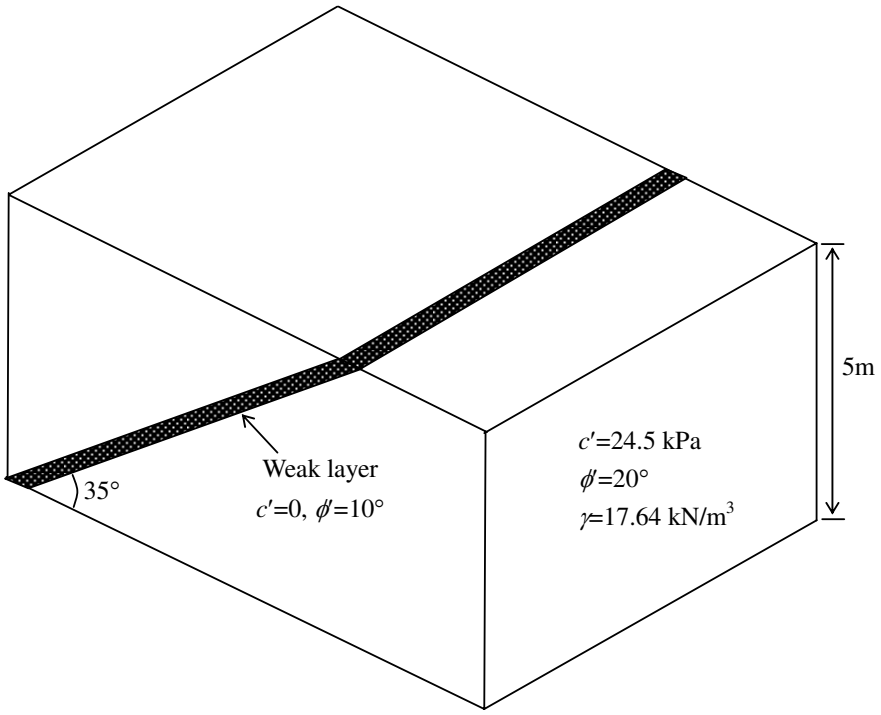

Figure 4.9 Geometry of a vertical cut with an inclined weak layer (after Huang and Tsai, 2000)

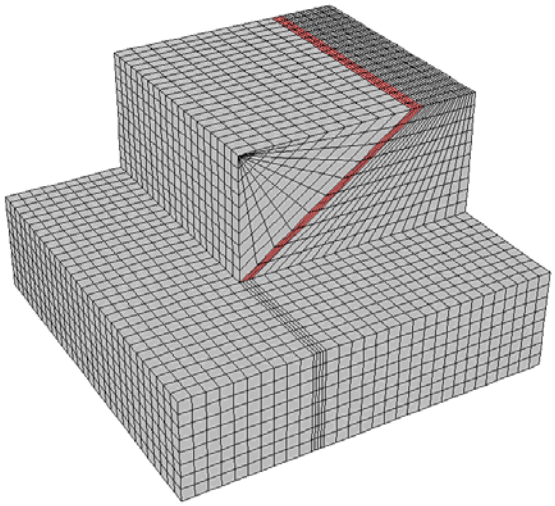

(a) mesh for the whole model

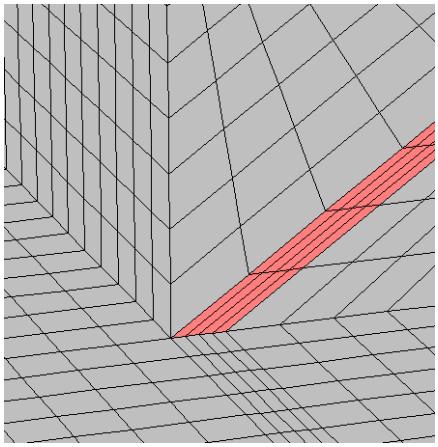

(b) enlarged view of mesh at toe

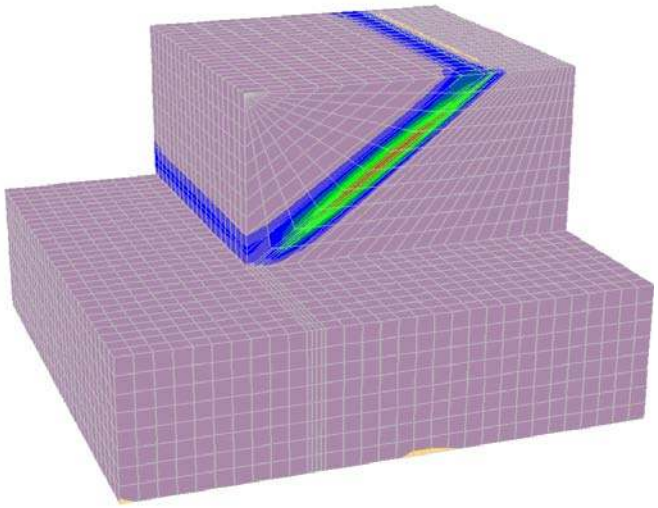

(c) slip surface (FOS=0.58)

Figure 4.10 Model one of the strength reduction analysis for a vertical cut with a weak layer

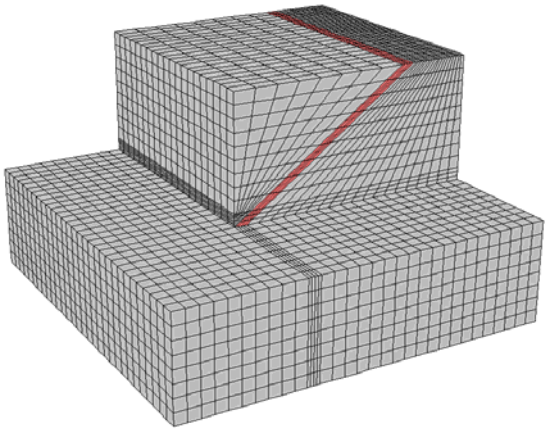

(a) mesh for the whole model

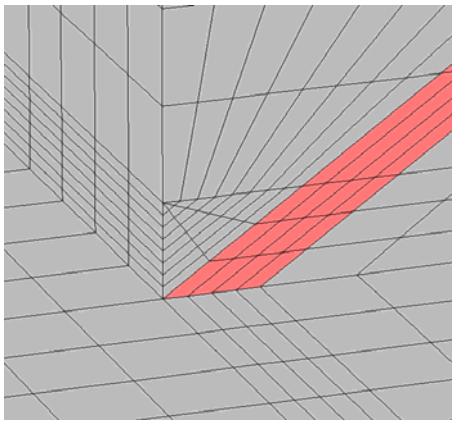

(b) enlarged view of mesh at toe

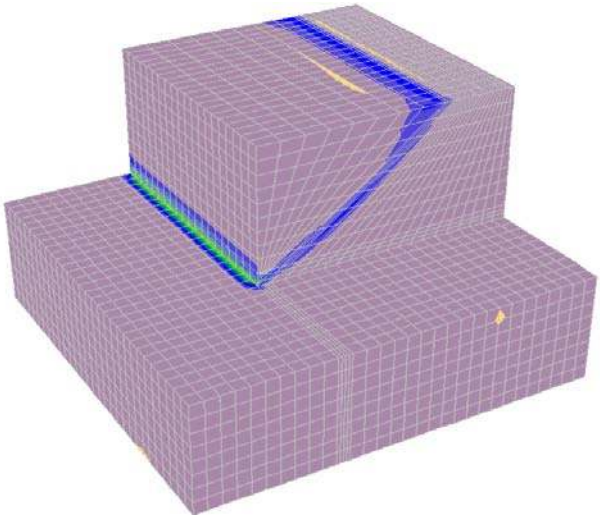

(c) slip surface (FOS=0.40)

Figure 4.11 Model two of the strength reduction analysis for a vertical cut with a weak layer

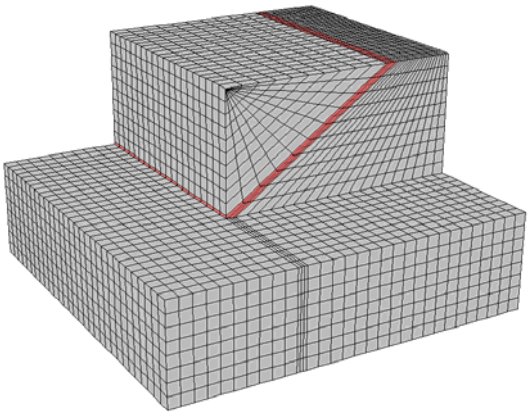

(a) mesh for the whole model

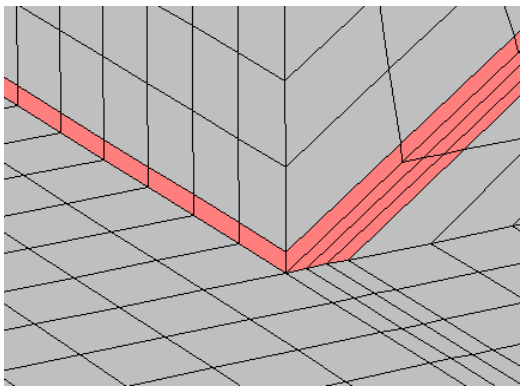

(b) enlarged view of mesh at toe

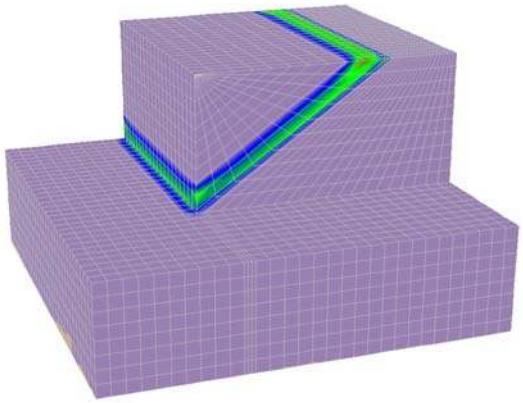

(c) slip surface (FOS=0.25)

Figure 4.12 Model three of the strength reduction analysis for a vertical cut with a weak layer

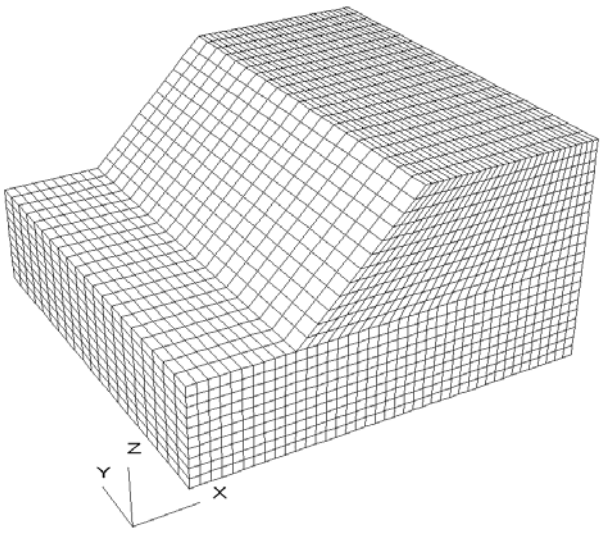

Figure 4.13 Mesh for a slope with transverse earthquake load

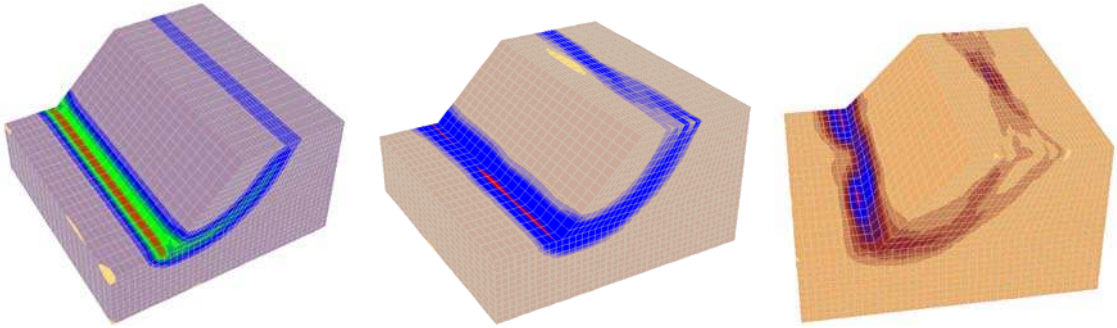

(a) homogeneous, m=∞, FOS=1.17 (b) *m*=3, FOS=1.14 (c) *m*=1, FOS=1.04

Figure 4.14 Simple slope stability analysis with varying heterogeneity

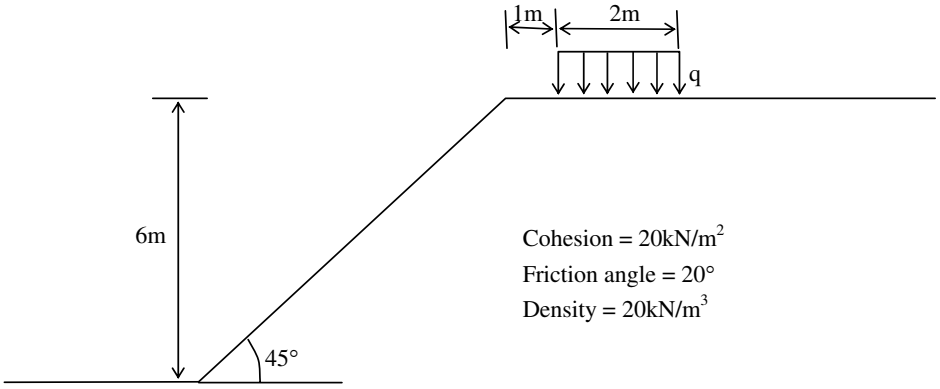

Figure 4.15 The geometry of the slope under local loading

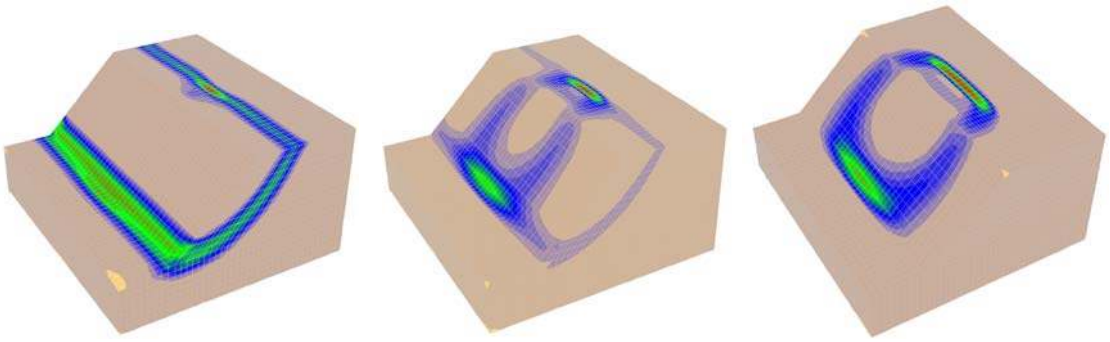

(a) L/B=1 (b) L/B=2 (c) L/B=4

Figure 4.16 The slip surfaces for different loading lengths when B=2m

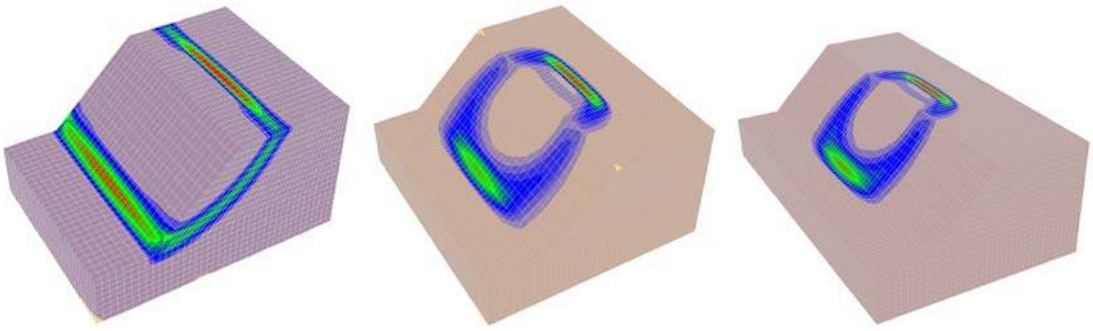

(a) 14 m, FOS=1.37 (b) 20 m, FOS=1.41 (c) 30 m, FOS=1.41

Figure 4.17 The slip surfaces for different model lengths when L/B=4

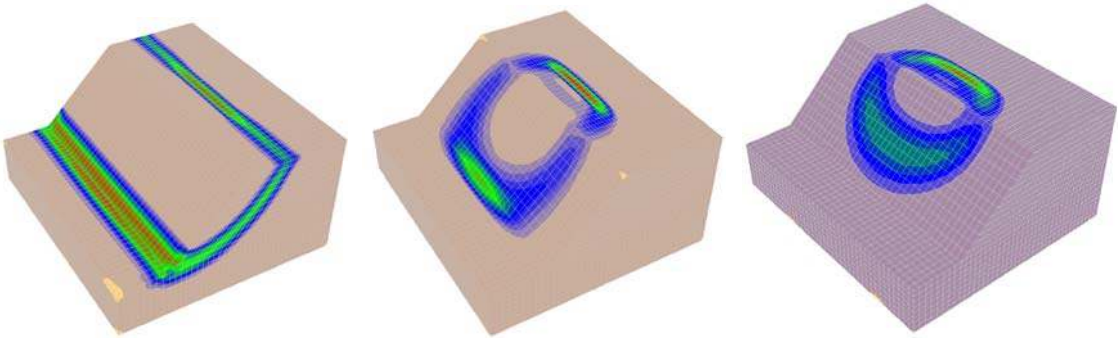

(a) 20 kPa, FOS=1.74 (b) 100 kPa, FOS=1.41 (c) 300 kPa, FOS=0.89

Figure 4.18 The slip surfaces for different local loadings when L/B=4 and model length=20m

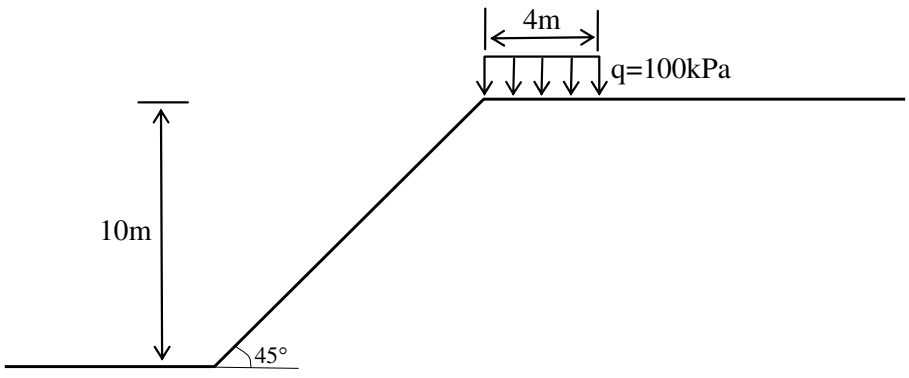

Figure 4.19 The geometry of the slope section

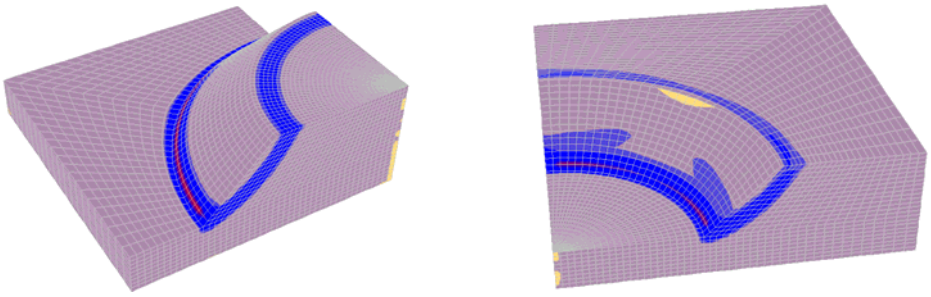

(a) convex (b) concave

Figure 4.20 Typical geometry of convex and concave slope

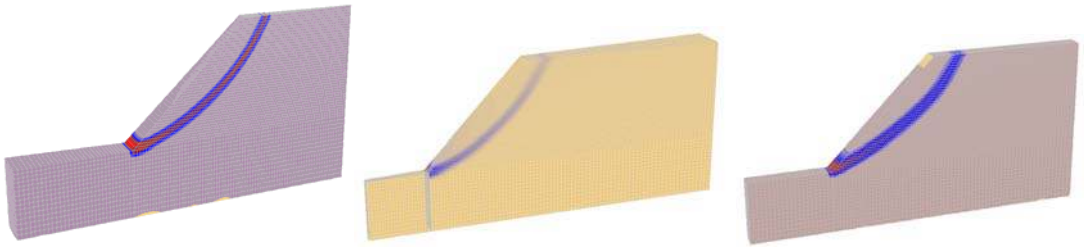

(a) convex (b) concave (c) plane

Figure 4.21 Mesh plot and slip surface of concave and convex models

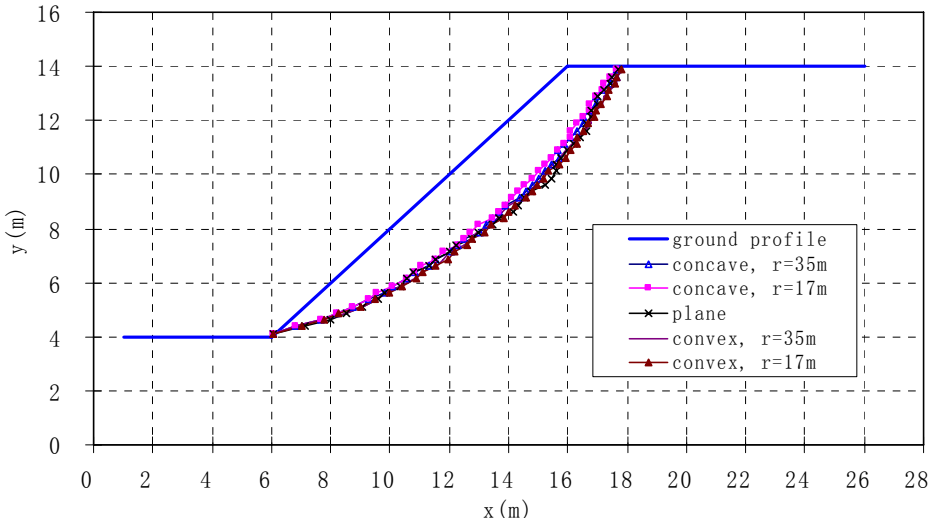

Figure 4.22 Slip surfaces at different curvatures (no load)

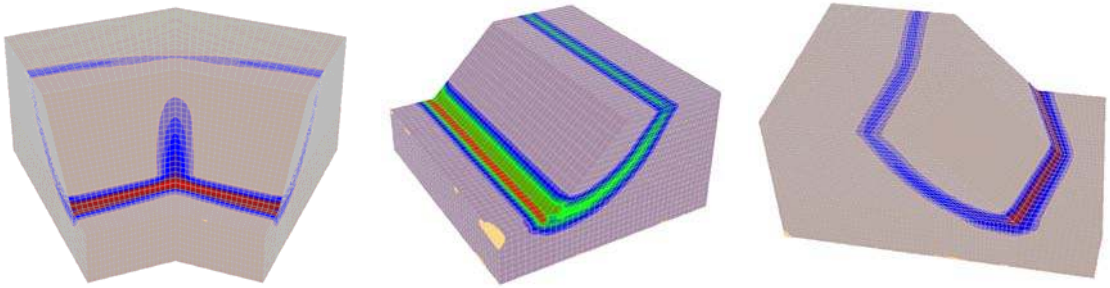

(a) 135° concave, FOS=1.91 (b) no curvature, FOS=1.82 (c) 145° convex, FOS=1.83

Figure 4.23 Slip surfaces for different curvatures (no load)

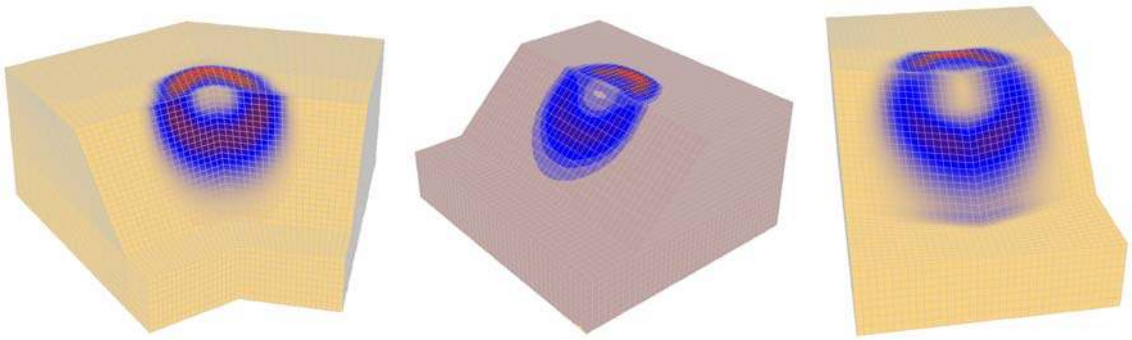

(a) 135° concave, FOS=1.36 (b) no curvature, FOS=1.22 (c) 145° convex, FOS=1.22

Figure 4.24 Slip surfaces for different curvatures with 200kPa loading

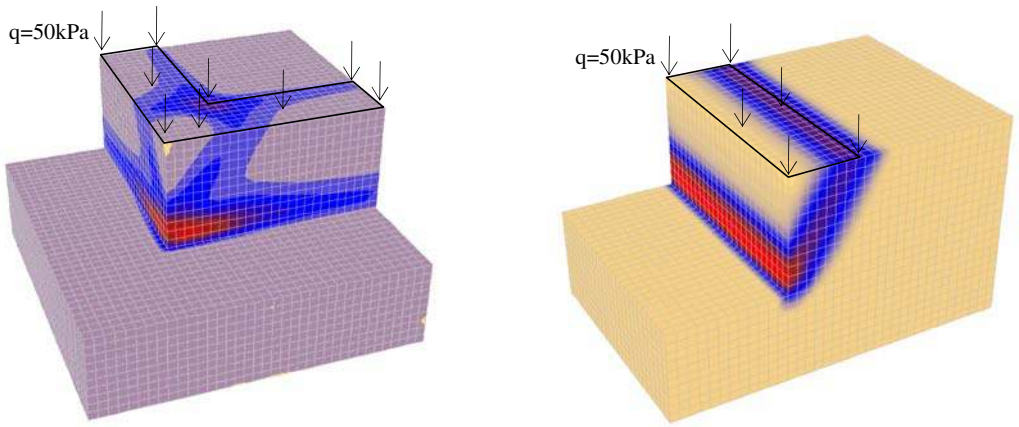

(a) convex, FOS=0.88 (b) plane, FOS=0.90

Figure 4.25 Vertical cut slope with 3m width 50kPa loading along the edge of the crest

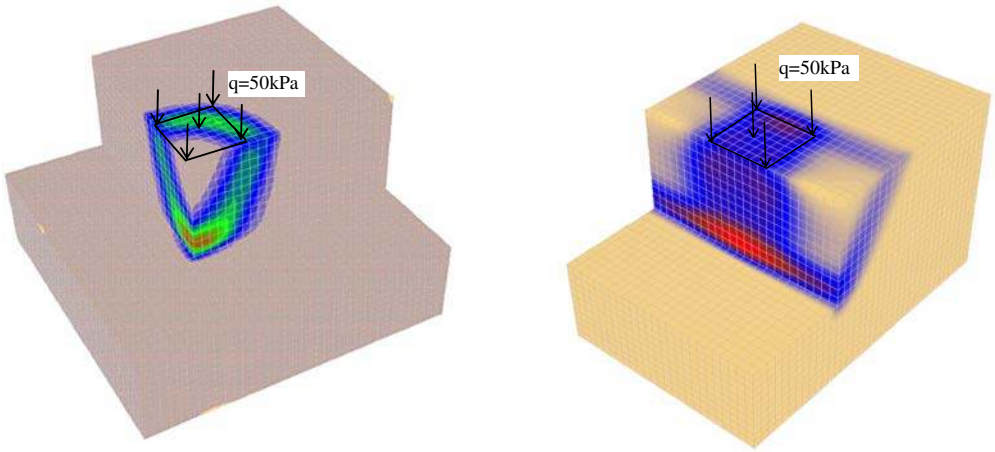

(a) convex, FOS=0.95 (b) plane, FOS=1.26

Figure 4.26 Vertical cut slope with 3m long and 3m wide 50kPa loading

CHAPTER 5: SOIL NAILED SLOPE BY STRENGTH REDUCTION AND LIMIT EQUILIBRIUM METHODS

5.1 Introduction

Soil nailing is a simple and economic slope stabilization technique, and is particularly useful for the strengthening of existing slopes. There are many different design methods for soil nailing which include the limit equilibrium methods and several working stress design methods, and the most commonly used method for soil nailing design is still limit equilibrium method. The Federal Highway Administration of US has also published series of design guidelines (Elias and Christopher, 1997; Byrne et al., 1998; Elias et al., 2001; Lazarte et al., 2003) for soil nailed and reinforced earth structures which are based on the limit equilibrium method and are currently used by many engineers.

The two-dimensional finite element or finite difference method has also been applied for the analysis of nailed slope which may be more suitable for slopes reinforced with geotextile but not soil nails. Although two-dimensional analysis is useful, the effect of soil-nail interaction is not adequately taken into account as a soil nail has a finite diameter with a spacing much larger than the nail diameter. Some researchers have also employed 3D finite element method to soil nailed slope analysis, and they focus mainly on the deformation and soil-nail interaction while the factor of safety is seldom considered. For a soil nailed slope, there is still a lack of detailed study, in particular for three-dimensional analysis. This chapter will try to conduct a detailed analysis for soil nailed slope by SRM and LEM for which there are only few previous studies, and some

interesting results are obtained which are worth further consideration and discussion for analysis and design.

One of the important factors for a proper analysis of soil nailed slope is the determination of the nail load. According to Hong Kong's practice (which is a special case of the Davis's method by Shen et al. 1981a), the ultimate bond stress of a soil nail τ_f is expressed as $\tau_f = \pi D c' + 2D\sigma_v' \tan\phi'$, where D is hole diameter, σ'_v is effective vertical stress on the nail, tanϕ' is frictional coefficient between the soil and the nail, c' is cohesion of the soil. Since the adhesion and friction between the soil and nail will be less than c' and tanϕ', a factor of safety 2.0 is given to the ultimate bond stress for design purpose. There is also another soil nail design practice in which the bond stress is assumed to be independent of the confining/overburden stress. The laboratory and field tests in Hong Kong have suggested that both design methods may be correct under different cases, and the actual nail load appears to be dependent on the soil type, time, the grouting pressure and the topography. In the following studies, the two methods of bond load determination are considered and the SRM and LEM are compared on the same basis for comparisons.

For LEM analysis, the effect of soil nail is considered by applying a point load provided by the nail on the slip surface. The effective nail load is taken as the minimum of: (a) the bond strength between grout and soil; (b) the tensile strength of the nail; (c) the bond strength between the grout and the nail. The software Slope2000 developed by Cheng is used for LEM analysis of soil nailed slope.

For the present SRM analysis, FLAC3D software is used. If the bending effects are not important, the nails can be modelled by cable elements in FLAC3D because cable

elements provide a shearing resistance (by means of the grout properties) along their length. In FLAC3D, the system is idealized as shown in Figure 5.1, and is represented numerically as a spring-slider system located at the nodal points along the cable axis. The shear behavior of the grout annulus under relative shear displacement between the cable/grout interface and the grout/rock interface as shown in Figure 5.1b is described numerically by: the grout shear stiffness, the grout cohesive strength, the grout friction angle, the grout exposed perimeter, and the effective confining stress σ_m (Figure 5.1c). In the above model, it is assumed that the surrounding rock is very hard and stiff and the grout is relatively weak. In soil-nail system, the surrounding soil is relatively weak and both the steel bar and cement grout stiffness are much higher than the soil, so in the present study the steel bar and cement grout are taken as a whole. At the same time, a thin layer of material with a thickness of 4.0mm surrounding the nail is used to simulate the shearing zone. The soil nail model used in this analysis and its corresponding meaning compared with the idealized model in FLAC3D is shown in Figure 5.2. In SRM analysis, the failure of the soil nail system is controlled by the pullout strength between the soil and nail or the tensile strength of the nail tendon, and this is similar to the LEM analysis. The confining force acting around the nail is approximately calculated by the formula $2D\sigma'_v$ per unit length in LEM analysis, while it is computed automatically in SRM analysis, and this will cause some difference, but this difference will be small for common problems. So the results obtained by LEM and SRM according to the above analyzing approaches will be comparable.

In this chapter, the effects of the nail head, some special results from SRM, the effects of failure induced by external loads and the analysis of some model tests will be discussed. These results are actually important for the proper understanding and analysis of a nailed slope.

5.2 Importance of nail head in analysis

Firstly, a 6m height soil nailed slope with 45° slope angle is analyzed. 8m length nails are installed at 1.5m centers horizontally and vertically. The diameter of the steel bar is 40mm and the grout hole diameter is 100mm. The numerical model and soil properties are shown in Figure 5.3a. The minimum factor of safety (FOS) by the Spencer's method using the simulated annealing search by Cheng (2003) is 1.2231 for pull out failure and 1.146 for face failure.

For SRM analysis, the material properties of the grouted nail are calculated considering a combination of the stiffness of the steel bar and the cement grout, and the Young's Modulus of the grouted nail is determined as 45.44GPa.

In this analysis, the elastic modulus and Poisson ratio of the soil are 15MPa and 0.42 respectively, so the shear modulus of the shear zone is 5.28MPa. The shear stiffness of the shear zone k_g can be estimated as (Itasca 2006):

$$k_g = \frac{2\pi G}{10\ln(1+2t/D)} = 43.1\text{MPa}$$

where G is shear modulus of the shear zone and equals to 5.28MPa; D is grout hole diameter and is equal to 0.1m; t is annulus thickness and is equal to 0.004m. The parameters used for the study are shown in Table 5.1.

The numerical model for the nailed slope without nail head is shown in Figure 5.3b with a FOS 1.2 by the SRM (associated flow rule) which is slightly smaller than the FOS for pull out failure by the LEM analysis but is slightly larger than that by the face failure for LEM analysis. It has been established in the previous two chapters (also the results in the following section) that the FOS from SRM is usually larger than that from the LEM.

It can be concluded that the FOS by the SRM corresponds to the face failure, and this conclusion can be further supported by the results if a nail head is modeled in the analysis. The slip surface and the tension stress of the nail are shown in Figure 5.4. The critical slip surfaces corresponding to the pull out failure and face failure from the LEM as shown in Figure 5.5 are compared with the SRM result. The slip surface by the SRM agrees well with the face failure surface from the LEM, but is greatly different from the pullout failure surface by the LEM. Another interesting phenomenon (Figure 5.5) is that the slip surface from the SRM for this case is virtually the same as the one when the slope is un-reinforced (FOS=1.11). Several other examples have been tried, and it appears that the slip surfaces by the SRM for nailed slope without nail head are usually similar to the un-reinforced slopes. This phenomenon appears to be not noticed in the past. More detailed study about this phenomenon will be considered in the later part of this chapter. If a continuous elastic surface is simulated as the nail head with 0.15 m thickness, the FOS for this model is 1.28 and the slip surface is shown in Figure 5.6, and this failure surface is comparable to the one by LEM for pullout failure as shown in Figure 5.7.

The results in Figures 5.4-5.7 demonstrate the effect of nail head on the failure mode which is seldom considered in the past, and there is little previous SRM study on this issue. For the model with no nail head, the failure mode is actually a face failure which is similar to that in Figure 2.2a. The soil nail with no nail head is restrained by the soil behind the failure surface while the soil failure mass is separated from the nail, so only the bond stress within the failure mass is effective in the stabilization. For the model with a nail head, the failure mode is a pullout failure which is similar to that in Figure 2.2b. The failure along the nail is initiated along the portion behind the failure mass, so the bond load from the “effective length” behind the failure surface is effective in the

slope stabilization. The two failure modes as found from the study of nailed slope with and without nail head can be compared to the design of geotextile for embankment stabilization, where the bond loads for the two sides of geotextiles have to be checked (usually no head/anchorage to the geotextile).

To figure out the influence of the nail head with different shape and parameters, two different types of nail head are considered. In the first model, a 0.5m width and 0.5m height nail head with 0.15m thickness is used and its elastic modulus varies from 15MPa to 30GPa. In the second model, a continuous elastic surface is simulated as the nail head, and its elastic modulus also varies from 15MPa to 30GPa. The results as shown in Table 5.2 show that there is only very small difference between the two nail head configurations. That means, there are noticeable differences for a nailed slope with and without nail head, but the influence of the size and material parameters of the nail head are not important (provided that the material parameters are normal and reasonable). For example, when the nail head with 0.14m width and 0.15m height is used (elastic modulus is 15GPa), a factor of safety of 1.25 is determined from the SRM, and the slip surface and nail force distribution are shown in Figure 5.8.

The influence of the Poisson ratio of the soil is also investigated by varying the Poisson ratio from 0.15 to 0.45 in the above model, and it is found this parameter has little effect on the factor of safety of the soil nailing slope.

5.3 Soil nailed slope stability with different soil properties

In this section, a parametric study for a homogeneous soil slope with a slope height equal to 6m and slope angle equal to 45° is conducted, and the slope geometry and soil nail distribution is the same as the example in Figure 5.1. In the parametric study,

different shear strength properties are used and both the LEM and SRM analyses are carried out. The cohesion of the soil varies from 2, 5, 10 to 20 kPa while the friction angle varies from 5, 15, 25, 35 to 45° respectively. The density, elastic modulus and Poisson ratio of the soil are kept constant at 20kN/m^3, 15MPa and 0.35 respectively in all the analyses, and the results of analyses are shown in Table 5.3. For the LEM, the Spencer's method is adopted and the tolerance in the location of the critical failure surface is 0.0001 which is good enough for the present study.

From Table 5.3, it is found that the factors of safety by the SRM and LEM are very similar under different combinations of soil parameters, and all the FOS obtained from the SRM (associated flow rule) are slightly larger than those obtained by LEM with a maximum difference of 12.4 %. This phenomenon is also similar to that as obtained in previous chapters for un-reinforced slopes. The slip surfaces for this study are shown in Figures 5.9 to 5.11. It can be seen that when the friction angle of the soil is small, the slip surfaces by the SRM and LEM are in good agreement. When the friction angle of the soil becomes very large (for example, ϕ'=45°), the slip surfaces by the SRM are deeper than those by the LEM.

It has been observed that there are several special cases where a combined failure surface may occur. For example, when c'=5kPa and ϕ'=35° (Figure 5.12), a combined slip surfaces given by Figure 5.12b will be detected by the use of a very fine mesh, and such a special slip surface will not occur when the mesh size is slightly increased (Figure 5.12a). Even though there are major differences in the two slip surfaces, the differences in the FOS are very small, and such phenomenon does not appear for the LEM. It appears that that the determination of a combined failure surface is controlled by the size of the mesh in the computation. Such combined failure surface, however,

may be not a true phenomenon as such failure surface possesses a high factor of safety when the LEM is used. It is suspected that due to the use of extremely fine mesh, stress concentration occurs around the grout/nail interfaces so that the combined failure surface will come out during the nonlinear iteration analysis. Actually, it has also been demonstrated the limitations of the nonlinear solution algorithms in evaluating the ultimate limit states of a slope in the previous chapters. In this respect, the engineers need to be very careful in assessing the results from the SRM, particularly for a nailed slope using three-dimensional analysis.

5.4 Slope with different nail inclination angle

In this section, the influence of the nail inclination is discussed. The slope geometry and the soil nail distribution is the same as the example in Figure 5.1. The nail length is 8m and the nail inclination varied from zero to 60 degree. Both the LEM and SRM are used and the results are compared in Table 5.4. Two different models are developed for the SRM. In the first model, the soil nail is simulated by cable structure element which considers only the tension effect (SRM1). In the second model, the soil nail is simulated by pile-structure element which can consider both the tension and bending effect (SRM2).

With the increase of nail inclination angle, the factor of safety firstly increases and then decreases. It means that the nail inclination angle can be optimized in practice. The maximum FOS occurs when inclined angle is between 10 to 30 degree (for LEM=10°; for SRM1= 20°; for SRM2= 30°). Although the optimized inclined angle is different for these three methods, the variation of the FOS is very small when the inclination angle varies within 10 to 30. There are two common views about the optimum nail

inclination: the nail should be horizontal; the nail should be perpendicular to the slip surface. For this example, the factor of safety is insensitive to the inclination angle (from 10° to 30°), which is basically equivalent to the inclination varies from horizontal to nearly perpendicular to the slip surface. When the inclination is very great (say 60° or more), the FOS will drop quickly then.

The slip surface, nail axial force distribution and bending moment distribution are shown in Figures 5.13 to 5.15 and Table 5.4. The maximum mobilized nail axial force increases initially and then decreases with the nail inclination, and this also explains why the FOS increases firstly and then decreases finally. It can also be seen that some bending effect is mobilized in the nail (Figure 5.15), especially when the nail inclination is large (30 to 60°), but the effect of the bending moment in the nail force is very small compared with the axial nail force (Table 5.4) so that the contribution of the bending effect to the factor of safety is also very small. This result also supports the current method of design where the bending effect of soil nail is neglected in the analysis.

5.5 Slope with different nail length

In this section, the influence of the nail length is discussed. The slope geometry and the soil nail distribution are the same as example 1 in previous section. The nail length varies from 6m to 16m. Both the LEM and SRM are used and the results are compared (shown in Table 5.5).

In general, with the increase of the nail length, the FOS will increase which is reasonable and obvious. There are also no major differences between the results from

the SRM and LEM. From Figure 5.16, it can also be seen with the increase of the nail length, the slip surface gradually gets deeper.

5.6 Slope with different soil nail layout

In this section, the influence of the soil nail layout is discussed by two different cases. The slope geometry and the soil nail distribution is also the same as example 1 in the previous section. In case 1, the soil nails are shorter at the upper part and longer at the bottom part (the nail lengths of the top row, middle row and bottom row are 4m, 8m and 12m respectively). In case 2, the design is reversed (the nail lengths of the top row, middle row and bottom row are 12m, 8m and 4m respectively). Two different nail inclination angles are also considered: zero and 20° (Figures 5.17 and 5.18). For both nail inclination angles, the FOS for case 1 is larger than that for case 2. Since the nail pull out strength is assumed to be defined by the overburden/confining pressure for the results in Figures 5.17 and 5.18, such results are not surprising. To eliminate the influence of the overburden confining pressure, two other models are developed in which the pull out strength (5.6kN/m) is assumed to be independent of the confining pressure and the results are shown in Figures 5.19 and 5.20. For these new models, the FOS by case 1 is still larger than that for case 2. Case 1 appears to be a more effective solution for enhancing the stability of slope.

Classically, case 2 is recommended for reinforced earth structure as it is better in controlling the displacement of the slope crest. For the ultimate limit state of slope stability, case 1 is however found to more effective as more nail forces can be mobilized. For the reinforcement of existing slopes, the displacement control is usually not an important issue and the failure will start to initiate at the lower part of the slope. If longer soil nail is installed at the bottom, it will be more effective in taking up the

loading so that it is better for the slope stability. On the other hand, if the slope is formed by excavation, a relatively large displacement will usually induced in the slope crest by the releasing of stresses and the failure will start from the top to bottom. If longer nail is installed at the top, it will be more effective in controlling the development of the displacement and the initiation of the failure. It can therefore be concluded that the soil nail should be installed at locations where the failure start to initiate for the maximum efficiency.

5.7 Soil nailed slope with external pressure on the top

In this section, the influence of the external pressure on SRM analysis is discussed, and there is a major difference between the SRM and LEM in dealing with external load which is seldom discussed in the past. The slope height, slope angle and the soil nail distribution is also the same as example 1. A 200 kPa pressure is applied on the top of the slope and both the SRM and LEM results for different nail length are shown in Tables 5.6 and 5.7. Two different SRM models are developed for this study. In the first model, the bond stress is assumed to be controlled by the confining pressure. The results for the first model are shown in Table 5.6 and are compared with the results by LEM. There are major differences between the results from the SRM and the LEM, and this phenomenon can be explained that such major differences arise from the increased confining pressure and hence the bond stress in the SRM analysis. On the other hand, the overburden pressure on the nail from the external load is usually not considered in the bond stress calculation (appear to be the practice for all commercial programs), so a lower bond stress is determined from the LEM. In this respect, there is a major difference in the soil nail design by the SRM and LEM under the action of the external loads if the bond load is the function of the confining stresses.

In order to eliminate the influence of the confining stresses on the bond stress, the second model is developed in which the bond stress is assumed to be independent of the confining pressure (bond stress= 5.6 kN/m), and the results of analyses are shown in Table 5.7. Since the basic assumption for the bond stress is the same for SRM and LEM, the differences between the results from the LEM and SRM are smaller than the case in Table 5.6. It can be concluded that the SRM and LEM may give greatly different results depending on the bond load determination method, and engineers should be aware of this difference.

5.8 Influence of nail elastic modulus

In the previous sections, the elastic modulus of the soil nail used for the analysis is 45.44 GPa, which is determined by the combination of the stiffness from the steel bar and the cement grout (shown in Table 5.1). In the LEM, the nail stiffness is however not required in the analysis. To investigate the influence of the nail elastic modulus on the stability of slope, two different kinds of nail elastic moduli for two different slope angles are considered. The first nail stiffness is 45.44 GPa which corresponds to the grouted steel bar nail. The second nail stiffness is 4.544 GPa which approximately corresponds to the glass fibre reinforced plastic nail which is much more flexible in nature. Two cases are considered here, and the slope angles under consideration are 45° (same as example 1) and vertical as shown in Figure 5.21. It can be seen from Table 5.8 that the FOS for the two different nail elastic moduli are nearly the same for the first case. On the other hand, there are noticeable effects from the soil nail stiffness which are shown in Table 5.9 when the slope is very steep. It means that a softer soil nail is better for the slope stability, provided that the nail pull out strength or the nail tensile strength is not reduced. This phenomenon can be explained from the fact that more soil movement and hence stress-redistribution is mobilized for softer nail so that the

mobilization of the bond stress will be greater. This phenomenon can also be compared with the extensible and inextensible design for reinforced earth design (Elias et al., 2001). It should also be noted that a 100 kPa loading is applied at the toe of the slope to prevent the local failure, otherwise, a slip surface passing through the soil nails will not appear as the analysis will be controlled by the toe slope failure. The use of a strong material or the removal of the lower solution domain in Figure 5.21 will have similar function as the application of a 100 kPa distribution load, and the prevention of the toe failure will only have small influence on the results of analyses.

5.9 Analysis of a vertical soil nailed wall in Seattle, Washington

Thompson and Miller (1990) described the design, construction and performance of one of Seattle's first soil nailed walls. For this vertical soil nailed wall, nails were mostly installed at 1.8m spacing horizontally and vertically. The nail length is 10.7m, except for the length of the top row which is 9.8m. The diameter of the drilled holes is 203mm. Nail bars varied from 25mm to 32mm in diameter are installed at an inclination of 15 degree, though the first row on the high wall was installed at 20 degree to avoid utilities. A typical section of the high wall is shown in Figure 5.22. In this section, the stability of this soil nailed vertical cut will be analyzed by the SRM.

The FOS by the SRM is 1.76 while the FOS by the LEM is 1.90 (Figure 5.23). From Figure 5.22, it can be found that the failure is located at the toe of the slope, which means that this is actually a bearing capacity failure, so this factor of safety is not the real FOS of the nailed wall as toe of the slope is strengthened in practice to avoid bearing capacity failure. In order to find the FOS of the nailed wall, two additional models are developed. In the first model, the soil shear strength is increased to a very large value at the toe of the slope to avoid the local bearing capacity failure with a FOS

equals 2.10 from the SRM (Figure 5.24). In the second model, a 200 kPa pressure is applied at the toe of the slope and the FOS is 2.29 from the SRM (Figure 5.25). In these two additional models, two failure modes are detected which are much clearer in the second model (Figure 5.25). In the first failure mode, the upper part of the slip surface is nearly vertical which is basically the inextensible strip failure mode as stated in FHWA (Elias et al., 2001). In the second failure mode, the slip surface is nearly the same as the one by the LEM and is approaching that for the extensible strip failure mode. Since the inextensible strip failure mode is not obtained from the LEM analysis, the SRM have some advantage over the LEM for this case.

5.10 Distribution of the nail tension force and critical slip surface

The line of maximum tension within the nail is often considered as the failure surface which divides the soil mass into two regions: (1) active zone, which is near to the ground surface and in this region the shear stress mobilized on the nail surface is toward outside and tend to pull the nail out of the soil; (2) resistant zone, which is behind the slip surface and in this region the shear stress generated on the nail is toward inside and tend to prevent the nail from being pulled out. This concept is shown in Figure 5.26 (after Byrne et al., 1998) and many reinforced earth structures are designed in this way. It should be realized that the maximum tensile force location is not necessarily the traditional critical failure surface at the limit state, but is the consequence of the interaction between soil and nail (Byrne et al., 1998). Classically, many researchers assume that the maximum tensile force line coincides with the potential sliding surface, and such view is supported by some model tests (Juran et al., 1984) and full-scale tests (Clouterre, 1993). In this section, this issue will be discussed by conducting strength reduction analysis of several soil nailed slopes.

Firstly, the influence of the failure modes is investigated. The soil nailed slope failure can be broadly classified into external failure modes and internal failure modes. For external failure modes, the slip surface does not intersect with the nails, so the maximum tensile force line will not coincide with the potential sliding surface. Three different external failure modes are shown in Figure 5.27. In Figure 5.27a, if the soil nail is very short, it will be a global failure where the nails are totally within the failure mass. In Figure 5.27b, the soil nail is long and the soil mass/nail becomes an integral body and fails by a sliding mode. In Figure 5.27c which is one of Seattle's first soil nailed walls discussed in the previous section, the reinforced soil nailed wall is more stable than the toe of the slope so that it is a local bearing capacity failure. For internal failure modes, they are usually classified into three different types – face failure, pullout failure and nail tensile failure which are shown in Figure 2.2 (after Byrne et al., 1998). These three different internal failure modes are modeled for the slope as shown in Figure 5.1, and the results are shown in Figure 5.28. In Figure 5.28a which is a face failure, no nail head is used and the soil nail is restrained by the soil mass behind the failure surface so that only the friction within the failure mass is effective in the stabilization. In this case, the line of the maximum tension force is located behind the slip surface. In Figure 5.28b, the line of the maximum tension force is near to the nail head and is in front of the slip surface. In Figure 5.28c where the tensile strength of the nail is only 10kN, the nail will reaches its tensile strength at ultimate limit state and the line of the maximum tension force will virtually coincides with the slip surface.

Secondly, the influence of the state of the slope (service state and limit state) is investigated. Slip surface should be referred to the condition of the failure mass at the limit state. For the maximum tension force line, it can be referenced at the service state or the limit state which should be stated clearly. To consider this, a model with 12 m

length soil nail with nail head is developed to compare these two states and the slope geometry and the soil nail distribution is the same as example 1. The results of analysis are shown in Figure 5.29. In Figure 5.29a (service state), the slip surface at the limit state is shown by the dash line for comparison. It can be seen that the line of the maximum tension force at service state is behind the slip surface. The force at the nail head connection at service state is very small. In the limit state (Figure 5.29b), the line of the maximum tension force is in front of the slip surface, and a relatively large force at the nail head connection is mobilized at the limit state. With the reduction of the soil shear strength, the soil nailed slope gradually transforms from service state to limit state, and during this process the nail force is gradually mobilized while the line of maximum nail force will gradually move towards the nail head. In this example which is an internal pullout failure, the slip surface appears to be located between the lines of maximum nail force at the service state and the limit state. Another example is shown in Figure 5.30 which is the Seattle's first soil nailed walls discussed in the previous section. For this example, during the transition from the service state to the limit state, the nail force is gradually mobilized and the line of the maximum nail force also gradually moved towards the nail head. Compared with Figures 5.24 and 5.25, it is clear that the line corresponding to the maximum tension is far away from the slip surface, but is very similar to the inextensible strip design method by FHWA (Elias et al., 2001).

In the above analysis, the limit state is achieved by reducing the shear strength which is easy to be conducted in numerical simulation but not for model tests or full-scale tests. The limit state can also be achieved by applying pressure on top of a slope, and an example is shown in Figure 5.31 where the results at the limit state are achieved by different ways. In Figure 5.31a, the limit state is achieved by reducing soil shear strength and the nail force at the bottom row is slightly more mobilized than the upper two rows. In Figure 5.31b, the limit state is achieved by applying a pressure near to the

crest of the slope with an internal failure, and the nail force at the top row is more mobilized. In Figure 5.31c, the limit state which is an external failure is achieved by applying a pressure on top of the slope near to end of the soil nails, and the nail force at the bottom row is very large while the nail forces at the upper two rows are much lower.

Some major test results in literature are summarized in Figure 5.32 and Figure 5.33. In Figure 5.32a (Gassler, 1993) and Figure 5.32b (Stocker et al., 1979), the limit state is achieved by applying a pressure on top of the slope. In Figure 5.32c (Clouterre, 1993), the limit state is achieved by gradually saturating the soil and this can be approximately viewed as equivalent to reducing the soil strength. At the limit state, the slip surface can be observed and both the slip surface and the nail tension force distribution are given in Figure 5.32. In Figures 5.32a and 5.32b, both the slip surfaces only partly intersect the soil nails. Actually, the limit state is caused by the applied load on top of the slope. The location of the slip surface is controlled mainly by the location of the loading as the slip surfaces starts from the edge of the loading (similar to those in Figure 5.31b and 5.31c). Since the location of the slip surfaces are controlled mainly by the location of the loading in Figures 5.32a and 5.32b and the slip surface only partly intersect the soil nails, the line of the maximum tension force will not coincides with the slip surface, and it can be seen that the maximum tension force at the lower rows of nails is very close to the nail head. In Figure 5.32c where the ultimate state is controlled by the shear strength reduction, it is an internal tension failure and the line of the maximum tension force coincides well with the slip surface. In this test, the structure had been designed with a sufficiently low safety factor for failure by the breakage of the nails (F=1.1). When the soil is gradually saturated, the system failed by the breakage of the nail which is similar to the SRM results in the previous section.

There are also four different soil nailed test results at service state shown in Figure 5.33. In service state, the slip surface does not exist so that only the tension force distribution is presented in these figures (in Figure 5.33b, two predicted slip surfaces are also shown). In Figure 5.33a (Shen et al., 1981c), the measured maximum tension force is near to the nail head. In Figure 5.33b, 5.33c and 5.33d, the maximum tension force at the lower part of the slope is also very close to the nail head while and the maximum tension force at the upper part is slightly further away from the nail head.

Based on the above analysis, it can be concluded that the line of the maximum tension does not correspond to the traditional critical slip surface in general, but is the representation of the soil structure interactions in the soil nailing system. Firstly, the tension stress distribution is influenced by the state of the slope and it is obviously different between the service state and the limit state. When the soil nailed slope gradually transforms from the service state to the limit state by reducing the shear strength, if face failure is prevented by the use of nail head, the maximum tension line will move towards the slope surface (such as Figure 5.29 and Figure 5.30) as the nail force is gradually mobilized and the resistant zone gets larger to maintain the slope in stable condition. Secondly, the tension stress distribution is influenced by the slope failure modes at limit state. For slope with internal failure modes, if it is face failure, the line of maximum tension usually is located behind the slip surface (Figure 5.28a). For a pullout failure, the line of the maximum tension is usually located in front of the slip surface (Figure 5.28b, Figure 5.29b). For a nail tensile failure, the line of the maximum tension will coincides well with the slip surface which is demonstrated by both the numerical simulation (Figure 5.28c) and the full scale test (Figure 5.32c). For slope with external failure modes, the line of the maximum tension force will not coincide with the

slip surface. Besides, both the nail tension force distribution and the slip surface are greatly controlled by the location of the external loading (Figure 5.31).

5.11 Slip surface for face failure

As presented in the previous section, for the soil nailed slope shown in Figure 5.1, if the nail head is not modeled, face failure will occurs and the slip surface by the SRM happened to be virtually the same as the one when the slope is not reinforced (though the FOS are not the same). Since such phenomenon is found for many cases (not shown in this chapter), the validity of this observation under different cases will be investigated. In this section, three different models are considered. In the first model, the horizontal and vertical interval of the nail is 1.5m (three nails are included in the model) which is the same as example 1 in previous sections. In the second model, the nail interval is 1.0m (five nails in the model) while the nail interval is 0.75m in the third model (eight nails in the model). At the same time, two different soil properties are considered: a soil with c'=9 kPa and ϕ'=18° (FOS=1.11 with no nail); the second case where c'=20 kPa and ϕ'=5° (FOS=1.2 with no nail). The results are shown in Figure 5.34 and 5.35 and the slip surface with no nail is shown in dashed line. It can be seen that when the nail interval is large, the slip surface is nearly the same with the one with no nail. When the nail interval gets smaller, the difference becomes obvious. For the first case where ϕ' is greater, the slip surface gets shallower with the decrease of the nail interval while the slip surface gets deeper with the decrease of the nail interval for the second case. It is however true that for normal nail spacing, the location of the slip surface for “face failure” is relatively insensitive to the presence of soil nail.

5.12 Influence of nail spacing on the failure modes

For the SRM analysis in previous sections, though the 3D analyzing is conducted for better consideration of the soil-nail interaction, the slip surfaces are still basically two dimensional (the slip surface is nearly the same at different section). This phenomenon is due to the relatively small nail spacing used in the analysis. If the spacing of the nail is large enough, a clear three dimensional failure surface may occur. A slope model is developed in this section to illustrate the influence of the nail interval on the failure mode. The slope geometry and soil property is the same as the example shown in Figure 5.1, but the horizontal and vertical intervals of the nail are 10m and 1m respectively (five nails in the model), and the nail length is 14m. When the soil-nail interface strength is set to be half of the soil shear strength, the slip surface is still nearly two dimensional (Figure 5.36). When the soil-nail interface strength is set to be the same as soil shear strength, a clear three dimensional slip surface will be mobilized (Figure 5.37). This means that the failure mode is influenced by both the nail interval and the load provided by the nail. Since the basic idea of the soil nailing technique is installing close spaced inclusions into the soil to increase the stability, a clear three-dimensional slip surface would not be easily mobilized simply due to the presence of nail. On the other hand, if the slope is reinforced by anchor technique which can provides large supporting load by each individual reinforcing element with a relatively large spacing, a clear three-dimensional slip surface may be easier to be mobilized.

5.13 Discussion and Conclusion

In this chapter, it is established that the Poisson ratio and the stiffness/arrangement of the nail head have little influence on the factor of safety and the failure mechanism of a slope. The presence of a nail head is however important and should be properly modeled. There have been slope failures in Hong Kong where the reason can be

attributed to the use of very small nail head (and hence face failure) so that this case should be checked in the analysis and design. The option of face failure is however absent in many commercial slope stability programs, and engineers should provide an adequate nail head in general for maximum efficiency. As long as the nail head is not too small, a pull out failure will be the failure mechanism which is investigated in the present study.

From the present study, it is found that the FOS from the SRM and the LEM are similar under most cases, and nearly all the FOS from the SRM are slightly greater than those from the LEM. Although the slip surfaces by the SRM and the LEM usually agree well, sometimes the slip surface from the SRM is not regular which is one of the limitations of the SRM. From the analysis of a soil nailed wall in Seattle, it is also found that several failure modes can easily be detected by the SRM which are absent in the corresponding LEM analyses. In this respect, the SRM can be an alternative or complementary method to the LEM analysis. On the other hand, some special combined failure surfaces similar to that in Figure 5.12b are found when a very fine mesh is used in the analysis. In this respect, the SRM also possesses numerical problems not found in the LEM.

It is found that the nail elastic modulus have little influence on the SRM analyses except for very steep slope. The FOS from the SRM also appears to increase with the decreasing of nail elastic modulus which can be attributed to the greater soil movement and mobilization of nail bond load. This phenomenon can also account for the differences in the design of reinforced earth wall using the extensible and inextensible strip methods (Elias et al., 2001) which is based on field observations but are also obtained from numerical modeling in the present study.

When there is an external pressure on top of a slope and the bond stress is assumed to be dependent on the overburden/confining stress, there are great differences between the SRM and LEM. In all the commercial slope stability programs based on the LEM, the increase in the overburden stress from the external loads on the nails are not included as there is not a reliable method in distributing the external loads under ultimate limit state. The simplified 1 in 2 rule of thumb or other empirical methods are all based on the service state instead of the ultimate limit state and are not included in normal LEM analysis. On the other hand, SRM can consider the external load easily and automatically which is an advantage not present in LEM. Engineers should also be aware of this difference in the bond load determination in LEM and SRM, and such difference has seldom been considered up to present.

In soil nailing design, the nail inclination angle and the layout can be optimized by the SRM or LEM analyses. Usually, with the increase of the nail inclination angle, the FOS increases slightly initially which will decreases if the inclination is large. An optimum soil nail design can be determined easily using whether the SRM or the LEM. It is also found that the mobilized bending moment in soil nail is small even when the nail inclined angle is large. The use of the bond stress for soil nail design which is a commonly adopted approach appears to be a reasonable design method.

An optimum design of longer nail at top and shorter nail at bottom has been recommended by some researchers and engineers for the control of the movement for soil nails installed by a top-down construction. For the stabilization of existing slopes, from the safety factor point of view, the SRM analysis shows that the reverse arrangement will be a more economic solution for the ultimate limit state. The final conclusion to the optimum soil nail layout from the present study is to place a longer

nail at locations where failure will start to initiate, and the choice of longer or shorter nail at top or bottom will depend on the initiation of the possible failure mechanism.

The tension force distribution along soil nail is found to be controlled by the state of the slope (service state, limit state) and the failure modes (external failure, internal failure). In general, the line of maximum tension does not correspond to the conventional critical slip surface which is different from the common believe, but is the consequence of the soil nail interaction. For slope with external failure modes, the line of maximum tension force will never coincide with the slip surface. For slope with internal face failure modes, the line of maximum tension is usually found to locate behind the slip surface. For a pullout failure, the line of maximum tension is usually in front of the slip surface while for a tensile failure, the line of maximum tension will coincides with the slip surface as the common belief.

The limit state can be achieved by reducing the soil shear strength or by applying external loading. It is demonstrated that there are differences in the nail force distribution and slip surface between these two modes. When the soil nailed slope gradually transforms from service state to limit state by reducing the shear strength, if the nail head is strong enough with no face failure, the maximum tension force line will move towards the slope surface.

The failure mode of soil nailed slope is controlled by both the nail spacing and the nail load. In practice, the nail is usually closely spaced, thus a clear three-dimensional slip surface would usually not easy to be mobilized if the slope geometry and boundary conditions have no obvious 3D effects. Most of the failure modes examined in this chapter are basically two dimensional slip surfaces, as the nail is densely populated and

the slope has no distinct irregular geometry or loading. In the next chapter, some soil nailing slopes with distinct 3D effect in geometry and boundary conditions will be investigated.

Table 5.1 Parameters of grout-soil-nail system

Young's modulus, E [GPa]	45.44
grout cohesive strength (force) per unit length, c_g [kN/m]	1.4135
grout friction angle, ϕ_g [degree]	9.23
grout stiffness per unit length, k_g[MPa]	43.1
grout exposed perimeter, p_g [m]	0.339
cross-sectional area, A [m^2]	0.00785
compressive yield strength (force), F_c [MN]	0.238
tensile yield strength (force), F_t [MN]	0.238

Table 5.2 Factor of safety for nail head with different elastic modulus

Elastic modulus	30GPa	15GPa	15MPa
FOS (0.5m*0.5m nail head)	1.28	1.27	1.28
FOS (continuous nail head)	1.26	1.27	1.27

Table 5.3 Factors of safety by LEM and SRM

case	c' (kPa)	ϕ' (°)	factor of safety (LEM)	factor of safety (SRM)	FOS difference between LEM and SRM (%)
1	2	5	0.27	0.28	3.70
2	2	15	0.59	0.63	6.78
3	2	25	0.99	1.09	10.10
4	2	35	1.55	1.72	10.97
5	2	45	2.34	2.63	12.39
6	5	5	0.44	0.46	4.55
7	5	15	0.80	0.86	7.50
8	5	25	1.23	1.33	8.13
9	5	35	1.80	1.96	8.89
10	5	45	2.59	2.9	11.97
11	10	5	0.70	0.74	5.71
12	10	15	1.14	1.19	4.39
13	10	25	1.63	1.71	4.91
14	10	35	2.17	2.37	9.22
15	10	45	2.97	3.3	11.11
16	20	5	1.15	1.26	9.57
17	20	15	1.67	1.79	7.19
18	20	25	2.20	2.34	6.36
19	20	35	2.82	3.04	7.80
20	20	45	3.67	3.95	7.63

Table 5.4 Results for different nail inclination

Inclination angle (°)	0	10	20	30	40	60
FOS by LEM	1.22	1.26	1.24	1.24	1.22	1.13
Maximum force of top nail by LEM (kN)	3.71	6.54	11.26	14.17	15.63	19.00
Maximum force of middle nail by LEM (kN)	5.9	9.21	13.85	17.06	18.80	21.54
Maximum force of bottom nail by LEM (kN)	8.74	12.39	17.28	20.47	21.72	23.10
FOS by SRM1	1.28	1.30	1.33	1.33	1.31	1.17
Maximum force of top nail by SRM1 (kN)	13.85	13.22	14.78	15.27	15.94	3.79
Maximum force of middle nail by SRM1 (kN)	17.22	21.55	26.92	30.25	33.00	23.33
Maximum force of bottom nail by SRM1 (kN)	28.15	31.41	35.80	39.57	41.69	24.65
FOS by SRM2	1.28	1.30	1.33	1.36	1.36	1.20
Maximum force of top nail by SRM2 (kN)	18.52	19.56	21.54	23.79	26.22	4.99
Maximum force of middle nail by SRM2 (kN)	21.35	26.49	28.77	33.46	36.15	22.13
Maximum force of bottom nail by SRM2 (kN)	30.32	34.98	38.84	41.59	44.76	23.77
Maximum moment (kN·m)	1.193	1.215	1.079	1.744	1.820	1.819

Table 5.5 Factor of safety for different soil nail length

Nail length (m)	0 (no nail)	6	8	10	12	14	16
FOS by SRM	1.11	1.17	1.28	1.36	1.41	1.48	1.54
FOS by LEM	1.05	1.12	1.22	1.27	1.32	1.35	1.40

Table 5.6 Factor of safety with 200 kPa top pressure (bond load controlled by overburden stress)

Nail length (m)	8	12	16
FOS by SRM	0.66	0.76	0.84
FOS by LEM	0.56	0.59	0.61

Table 5.7 Factor of safety with 200 kPa top pressure (constant pull out resistance)

Nail length (m)	8	12	16
FOS by SRM	0.60	0.67	0.73
FOS by LEM	0.58	0.61	0.65

Table 5.8 Factor of safety with different nail elastic modulus (slope angle 45 degree)

Nail length (m)	8	12	16
FOS by SRM (E=45.44 GPa)	1.28	1.41	1.54
FOS by SRM (E=4.544 GPa)	1.29	1.44	1.57

Table 5.9 Factor of safety with different nail elastic modulus (vertical cut slope)

Nail length (m)	6	8	12
FOS by SRM (E=45.44 GPa)	1.32	1.51	2.12
FOS by SRM (E=4.544 GPa)	1.57	1.79	2.37

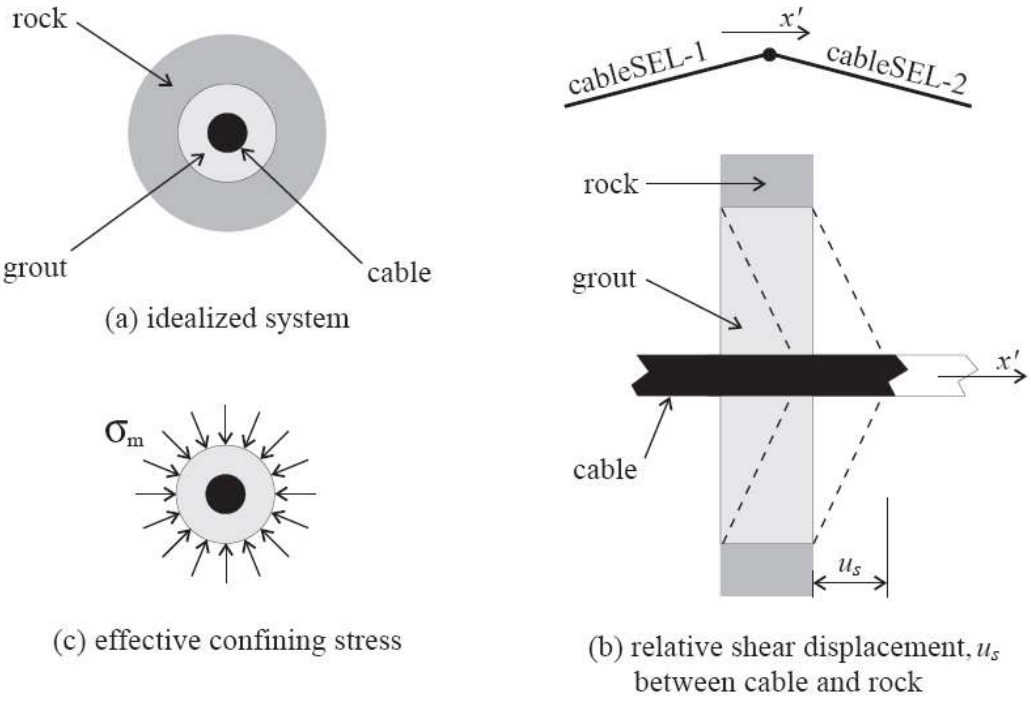

Figure 5.1 Idealization of grout-cable system (from Itasca, 2006)

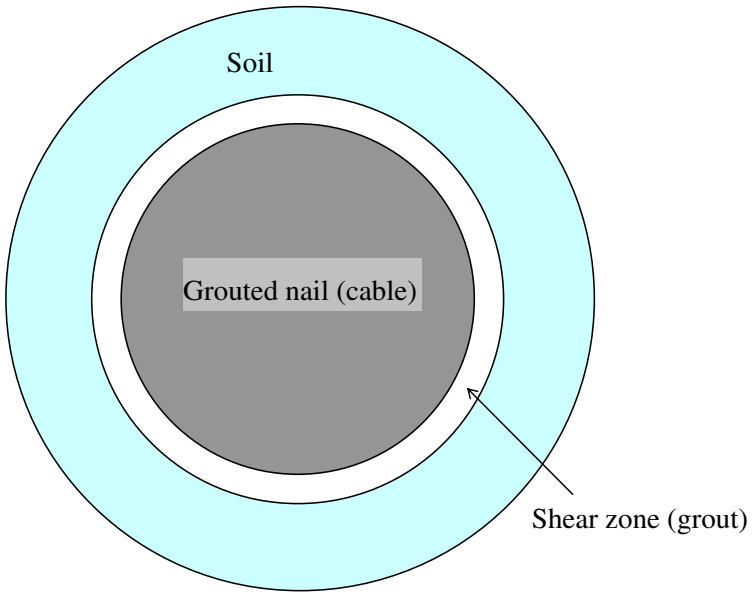

Figure 5.2 Idealization of soil nail system

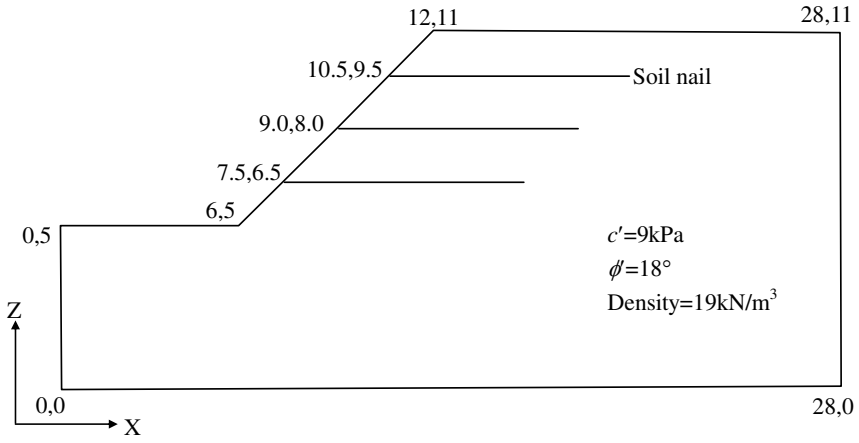

(a) cross section plot of the soil nailed slope model

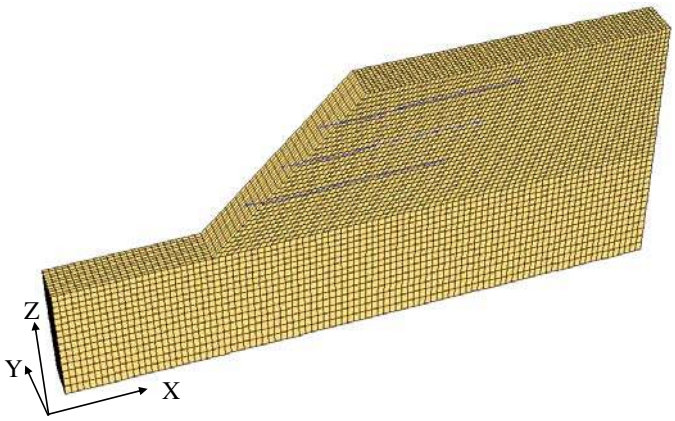

(b) three-dimensional mesh for SRM analysis

Figure 5.3 Plot of the soil nailed slope model

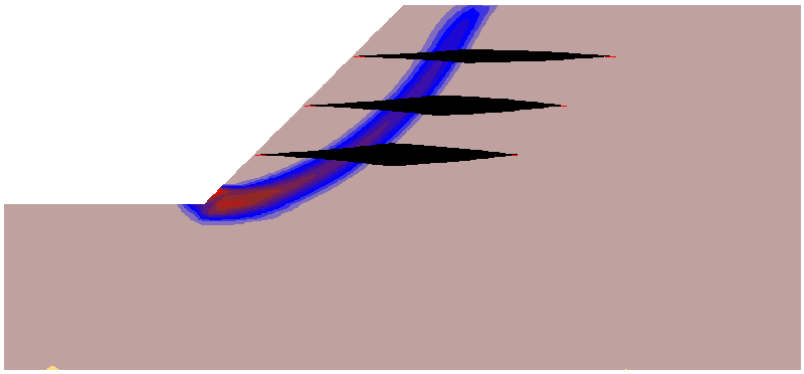

Figure 5.4 Slip surface and the tension stress of soil nail without nail head (FOS=1.20)

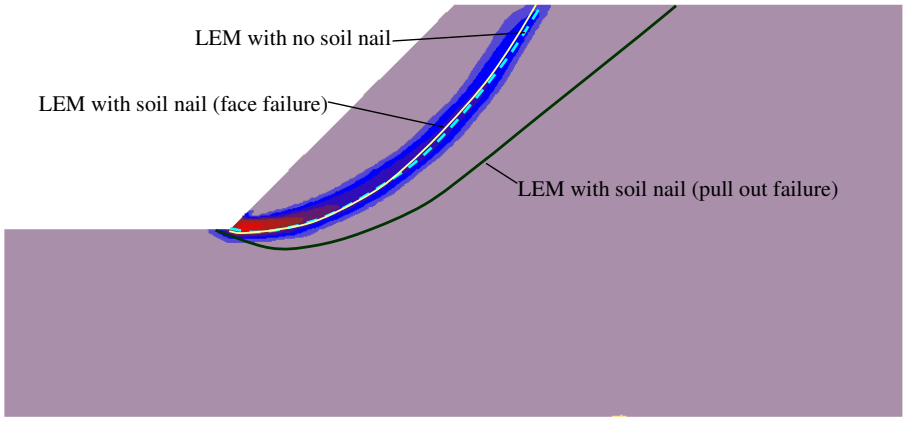

Figure 5.5 Slip surface for soil nailed slope without nail head by SRM and compared with LEM results

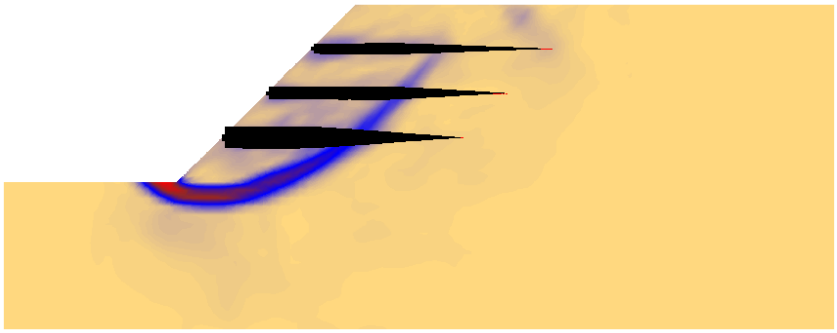

Figure 5.6 Slip surface and the tension stress of soil nail for model with nail head (FOS=1.28)

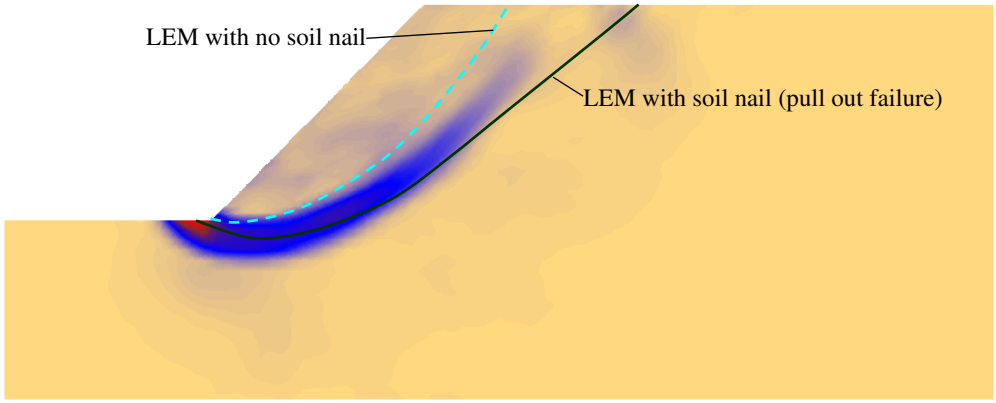

Figure 5.7 Slip surface for soil nailed slope by SRM for the model with nail head

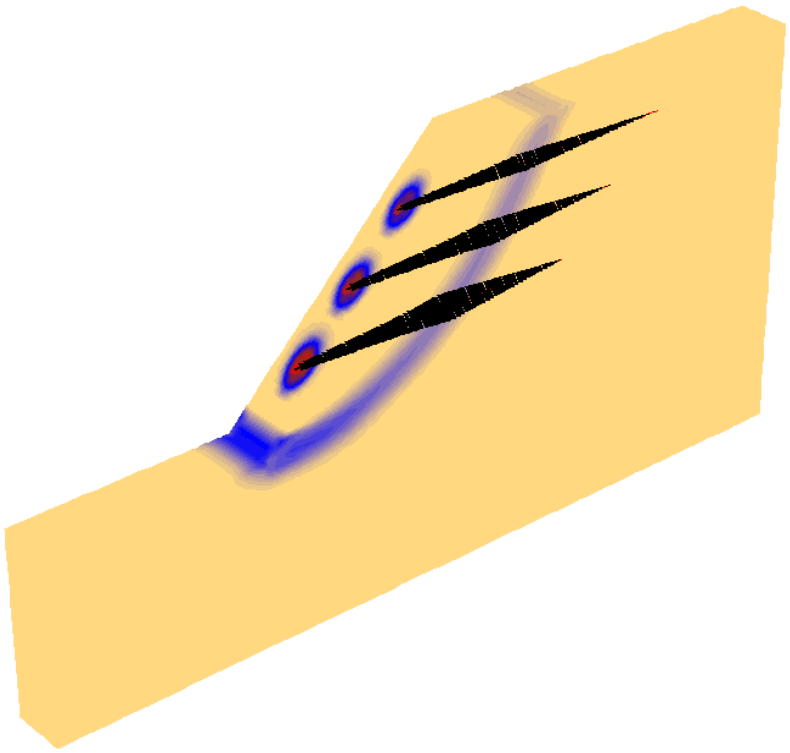

Figure 5.8 Slip surface of the slope with 0.14m width and 0.15m height nail head

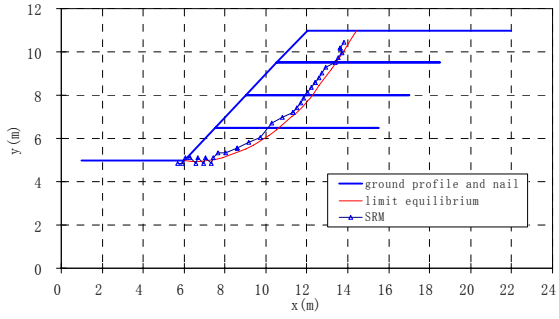

(a) c'=2kPa, ϕ'=5°

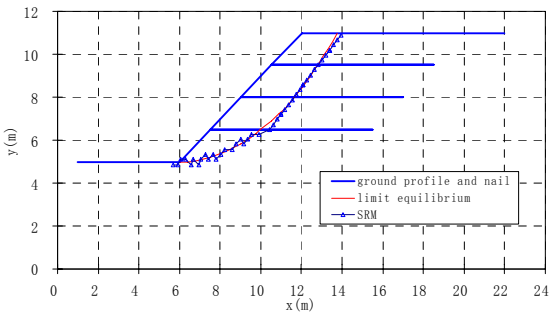

(b) c'=2kPa, ϕ'=15°

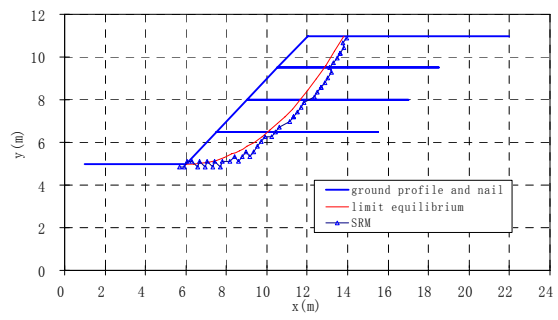

(c) c'=2kPa, ϕ'=25°

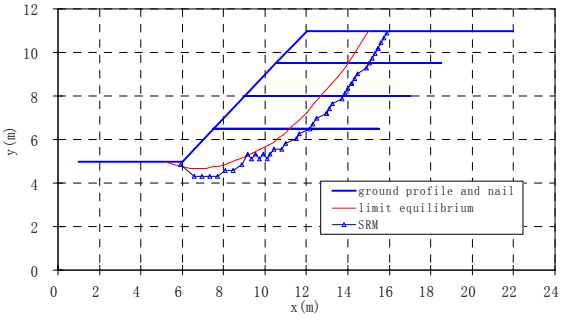

(d) c'=2kPa, ϕ'=45°

Figure 5.9 Slip surface comparison with increasing friction angle (c'=2kPa)

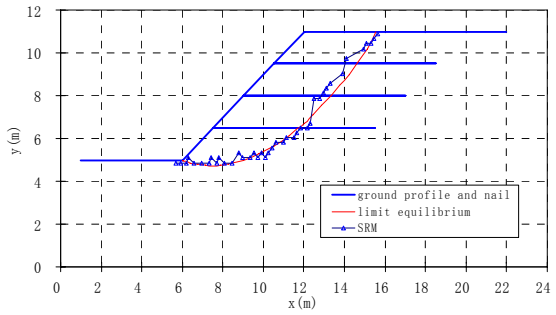

(a) c'=5kPa, ϕ'=5°

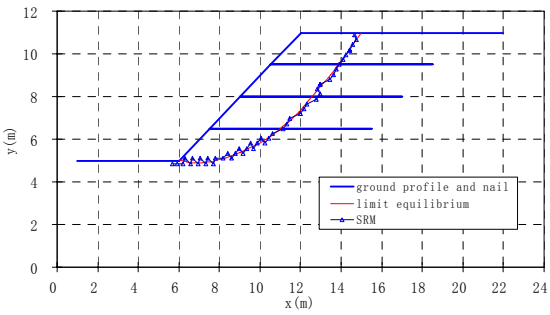

(b) c'=5kPa, ϕ'=15°

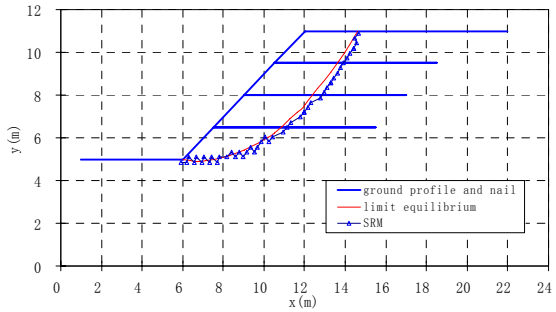

(c) c'=5kPa, ϕ'=25°

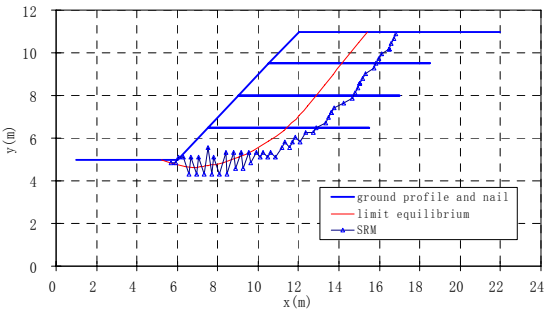

(d) c'=5kPa, ϕ'=45°

Figure 5.10 Slip surface comparison with increasing friction angle (c'=5kPa)

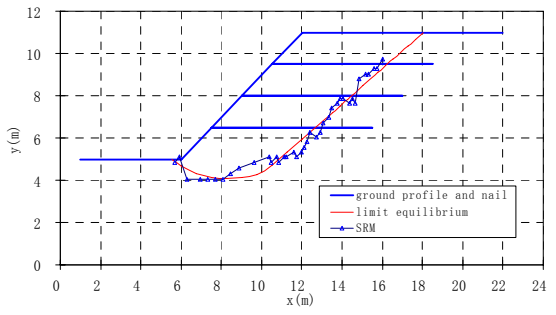

(a) c'=20kPa, ϕ'=5°

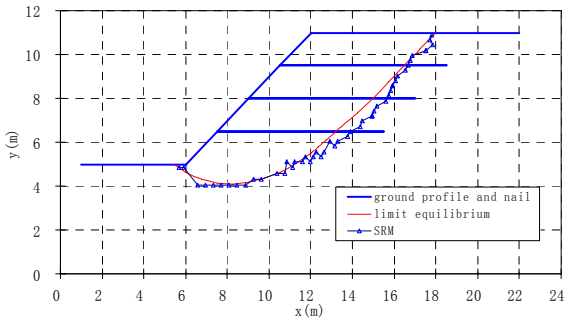

(b) c'=20kPa, ϕ'=15°

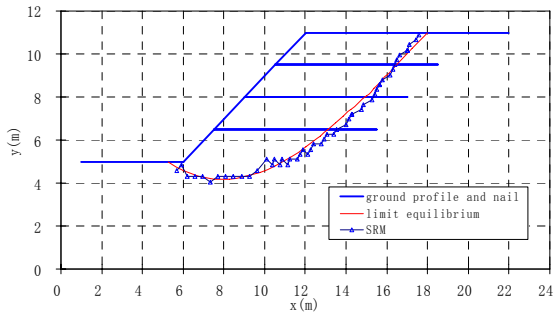

(c) c'=20kPa, ϕ'=25°

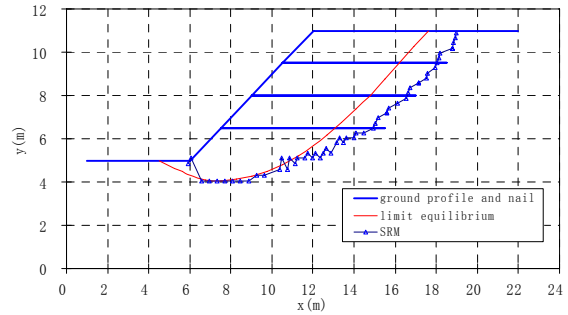

(d) c'=20kPa, ϕ'=45°

Figure 5.11 Slip surface comparison with increasing friction angle (c'=20kPa)

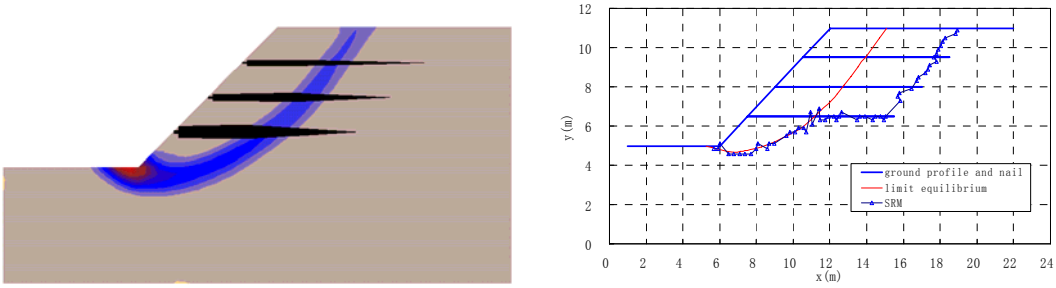

(a) FOS=1.96 for slightly increased element size (b) FOS=1.94 for very fine mesh

Figure 5.12 Slip surface obtained by different element size (c'=5kPa, ϕ'=35°)

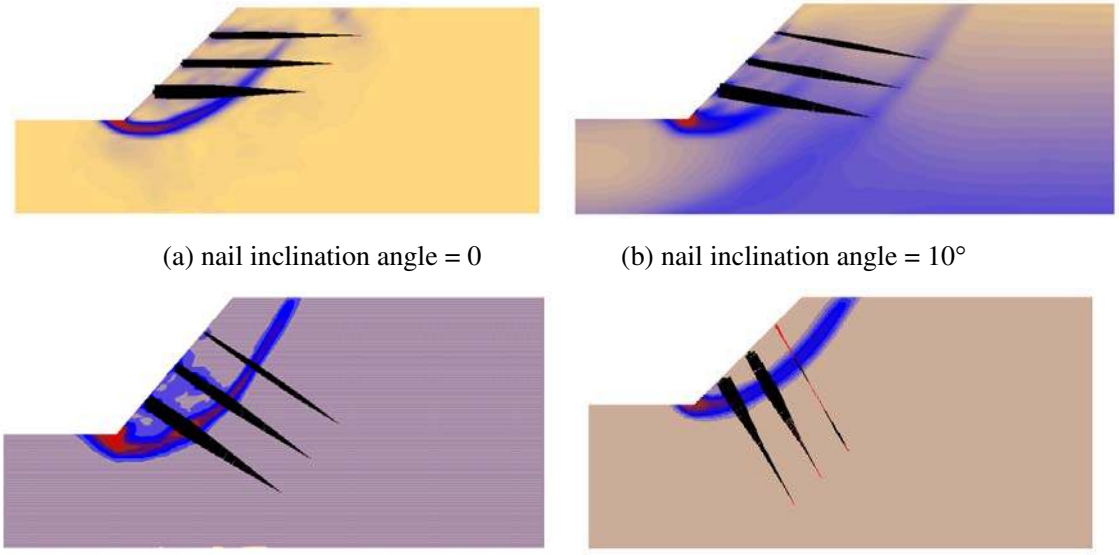

(a) nail inclination angle = 0 (b) nail inclination angle = 10°

(c) nail inclination angle = 30° (d) nail inclination angle = 60°

Figure 5.13 Slip surface and nail axial force distribution for different nail inclined angle (nail simulated by cable element)

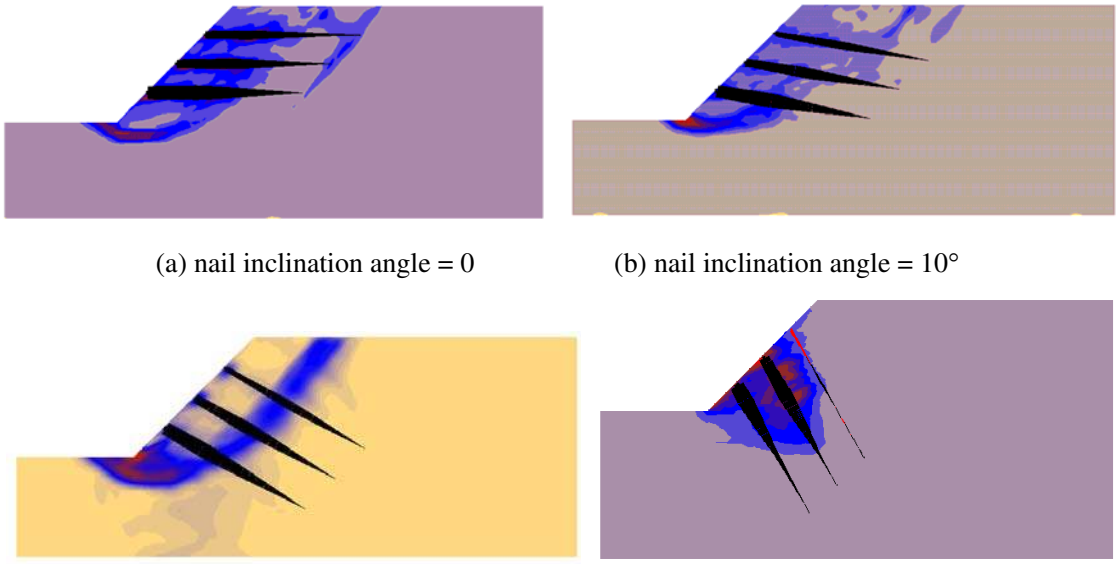

(a) nail inclination angle = 0 (b) nail inclination angle = 10°

(c) nail inclination angle = 30° (d) nail inclination angle = 60°

Figure 5.14 Slip surface and nail axial force distribution for different nail inclination (bending effect considered)

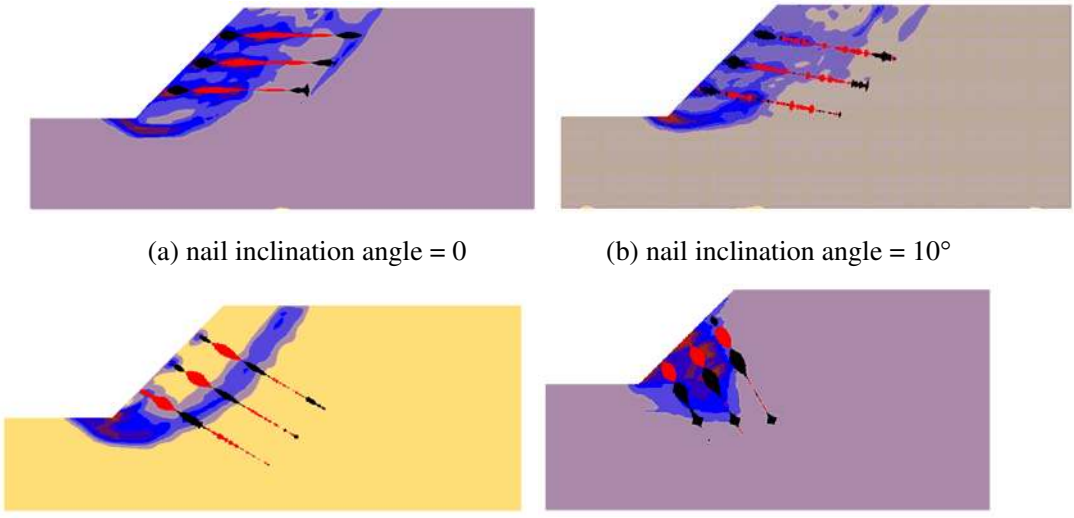

(a) nail inclination angle = 0 (b) nail inclination angle = 10°

(c) nail inclination angle = 30° (d) nail inclination angle = 60°

Figure 5.15 Slip surface and nail bending moment distribution for different nail inclination (bending effect considered)

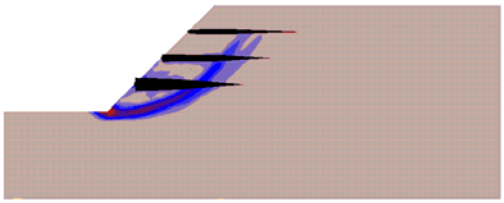

(a) L=6m

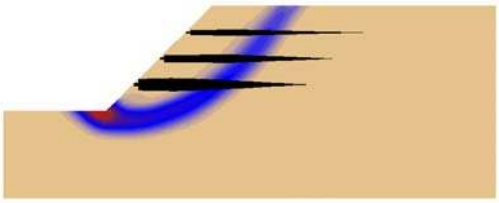

(b) L=10m

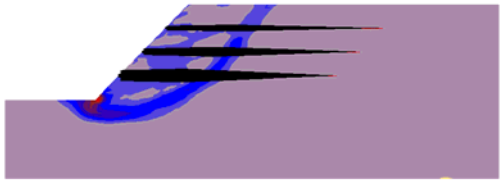

(c) L=14m

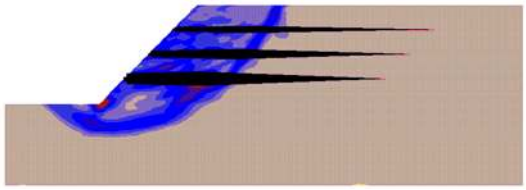

(d) L=16m

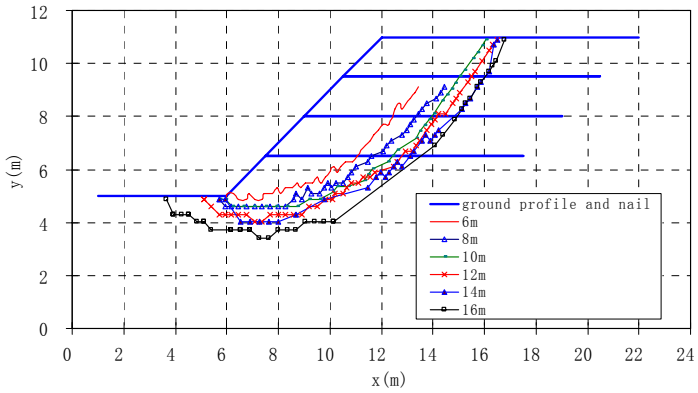

(e) Slip surface location comparison for different nail length

Figure 5.16 Slip surface and the nail tension force for different nail length

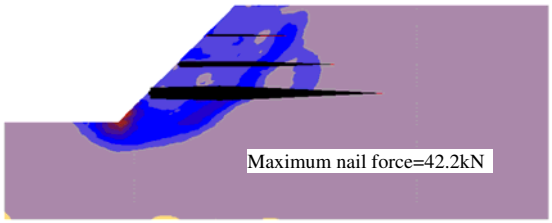

(a) Short nail at top, FOS=1.31

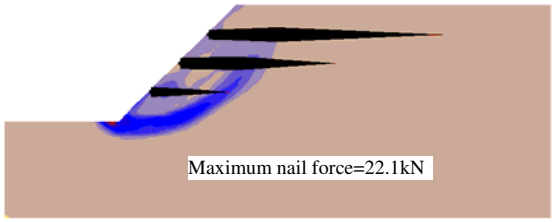

(b) short nail at bottom, FOS=1.22

Figure 5.17 Slip surface and the tension stress in different layout with zero inclined angle

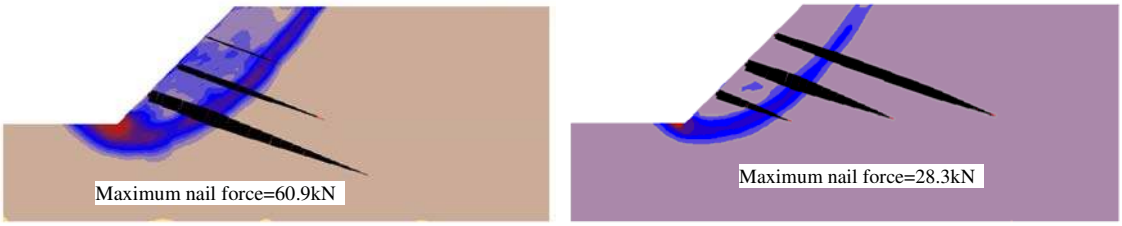

(a) short nail at top, FOS=1.40 (b) short nail at bottom, FOS=1.26

Figure 5.18 Slip surface and the nail load for different layout with 20° nail inclination

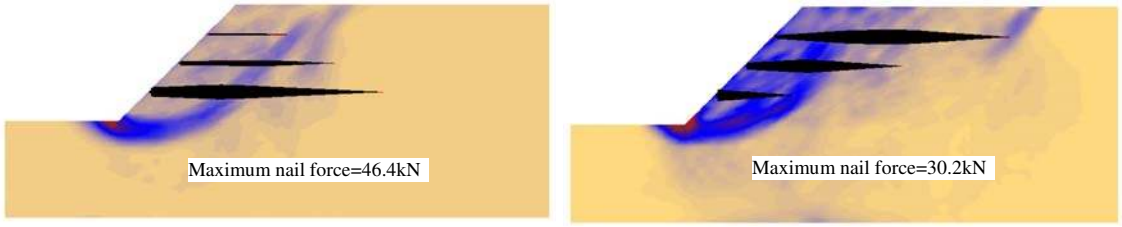

(a) short nail at top, FOS=1.34 (b) short nail at bottom, FOS=1.22

Figure 5.19 Results for different layout with zero inclined angle (constant nail pullout strength)

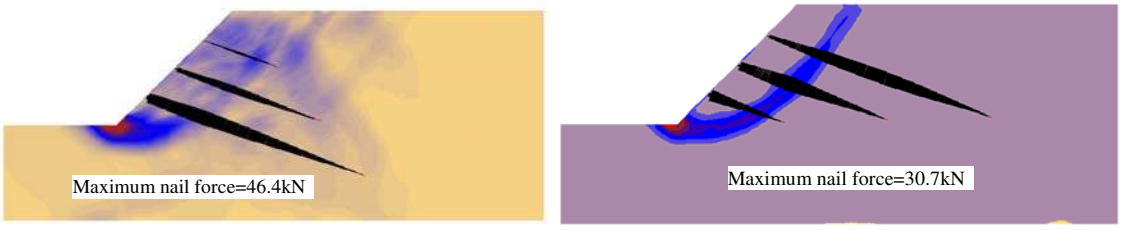

(a) short nail at top, FOS=1.35 (b) short nail at bottom, FOS=1.26

Figure 5.20 Results for different layout with 20° nail inclination (constant nail pullout strength)

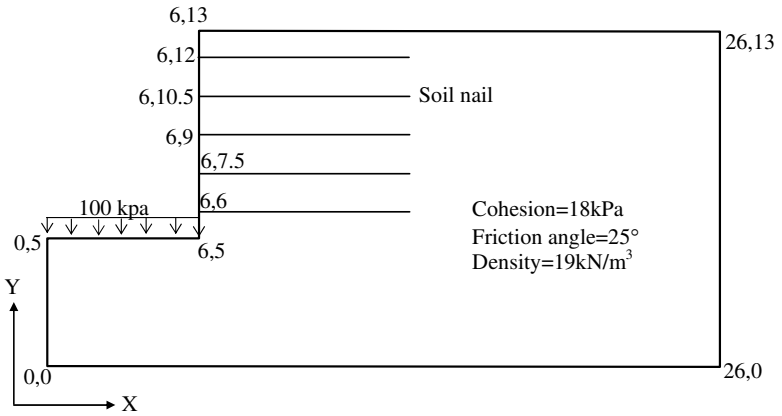

Figure 5.21 Vertical cut soil nailed slope model

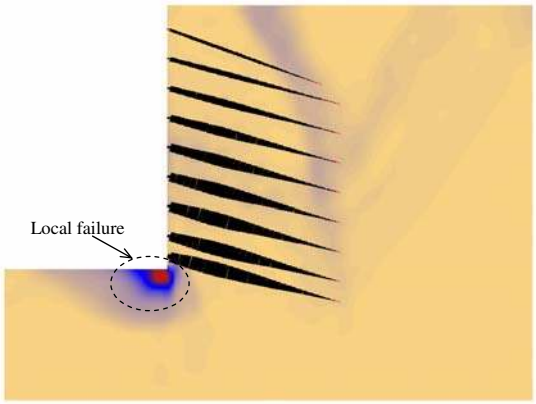

Figure 5.22 Slip surface and nail tension stress of the vertical soil nailed wall with FOS=1.76

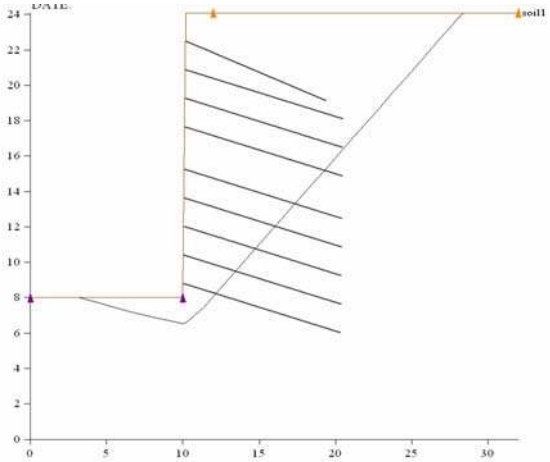

Figure 5.23 Slip surface of the vertical soil nailed wall by LEM with FOS=1.90

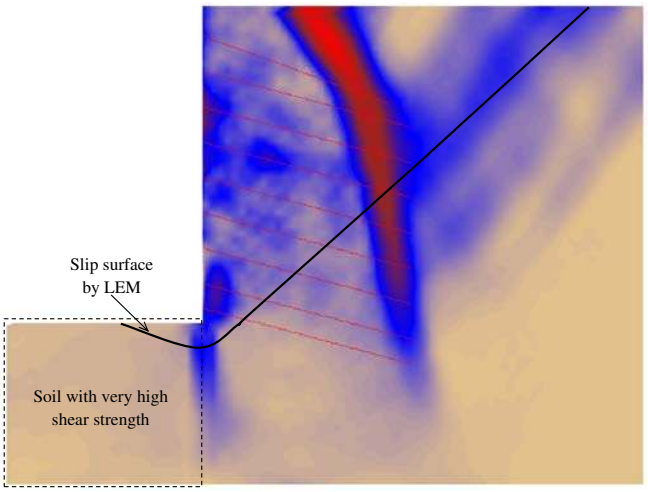

Figure 5.24 Slip surface of the vertical soil nailed wall with high shear strength at left part by SRM (FOS=2.10)

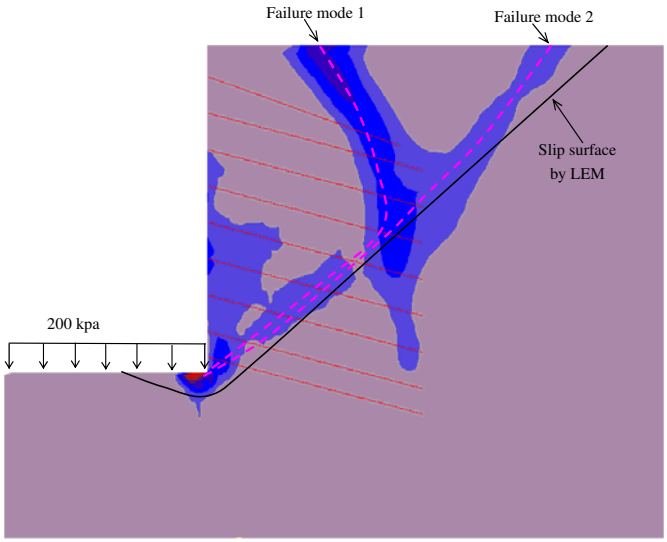

Figure 5.25 Slip surface of an excavated vertical cut with applied pressure 200kPa at left corner by SRM (FOS=2.29)

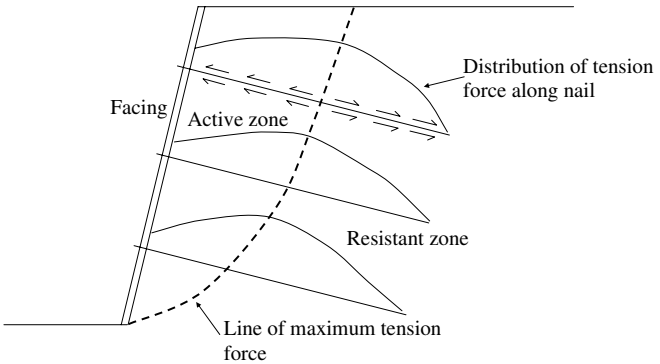

Figure 5.26 Load transfer mechanism in soil nails (after Byrne et al., 1998)

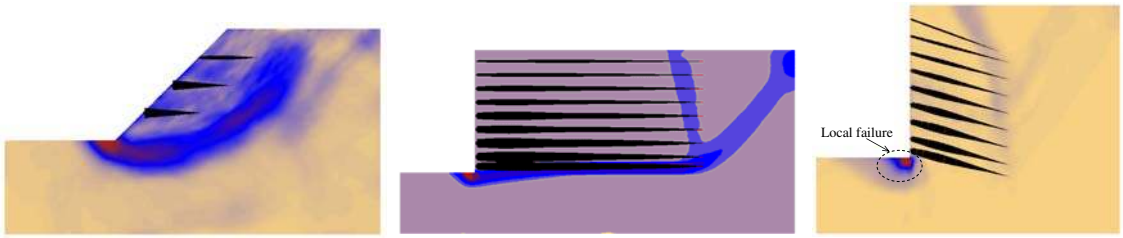

(a) global failure (b) sliding failure (c) bearing capacity failure

Figure 5.27 Axial tensile force distribution of soil nail in different external failure modes

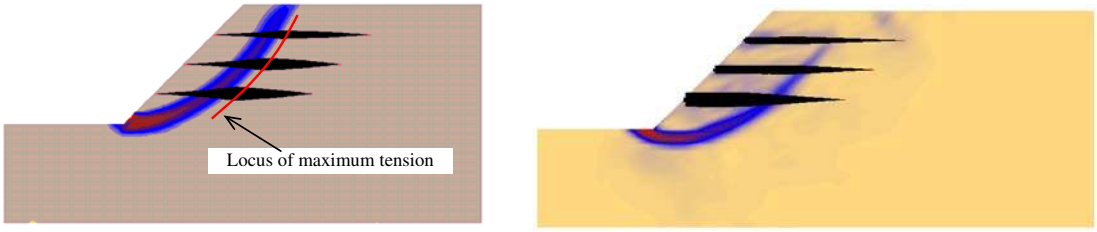

(a) no nail head, FOS=1.20, face failure (b) strong nail head, FOS=1.28, pullout failure

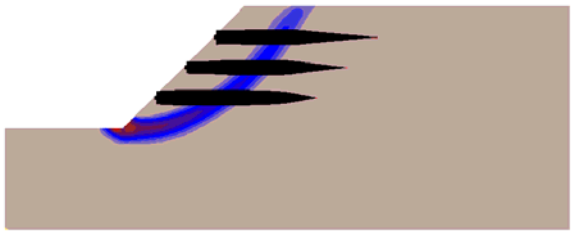

(c) nail head is strong, nail tensile strength=10kN, FOS=1.22 with nail tensile failure

Figure 5.28 Slip surface and nail tension stress distribution in different internal failure modes

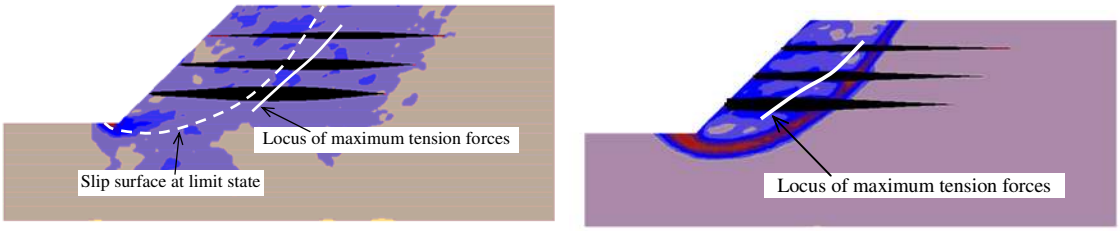

(a) service state (b) limit state, FOS=1.41

Figure 5.29 Axial tensile force distribution of soil nail in different state

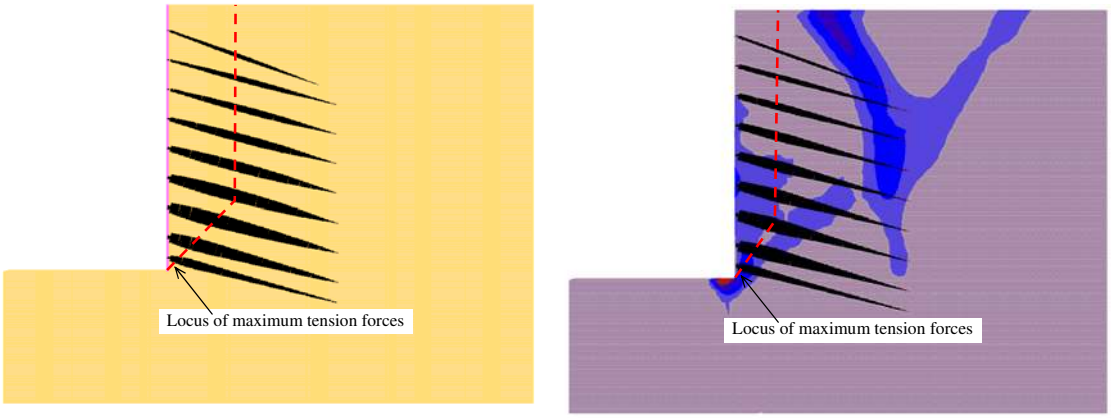

(a) service state (b) limit state

Figure 5.30 Axial tensile stress distribution in different state for a vertical cut slope

(a) limit state by reducing strength, f=1.31 (b) limit state by applying pressure near crest

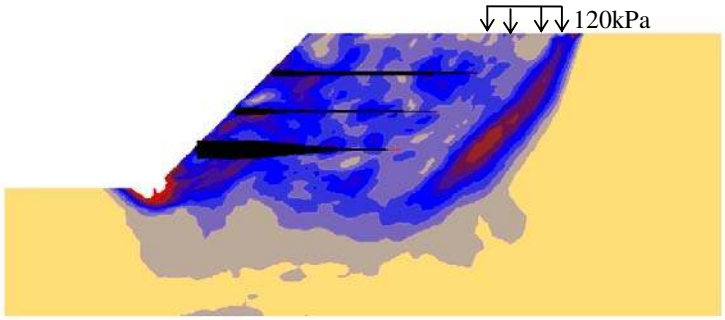

(c) limit state by applying 120kpa pressure at slope top near the nail end

Figure 5.31 Axial tensile stress distribution in different limit state

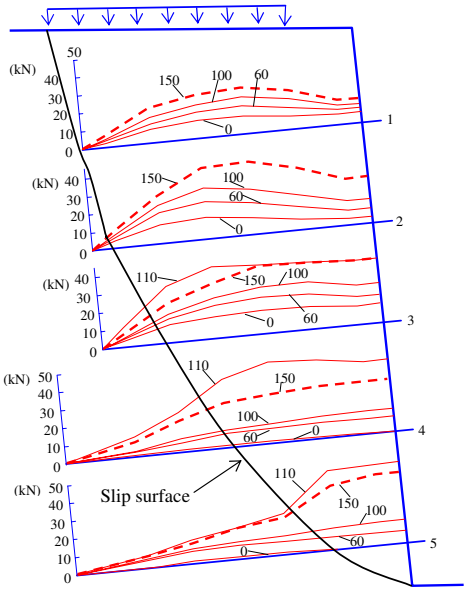

(a) Gassler (1993)

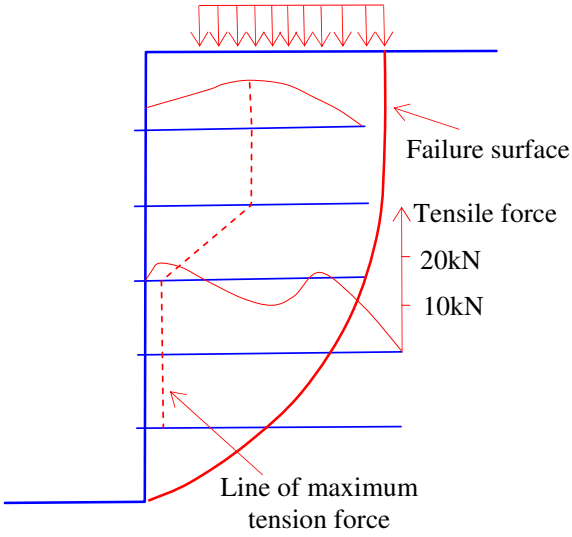

(b) Stocker et al. (1979)

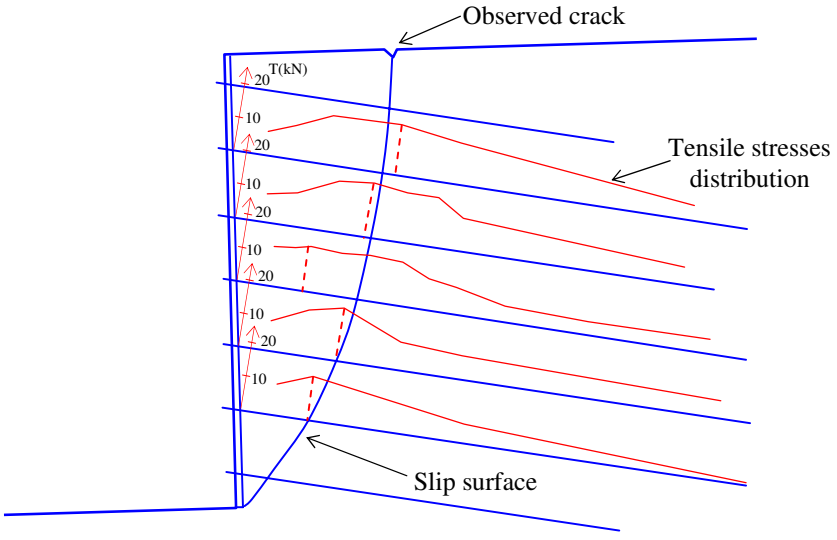

(c) Clouterre (1993)

Figure 5.32 Nail force distribution in limit state

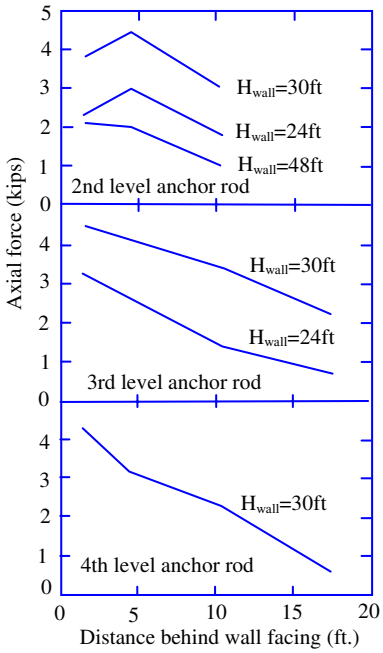

(a) Shen et al. (1981c)

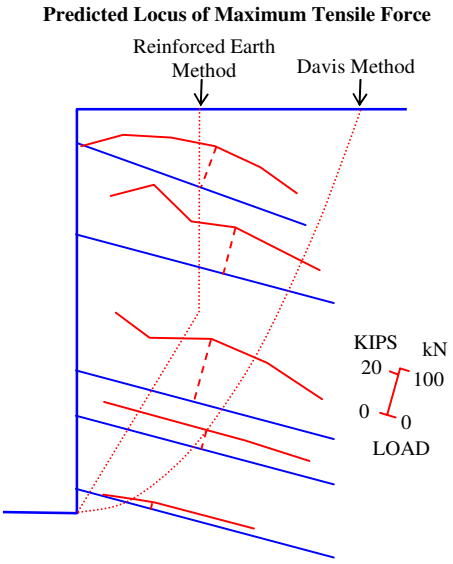

(b) Thompson and Miller (1990)

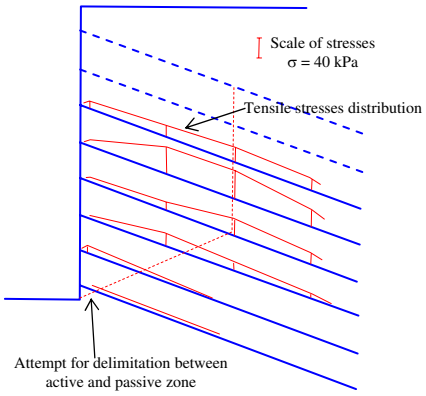

(c) Cartier and Gigan (1983)

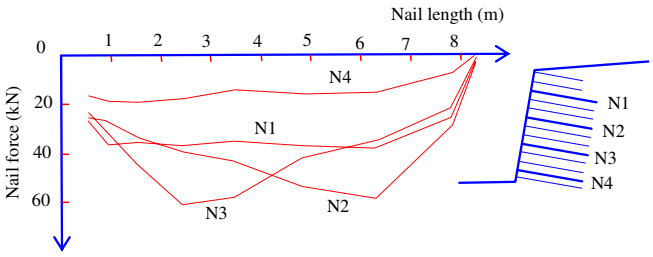

(d) Stocker and Riedinger (1990)

Figure 5.33 Nail force distribution in service state

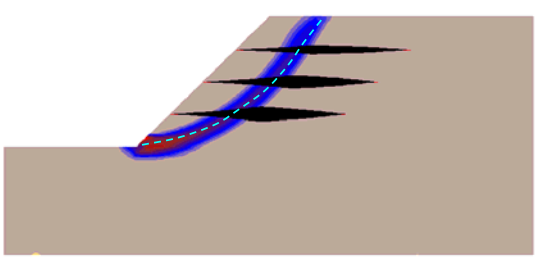

(a) nail interval 1.5m, FOS=1.20

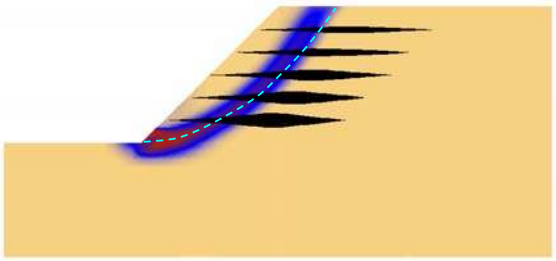

(b) nail interval 1.0m, FOS=1.35

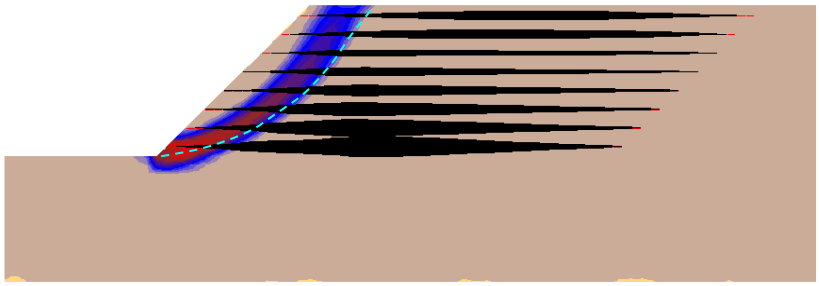

(c) nail interval 0.75m, FOS=1.65

Figure 5.34 Slip surface of soil 1 with face failure in different nail interval

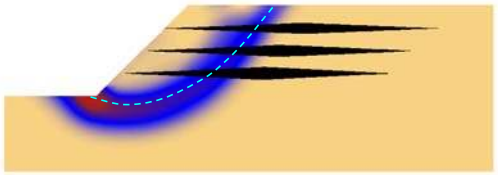

(a) nail interval 1.5m, FOS=1.32

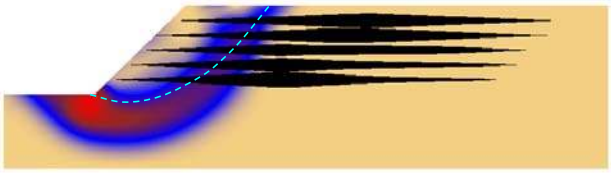

(b) nail interval 1.0m, FOS=1.49

(c) nail interval 0.75m, FOS=1.75

Figure 5.35 Slip surface of soil 2 with face failure in different nail interval

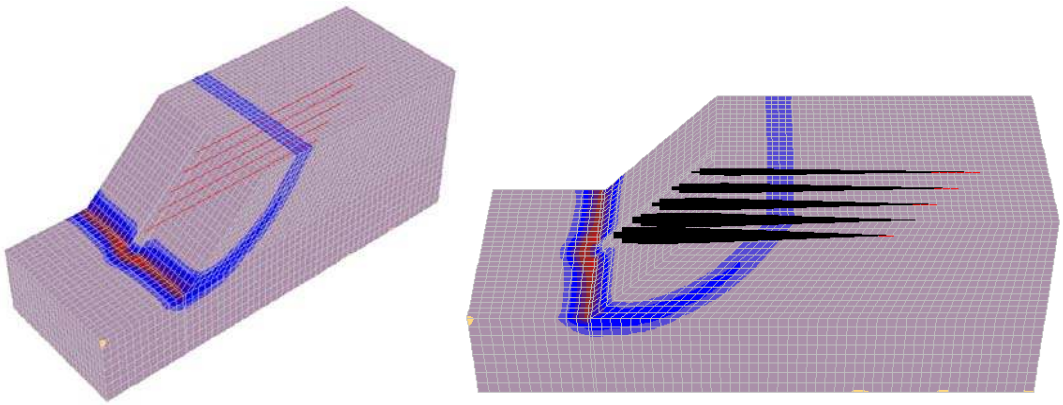

(a) slip surface (b) nail force distribution

Figure 5.36 Slip surface and nail force for slope with 10m horizontal nail interval and soil-nail interface strength is half of the soil strength (FOS=1.25)

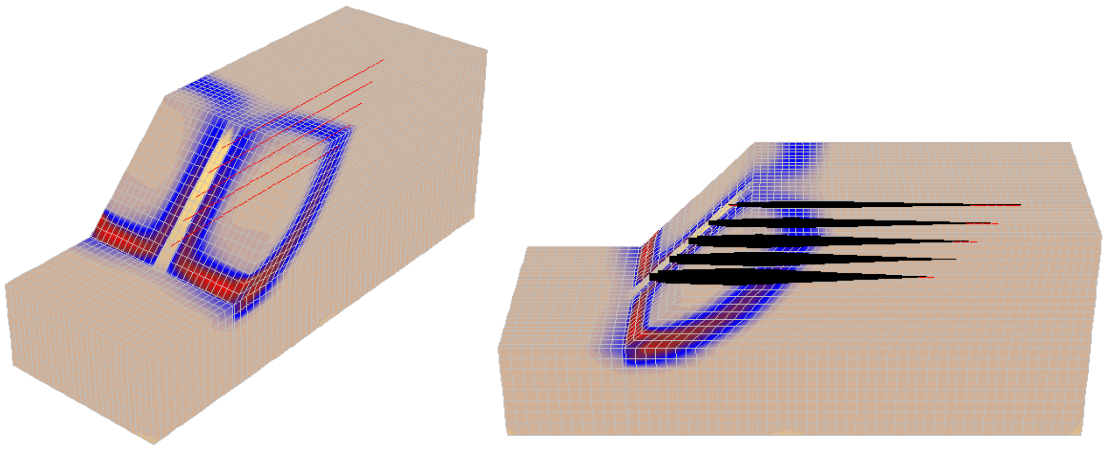

(a) slip surface (b) nail force distribution

Figure 5.37 Slip surface and nail force for slope with 10m horizontal nail interval and soil-nail interface strength is the same as the soil strength (FOS=1.30)

CHAPTER 6: EFFECTS OF CURVATURE AND LOCAL LOADING ON 3D SOIL NAILED SLOPE

6.1 Introduction

In traditional engineering design, soil nails are usually designed using 2D analysis which is reasonable when the soil nails are densely installed and the slope has no obvious 3D effect in geometry and boundary conditions. In most cases, 3D slope failure will be the prevailing failure mode for real problems, and chapter 4 has carried out detailed study on the 3D failure of unreinforced slopes. In this chapter, 3D analysis will be conducted for some soil nailed slopes with strong 3-D effect (locally loaded slope, curved slope and intersected slope), and the factor of safety of the slope will be obtained by the strength reduction method using software FLAC3D.

6.2 Numerical simulation for locally loaded soil nailing slope

In this section, a 6m height soil nailing slope with 45° slope angle under rectangular shape vertical loading as shown in Figure 6.1 is analyzed. The loading width B is 2m while the edge of the loading is 1m away from the crest of the slope. Nails are installed at 1.5m centers horizontally and vertically. The nail length is 8m and the inclination angle is zero. The slope geometry and the soil properties are shown in Figure 6.1, while the numerical model is 18m in length, so there are 36 nails included in this model (3 row and 12 nails in each row). When the loading q is 200kPa, the results of analysis are shown in Figure 6.2, where the ratio of the loading length L to loading width B varies from 1 to 4.

When the L/B ratio is 1.0, the failure is a local failure controlled by the top surcharge and does not pass through the toe of the slope. With the increase of the loading length (L/B increases from 1 to 4), the factor of safety becomes smaller and the slip surface becomes larger and extends towards the toe of the slope. The maximum nail tension force distribution at limit state under different local loading is shown in Figures 6.3 to 6.5, and the maximum nail force distribution for the slope with no local loading is shown in Figure 6.6. If no loading is applied on the nailing slope, the nail force at the bottom row is much more mobilized than the force at top and middle rows at the limit state (Figure 6.6). The tension force for the middle row is also slightly more mobilized than the top row, but the difference in the nail force between the middle row and top row is not large. The nail force of the bottom row is much larger than the middle and the top row. At the limit state, the movement of the slope is larger at the lower part and is smaller at upper part, so the nail force is more mobilized at the lower part. When there is local loading applied on the slope, the nail force of the top row at the centre of the model is much more mobilized (loading is applied at the range of the model center). For slope with local loading at the model center (Figures 6.3 to 6.5), the nail force distribution at the model edge has no great difference from the slope with no loading (the bottom row is more mobilized than the top row), since at the edge of the model, it is far away from the loading which is applied at the center of the model and the influence of the loading is small. Around the center of the model, when the loading length is small (L/B=1, Figure 6.3), the nail forces of the top and middle rows are more mobilized, but the nail force of the bottom row is nearly not affected. When the loading length is large (L/B=2 and 4, Figures 6.4 and 6.5), the nail forces of the top and middle rows are much more mobilized and the nail force of the bottom row is also slightly more mobilized.

6.3 Numerical simulation for idealized convex and concave slopes

In this section, several idealized concave and convex slope models are developed to investigate the effect of curvature on soil nailed slope. The slope height is 10m and slope angle is 45° with properties of density=19.5kN/m3, c'=10kPa and ϕ'=36° (same as the model in chapter 4, Figure 4.19). In this analysis, two different groups of slope models are developed. In the first group, 10m length soil nails are installed at 1.5m centers horizontally and 2m vertically and no external loading is applied on the slope. In the second group, 10m length soil nails are installed at 1.5m centers horizontally and 2m vertically together with a 4m width 100kPa external loading applied on the crest of the slope. In each group, five models are developed (two concave models with 17m and 35m radius at the slope middle height, two convex models with 17m and 35m radius at the slope middle height and one plane model with no curvature). The typical slope section is shown in Figure 6.7. Only a slice mode with a 1.5m thickness at the middle of the slope is adopted in the 3D analysis, and the typical models are shown in Figure 6.8.

The variation of the safety factors with different curvatures are shown in Tables 6.1 to 6.2. For concave slope, the effect of the curvature is obvious and the FOS increases with the decrease of radius. For convex slope, it seems that the curvature does not have distinct effect on the factor of safety which is similar to the un-reinforced slopes investigated in chapter 4.

The slip surfaces for different curvature with no loading is applied are shown in Figure 6.9. As discussed in chapter 4, when the slope is not reinforced, the curvature has nearly no influence on the location of slip surface. When the soil nail is included in the slope (Figure 6.9), it can be seen that the slip surface for reinforced slope is influenced by the curvature, particularly for concave slope. When the radius is smaller for concave slope,

the slip surface will be shallower. For convex slope with soil nails, the curvature has no major effect on the slip surface under normal curvature.

6.4 Numerical simulation for intersected slopes

In this section, two different intersected slope models are developed. For the concave slope model, the intersection angle is 135° and for the convex slope the intersection angle is 145°. The slope height is 6 m and the slope angle is 45° (same as the model in chapter 4, Figure 4.23).

Firstly, no loading is applied on the slope and the results are shown in Figure 6.10. For soil nailed slope, the effect of curvature for convex slope is still not obvious, and the FOS is nearly the same as that for a plane slope, and the effect of curvature is more obvious for concave slope with a larger FOS. Secondly, rectangular shaped vertical loading is applied on the soil nailed slope top. The loading length is 4m and the loading width B is 2m, while the edge of the loading is 1m away from the crest of the slope. For the locally loaded soil nailed slope, two different models are developed. In the first model, a very good nail head is simulated by a thin elastic plate and the nail is fixed on the nail head. There is no nail head failure in this model failure and the FOS and slip surface for different curvature are shown in Figure 6.11. In the second model, no nail head is simulated, so only the bond stress within the soil mass is mobilized and the FOS and slip surface for different curvature are shown in Figure 6.12. For the first model, the FOS has an obvious increase (Figure 6.11) compared with that for an unreinforced slope (Figure 4.24). For the second model which is a typical face failure, the increasing of FOS is very small (Figure 6.12) compared with an unreinforced slope (Figure 4.24). This example shows that a good nail head design is very important in practice. In both

the models, the effect of the curvature is not obvious for convex slope but is more obvious for concave slope.

The nail maximum tension force distribution is shown in Figures 6.13 to 6.19. For slope with no loading, the nail force of the bottom row is more mobilized (Figures 6.13 and 6.14). For convex slope, the nail force in a certain row is smaller at the slope intersection area, since in this area the nail density is a slightly larger because of the nail overlapping from both sides of the slope. For slope with loading (Figures 6.15 to 6.19), the nail force in the top and middle rows is much more mobilized, especially for the face failure situation in which the nail head is not simulated.

For un-reinforced slopes, it has been shown in chapter 4 that the curvature has little influence on the stability of normal convex slopes, but has distinct effect on the steep convex slope with local loading. In this chapter, it is shown in above that the effect of curvature can also be ignored for normal convex slope reinforced with nail. In order to examine the influence of curvature on steep convex slope with soil nails, the vertical cut model analyzed in chapter 4 (Figure 4.26) is investigated again, and the soil nails are installed in the model. The slope geometry and applied loading is the same as Figure 4.26. The nails are installed at 1.5m centers horizontally and vertically. Two different situations are considered. In the first situation, the nail head is simulated by thin elastic plate, and the failure is pullout failure (Figure 6.20). In the second situation, no nail head is simulated, and the failure is face failure (Figure 6.21). Compared with the un-reinforced slope (Figure 4.26), the factor of safety has an obvious increase in the first situation and has only a slight increase in the second situation. Both situations show that the curvature has distinct effect on the stability of this locally loaded vertical cut slope reinforced with nails, and the factor of safety is smaller for the convex slope model.

Based on the above analysis, the intersected slope reinforcement design should be as follows. For the concave intersection part, less reinforcement can be used as the effect of curvature can improve the slope stability. For the convex intersection part, if the slope is not steep, the reinforcement design can be the same as a plane slope, but if the slope is steep, more reinforcement should be used. When soil nail is used to reinforce intersected slope, even though the same soil nail design is used at the convex part, since there is some overlapping of the nail from the two intersected faces, the actual nail density at this part is slightly larger which will enhance the slope stability, but the improvement should be determined by a detailed analysis according to the situation in practice.

6.5 Some small scale model testing results

In recent years, some small scale tests are conducted in the laboratory of the Hong Kong Polytechnic University to investigate the effect of curvature and the soil nail performance. Three model tests have been conducted by Tsui (2007), and the results of these tests can be used to illustrate some of the numerical results in this chapter. These model slopes are relatively steep with a 65° slope angle and slope height is 0.8m. The first test is about a soil nailed intersected convex slope. The second test is a soil nailed slope with no curvature. The third test is a plane slope with no soil nail. In all these tests, the load is applied with a 130 mm offset from crest of the slope, and the load is increased gradually until the slope fails.

For the two soil nailed slopes, a good nail head is not constructed, so the soil nail is not pulled out and a face failure is mobilized where the bond stress within the soil mass is effective in the stabilization. The slope failure surfaces for different models are shown in Figure 6.22. For the weight of the failure mass, it is about 125kg in the Test 1, 194kg

in the Test 2 while it is about 382kg in the Test 3. For the maximum load, it is about 26kN in Test 1, 44.2kN in Test 2 while it is 35kN in Test 3.

For soil nailed slope, the maximum load for the convex slope is smaller than the one for the plane slope, and the sliding mass is also smaller. This shows that for steep slope, a convex slope is less safe than a plane slope under local loading which verifies the numerical simulation results of the vertical cut slope presented in the previous section. For the two slopes with no curvature, the maximum load for soil nailed slope is larger than the one for unreinfirced slope, but the sliding mass is smaller. It means that the soil nail has improved the safety of the slope.

6.6 Discussion and Conclusion

For a soil nailed slope without external load, the nail force of the bottom row is usually more mobilized at the limit state. For locally loaded soil nailed slopes, the nail force of the top row gets more mobilized as the movement of the top part of the slope is larger.

For the idealized curvature slope, it has been shown in chapter 4 that the curvature has no major effect on the location of the slip surface of unreinforced slope. When soil nail is included in the slope, the slip surface is influenced by the curvature, especially for concave slope. When the radius is smaller for concave slope, the slip surface is shallower.

The curvature does not have any noticeable effect on the factor of safety for normal convex slopes. When local loading is applied on the top of convex slope and if the slope is steep, the effect of curvature will be obvious and the FOS of convex slope gets smaller, and this phenomenon is similar with the result for un-reinforced slopes in

chapter 4. The present analysis also shows that a good nail head design is very important in practice.

Based on the above analysis, the intersected slope reinforcement design should be as follows. For the concave intersection part, less reinforcement can be used as the effect of curvature can improve the slope stability. For the convex intersection part, if the slope is not steep, the reinforcement design can be the same as that for an unreinforced slope. If the slope is steep, more reinforcement should be used. When soil nail is used to reinforce intersected slope, even though the same soil nail design is used at the convex part, since there is some overlapping of the nail from the two intersected faces, the actual nail density at this part is slightly larger which will further enhance the slope stability, but the actual contribution to the slope stability should be determined by a detailed analysis according to the situation in practice.

The physical model tests also show that for a steep slope, the convex slope is less safe than a plane slope under local loading.

Table 6.1 Variation of FOS respect to curvature (nail 10m, no load)

Radius of curvature (m)	17	35	∞ (plane)
Concave(SRM)	2.48	2.14	1.92
Convex(SRM)	1.97	1.92	1.92

Table 6.2 Variation of FOS respect to curvature (nail 10m, with 4m width load 100kPa)

Radius of curvature (m)	17	35	∞ (plane)
Concave(SRM)	1.57	1.46	1.39
Convex(SRM)	1.47	1.40	1.39

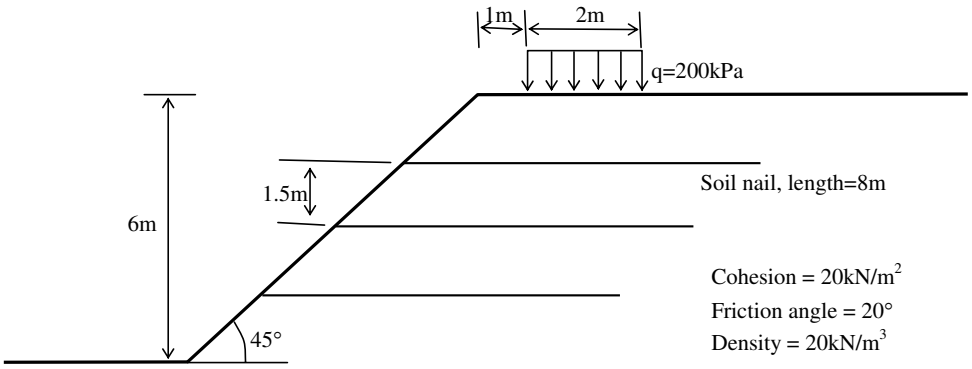

Figure 6.1 The geometry of the slope under local loading

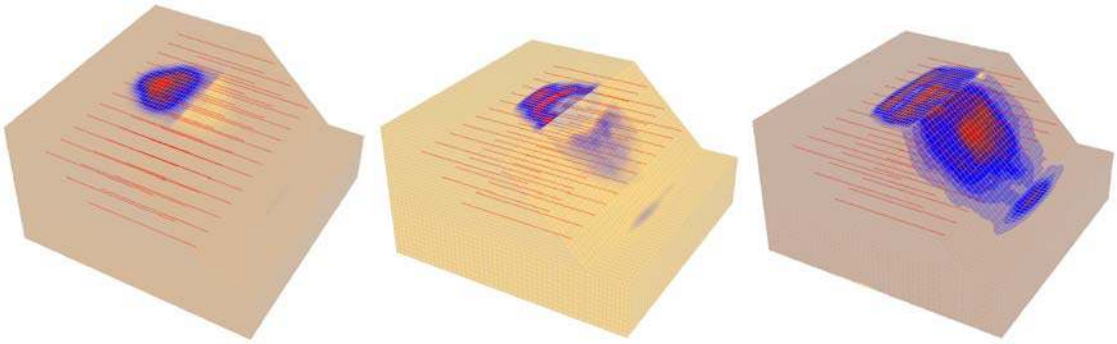

(a) L/B=1, FOS=1.61 (b) L/B=2, FOS=1.36 (c) L/B=4, FOS=1.17

Figure 6.2 The slip surface for different loading length when B=2m (nail 8m, load=200kPa)

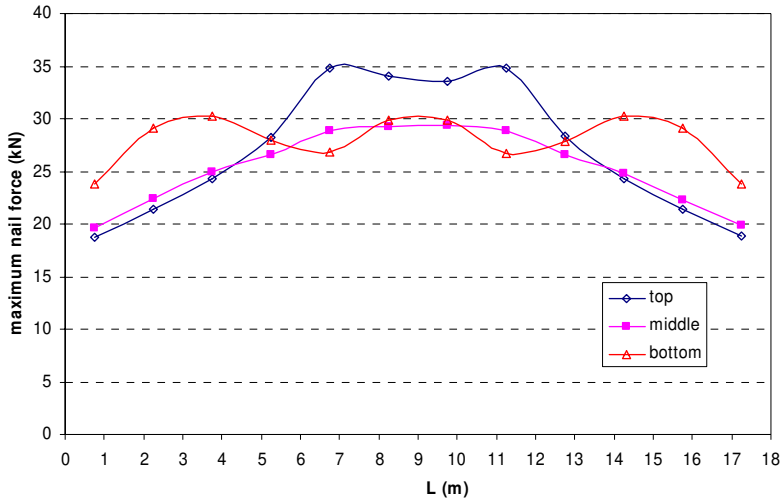

Figure 6.3 Nail maximum tension force distribution for L/B=1

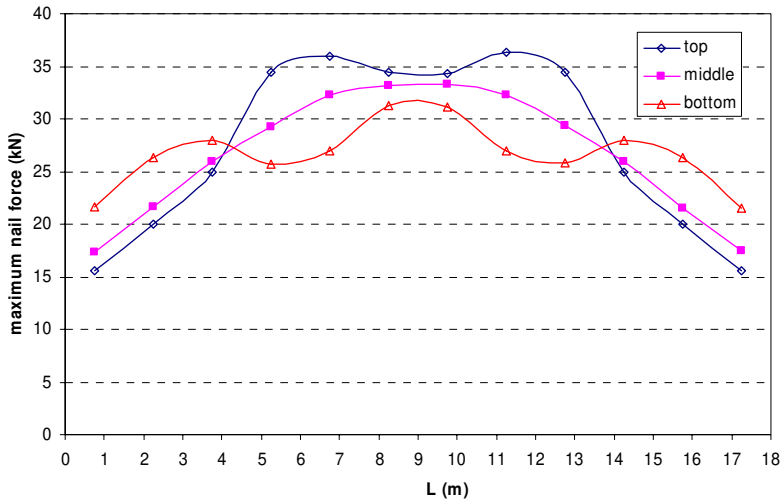

Figure 6.4 Nail maximum tension force distribution for L/B=2

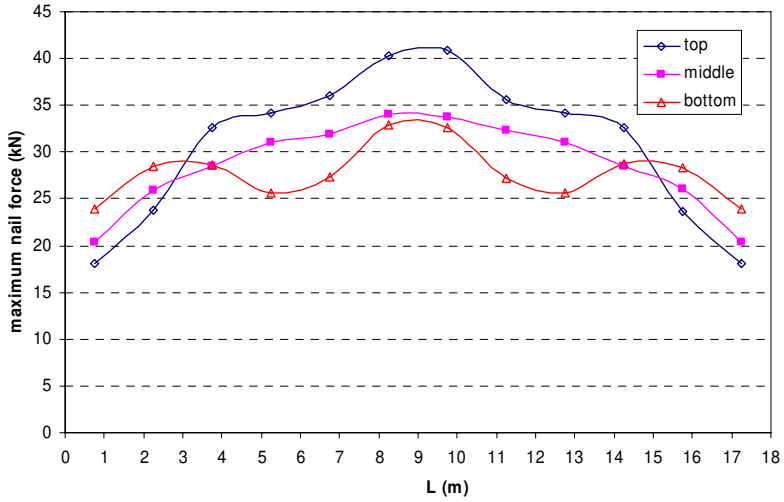

Figure 6.5 Nail maximum tension force distribution for L/B=4

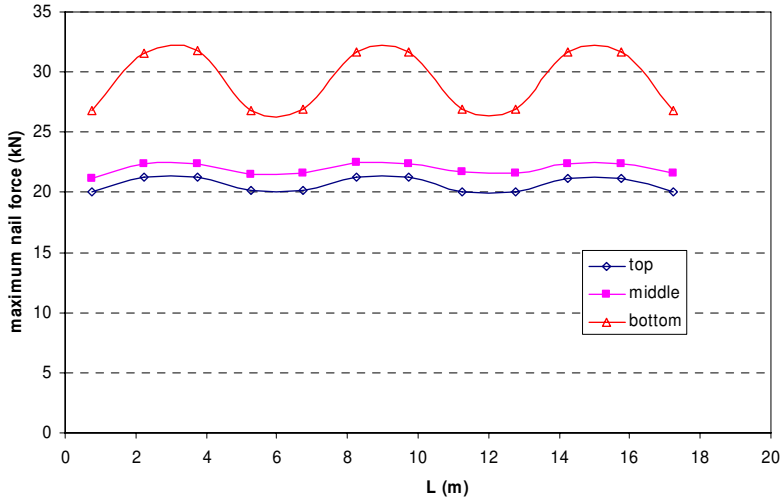

Figure 6.6 Nail maximum tension force distribution with no loading (FOS=1.94)

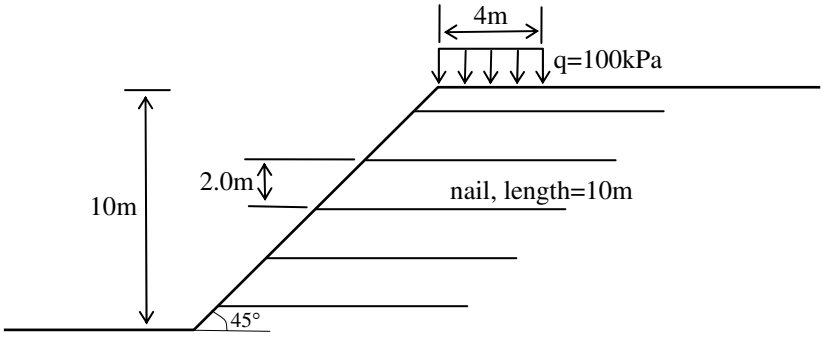

Figure 6.7 The geometry of the slope section

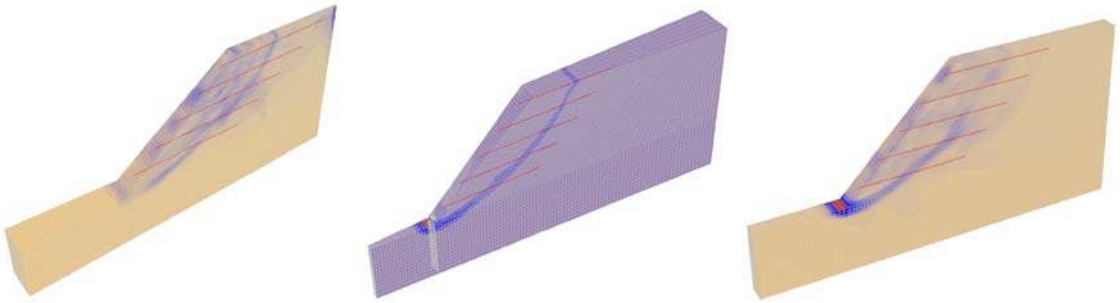

(a) convex (b) concave (c) plane

Figure 6.8 Mesh plot of concave and convex models reinforced with nails

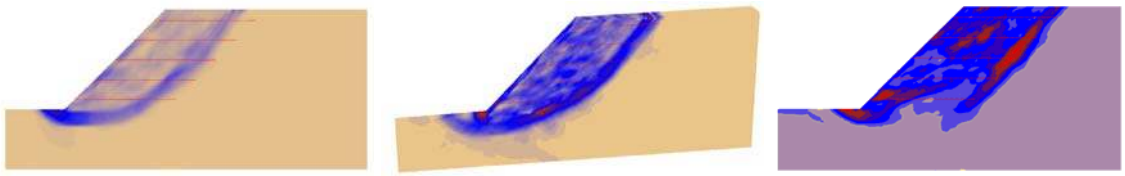

(a) concave, r=17m (b) concave, r=35m (c) plane, r=∞

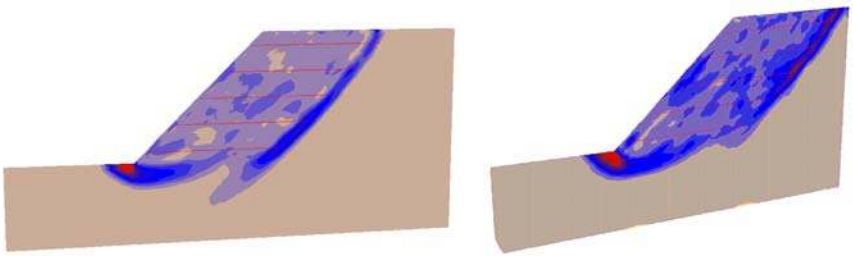

(d) convex, r=35m (e) convex, r=17m

Figure 6.9 Slip surfaces at different curvatures (with nail, no load)

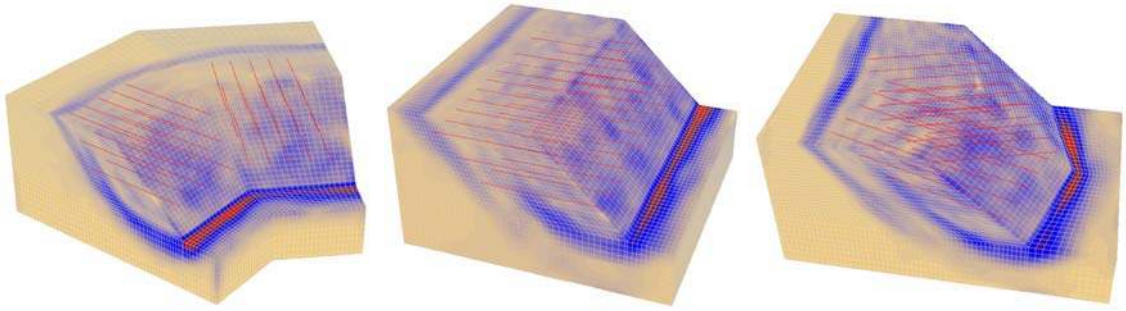

(a) 135° concave, FOS=2.08 (b) no curvature, FOS=1.94 (c) 145° convex, FOS=1.93

Figure 6.10 Slip surfaces for different curvatures with 200kPa loading (no load, nail 8m)

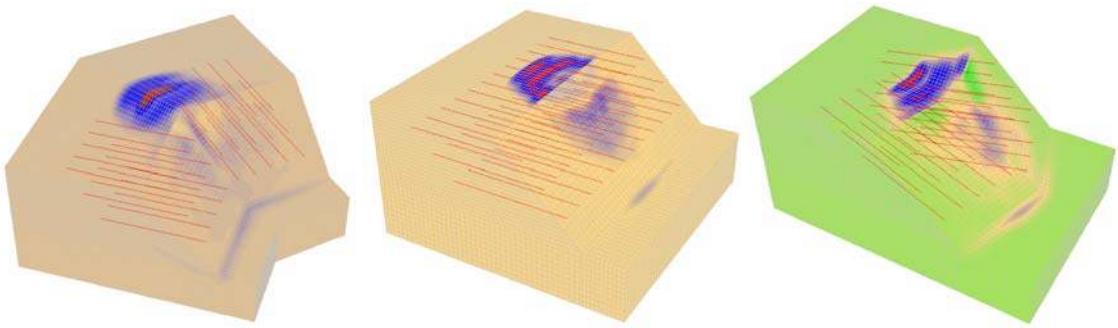

(a) 135° concave, FOS=1.59 (b) no curvature, FOS=1.36 (c) 145° convex, FOS=1.40

Figure 6.11 Slip surfaces for different curvatures with 200kPa loading (nail 8m, pullout failure)

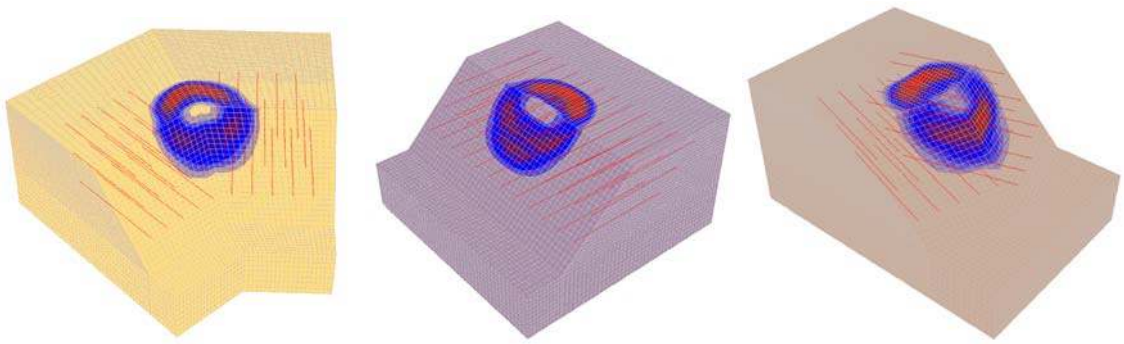

(a) 135° concave, FOS=1.39 (b) no curvature, FOS=1.23 (c) 145° convex, FOS=1.27

Figure 6.12 Slip surfaces for different curvatures with 200kPa loading (nail 8m, face failure)

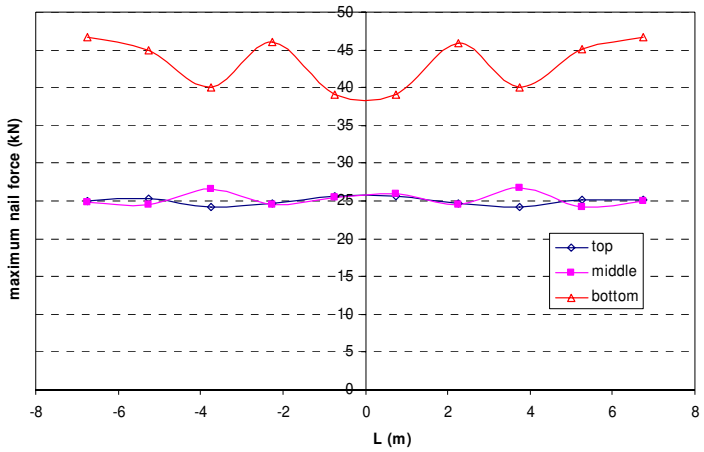

Figure 6.13 Nail maximum tension force distribution for a 135° concave slope with no loading

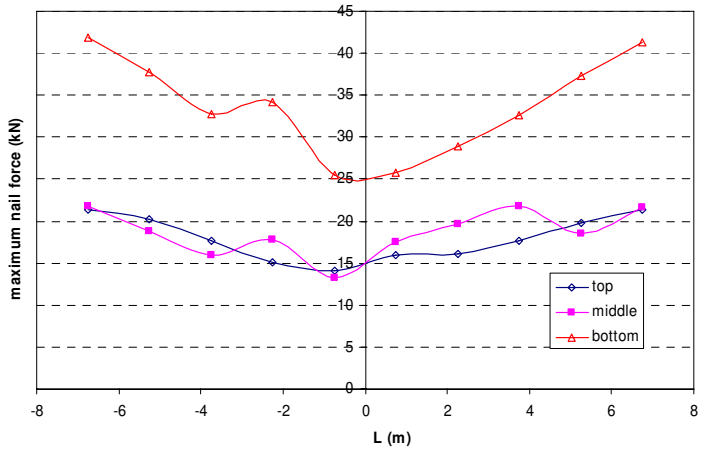

Figure 6.14 Nail maximum tension force distribution for a 145° convex slope with no loading

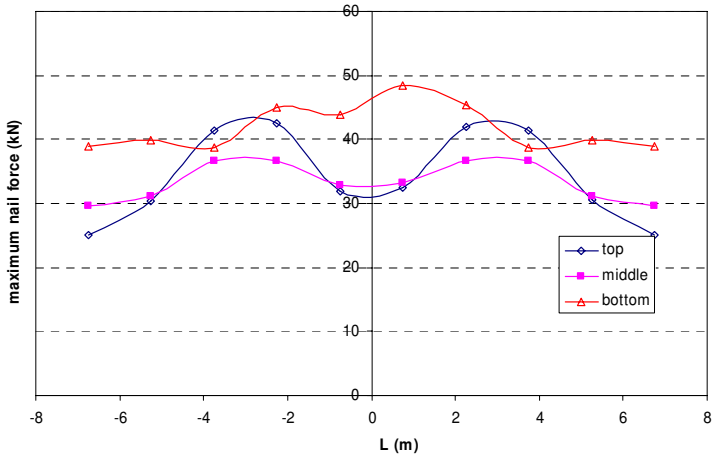

Figure 6.15 Nail maximum tension force distribution for a 135° concave slope with 200kPa loading

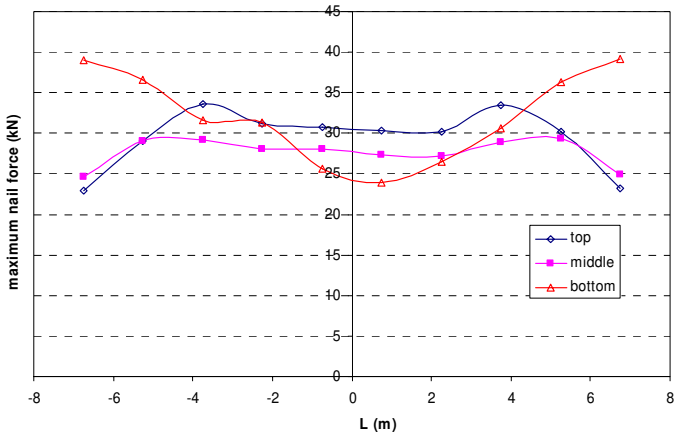

Figure 6.16 Nail maximum tension force distribution for a 145° convex slope with 200kPa loading

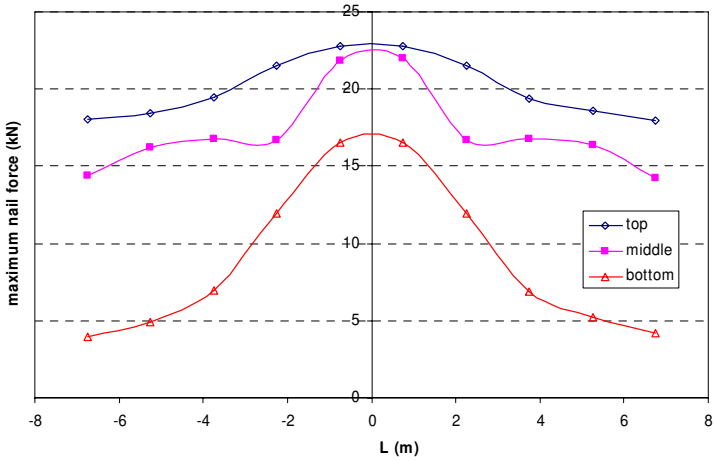

Figure 6.17 Nail maximum tension force distribution for a 135° concave slope with 200kPa loading (face failure)

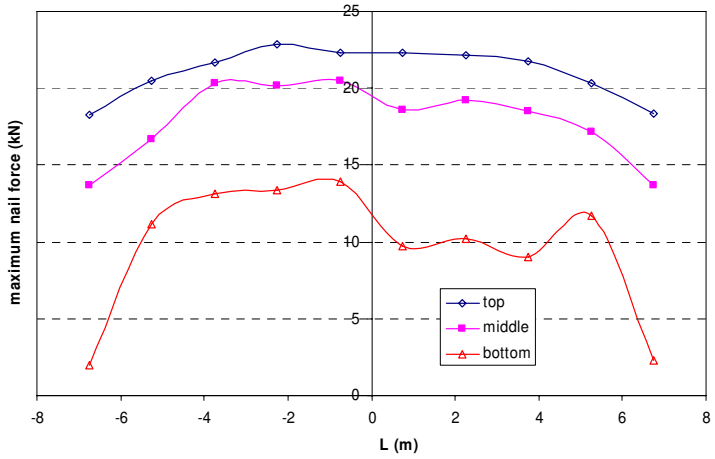

Figure 6.18 Nail maximum tension force distribution for a 145° convex slope with 200kpa loading (face failure)

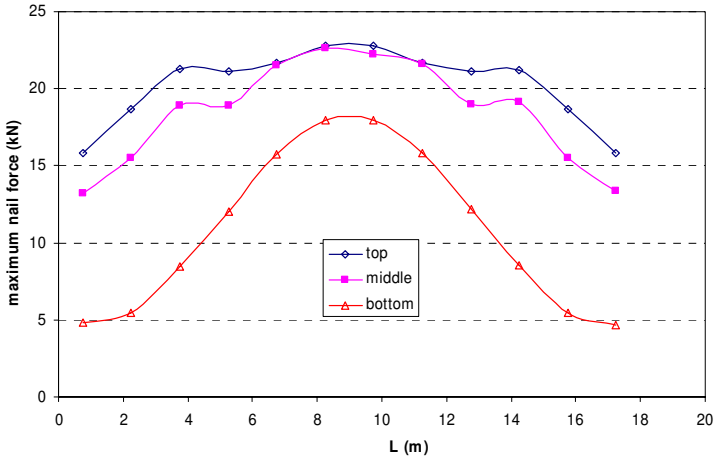

Figure 6.19 Nail maximum tension force distribution for a no curvature slope with 200kpa loading (face failure)

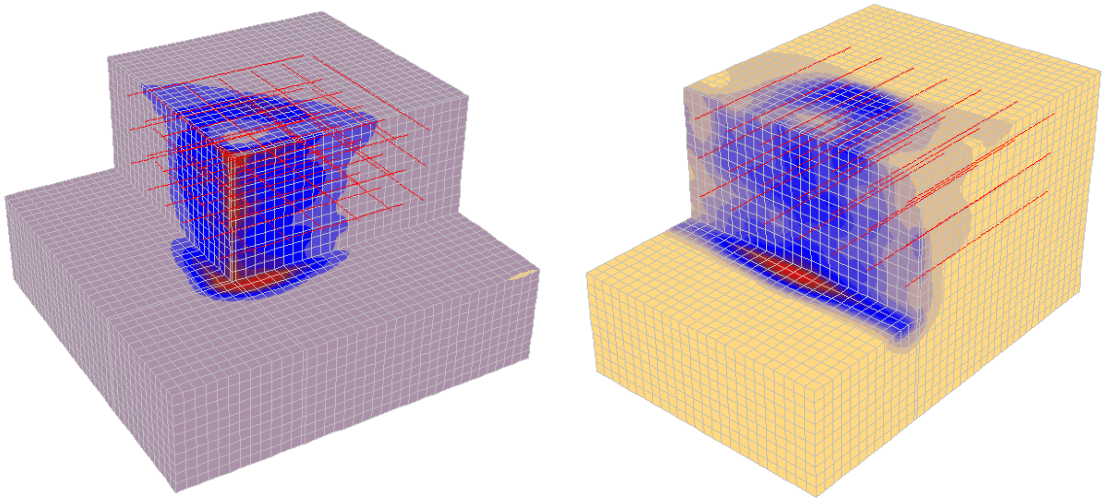

(a) convex, FOS=1.61 (b) plane, FOS=1.79

Figure 6.20 Slip surface of vertical cut slope with 3m long and 3m wide 50kPa loading (pullout failure)

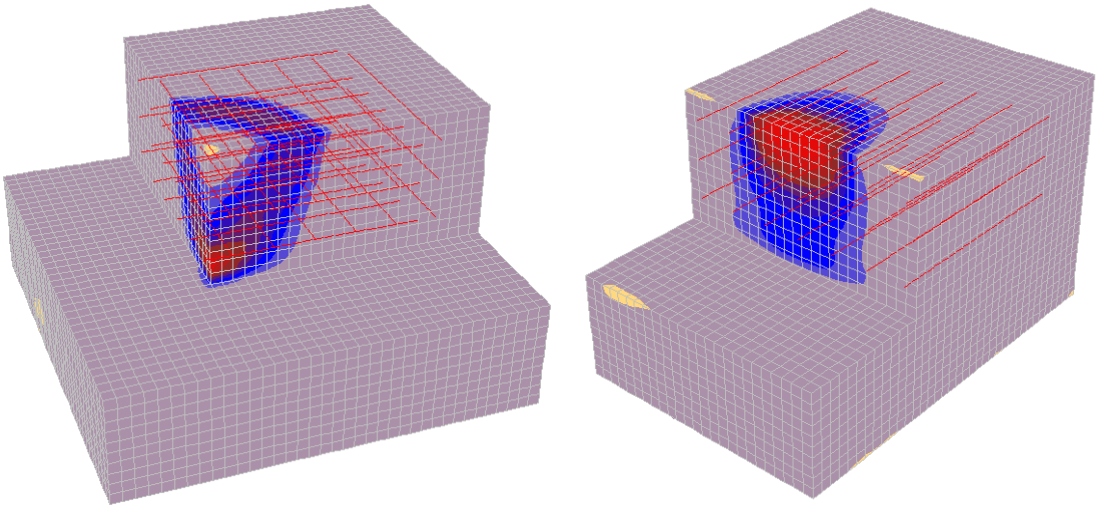

(a) convex, FOS=1.01 (b) plane, FOS=1.33

Figure 6.21 Slip surface of vertical cut slope with 3m long and 3m wide 50kPa loading (face failure)

(a) test 1, soil nailed convex slope

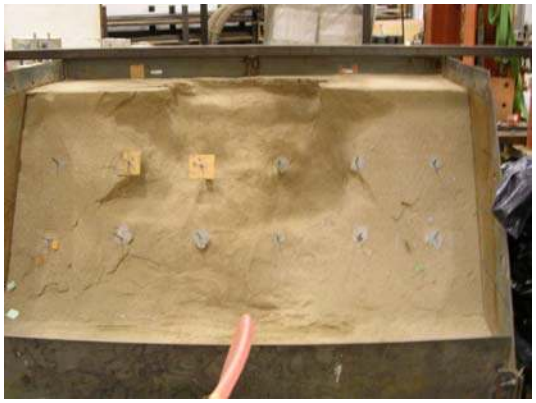

(b) test 2, soil nailed no curvature slope

(c) test 3, non soil nailed no curvature slope

Figure 6.22 Different failure shapes after failure mass was removed (after Tsui, 2007)

CHAPTER 7: STRENGTH REDUCTION ANALYSIS FOR SLOPE REINFORCED WITH ONE ROW OF PILES

7.1 Introduction

It is an effective solution to increase slope stability by installing piles. The piles used in slope stabilization are considered as passive piles because they are usually subjected to lateral force arising from the horizontal movements of the surrounding soil. The interaction between the passive piles and the soil is complicated, as the lateral forces exerting on the piles are related to the soil movements which are in turn influenced by the presence of the piles. A number of methods have been proposed to evaluate the performance and design of the piled slopes. These methods include limit equilibrium method, limit analysis method, strength reduction method, and others. Due to the complicated interaction between soil and pile, even though some limit equilibrium methods are employed for piled slope analysis, they are still not widely accepted by engineers. In this study, the strength reduction method will hence be used to conduct the piled slope analysis by software FLAC3D.

The shear strength reduction method has been used by Cai and Ugai (2000) for the analysis of slopes reinforced by one row of piles. Won et al. (2005) have also analyzed the same slope by Cai and Ugai (2000) using the three-dimensional finite difference code FLAC3D by the SRM. In the piled slope analysis by Won et al. (2005) and Cai and Ugai (2000), the location of the slip surface was determine by the maximum shear force in the pile so that a very deep slip surface was determined while the maximum shear strain in soil was not considered. In the present study, slip surface will be

determined by the shear strain rate and the failure mode is determined with respect to different pile spacing. It is found that the pile spacing has a major influence on the failure mode, and a more realistic slip surface is found from the present study. The upper and lower bounds of the factor of safety and the optimum pile location will also be discussed in the present study.

7.2 Failure mode of slopes with different pile spacing

For the slope considered by Won et al. (2005) and Cai and Ugai (2000), it is 10m in height with a gradient of 1V:1.5H (Figure 7.1). Two symmetric extreme boundaries are used so that the problem consists of a row of piles with a plane of symmetry. Steel tube pile with an outer diameter (D) of 0.8m is used in this study. The piles are treated as a linear elastic solid material and are installed in the middle of the slope with L_x=7.5m and center-to-center spacing (s) varies from 2D to 8D. The piles are embedded and fixed into the bedrock or a stable layer (infinite pile length assumption). In this model, the pile head is free. The cohesive strength, friction angle, elastic modulus, Poisson ratio and density of the soil are 10kPa, 20°, 200MPa, 0.25, and 20kN/m^3 respectively. The elastic modulus and Poisson ratio of the piles are 60000MPa and 0.2 respectively.

When the slope is not reinforced with piles, the factor of safety by the SRM is 1.20 and the slip surface is shown in Figure 7.2. The slip surfaces and the factors of safety for different pile spacing are shown in Figures 7.3 to 7.8. It is reasonable that the factor of safety decreases with the increase of pile spacing. In Figures 7.3 to 7.8, the slip surfaces through different sections are shown (section y=0 is the plane through pile centerline; section y=0.4 is the plane tangent to the pile outer surface; and for the section through soil midway between piles, y varies from 0.8 to 3.2 with respect to pile spacing varies from 2D to 8D). When s=2D (Figure 7.3), the slip surface is clearly divided into two

parts even at the section through the soil midway between the piles. When the section varies from the plane through the pile centerline to the plane through the soil midway between the piles, the shear strain in the soil gets more mobilized. When s=3D (Figure 7.4), the slip surface near the pile is still clearly divided into two parts. The slip surfaces at the section through the soil midway between the piles are slightly connected, but the overall slip surface is still nearly divided into two parts. When the pile spacing increases from 4D to 6D (Figures 7.5 to 7.7), the slip surface at the sections near the pile is also divided into two parts due to the presence of the piles, but the two parts of slip surfaces gets deeper near the pile location, so there is a clear shear strain mobilization at the interface of the pile-soil in the vertical direction. The slip surface at the section through the soil midway between the piles gets more connected and deeper, and at the connection of the two parts of the slip surfaces, there is clear shear strain mobilization in the vertical direction. When the pile spacing increases to 8D (Figure 7.8), the slip surface at the section through the soil midway between the piles is clearly one single slip surface, though the slip surface at the sections near the pile is still divided into two parts due to the presence of the piles. For a section which is not far from the pile, for example y=1.0 (Figure 7.8d), a clear shear strain mobilization in the vertical direction is also found at the pile location. When the section is far enough from the pile, for example y=1.8 (Figure 7.8e), the vertical shear strain mobilization at the slip surface center disappears.

The slip surfaces at the section through the soil midway between the piles are compared for different pile spacing in Figure 7.9 (slip surface can be seen easily from the shear strain mobilization and are also shown in dashed lines). The slip surface for the slope with no pile is shown by the solid line. When the pile spacing is small, the slip surface is shallow and is nearly divided into two parts. With the increase in pile spacing, the slip

surface gets deeper and the two parts of the slip surface gets more connected. When the pile spacing is large enough, the two parts of the slip surface gradually merge to a clear single slip surface which is nearly the same as the slip surface for unreinforced slope. This means that the slip surface of a piled slope is usually shallower than that with no pile, and this result is totally different from that by Won et al. (2005) and Cai and Ugai (2000) who obtained a very deep slip surface for piled slopes based on the maximum shear force in the pile (Figure 7.10). The shear force distribution for pile spacing equal to 3D is shown in Figure 7.11. It is clearly seen that the location of the maximum shear force is very deep and is far away from the real slip surface, therefore, the maximum shear force location is not necessarily the location of the critical slip surface for a piled slope.

7.3 Upper and lower bound of the factor of safety

Identifying the upper and lower bounds of the factor of safety is very useful and important before the detailed design of a pile supported slope. The factor of safety for slopes with no pile can be taken as the lower bound, while the FOS for a slope with a pile wall can be taken as the upper bound. For the slope model analyzed in the previous section, the lower and upper bounds of the FOS are 1.20 (Figure 7.2) and 1.89 (Figure 7.12) respectively. The FOS for different pile spacing is shown in Table 7.1.

Based on the above study, a very simple approach for the piled slope SRM analysis is proposed before conducting a detailed design. Firstly, a slope with no pile and with a pile wall is analyzed to determine the lower and upper bounds of the factor of safety. For these two cases, only a 2D analysis will be required and this will save significant time and effort. Secondly, the upper bound solution is actually equivalent to the case of s=D, while the lower bound is equivalent to s=∞. The general curve of the safety factor

variation with respect to spacing is shown in Figure 7.13a. When s/D increases from 1 to infinity, the factor of safety will decrease from the upper bound to the lower bound. The FOS usually decreases quicker when the spacing is relatively small and becomes gradual when the spacing is large. In practice, the pile spacing will not be very large, therefore, we only need to consider the range for relatively small spacing. Although the decrease of the FOS from the upper bound to the lower bound is not easy to predict for a general problem, at the preliminary design, we can assume the FOS decreases linearly from the upper bound to the lower bound when the spacing increases from 1D to X times D (shown in Figure 7.13a). For the example analyzed above, when X equals to 10 or 12, a good approximate prediction can be obtained by a simple interpolation (the result is shown in Figure 7.13b for X=12). The X value in the range of 10 to 14 is recommended after a serious of different case studies. According to the proposed approach, an approximate pile spacing can be determined and fine tune of the spacing by a detailed 3D analysis can be conducted afterwards.

7.4 Optimization of the pile position

In piled slopes, the position of the pile is very important and its effect has been discussed by Won et al. (2005) and Cai and Ugai (2000), who came to the same conclusion that the improvement of the slope stability will be largest when the piles are located in the middle of the slopes. In general, the optimal position should also be dependent on the s/D ratio, but it is found that the optimum pile location is not sensitive to this ratio based on a series of trials. For simplicity, the situation of a pile wall (s=D) will be used to conduct the pile position optimization since this 2D analysis is a time saving analysis (3D SRM is extremely time consuming in the analysis and some problems takes 2-3 weeks by a Pentium 4 for the analysis). As shown in Figure 7.12, if a pile wall is installed in the middle of the slope, the slip surface is nearly divided into

two equal parts (actually when the pile spacing is very small, for example s=2D, the slip surface is also divided into two parts). If the two equal half do not interfere with each other, the two local factors of safety will be identical and the overall factor of safety will be the optimum as proposed by Won et al. (2005) and Cai and Ugai (2000). It is however found that the two half of soil mass interfere with each other so that there is some small difference between the lower and upper parts. As shown in Figure 7.12, the slip surface is divided into two parts, but the shear strain in the upper part is slightly more mobilized at the limit state. This means that the factor of safety for the upper part is lower than that for the lower part, and the overall FOS of the slope will be controlled by the upper part of the slip surface. In order to compare the safety of the lower and upper parts, two additional models are developed. In the first model, the shear strength of the soil at the upper part of the pile is increased to a very large value, so slope failure will occurs only at the lower part and the FOS is 1.94 (Figure 7.14). In the second model, the shear strength of the soil at the lower part of the pile is increased to a very large value, so slope failure will occur only at the upper part and the FOS is 1.87 (Figure 7.15). It can be seen that the FOS of the lower part is a little larger than the upper part, but the difference is not large. If the pile position is 0.2m above the middle of the slope, the factors of safety of the lower part and the upper part are both 1.91 (Figure 7.16) which will be the optimal solution. This means that the optimal pile position for this slope model is 0.2m above the middle of the slope.

For the optimal location of the piles, Poulos (1995) has proposed another guideline where the piles are installed around the center of the critical slip surface to avoid shifting the slip surface either in front of or behind the piles. For the slope model analyzed above, the slip surface with no pile is shown in Figure 7.17 and it is compared with the optimized pile location. It can be seen that the exact optimized pile location lies

between the middle of the slope and the middle of the slip surface of the slope with no pile, but it is much closer to the middle of the slope.

In order to get more insight into this issue, another slope model with different soil property is analyzed. The soil cohesion and friction angle are 20kPa and 10 degree respectively for this model. The FOS is 1.14 for this slope with no pile and the slip surface (Figure 7.18) is much deeper than the previous slope model. For this model, if the pile is installed at the middle of the slope, the FOS is 2.22 and the slip surface is shown in Figure 7.19a. It can be seen that obvious shear strain is mobilized only at the upper part. This means the lower part is much safer than the upper part which is also verified by Figure 7.19b (FOS is 2.48 for the lower part) and Figure 7.19c (FOS is 2.16 for the upper part). If the pile is installed 0.55m towards the crest of the slope (Figure 7.20), the FOS of the lower part (2.32) is nearly the same as the upper part (2.33). The optimized pile position is shown in Figure 7.21, which also lies between the middle of the slope and the middle of the slip surface of the slope with no pile, but it is still much closer to the middle of the slope. The optimal pile position for the above two models are both at some distance towards the crest of the slope as measured from the middle of the slope, and it is interesting that this distance for both models are nearly one sixth of the interval between the center of the slope and the center of the slip surface.

Based on the above analysis, the main conclusions are as follows. For slopes reinforced with one row of piles, the optimal pile position lies between the middle of slope and the middle of the slip surface of the slope with no pile, and is very close to the middle of the slope. For slopes with sandy soil (soil cohesion is small but friction angle is large), the slip surface is shallow and the upper end of the slip surface is very close to the slope crest. The middle of the slip surface will also be close to the middle of the slope, and the

optimal pile position is nearly located at the middle of the sandy soil slope. For slopes with clayey soil (soil cohesion is large but friction angle is small), the slip surface is deep and the upper end of the slip surface is far away from the slope crest, so the middle of the slip surface is also far away from the middle of the slope while the optimal pile position will be slightly more away from the middle of the slope.

7.5 Conclusion

For slopes reinforced with one row of piles, when the pile spacing is small, the slip surface is shallow and is nearly divided into two parts. With the increase in the pile spacing, the slip surface becomes deeper and the two parts of slip surface become more connected. When the pile spacing is large enough, the two parts of the slip surface gradually turn into a clear single slip surface which is nearly the same as the slip surface with no pile. This means that the slip surface of the piled slope is usually shallower than that of a slope with no pile. This result is totally different from the results based on the maximum point of shear force by which a very deep slip surface for the piled slope is usually obtained. The present study has revealed that the maximum point of shear force is very deep and is far away from the real slip surface, therefore, the pile maximum shear force location is not necessarily the location of the critical slip surface of a piled slope.

It is extremely time-consuming to carry out a detailed 3D piled slope analysis, and lots of time has been spent in carrying out the analysis for the present study. For practical analysis and design, a useful guideline to the engineers has been proposed in this study. The upper and lower bounds of the factor of safety can be determined easily by a 2D analysis and they are useful for the preliminary design before conducting a detailed 3D

analysis and design. Based on the guideline as shown in Figure 7.13, an economical design can be obtained without tedious efforts in finding an optimal pile spacing.

The optimal pile position for a slope reinforced with one row of piles is found to lie between the middle of slope and the middle of slip surface of the slope with no pile. The precise location is usually very closer to the middle of the slope. For slopes with sandy soil, the optimal pile position will be nearly located at the middle of the slope so that the middle of the slope can be chosen for the optimum design. For slope with clayey soil, the exact optimal pile position is usually located slightly towards the crest of the slope instead of being located at the middle of the slope.

Table 7.1 Factor of safety with different pile spacing

pile spacing	pile wall (s=D)	s=2D	s=3D	s=4D	s=5D	s=6D	s=8D	No pile (s=∞)
FOS	1.89 (upper bound)	1.78	1.72	1.61	1.55	1.52	1.42	1.20 (lower bound)

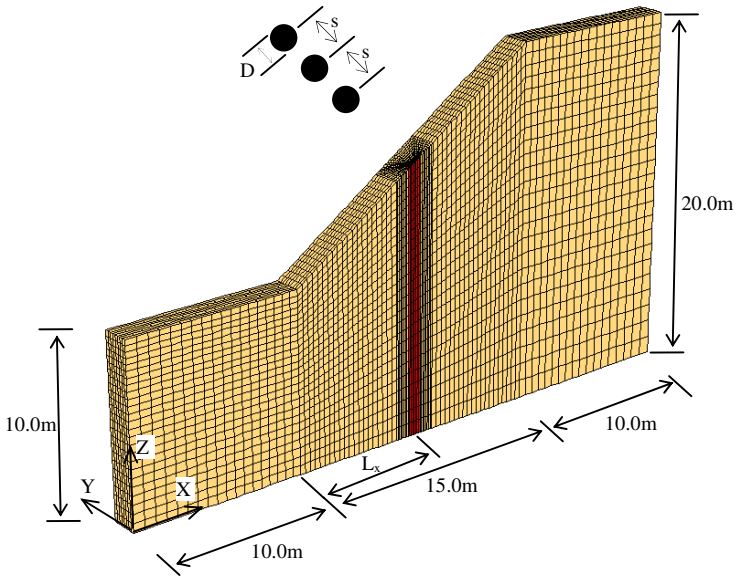

Figure 7.1 Slope model and finite difference mesh

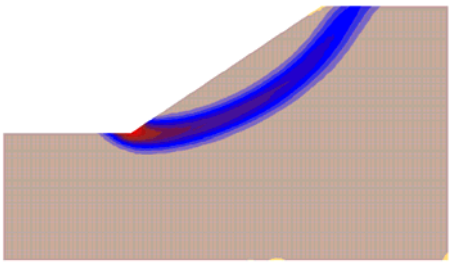

Figure 7.2 Slip surface of the slope with no pile (FOS=1.20)

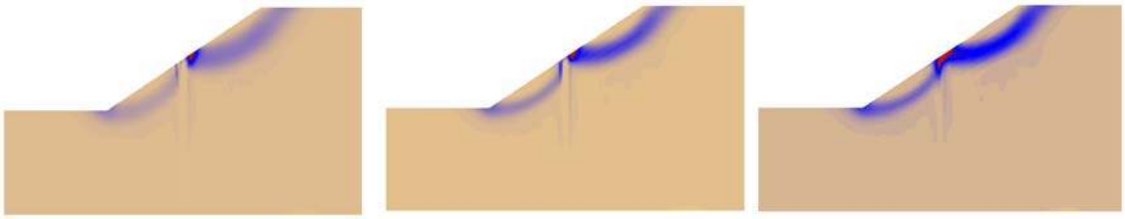

(a) y=0, through pile centerline (b) y=0.2 (c) y=0.4

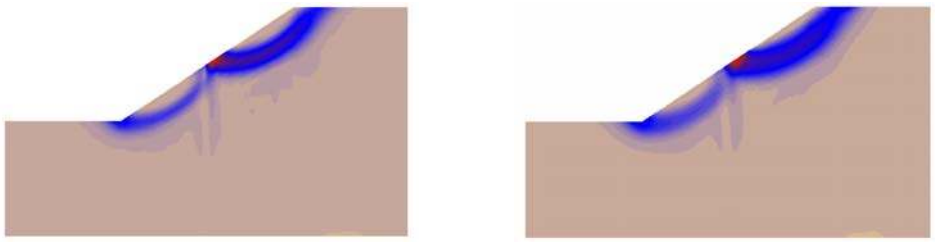

(d) y=0.6 (e) y=0.8, through soil midway between piles

Figure 7.3 Slip surface at different sections for s=2D (FOS=1.78)

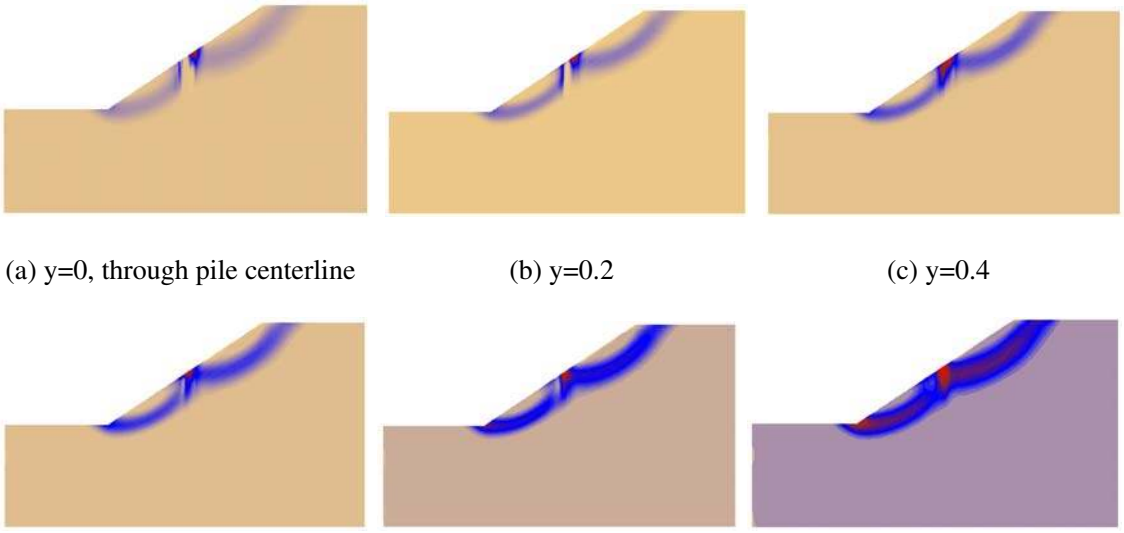

(a) y=0, through pile centerline (b) y=0.2 (c) y=0.4

(d) y=0.6 (e) y=0.8 (f) y=1.2, midway through soil

Figure 7.4 Slip surface at different sections for s=3D (FOS=1.72)

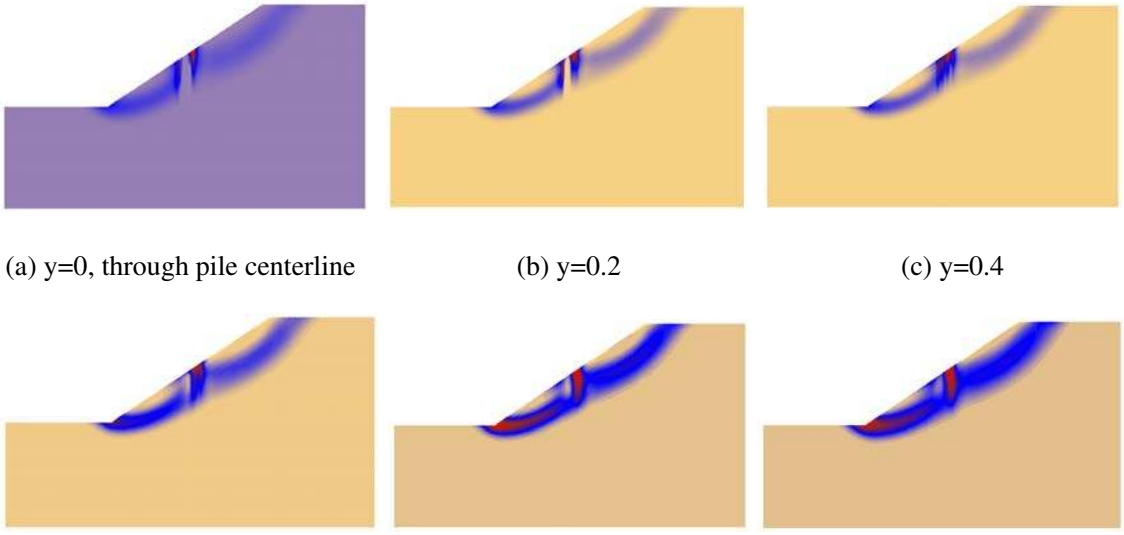

(a) y=0, through pile centerline (b) y=0.2 (c) y=0.4

(d) y=0.8 (e) y=1.2 (f) y=1.6, midway through soil

Figure 7.5 Slip surface at different sections for s=4D (FOS=1.61)

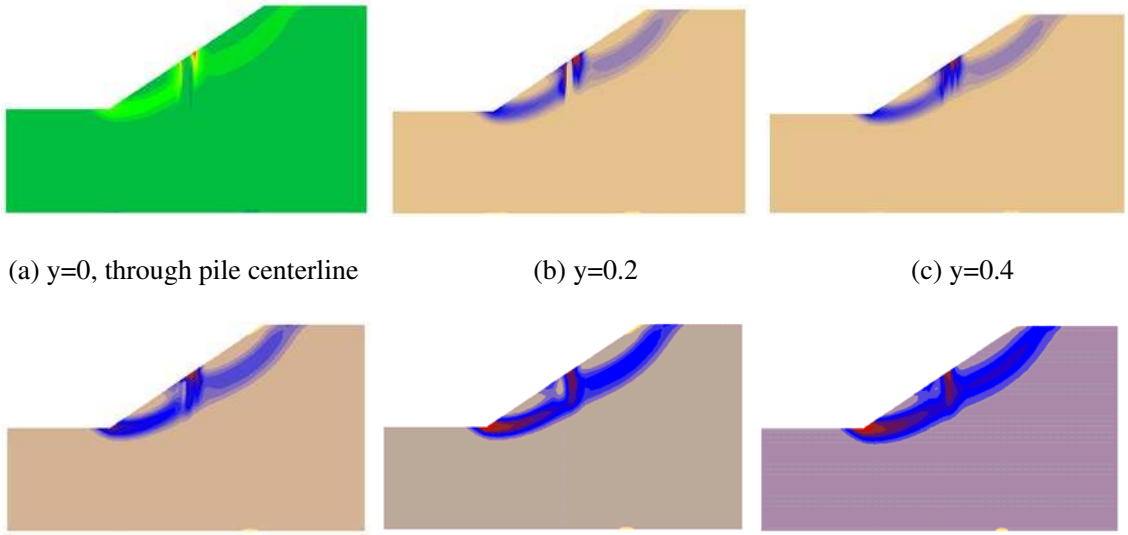

(a) y=0, through pile centerline (b) y=0.2 (c) y=0.4

(d) y=0.8 (e) y=1.4 (f) y=2.0, midway through soil

Figure 7.6 Slip surface at different sections for s=5D (FOS=1.55)

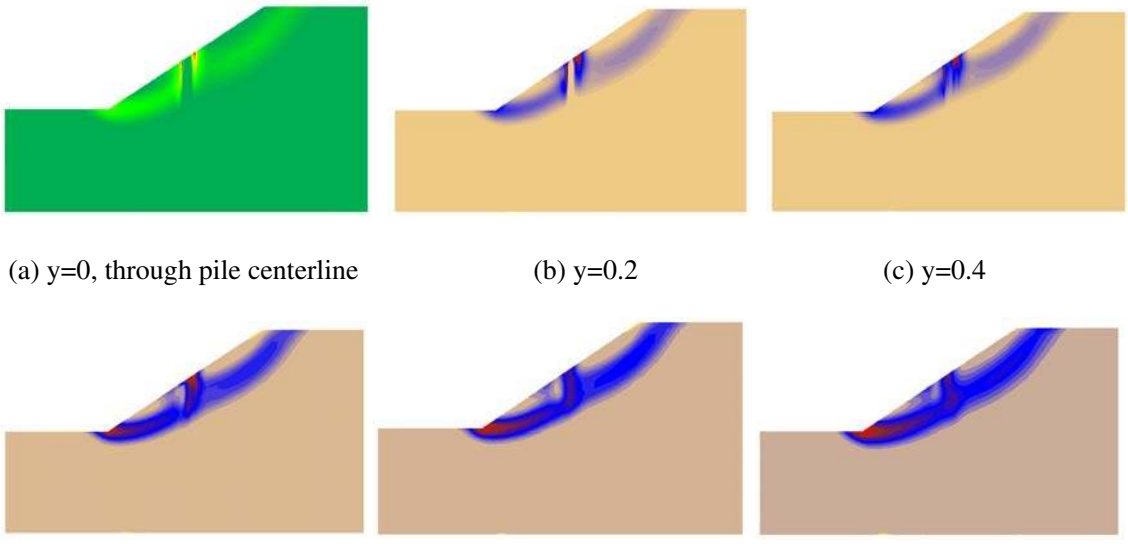

(a) y=0, through pile centerline (b) y=0.2 (c) y=0.4

(d) y=1.0 (e) y=1.6 (f) y=2.4, midway through soil

Figure 7.7 Slip surface at different sections for s=6D (FOS=1.52)

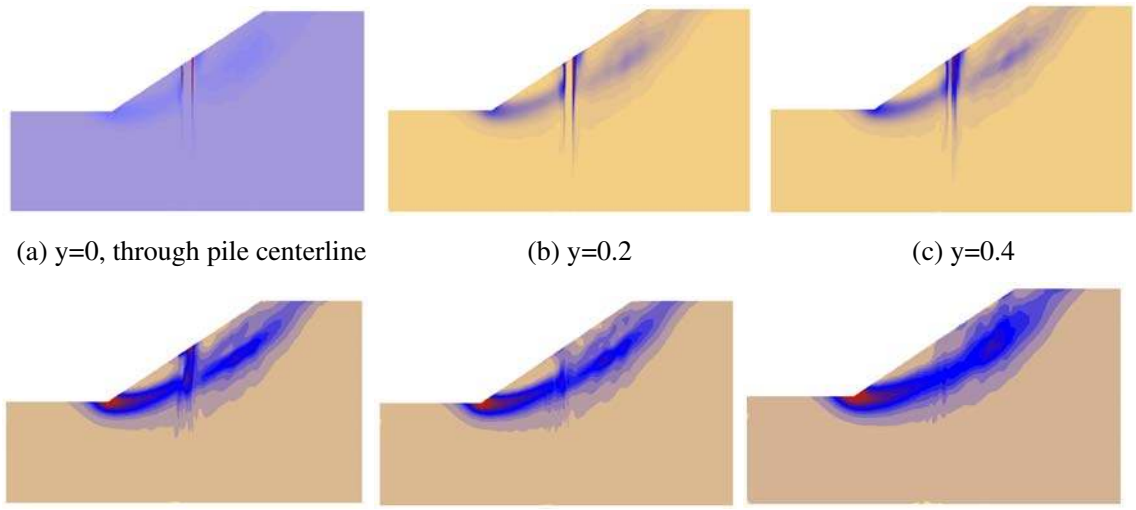

(a) y=0, through pile centerline (b) y=0.2 (c) y=0.4

(d) y=1.0 (e) y=1.8 (f) y=3.2, midway through soil

Figure 7.8 Slip surface at different sections for s=8D (FOS=1.42)

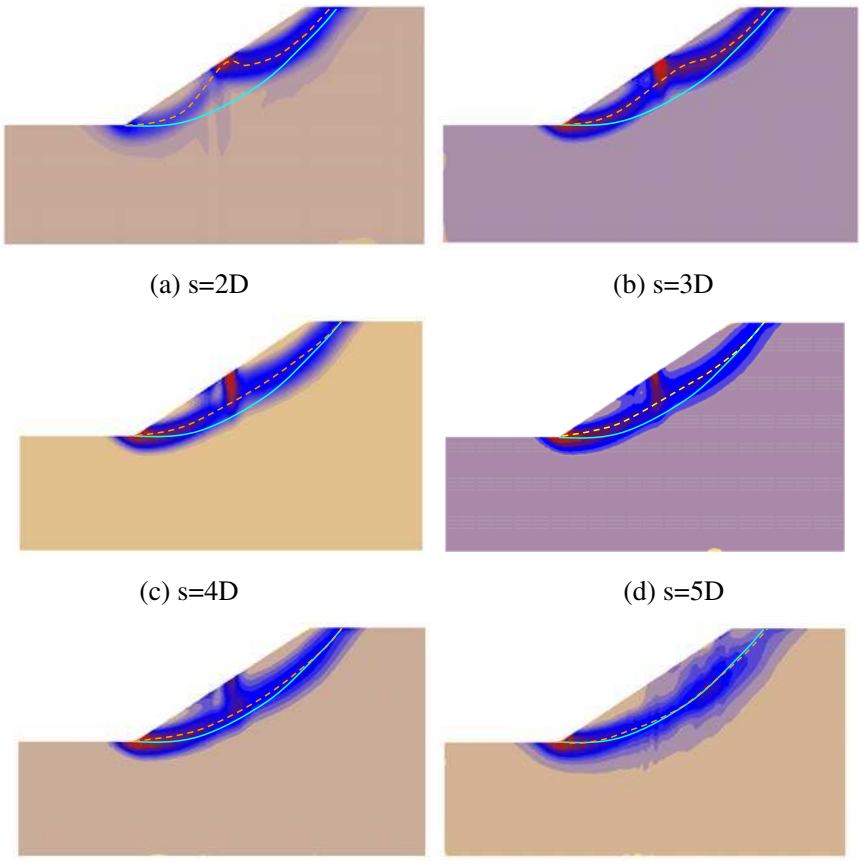

(a) s=2D (b) s=3D

(c) s=4D (d) s=5D

(e) s=6D (f) s=8D

Figure 7.9 Slip surface at the section of soil midway between piles

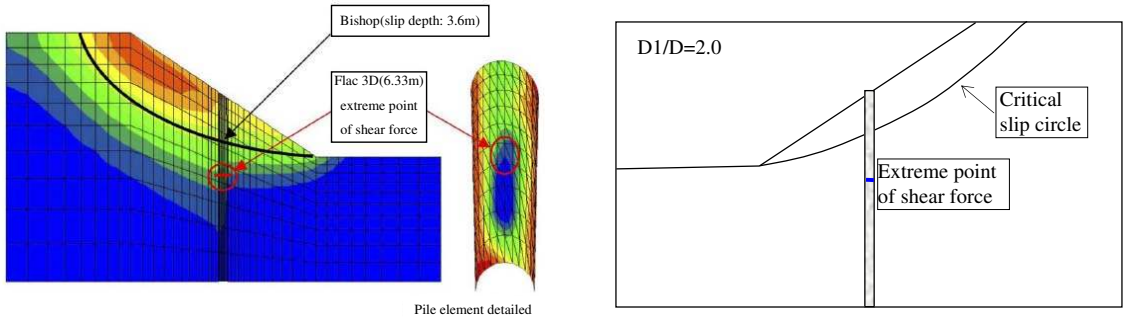

(a) Won et al. (2005) (b) Cai and Ugai (2000)

Figure 7.10 Slip surface obtained by SRM based on extreme point of shear force and comparison with critical slip circle obtained by Bishop's simplified method

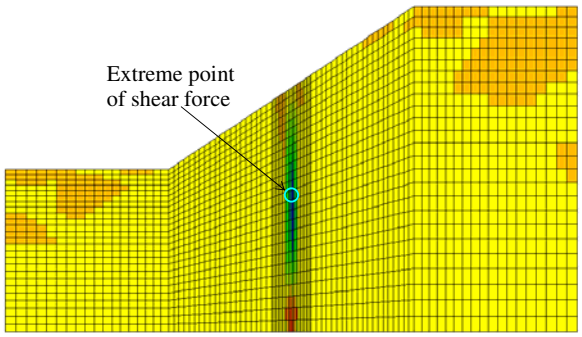

Figure 7.11 Shear force distribution of the piled slope for s=3D

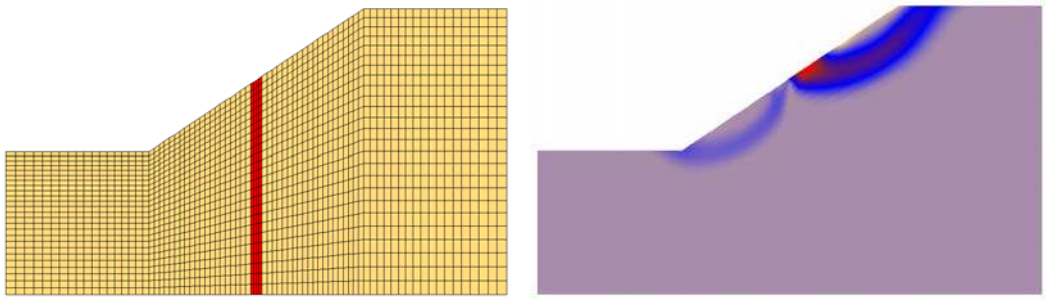

(a) mesh plot (b) slip surface

Figure 7.12 Slip surface and mesh for the slope with pile wall (FOS=1.89)

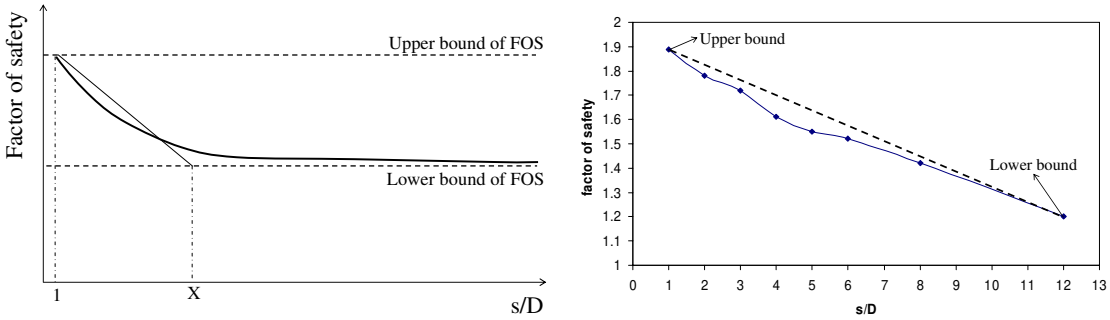

(a) general curve (b) X=12

Figure 7.13 Factor of safety with respect to different pile spacing

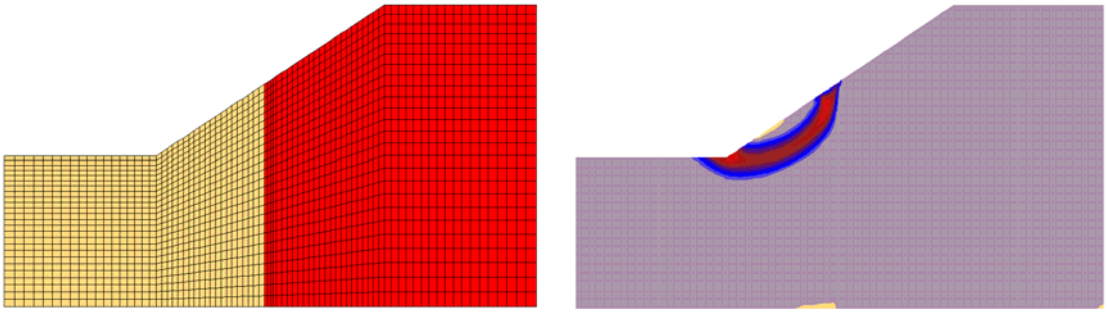

(a) mesh plot (b) slip surface

Figure 7.14 Slip surface and mesh for the slope with strong soil at upper part (FOS=1.94)

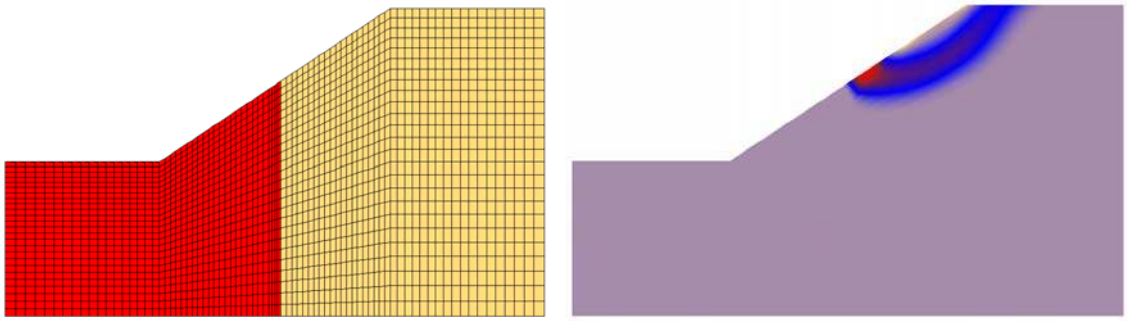

(a) mesh plot (b) slip surface

Figure 7.15 Slip surface and mesh for the slope with strong soil at lower part (FOS=1.87)

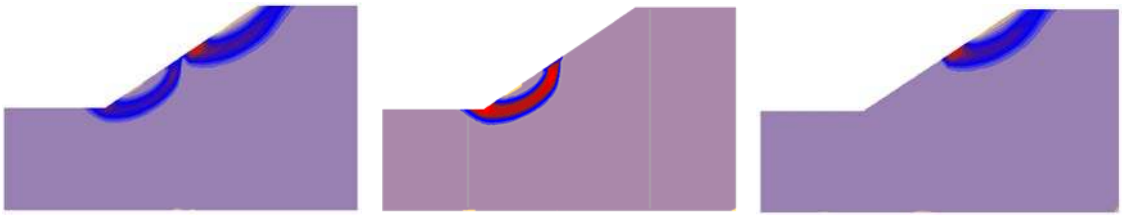

(a) pile wall, FOS=1.88 (b) strong soil up part, FOS=1.91 (c) strong soil low part, FOS=1.91

Figure 7.16 Slip surface for the slope with pile wall installed at 0.2m towards the slope crest as measured from the middle of slope

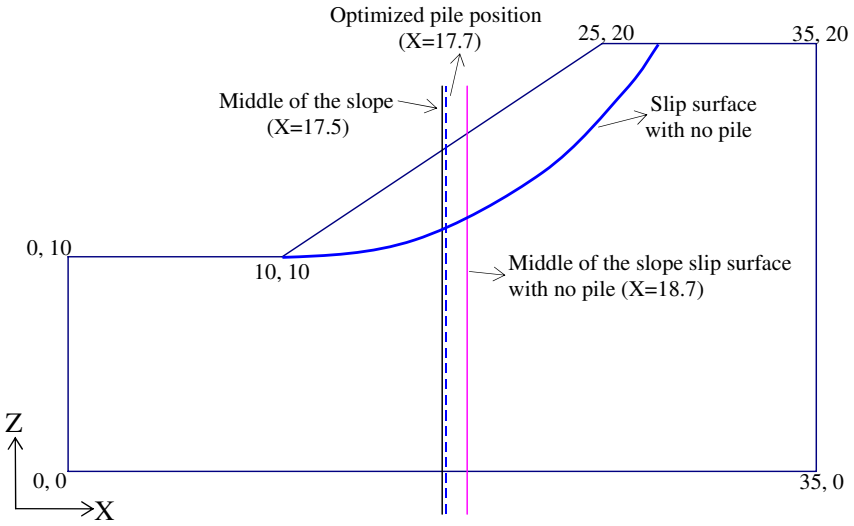

Figure 7.17 Pile position for the slope with soil cohesion 10kpa and friction angle 20 degree

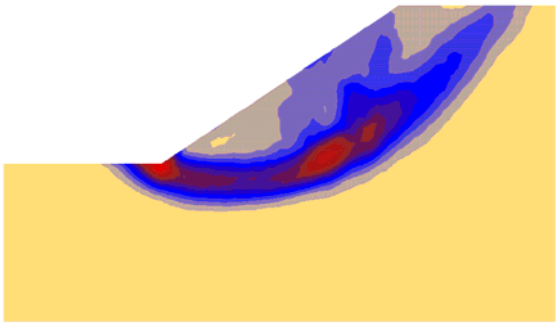

Figure 7.18 Slip surface of the slope with no pile for soil cohesion= 20kpa and friction angle 10 degree (FOS=1.14)

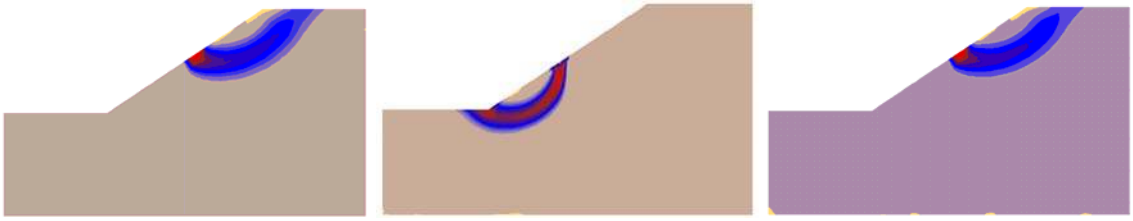

(a) pile wall, FOS=2.22 (b) strong soil up part, FOS=2.48 (c) strong soil low part, FOS=2.16

Figure 7.19 Slip surface for the slope with pile installed in the middle of slope (soil cohesion=20kpa, friction angle=10 degree)

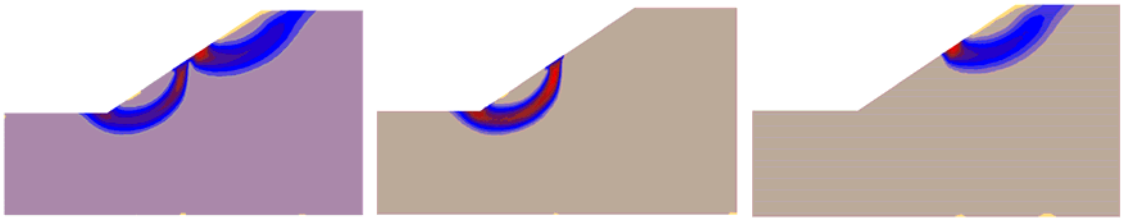

(a) pile wall, FOS=2.33 (b) strong soil up part, FOS=2.32 (c) strong soil low part, FOS=2.33

Figure 7.20 Slip surface for the slope with pile installed 0.55m upper of the middle of slope (soil cohesion=20kpa, friction angle=10 degree)

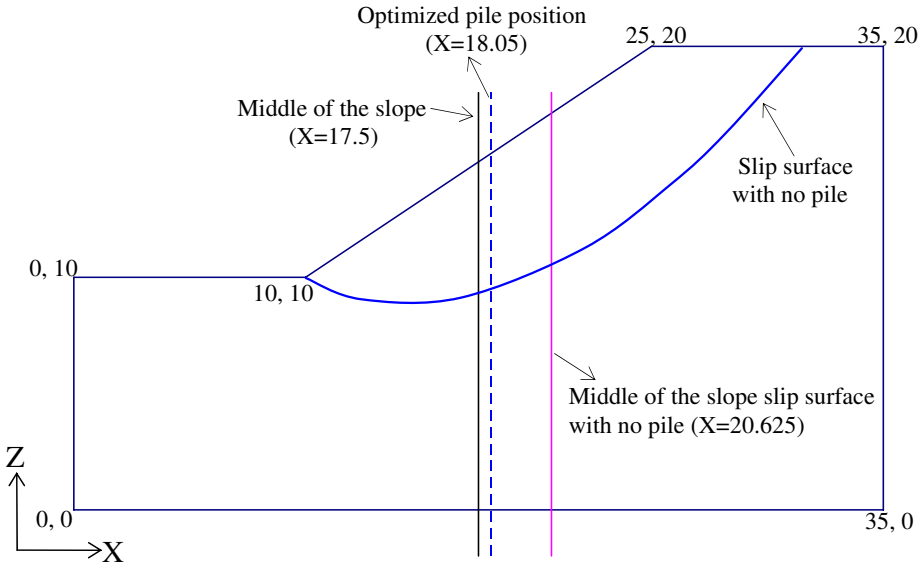

Figure 7.21 Pile position for the slope with soil cohesion 20kpa and friction angle 10 degree

CHAPTER 8: STABILITY ANALYSIS OF SLOPE WITH WATER FLOW BY STRENGTH REDUCTION METHOD

8.1 Introduction

Pore water pressure is one of the major reasons for slope instability. In limit equilibrium method which is widely used in engineering practice, the most common way in defining the pore-water pressure is the piezometric line, which is actually a hydrostatic condition. Since the assumption of a hydrostatic pore-water pressure is strictly not correct for most seepage situations, a correction factor is used in some software. Furthermore, if the pore-water pressure distribution is known by finite element or finite difference analysis, the LEM can also be integrated with the pore water pressure from the seepage analysis in the stability calculation. The SRM can also adopt the results from the seepage analysis easily, and the mesh for the SRM and seepage analysis can actually be the same.

As mentioned in chapter 2, for slope stability analysis with water flow, the way to include seepage forces in the LEM has caused various confusions, and some researchers (Greenwood, 1983, 1985; King, 1989) have introduced some effective-stress methods of slices which include the interslice water forces. These approaches are however more complicated in the analysis and are not adopted in commercial programs. Greenwood (1983) and Duncan and Wright (2005) have shown that there are cases where the refined approaches may have noticeable differences with the classical methods. If the SRM is used, the pore-pressure will affect the effective stress for which the stability

analysis is based on. The confusions about the effect of water in the LEM will not appear in the SRM.

In this chapter, two and three-dimensional strength reduction analyses will be carried out by software FLAC3D to study the effects of water flow on slope under several cases. In the following examples, the main focus is the steady state flow situation while the transient flow effect is not considered, so the value of the soil permeability has no influence on the SRM results. In order to reduce the running time, a relatively large value is assigned to the soil permeability (0.01cm/s). This study has demonstrated that besides the lowering of the factor of safety, the failure mechanism may also be affected by the seepage flow. Many engineers view that densely populated soil nails may affect seepage flow, but it is demonstrated in this study that for practical purposes, the effect of soil nail on the seepage flow can be neglected.

8.2 Stability analysis for a simple slope with seepage flow

In this section, a two-dimensional 6m height slope with 45° slope angle is analyzed. A 10m height model is developed in which the water is 4m height on the left and 10m height on the right side. The pore-pressure and the flow vector distribution for the free-surface seepage flow analysis are shown in Figure 8.1. For different soil properties, the FOS and slip surfaces are shown in Figures 8.2 to 8.5, and the results are compared with the case with no water. Obviously, with the seepage flow, the FOS is much smaller than the corresponding case without water. For sandy soil, the decrease of the FOS with seepage flow is larger than that for the clayey soil. This means that a sandy soil slope is easier to be destroyed by seepage flow than a clayey soil slope, so more attention should be paid to the prevention of seepage flow from destroying a sandy soil slope. Actually, Hong Kong is famous for slope failures and there are many sandy slopes failures (soil is

completely decomposed granite) during raining time each year. On the other hand, there is much less slope failures in those slopes with finer grain size (completely decomposed volcanic) in Hong Kong (GEO 1996) based on thirty years observations in Hong Kong. The sandy and finer grain soils in Hong Kong are derived from granitic and volcanic rock with similar chemical composition, and the main differences between the two types of soil are the grain size and the cohesive strength. It is also found that the location of the slip surface for sandy soil is greatly influenced by the water flow from various parametric studies, and the failure surface becomes shallower and closer to the slope toe under the influence of water seepage flow. These results are also similar to the observations of the slopes failures in Hong Kong over the last thirty years (GEO 1996), where many slopes failures are initiated from toe failures under heavy rain.

In the above analysis, the pore water pressure is generated by a seepage flow analysis which is a reasonable way to obtain the pore pressure distribution. It is however possible to define the pore water pressure by a water table in SRM similar to that in the LEM analysis. In order to investigate the difference between the two approaches, another model is developed in which the pore pressure is generated by the water table and the pore pressure distribution is shown in Figure 8.6 (the water table location is the free-surface obtained from Figure 8.1). The factors of safety for the two cases are compared in Table 8.1. The FOS for the case where the pore pressure is generated by the water table is smaller than the case generated by the seepage flow analysis, as the pore water pressure calculated by the water table (free-surface) is larger. It means that the use of the water table (or piezometric line) is a conservative method of analysis, and the difference is very small for a clayey soil slope but is much larger for a sandy soil.

8.3 Stability analysis for a simple slope with irregular pore pressure

In this section, two more models are analyzed for the 6m height slope with 45° slope angle discussed in the previous section, but the pore pressure distribution is irregular due to some blocking effects in the slope. In the first model, the soil on the left side of the slope crest and on the left side of slope toe is assigned as impermeable zone. The slip surface and the pore pressure distribution are shown in Figure 8.7. In the second model, an 8 m height thin impermeable wall near the slope crest is applied. The slip surface and the pore pressure distribution are shown in Figure 8.8. In the second model, the FOS (1.30) is much larger than the case with no soil blocking in Figure 8.3 (0.96) and the case in Figure 8.7 (1.07). With the blockage from the soil wall, the seepage path gets much longer which will greatly reduce the pore water pressure, so the FOS gets much larger. This result also shows that the installation of retaining wall to increase the seepage length is a good method to prevent slope failure caused by seepage flow.

8.4 Stability analysis for soil nailing slope with seepage flow

In this section, a 6m height soil nailed slope with water flow is analyzed and the slope angle is 45°. Nails are installed on 1.5m centers horizontally and vertically. The nail length is 8m and the inclination angle is zero. The cohesion of the soil is 2 kPa and the friction angle is 35°, and the slope model is shown in Figure 8.9. In Hong Kong where the density of soil nail is high (spacing around 1m to 1.5m) and the diameter and length of the soil nails are large (32mm or 40mm diameter bar is commonly used while a length of 10m to 20m is also common), many engineers have questioned that the densely populated soil nails may affect the seepage pattern. Towards this problem, two models are developed. In the first model, the pore pressure is determined without the presence of the nail. In the second model, the soil nails together with the grout are

treated as impermeable zone and the pore pressure distribution for this case is shown in Figure 8.10. For these two models, the soil is given a relatively large permeability (0.01cm/s). In the first model, the nail is given the same permeability as the soil, while in the second model, the nail is given a very small permeability (10^{-8}cm/s). The water boundary conditions are: at the right hand side, the water height is 10m; at the slope toe side, the water height is 4m (Figure 8.10b). It is noticed that the pore pressure distribution considering the blockage effect from soil nails is actually close to that for the first case at the section where there is no soil nail. The FOS by these two models is also the same (both are 0.95 and the slip surface as shown in Figure 8.11 apply for both cases). This means that the blockage effect of the soil nail can be ignored in a soil nailed slope analysis as the nail diameter is small as compared with the nail spacing, even when large diameter soil nails as used in Hong Kong are used in the analysis.

For this soil nailed slope, the FOS is 1.71 with no water flow. If no nail is included in this slope, the FOS with and without water flow is 0.72 and 1.07 respectively. It can be seen that the factor of the safety for soil nailed slope is more influenced by the water flow, as the percentage decrease of the FOS is much larger when compared with a slope without nail. In this analysis, the nail is simulated by cable element and its pullout strength is related to the confining pressure. When there is water, the confining pressure around the nail is decreased due to the pore water pressure, so water has two effects on a soil nailed slope. Firstly, the FOS is decreased by the seepage force, and secondly, the FOS is lowered by the lowering of the nail pullout strength which is related to the effective confining pressure. To remove the influence of the confining pressure on the nail pullout strength, the second model is re-considered in which the nail has a constant pullout strength which is not affected by the effective overburden stress (only grout cohesive strength is given and grout friction is zero) and the results are shown in Table

8.2. The decrease of the FOS with the presence of water is now smaller when compared with the previous model. It is clear that the relation of the soil nail pullout strength and the effective overburden stress is a very critical factor in the stability of a soil nailed slope.

8.5 Stability analysis for piled slope with seepage flow

In this section, a piled slope with water flow is analyzed. The slope geometry and the properties of soil and pile are the same as the first example analyzed in chapter 7 (Figure 7.1). Only the case of pile spacing equal to 3D is considered. Since the solution time of SRM analysis for slope with water flow is much longer than for no water slope, the model with a relatively coarse mesh is developed to reduce solution time, and the mesh plot is shown in Figure 8.12. When the slope is not reinforced with pile, the factor of safety by the SRM is 0.85 and the slip surface is shown in Figure 8.13.

Two models are developed to investigate the influence of seepage flow on the failure mechanism for pile reinforced slope. The FOS and slip surface obtained by the models with and without water blocking effect are the same for the two cases (FOS is 1.29 and the results are shown in Figures 8.14 and 8.15). It is clear that the blocking effect of the pile to the seepage can also be ignored which is similar to the case for soil nails.

If no water is involved in this model, it is found the optimal pile position is about at the middle of the slope which is shown in chapter 7. The slip surface is practically divided into two parts, and obvious shear strain is mobilized in both the lower and upper parts. When there is water seepage, the slip surface is mainly located at the lower part of the slope (Figure 8.15) which is different from the case without seepage, which means that the upper part of the slope is safer than the lower part. This phenomenon clearly arises

from the effect of the seepage force. Without the seepage force, there is only a minor interaction between the upper and lower parts of the failure mass. The optimized pile position under seepage moves towards the slope toe instead of locating at about the middle of the slope, and this is different from that without seepage. It is found that the optimal pile location for this case is 2.0m towards the slope toe as measured from the middle of the slope (Figure 8.16). The effect of the water seepage is hence important in controlling the failure mechanism of a pile reinforced slope.

8.6 Stability analysis for locally loaded slope with seepage flow

In this section, a 6m height slope with 45° slope angle under rectangular shape vertical loading is analyzed. The width and length of the loading are 2m and 4m respectively, while the edge of the loading is 1m away from the crest of the slope. The cohesion of the soil is 20kPa and the friction angle is 20°. The length of the computer model is 20m. When the loading q is 100kPa, the results of analysis are shown in Figure 8.17. This slope model with no water has been analyzed in chapter 4, and the result is shown in Figure 4.16b. It can be seen from this model that the failure mechanisms for the slope with water and without water are different. For the slope with a two-dimensional seepage flow, the slip surface is basically two-dimensional. On the other hand, for the slope without water, a nearly three-dimensional slip surface is mobilized around the local loading. In chapter 4, the failure mechanism of the locally loaded slope with no water has been investigated. When the loading is small, the slip surface is still basically two-dimensional until the loading becomes sufficiently large to mobilize a three-dimensional slip surface. For this model, the failure mechanism with and without seepage are different even though the applied loading is the same because the seepage force is included in the analysis, and the ability to mobilize a three-dimensional slip surface for the local loading is weakened by the two-dimensional seepage flow.

8.7 Conclusion

In this chapter, the strength reduction method is employed for slope stability analysis with water flow. The pore water pressure is generated by seepage flow analysis according to the boundary conditions. With seepage flow, the FOS is usually much smaller than the corresponding case with no water. For the sandy soil slope, the decrease of the FOS by seepage is usually larger than that for the clayey soil slope. This means that sandy soil slope is easier to be destroyed by seepage flow than clayey soil slope which agrees well with the observations in Hong Kong over the last thirty years. The reduction of seepage flow in sandy soil slope hence deserves more attention. Furthermore, the location of the slip surface for sandy soil slope is more sensitive to seepage, and it becomes shallower and closer to the slope toe under the influence of seepage flow. If the pore pressure is generated by the use of piezometric line, usually the FOS will be smaller than the case where the pore pressure is generated by seepage flow analysis. It means that the water table (or piezometric line) option is a conservative method for analysis. For clayey soil, the difference between the two ways in defining the pore water pressure is usually small, but for sandy soil, the difference is much larger.

It has been demonstrated that the use of a retaining wall to increase the seepage path is a very effective solution to enhance slope stability under seepage flow. On the other hand, the results of the seepage analysis are virtually independent of the soil nails or reinforcing piles (under practical spacing) so that engineers need not consider the soil nail/pile in the seepage analysis. The water flow has two effects on the stability of a soil nailed slope. Firstly, the FOS is decreased by the seepage force. Secondly, the FOS is decreased by the reduction of the nail pullout strength as the confining pressure around

the nail is decreased by the pore water pressure. Water is hence a major factor in controlling the stability of slope.

For locally loaded slope with water flow and pile reinforced slope, the failure mechanism can be strongly influenced by the seepage force. To get a realistic failure mechanism, the pore pressure must be carefully considered in the analysis.

Table 8.1 Factor of safety for different situations by SRM

Cohesion and Friction angle	1kPa, 45°	2kPa, 45°	5kPa, 35°	10kPa, 25°
FOS with water (pore pressure generated by seepage analysis)	0.82	0.96	0.98	1.07
FOS with water (pore pressure generated by water table)	0.66	0.82	0.92	1.03
FOS for no water	1.3	1.44	1.35	1.37

Table 8.2 Factor of safety of nailed slope by SRM

Case	No water	With water flow
With no nail	1.07	0.72
Nail pull out strength related to confining pressure	1.71	0.95
Nail with constant pull out strength 5.6kN/m	1.61	1.01

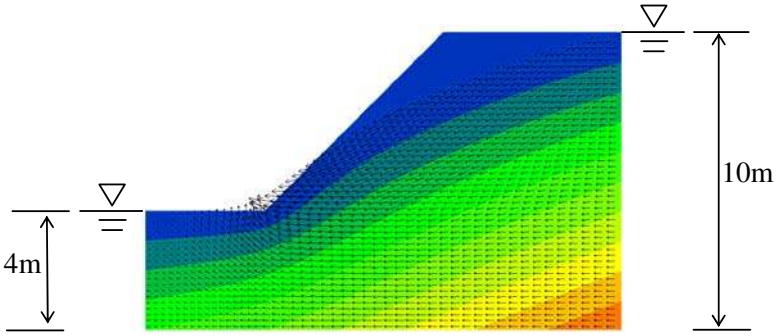

Figure 8.1 Pore water pressure and flow vector of a simple slope from a free-surface seepage analysis

(a) with water flow, FOS=0.82 (b) no water, FOS=1.30

Figure 8.2 Slip surface for slope with cohesion 1kPa and friction angle 45°

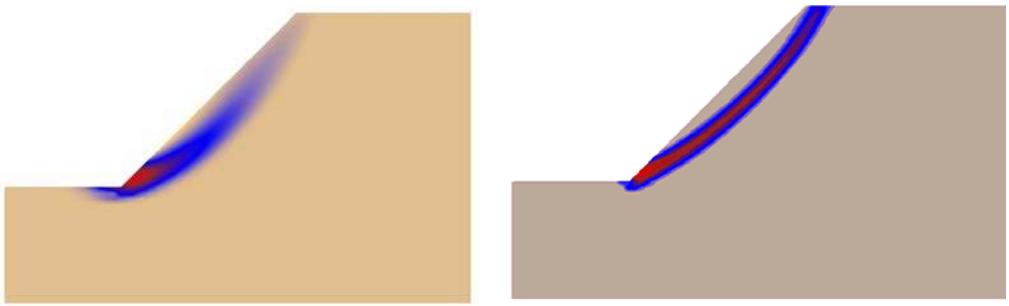

(a) with water flow, FOS=0.96 (b) no water, FOS=1.44

Figure 8.3 Slip surface for slope with cohesion 2kPa and friction angle 45°

(a) with water flow, FOS=0.98 (b) no water, FOS=1.35

Figure 8.4 Slip surface for slope with cohesion 5kPa and friction angle 35°

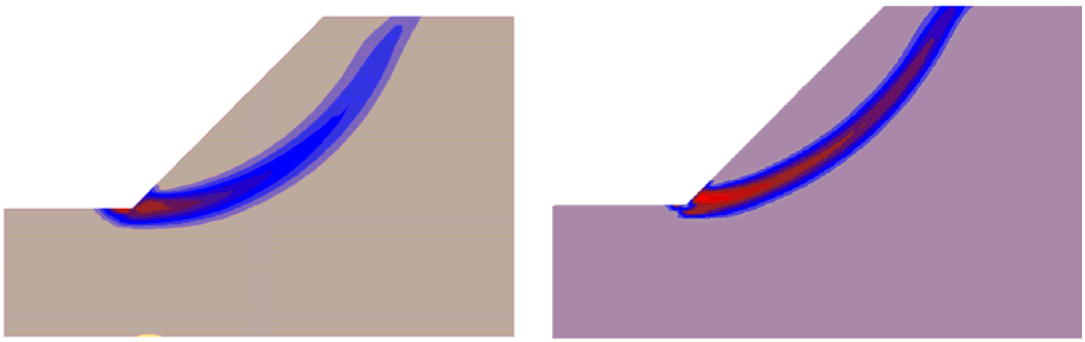

(a) with water flow, FOS=1.07 (b) no water, FOS=1.37

Figure 8.5 Slip surface for slope with cohesion 10kPa and friction angle 25°

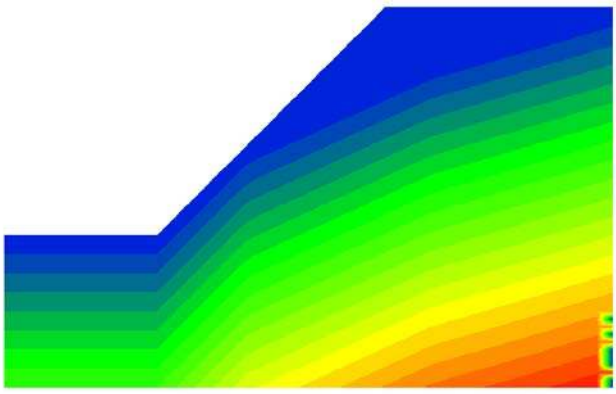

Figure 8.6 Water pressure by water table (piezometric line) assuming hydrostatic condition

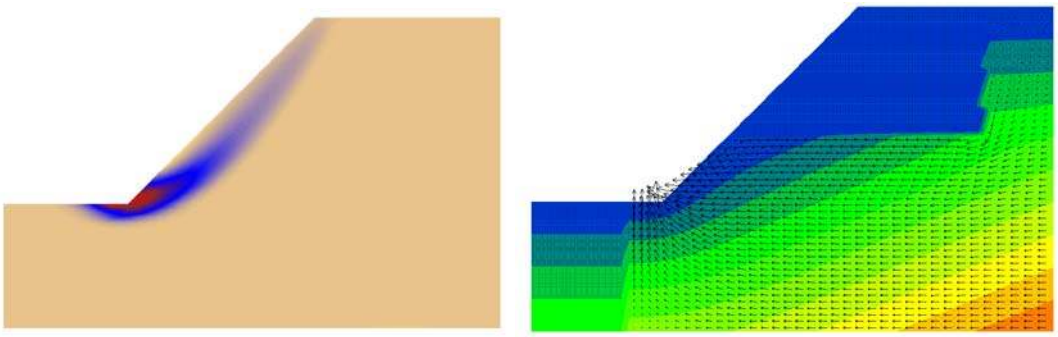

(a) slip surface, FOS=1.07 (b) pore water pressure

Figure 8.7 Slip surface and pore pressure with water block at upper and bottom left for slope with cohesion 2kPa and friction angle 45°

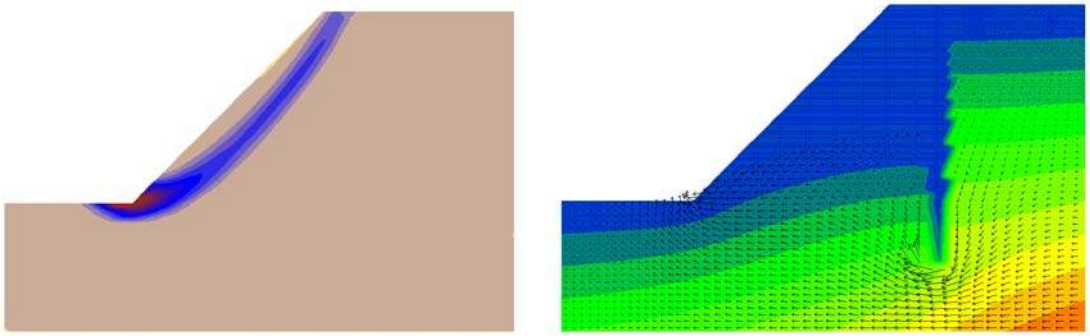

(a) slip surface, FOS=1.31 (b) pore water pressure

Figure 8.8 Slip surface and pore pressure with water block wall for slope with cohesion 2kPa and friction angle 45°

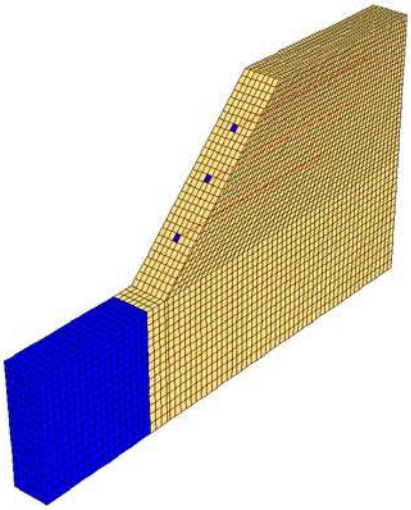

Figure 8.9 Model plot of the soil nailing slope

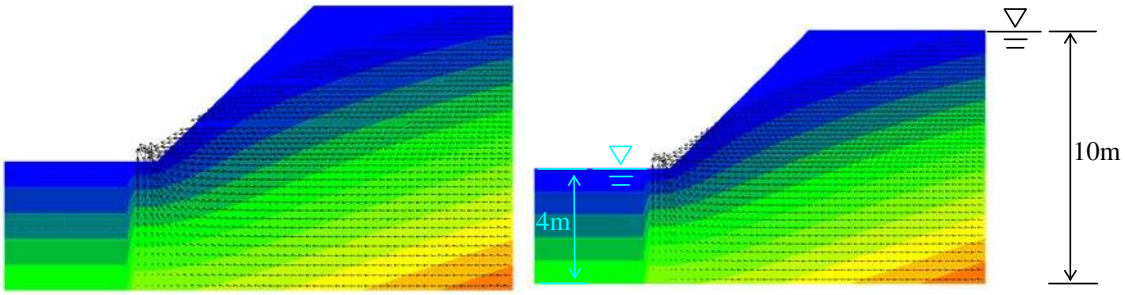

(a) cutting plane through the nail (b) cutting plane not including nail

Figure 8.10 Pore pressure distribution of the soil nailing slope with water blocking effect

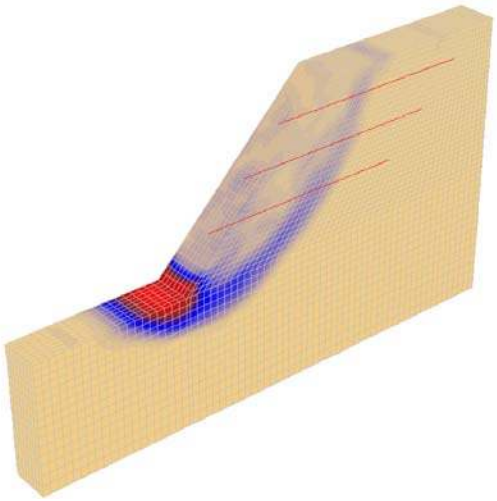

Figure 8.11 Slip surface for the nailed slope with water flow (FOS=0.95)

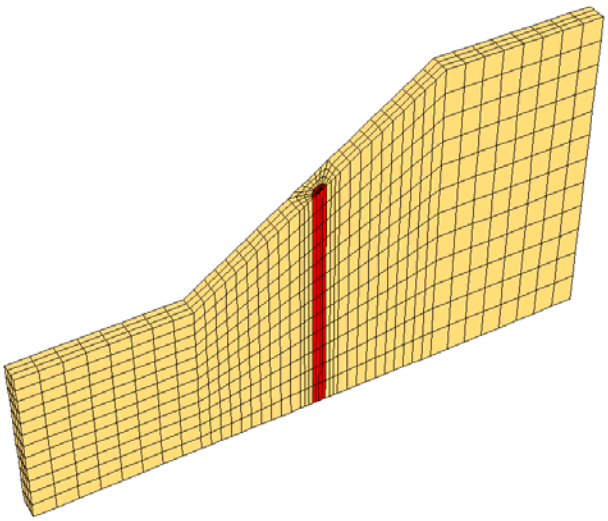

Figure 8.12 Model plot of the piled slope

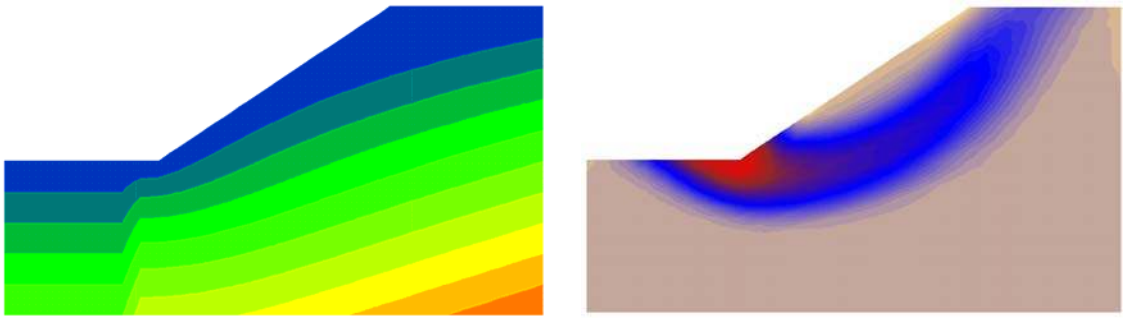

(a) pore pressure (b) slip surface

Figure 8.13 Pore pressure and slip surface of the slope without pile (FOS=0.85)

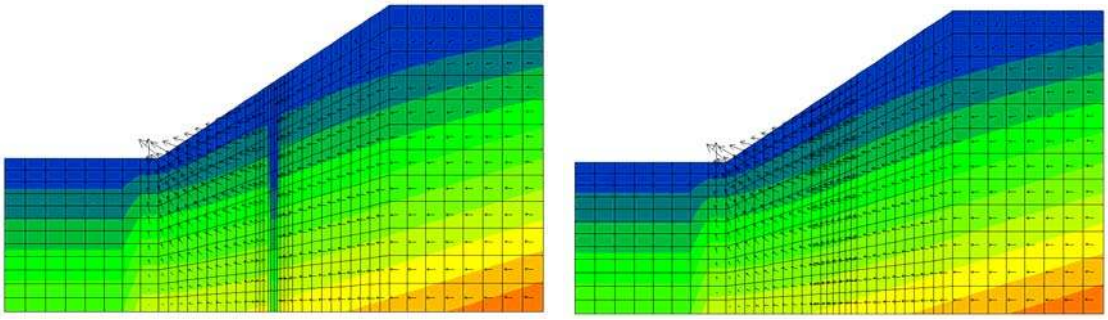

(a) cutting plane through the pile center (b) cutting plane through soil midway

Figure 8.14 Pore pressure distribution of the piled slope with water blocking effect

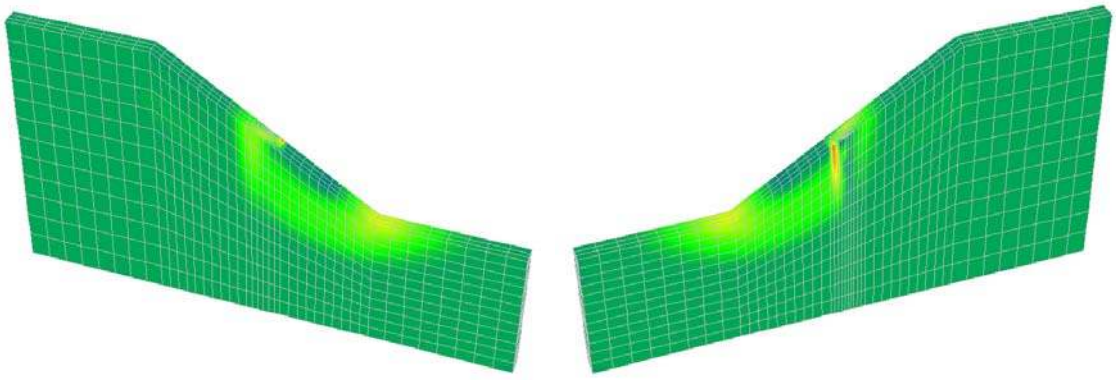

(a) back view (b) front view

Figure 8.15 Slip surface for the piled slope with water flow (FOS=1.29)

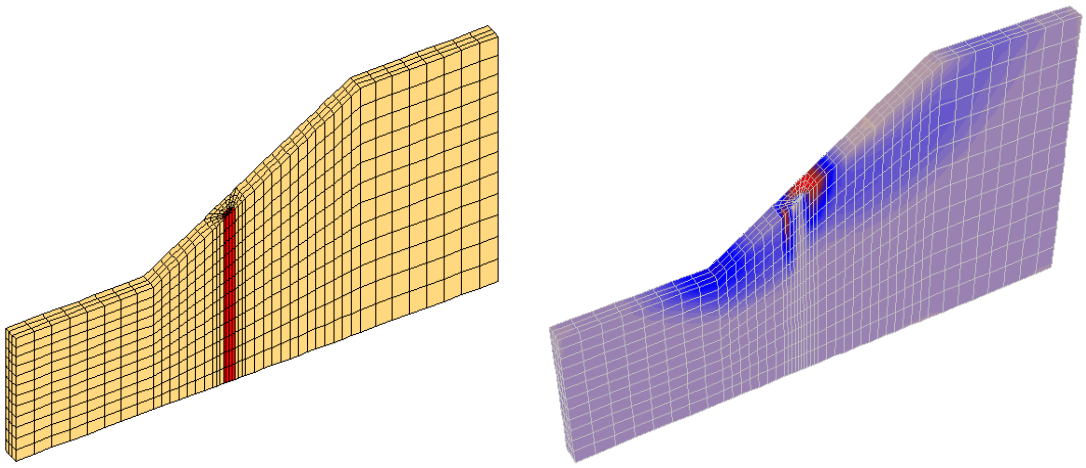

(a) model plot (b) slip surface

Figure 8.16 Slip surface for the slope with pile installed at 2.0m towards the slope toe as measured from the middle of slope (FOS=1.34)

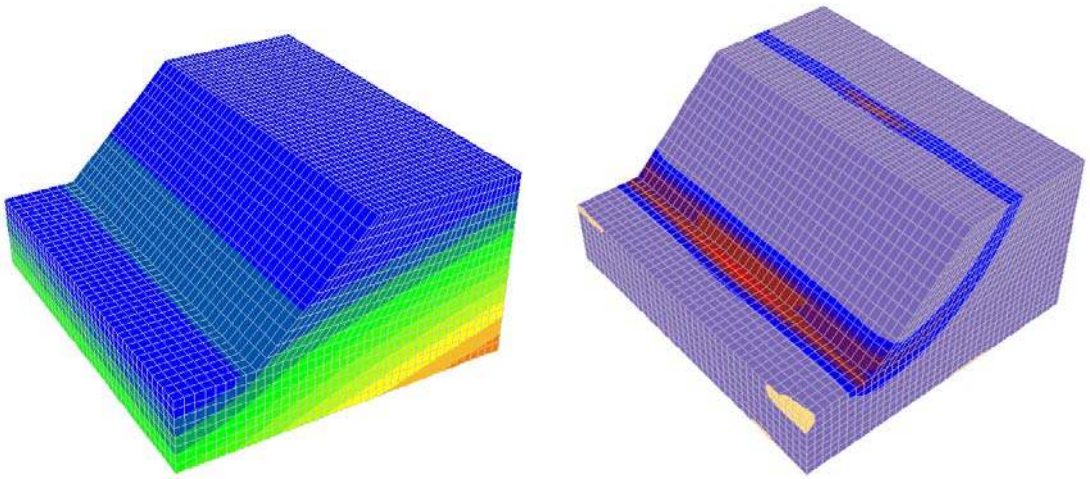

(a) pore pressure distribution (b) slip surface, FOS=1.29

Figure 8.17 Pore water pressure and slip surface for the locally loaded slope with water

CHAPTER 9: CONCLUSIONS AND RECOMMENDATIONS

9.1 Conclusions

This study has attempted to conduct a comprehensive analysis of three-dimensional slopes. The 3D effects include irregular slope geometry, soil property distribution and boundary conditions as well as the effects of soil nail/pile and water flow. Both limit equilibrium and strength reduction methods have been used in this study, and an extensive comparison between these two methods are also conducted. The main conclusions of the present study are summarized in five aspects which are described as follows.

9.1.1 Comments on limit equilibrium and strength reduction methods

The main advantage of strength reduction method is that it can automatically locate the critical slip surface, and the failure modes can be detected by the shear strain distribution. Another advantage of SRM is that it can easily simulate more complex conditions with inclusions. Concerning the piled slope, the SRM can be a better alternative to the LEM, as the LEM is still not very mature for piled slope analysis. This advantage may be more pronounced when different reinforcements are included in the same slope, and a complicated water flow conditions is involved in the analysis.

The major limitations of SRM are: it is sensitive to the nonlinear solution algorithm for the case of a soft band especially for frictional material, and it is incapable of determining other failure surfaces which may be only slightly less critical than the SRM solution but still require treatment for good engineering practice. Another issue is that the SRM can be sensitive to the convergence criterion, and if it is necessary, the result

should be checked by the criterion of sudden change of displacement which is found to be a more reliable criterion to determine the failure state but is not the default option in some commercial program (but require human judgment instead of automatic analysis). The long solution time for SRM has been a major problem in the past, but this problem becomes moderate now with the continuing improvement of computational power.

The main shortcoming of the LEM is that it includes many assumptions to make the solution statically determinate. It is also not as powerful as SRM to simulate interaction between reinforcement and soil, and to analyze some very complex situations. The primary benefit of the LEM is the short solution time, and it is still more suitable and generally accepted for routine design and analysis. The LEM is also flexible in finding different local minima factor of safety and the corresponding slip surface. Through the present study, it can be concluded that both the LEM and SRM have their own merits and demerits, and the final choice will heavily depends on the engineering judgment of the results.

9.1.2 Main findings from analysis of non-reinforced slopes with obvious 3D effects

The results from the 3D LEM and SRM agree reasonably well for normal situations, and the factors of safety obtained by the SRM are slightly higher than those from the LEM, which is similar to the corresponding 2D analysis. Such results also agree well with previous studies by other researchers.

For an infinite slope with local loading, whether the critical failure surface is 2D or 3D depends on the magnitude of the external load. It is also interesting to find that the suitable domain size for analysis is largely controlled by the failure mechanism instead of the length of the external load, as the failure mechanism may be greatly affected by

the boundary effect. For a proper SRM or LEM analysis, the engineers may either adopt a large domain size at the expense of computer time, or pursue a trial and error analysis as discussed in previous chapters to determine the proper domain size.

For concave slope, the effect of curvature is distinct and the FOS increases with the decrease of radius of curvature. For convex slope with no local loading, the curvature effect can be ignored, but for the steep convex slope with local loading, the curvature effect is apparent.

9.1.3 Main findings from analysis of soil nailing slope

For soil nailed slope, it is also found that there are not major differences in the factor of safety and slip surfaces from the strength reduction method and the limit equilibrium method in general. Appreciable difference between the SRM and LEM will however be found if the nail load is controlled by the overburden stress.

It is demonstrated that a nail head is important in determining the failure mode and the factor of safety of a nailed slope, while the effect of the nail elastic modulus is more noticeable only when the slope is very steep.

The optimum layout of the soil nail is found to be longer at the bottom of the slope and shorter at the top which is contrary to some of the engineers' guideline for design of soil nail during top-down construction. In general, longer soil nail should be placed at the location where failure first initiates.

It is found that the mobilized bending moment in soil nail is small even when the nail inclined angle is large. In this respect, the conventional method of soil design appears to be adequate and is slightly on the conservative side.

From the tension force distribution along the soil nail, it is found that the tension force distribution is influenced by the state of the slope (service state, limit state) and the failure modes (external failure, internal failure). In general, the line of the maximum tension may not correspond to the critical slip surface as commonly believed, except when the failure mode is an internal tensile failure. This result is contrary to the common belief by the engineers, but the detailed study in chapter 5 has demonstrated that this is actually a better representation of the nail load distribution.

For locally loaded slopes, the nail force of the top row is usually more mobilized, but for non-locally loaded slopes, the nail force of the bottom row is usually more mobilized at the limit state.

For the reinforcement design of intersected slope, less reinforcement can be used for the concave intersection part as the effect of curvature can improve the slope stability. For convex intersection slope, if the slope angle is not high, the reinforcement design can be the same as no curvature slopes. If the slope is steep, more reinforcement should be used for convex intersection slope.

9.1.4 Main findings from analysis of piled slope

For slope reinforced with one row of piles, the slip surface is found to be divided into two parts when the pile spacing is very small, and these two parts gradually get connected with the increase of pile spacing until a clear single slip surface is formed

when the pile spacing is large enough. The slip surface of the piled slope is usually shallower than the corresponding slope with no pile, and this result is totally different from the previous results based on the maximum point of shear force where a very deep slip surface for piled slope is usually obtained.

The optimal pile position for slope reinforced with one row of piles is found to locate between the middle of the slope and the middle of the slip surface for an unreinforced slope.

An optimal design procedure for the pile spacing has also been suggested in the present study based on the upper bound and lower bound of the factor of safety, and the procedure will help to reduce the time required for a piled slope three-dimensional analysis.

9.1.5 Main findings from analysis of slopes with water flow

From the analysis, it demonstrates that the factor of safety for sandy soil slope is more influenced by seepage flow. Thus sandy soil slope deserves more attention in prevention of destroy from water flow. This phenomenon is also in compliance with the observation in Hong Kong where less slope failures are found for slopes with completely decomposed volcanic which has higher cohesive strength than the slopes with completely decomposed granite.

If the pore pressure is generated by the use of piezometric line, the FOS will be smaller than that generated by seepage flow analysis. The difference is small for clayey soil slope but is much larger for sandy soil slope. This result has demonstrated that the classical method in treating the water table is conservative for analysis and design.

The analysis also shows that the installation of retaining wall to increase the length of the seepage path is a good method to prevent slope failure induced by seepage flow.

The water flow has two effects on the soil nailing slope stability. Firstly, the FOS is decreased by the seepage force and secondly, the FOS is decreased by the weakening of the nail pullout strength as the effective confining pressure around the nail is decreased by the pore water pressure.

For locally loaded slope with water flow, the failure mechanism is influenced by the seepage force. The three-dimensional slip surface is more difficult to be mobilized when a two-dimensional seepage force is included.

The present study also shows that the effect of pile and densely populated soil nail on the seepage flow can be neglected for practical purpose. This result is important to many engineers in Hong Kong, as this question has been raised among the engineers in Hong Kong due to the densely populated soil nails used locally.

9.2 Recommendations and suggestions

For problems with a soft band or major differences in the soil parameters between soil layers, the numerical model and results should be checked carefully. Since both the SRM and LEM have their specific advantages and limitations, the results come from the complex slope models should be cross checked by these two methods. The final results have to be assessed carefully using engineering judgment.

It is found that the non-convergence criterion in commercial SRM programs should be assessed carefully, and engineers should not rely completely on the default setting in the

computer programs. It has also been found that a sudden change of the displacement may sometimes be a better criterion than the default setting in the computer programs for some cases. Therefore, more research to establish a more robust criterion for the ultimate limit state under general condition is required. A proper and successful combination of the above two criteria may be a prospective way.

For piled slope analysis, only one row of piles is considered and infinite pile length assumption is used in this study. Further research should be conducted on the slope with multi rows of piles, and the influence of the pile length on the slope failure mode should also be investigated.

In the present study, only one kind of reinforcement (soil nail or pile) is included in an individual slope. Further study should be carried out on the stability and failure modes of the slope with the presence of different types of reinforcement.

Many 3D effects and failure modes are revealed by numerical simulation in the present study, and some of them are verified by limit equilibrium method or testing results obtained in the literature. Further study is still suggested by conducting full scale or reduced scale model tests to confirm some of the results from the numerical simulation.

REFERENCES

Abramson, L. W., Lee, T. S., Sharma, S., and Boyce, G. M. (2002). Slope Stability and Stabilization Methods, 2nd edition, John Wiley, USA

Anderheggen, E. and Knopfel, H. (1972). Finite element limit analysis using linear programming. International Journal of Solids and Structures, 8, 1413-1431

ASCE. (1997). Committee report "Soil nailed retaining structures". Ground Improvement, Ground Reinforcement, Ground Treatment: developments 1987-1997, ASCE Geotechnical Special Publication No. 69, edited by Vernon R. Schaefer, Section 2.8, 201-232

Ausilio, E., Conte, E., and Dente, G. (2001). Stability analysis of slopes reinforced with piles. Computers and Geotechnics, 28(8), 591-611

Azzouz, A. S. and Baligh, M. M. (1983). Loaded areas on cohesive slopes. Journal of Geotechnical Engineering, ASCE, 109(5), 724-729

Babu, G. L. S., Murthy, B. R. S., and Srinivas, A. (2002). Analysis of construction factors influencing the behaviour of soil-nailed earth retaining walls. Ground Improvement, 6(3), 137-143

Baker, R. and Garber, M. (1978). Theoretical analysis of the stability of slopes. Geotechnique, 28(4), 395-411

Baker, R., and Leshchinsky, D. (1987). Stability analysis of conical heaps. Soils and Foundations, 27(4), 99-110

Baker, R. and Leshchinsky, D. (2001). Spatial distribution of safety factors. Journal of Geotechnical and Geoenvironmental Engineering, 127(2), 135-145

Baligh, M. M. and Azzouz, A. S. (1975). End effects on stability of cohesive slopes. Journal of the Geotechnical Engineering Division, ASCE, 101(GT11), 1105-1118

Bell, J. M. (1968). General slope stability analysis. Journal of the Soil Mechanics and Foundations Division, ASCE, 94(SM6), 1253-1270

Bishop, A. W. (1955). The use of the slip circle in stability analysis of slopes. Geotehnique, 5(1), 7-17

Bottero, A., Negre, R., Pastor, J., and Turgeman, S. (1980). Finite element method and limit analysis theory for soil mechanics problems. Computer Methods in Applied Mechanics and Engineering, 22, 131-149

Briaud, J. L. and Lim, Y. (1997). Soil-nailed wall under piled bridge abutment: simulation and guidelines. Journal of Geotechnical and Geoenvironmental Engineering, 123(11), 1043-1050

Brinkgreve, R. B. J. and Bakker, H. L. (1991). Non-linear finite element analysis of safety factors. Proceedings of the seventh international conference on computer methods and advances in geomechanics, Cairns, 6-10 May 1991, 1117-1122

Bruce, D. A. and Jewell, R. A. (1986). Soil nailing: Application and Practice-Part 1. Ground Engineering, 19(8), 10-15

Byrne, R. J., Cotton, D., Porterfield, J., Wolschlag, C., and Ueblacker, G. (1998). Manual for Design & Construction of Soil Nail Walls. FHWA-SA-96-069R, Federal Highway Administration (FHWA), Washington DC, USA.

Cai, F., Ugai, K., Wakai, A., and Li, Q. (1999). Effects of horizontal drains on slope stability under rainfall by three-dimensional finite elements analysis. Computers and Geotechnics, 23, 255-275

Cai, F. and Ugai, K. (2000). Numerical analysis of the stability of a slope reinforced with piles. Soils and Foundations, 40(1), 73-84

Cai, F. and Ugai, K. (2003). Response of flexible piles under laterally linear movement of the sliding layer in landslides. Canadian Geotechnical Journal, 40(1), 46-53

Cai, F. and Ugai, K. (2004). Numerical analysis of rainfall effects on slope stability. International Journal of Geomechanics, 4(2), 69-78

Cartier, G. and Gigan, J. P. (1983). Experiments and observations on soil nailing structures. Proc. Enropean Conf. Soil Mechanics and Foundation Engineering, Helsinki, 473-476

Cavounidis, S. (1987). On the ratio of factors of safety in slope stability analyses. Geotechnique, 37 (2), 207- 210

Chai, X. J. and Hayashi, S. (2005). Effect of constrained dilatancy on pull-out resistance of nails in sandy clay. Ground Improvement, 9(3), 127-135

Chang, M. (2002). A 3D slope stability analysis method assuming parallel lines of intersection and differential straining of block contacts. Canadian Geotechnical Journal, 39, 799-811

Chen, C. Y. and Martin, G. R. (2002). Soil-structure interaction for landslide stabilizing piles. Computers and Geotechnics, 29(5), 363-386

Chen, L. T. and Poulos, H. G. (1997). Piles subjected to lateral soil movements. Journal of Geotechnical and Geoenvironmental Engineering, 123(9), 802-811

Chen, Z., Wang, X., Haberfield, C., Yin, J. H., and Wang, Y. (2001a). A three-dimensional slope stability analysis method using the upper bound theorem, Part 1: theory and methods. International Journal of Rock Mechanics and Mining Sciences, 38, 369-378

Chen, Z., Wang, J., Wang, Y., Yin, J. H., and Haberfield, C. (2001b). A three-dimensional slope stability analysis method using the upper bound theorem, Part 2: numerical approaches, applications and extensions. International Journal of Rock Mechanics and Mining Sciences, 38, 379-397

Chen, Z. Y., Mi, H. L., Zhang, F. M., and Wang, X. G. (2003a). A simplified method for 3D slope stability analysis. Canadian Geotechnical Journal, 40, 675-683

Chen, J. (2004). Slope stability analysis using rigid elements. PhD Thesis, The Hong Kong Polytechnic University

Chen, J., Yin, J. H., and Lee, C. F. (2003b). Upper bound limit analysis of slope stability using rigid finite elements and nonlinear programming. Canadian Geotechnical Journal, 40, 742-752

Chen, J., Yin, J. H., and Lee, C. F. (2004). Rigid finite element method for upper bound limit analysis of soil slopes subjected to pore water pressure. Journal of Engineering Mechanics, 130(8), 886-893

Chen, J., Yin, J. H., and Lee, C. F. (2005a). The use of an SQP algorithm in slope stability analysis. Communications in Numerical Methods in Engineering, 21, 23-37

Chen, J., Yin, J. H., and Lee, C. F. (2005b). A three-dimensional upper-bound approach to slope stability analysis based on RFEM. Geotechnique, 55(7), 549-556

Chen, R. H. and Chameau, J. L. (1982). Three-dimensional limit equilibrium analysis of slopes. Geotechnique, 32(1), 31-40

Chen, W. F. (1975). Limit Analysis and Soil Plasticity. Elsevier Scientific Publishing Co., New York

Chen, W. F. and Giger, M. W. (1971). Limit analysis of stability of slopes. Journal of the Soil Mechanics and Foundations Division, 97(1), 19-26

Cheng, Y. M., Liu, H. T., Wei, W. B., and Au, S. K. (2005). Location of critical three-dimensional non-spherical failure surface by Nurbs Functions and Ellipsoid with applications to highway slopes. Computers and Geotechnics, 32, 387-399

Cheng, Y. M. (2003). Locations of critical failure surface and some further studies on slope stability analysis. Computers and Geotechnics, 30, 255-267

Cheng, Y. M. and Zhu, L. J. (2004). Unified formulation for two dimensional slope stability analysis and limitations in factor of safety determination. Soils and Foundations, 44(6), 121-127

Cheng, Y. M. and Yip, C. J. (2007). Three-dimensional asymmetrical slope stability analysis extension of Bishop's, Janbu's, and Morgenstern-Price's techniques. Journal of Geotechnical and Geoenvironmental engineering, ASCE, 133(12), 1544-1555

Cheng, Y. M., Li, L. and Chi, S. C. (2007). Performance studies on six heuristic global optimization methods in the location of critical slip surface. Computers and Geotechnics, 34(6), 462-484

Cheng, Y. M. (2007). Global optimization analysis of slope stability by simulated annealing with dynamic bounds and Dirac function, Engineering Optimization, 39(1), 17-32

Cheng, Y. M., Zhao, Z. H., and Wang, J. A. (2008). Realization of Pan Jiazheng's extremum principle with optimization methods. Chinese Journal of Rock Mechanics and Engineering, 27(4), 782-788 (in Chinese)

Cheuk, C. Y., Ng, C. W. W., and Sun, H. W. (2005). Numerical experiments of soil nails in loose fill slopes subjected to rainfall infiltration effects. Computers and Geotechnics, 32(4), 290-303

Cho, S. E. and Lee, S. R. (2001). Instability of unsaturated soil slope due to infiltration. Computers and Geotechnics, 28, 185-208

Choukeir, M. H. (1996). Seismic analysis of reinforced earth and soil-nailed structures. Ph.D Thesis, New York Polytechnic University

Chow, Y. K. (1996). Analysis of piles used for slope stabilization. International Journal for Numerical and Analytical Methods in Geomechanics, 20, 635-646

Chu, L. M. (2003). Study on the interface shear strength of soil nailing in completely decomposed granite (CDG) soil. M.Phil thesis, Sept. 2003, The Hong Kong Polytechnic University

Chu, L. M. and Yin, J. H. (2005). Comparison of interface shear strength of soil nails measured by both direct shear box tests and pullout tests. Journal of Geotechnical and Geoenvironmental Engineering, 131(9), 1097-1107

Clouterre. (1993). Recommendations Clouterre 1991. US Department of Transportation, Federal Highway Administration (English translation, Report on the French National Project Clouterre, Rep. No. FHWA-SA-93-026, Washington, D.C.)

D'Appolonia, E., Alperstein, R., and D'Appolonia, D. J. (1967). Behavior of a colluvial slope. Journal of the Soil Mechanics and Foundation Division, ASCE, 93(SM4), 447-473

Dawson, E. M., Roth, W. H., and Drescher, A. (1999). Slope stability analysis by strength reduction. Geotechnique, 49(6), 835-840

Dawson, E., Motamed, F., Nesarajah, S., and Roth, W. (2000). Geotechnical stability analysis by strength reduction. Slope stability 2000: proceedings of sessions of Geo-Denver 2000, August 5-8, 2000, Denver, Colorado, 99-113

De Beer, E. E. and Wallays, M. (1970). Stabilization of a slope in schist by means of bored piles reinforced with steel beams. Proc. 2nd Int. Congress Rock Mech., Vol. 3, 361-369

Deng, J. H., Tham, L. G., Lee, C. F., and Yang, Z. Y. (2007). Three-dimensional stability evaluation of a preexisting landslide with multiple sliding directions by the strength-reduction technique. Canadian Geotechnical Journal, 44, 343-354

Donald, I. and Chen, Z. Y. (1997). Slope stability analysis by the upper bound approach: fundamentals and methods. Canadian Geotechnical Journal, 34, 853-862

Donald, I. B. and Giam, S. K. (1988). Application of the nodal displacement method to slope stability analysis. Proceedings of the 5th Australia-New Zealand conference on geomechanics, Sydney, Australia, 456-460

Drucker, D. C. and Prager, W. (1952). Soil mechanics and plastic analysis or limit design. Quarterly of Applied Mathematics, 10, 157-165

Duncan, J. M. (1996). State of the art: limit equilibrium and finite-element analysis of slopes. Journal of Geotechnical Engineering, 122(7), 577-596

Duncan, J. M. and Wright, S. G. (2005). Soil Strength and Slope Stability. John Wiley & Sons, Inc.

Elias, V. and Christopher, B. R. (1997). Mechanically Stabilized Earth Walls and Reinforced Soil Slopes Design and Construction Guidelines. FHWA DM 82 Manual, Report No. FHWA A-SA-96-071, USA

Elias, V., Christopher, B. R., and Berg, R. R. (2001). Mechanically Stabilized Earth Walls and Reinforced Soil Slopes Design and Construction Guidelines. Federal Highway Administration (FHWA), FHWA-NHI-00-043, USA

Farzaneh, O. and Askari, F. (2003). Three-dimensional analysis of nonhomogeneous slopes. Journal of Geotechnical and Geoenvironmental Engineering, 129(2), 137-145

Fredlund, D. G. and Krahn, J. (1984). Analytical methods for slope analysis. International Symposium on Landslides, 229-250

Fredlund, D. G., Scoular, R. E. G., and Zakerzadeh, N. (1999). Using a finite element stress analysis to compute the factor of safety. Proceedings of the 52nd Canadian Geotechnical Conference, Regina, Saskatchewan, 73-80

Fukuoka, M. (1977). The effects of horizontal loads on piles due to landslides. Proc. 10th Spec. Session, 9th Int. Conf. Soil Mech. and Found. Eng., Tokyo, 27-42

Gasmo, J. M., Rahardjo, H., and Leong, E. C. (2000). Infiltration effects on stability of a residual soil slope. Computers and Geotechnics, 26, 145-165

Gassler, G. and Gudehus, G. (1981). Soil nailing – Some aspects of a new technique. Proceedings of the Tenth International Conference on Soil Mechanics and Foundation Engineering, Sweden, Vol. 3, 665-670

Gassler, G. (1988). Soil-nailing - theoretical basis and practical design. Pro. Int. Geotechnical Symp. on Theory and Practice of Earth Reinforcement, Fukuoka Kyushu, 283–288

Gassler, G. (1992). Full scale test on a nailed wall in consolidated clay. Proc. Int. Symp. on Earth Reinforcement Practice, Fukuoka, Kyushu, Japan, Vol. 1, 475-480

Gassler, G. (1993). The first two field tests in the history of soil nailing on nailed walls pushed to failure. Soil reinforcement: full scale experiments of the 80's, Presses de l'ecole Nationale des Ponts et Chaussees, CEEC, 7-34

Gens, A., Hutchinson, J. N., and Cavounidis, S. (1988). Three-dimensional analysis of slides in cohesive soils. Geotechnique, 38(1), 1-23

GEO. (1996). GEO Report No. 52: Investigation of Some Major Slope Failures between 1992 and 1995. The Hong Kong Special Administrative Region Government

Giger, M. W. and Krizek, R. J. (1975). Stability analysis of vertical cut with variable conner angle. Soils and Foundations, 15(2), 63-71

Giger, M. W. and Krizek, R. J. (1976). Stability of vertical corner cut with concentrated surcharge load. Journal of the Geotechnical Engineering Division, 102(1), 31-40

Greenwood, J. R. (1983). A simple approach to slope stability. Ground Engineering, 16(4), 45-48

Greenwood, J. R. (1985). Correspondence on stability of compacted rockfill slopes, Charles, J. A. and Soares, M. M. (1984). Geotechnique, 35(2), 217-218

Griffiths, D. V. and Lane, P. A. (1999). Slope stability analysis by finite elements. Geotechnique, 49(3), 387-403

Griffiths, D. V. and Marquez, R. M. (2007). Three-dimensional slope stability analysis by elasto-plastic finite elements. Geotechnique, 57(6), 537-546

Gurocak, Z., Alemdag, S., and Zaman, M. M. (2008). Rock slope stability and excavatability assessment of rocks at the Kapikaya dam site, Turkey. Engineering Geology, 96, 17-27

Hassiotis, S., Chameau, J. L., and Gunaratne, M. (1997). Design method for stabilization of slopes with piles. Journal of Geotechnical and Geoenvironmental Engineering, 123(4), 314-323

Hayashi, S., Ochiai, H., Otani, J., and Umezaki, T. (1992). Function and evaluation of steel bars in earth reinforcement. Proc. of the Int. Symp. on Earth Reinforcement, Kyushu, Japan, Vol. 1, 481-486

Hong, Y. S., Wu, C. S., and Yang, S. H. (2003). Pullout resistance of single and double nails in a model sandbox. Canadian Geotechnical Journal, 40, 1039-1047

Hovland, H. J. (1977). Three-dimensional slope stability analysis method. Journal of the Geotechnical Engineering Division, ASCE, 103(GT9), 971-986

Huang, C. C. and Tsai, C. C. (2000). New method for 3D and asymmetrical slope stability analysis. Journal of Geotechnical and Geoenvironmental Engineering, ASCE, 126(10), 917-927

Huang, C. C. and Tsai, C. C. (2002). General method for three-dimensional slope stability analysis. Journal of Geotechnical and Geoenvironmental Engineering, ASCE, 128(10), 836-848

Hungr, O. (1987). An extension of Bishop's simplified method of slope stability analysis to three dimensions. Geotechnique, 37(1), 113-117

Itasca Consulting Group, Inc. (2006). FLAC 3D Version 3.1 User's Guide. Minneapolis, Minnesota, USA

Ito, T. and Matsui, T. (1975). Methods to estimate lateral force acting on stabilizing piles. Soils and Foundations, 15(4), 43-60

Ito, T., Matsui, T., and Hong, W. P. (1981). Design method for stabilizing piles against landslide - one row of piles. Soils and Foundations, 21(1), 21-37

Ito, T., Matsui, T., and Hong, W. P. (1982). Extended design method for multi-row stabilising piles against landslide. Soils and Foundations, 22(1), 1-13

Izbicki, R. J. (1981). Limit plasticity approach to slope stability problems. Journal of the Geotechnical Engineering Division, 107(2), 228-233

Janbu, N. (1973). Slope stability computation. Embankment Dam Engineering – Cassagrande Volume, John Wiley

Jewell, R. A. (1990). Review of theoretical models of soil nailing. Proc. Int. Reinforced Soil Conf., Glasgow, Scotland, 265-275

Jewell, R. A. and Pedley, M. J. (1992). Analysis for soil reinforcement with bending stiffness. Journal of Geotechnical Engineering Division, 118(10), 1505-1528

Jiang, J. C. and Yamagami, T. (1999). Determination of the sliding direction in three-dimensional slope stability analysis. Proc. 44th Symposium on Geotechnical Engineering, 193-200

Jong, G. D. J. D. (1980). Application of the calculus of variations to the vertical cut off in cohesive frictionless soil. Geotechnique, 30(1), 1-16

Junaideen, S. M., Tham, L. G., Law, K. T., Lee, C. F., and Yue, Z. Q. (2004). Laboratory study of soil-nail interaction in loose, completely decomposed granite. Canadian Geotechnical Journal, 41, 274-286

Juran, I., Beech, J., and De Laure, E. (1984). Experimental study of the behaviour of nailed soil retaining structures on reduced scale models. Proceedings of

International Symposium on In Situ Soil and Rock Reinforcement, Paris, France, 309-314 (in French)

Juran, I., Shafiee, S., and Schlosser, F. (1985). Numerical study of nailed soil retaining structures. Proceedings of the Eleventh International Conference on Soil Mechanics and Foundation Engineering, San Franciso, Vol. 3, 1713-1716

Juran, I. and Elias, V. (1987). Soil nailed retaining structures: analysis of case histories, Soil improvement – A ten year update, ASCE Special Geotechnical Publication No. 12, Edited by Joseph P. Welsh, 232-244

Juran, I., Baudrand, G., Farrag, K., and Elias, V. (1990). Kinematical limit analysis for design of soil-nailed structures. Journal of Geotechnical Engineering, 116(1), 54-72

Juran, I., Baudrand, G., Farrag, K. and Elias, V. (1992). Kinematical limit analysis for design of soil-nailed structures (discussion). Journal of Geotechnical Engineering, 118, 1640-1647

Karal, K. (1977a). Application of energy method. Journal of the Geotechnical Engineering Division, 103(5), 381-397

Karal, K. (1977b). Energy method for soil stability analyses. Journal of the Geotechnical Engineering Division, 103(5), 431-445

Kim, D. S., Juran, I., Nasimov, R., and Drabkin, S. (1995). Model study on the failure mechanism of soil-nailed structure under surcharge loading. Geotechnical Testing Journal, 18(4), 421-430

Kim, J. S., Park, C. L., Lee, S. D., and Lee, S. R. (1996). A large-scale experimental study of soil-nailed structures. Proc. of the 3rd Int. Symp. on Earth Reinforcement, Fukuoka, Kyushu, Japan, 775-780

Kim, J., Salgado, R., and Yu, H. S. (1999). Limit analysis of soil slopes subjected to pore- water pressures. Journal of Geotechnical and Geoenvironmental Engineering, 125(1), 49-58

Kim, J., Salgado, R., and Lee, J. (2002). Stability analysis of complex soil slopes using limit analysis. Journal of Geotechnical and Geoenvironmental engineering, ASCE, 128(7), 546-557

Kim, J., Jeong, S., Park, S., and Sharma, J. (2004). Influence of rainfall-induced wetting on the stability of slopes in weathered soils. Engineering Geology, 75, 251-262

King, G. J. W. (1989). Revision of effective-stress method of slices. Geotechnique, 39(3), 497-502

Kitamura, T., Nagao, A., and Uehara, S. (1988). Model loading tests of reinforced slopes with steel bars. Proc. Int. Geotechnical Symp. on Theory and Practice of Earth Reinforcement, Fukuoka, Japan, 5-7 October, 311-316

Krahn, J. (2003). The 2001 R.M. Hardy Lecture: the limits of limit equilibrium analyses. Canadian Geotechnical Journal, 40(3), 643-660

Lam, L. and Fredlund, D. G. (1993). A general limit equilibrium model for three-dimensional slope stability analysis. Canadian Geotechnical Journal, 30, 905-919

Lazarte, C. A., Elias, V., Espinoza, R. D., and Sabatini, P. J. (2003). Geotechnical Engineering Circular No. 7 - Soil Nail Walls. FHWA-IF-03-017, Federal Highway Administration, USA

Lee, C. Y., Poulos, H. G., and Hull, T. S. (1991). Effect of seafloor instability on offshore pile foundations. Canadian Geotechnical Journal, 28(5), 729-737

Lee, C. Y., Hull, T. S., and Poulos, H. G. (1995). Simplified pile-slope stability analysis. Computers and Geotechnics, 17(1), 1-16

Leshchinsky, D., Baker, R., and Silver, M. L. (1985). Three-dimensional analysis of slope stability. International Journal for Numerical and Analytical Methods in Geomechanics, 9(2), 199-223

Leshchinsky, D. and Baker, R. (1986). Three-dimensional slope stability: end effects. Soils and Foundations, 26(4), 98-110

Leshchinsky, D. and Huang, C. C. (1992a). Generalized slope stability analysis: interpretation, modification, and comparison. Journal of Geotechnical Engineering, 118(10), 1559-1576

Leshchinsky, D. and Huang, C. C. (1992b). Generalized three-dimensional slope stability analysis. Journal of Geotechnical Engineering, 118(11), 1748-1764

Li, J. (2003). Field study of a soil nailed loose fill slope. PhD thesis, July 2003, The University of Hong Kong

Li, J., Tham, L. G., Junaideen, S. M., Yue, Z. Q., and Lee, C. F. (2008). Loose fill slope stabilization with soil nails: full-scale test. Journal of Geotechnical and Geoenvironmental Engineering, ASCE, 134(3), 277-288

Loehr, J. E., McCoy, B. F., and Wright, S. G. (2004). Quasi-three-dimensional slope stability analysis method for general sliding bodies. Journal of Geotechnical and Geoenvironmental Engineering, 130(6), 551-560

Loukidis, D., Bandini, P., and Salgado, R. (2003). Stability of seismically loaded slopes using limit analysis. Geotechnique, 53(5), 463-479

Lowe, J. and Karafiath, L. (1960). Stability of earth dams upon drawdown. Proceedings of the 1th Pan-American on Soil Mechanics and Foundations Engineering, Mexico City, Vol. 2, 537-552

Luo, S. Q., Tan, S. A., and Yong, K. Y. (2000). Pull-out resistance mechanism of a soil nail reinforcement in dilative soils. Soils and Foundations, 40(1), 47-56

Luo, S. Q., Tan, S. A., Cheang, W., and Yong, K. Y. (2002). Elastoplastic analysis of pull-out resistance of soil nails in dilatant soils. Ground Improvement, 6(4), 153-161

Lyamin, A. V. (1999). Three-dimensional lower bound limit analysis using nonlinear programming. Ph.D Thesis, University of Newcastle, Australia

Lyamin, A. V. and Sloan, S. W. (2002a). Lower bound limit analysis using nonlinear programming. International Journal for Numerical Methods in Engineering, 55(5), 573-611

Lyamin, A. V. and Sloan, S. W. (2002b). Upper bound limit analysis using linear finite elements and non-linear programming. International Journal for Numerical and Analytical Methods in Geomechanics, 26, 181-216

Martin, G. R. and Chen, C. Y. (2005). Response of piles due to lateral slope movement. Computers and Structures, 83(8), 588-598

Matsui, T. and San, K. C. (1992). Finite element slope stability analysis by shear strength reduction technique. Soils and Foundations, 32(1), 59-70

Miao, L. F., Goh, A. T. C., Wong, K. S., and Teh, C. I. (2006). Three-dimensional finite element analyses of passive pile behaviour. International Journal for Numerical and Analytical Methods in Geomechanics, 30(7), 599-613

Michalowski, R. L. (1989). Three-dimensional analysis of locally loaded slopes. Geotechnique, 39(1), 27-38

Michalowski, R. L. (1995). Slope stability analysis: a kinematical approach. Geotechnique, 45(2), 283-293

Morgenstern, N. R. and Price, V. E. (1965). The analysis of stability of general slip surfaces. Geotechnique, 15(1), 79-93

Morgenstern, N. R. (1992). The evaluation of slope stability – A 25 year perspective, stability and performance of slopes and embankments – II. Geotechnical Special Publication No. 31, ASCE, 1-26

Murthy, B. R. S., Babu, G. L. S., and Srinivas, A. (2002). Analysis of prototype soil-nailed retaining wall. Ground Improvement, 6(3), 129-136

Naylor, D. J. (1982). Finite elements and slope stability. Numerical Methods in Geomechanics, Proceedings of the NATO Advanced Study Institute, University of Minho, Braga, Portugal, 1981, edited by Martins J. B., 229-244

Ng, C. W. W. and Shi, Q. (1998). A numerical investigation of the stability of unsaturated soil slopes subjected to transient seepage. Computers and Geotechnics, 22(1), 1-28

Ng, C. W. W. and Zhang, L. M. (2001). Three-dimensional analysis of performance of laterally loaded sleeved piles in sloping ground. Journal of Geotechnical and Geoenvironmental Engineering, 127(6), 499-509

Ng, C. W. W., Zhang, L. M., and Ho, K. K. S. (2001). Influence of laterally loaded sleeved piles and pile groups on slope stability. Canadian Geotechnical Journal, 38(3), 553-566

Pan, J. L., Goh, A. T. C., Wong, K. S., and Selby, A. R. (2002). Three-dimensional analysis of single pile response to lateral soil movements. International Journal for Numerical and Analytical Methods in Geomechanics, 26(8), 747-758

Patra, C. R. and Basudhar, P. K. (2005). Optimum design of nailed soil slopes. Geotechnical and Geological Engineering, 23, 273-296

Pedley, M. J. (1990). The performance of soil reinforcement in bending and shear. Ph.D. Thesis, University of Oxford

Pedley, M. J., Jewell, R. A., and Milligan, G. W. E. (1990a). A large scale experimental study of soil-reinforced interaction – Part I. Ground Engineering, 23(6), 44-50

Pedley, M. J., Jewell, R. A., and Milligan, G. W. E. (1990b). A large scale experimental study of soil reinforcement interaction – Part II. Ground Engineering, 23(7), 45-49

Plumelle, B. C., Schlosser, F., Delage, P., and Knochenmus, G. (1990). French national research project on soil nailing Clouterre. Design and performance of earth retaining structures: proceedings of a conference / sponsored by the Geotechnical

Engineering Division of the American Society of Civil Engineers in cooperation with the Ithaca Section, ASCE, Cornell University, Ithaca, New York, June 18-21, 1990 ; edited by Philip C. Lambe and Lawrence A. Hansen, 660-675

Poulos, H. G. (1973). Analysis of piles in soil undergoing lateral movement. Journal of the Soil Mechanics and Foundation Division, ASCE, 99(SM5), 391-406

Poulos, H. G. and Davis, E. H. (1980). Pile Foundation Analysis and Design. John Wiley & Sons, New York, etc.

Poulos, H. G. (1995). Design of reinforcing piles to increase slope stability. Canadian Geotechnical Journal, 32(5), 808-818

Pradhan, B., Tham, L. G., Yue, Z. Q., Junaideen, S. M., and Lee, C. F. (2006). Soil-nail pullout interaction on loose fill materials. International Journal of Geomechanics, 6(4), 238-247

Rahardjo, H., Ong, T. H., Rezaur, R. B., and Leong, E. C. (2007). Factors controlling instability of homogeneous soil slopes under rainfall. Journal of Geotechnical and Geoenvironmental Engineering, 133(12), 1532-1543

Raju, G. V. R., Wong, I. H., and Low, B. K. (1997). Experimental nailed soil walls. Geotechnical Testing Journal, 20(1), 90-102

Reese, L. C., Wang, S. T., and Fouse, J. L. (1992). Use of drilled shafts in stabilising a slope. In stability and performance of slopes and embankments – II. Edited by Seed R. B. and Boulanger R. W. American Society of Civil Engineers, Vol. 2, 1318-1332

Sabhahit, N., Basudhar, P. K., and Madhav, M. R. (1995). A generalized procedure for the optimum design of nailed soil slopes. International Journal for Numerical and Analytical Methods in Geomechanics, 19, 437-452

Schlosser, F. and Guilloux, A. (1981). Le frottement dens les sols. Revue Francaise de Geotechnique, No.16, 65-77

Schlosser, F. (1982). Behaviour and design of soil nailing. Proc. Symp. on Recent Developments in Ground Improvement Techniques, Bangkok, Thailand, 399-413

Schlosser, F. (1991). The multicriteria theory in soil nailing. Ground Engineering, Vol. 24, November 1991, 30-39

Schlosser, F., Unterreiner, P., Plumelle, C., and Benoit, J. (1992). Failure of a full scale experimental soil nailed wall by reducing the nails lengths (French research project Clouterre). Proc. Int. Symp. on Earth Reinforcement Practice, Fukuoka, Kyushu, Japan, Vol.1, 531-535

Sheahan, T. C. and Ho, C. L. (2003). Simplified trial wedge method for soil nailed wall analysis. Journal of Geotechnical and Geoenvironmental Engineering, 129(2), 117-124

Shen, C. K., Herrmann, L.R., Romstad, K. M., Bang, S., Kim, Y. S., and DeNatale, J. S. (1981a). In situ earth reinforcement lateral support system. Department of Civil Engineering, University of California, Davis, Report No. 81-03

Shen, C. K., Bang, S., Romstad, K. M., Kulchin, L., and DeNatale, J. S. (1981b). Ground movement analysis of an earth support system. Journal of the Geotechnical Engineering Division, 107, 1609-1624

Shen, C. K., Bang, S., Romstad, K. M., Kulchin, L., and DeNatale, J. S. (1981c). Field measurements of an earth support system. Journal of the Geotechnical Engineering Division, 107, 1625-1642

Shukha, R. and Baker, R. (2003). Mesh geometry effects on slope stability calculation by FLAC strength reduction method – linear and non-linear failure criteria. 3rd International Conference on FLAC and Numerical modeling in Geomechanics, Sudbury, Ontario, Canada, 109-116

Shukha, R. and Baker, R. (2008). Design implications of the vertical pseudo-static coefficient in slope analysis. Computers and Geotechnics, 35, 86-96

Sloan, S. W. (1988). A steepest edge active set algorithm for solving sparse linear programming problems. International Journal for Numerical Methods in Engineering, 26, 2671-2685

Sloan, S. W. (1989). Upper bound limit analysis using finite elements and linear programming. International Journal for Numerical and Analytical Methods in Geomechanics, 13, 263-282

Sloan, S. W. and Kleeman, P. W. (1995). Upper bound limit analysis using discontinuous velocity fields. Computer Methods in Applied Mechanics and Engineering, 127, 293-314

SLOPE/W Engineering Book. (2004). Stability modelling with SLOPE/W. GEO-SLOPE/W International, Ltd.

Smith, I. M. and Su, N. (1997). Three-dimensional FE analysis of a nailed soil wall curved in plan. International Journal for Numerical and Analytical Method in Geomechanics, 21, 583-597

Song, E. (1997). Finite element analysis of safety factor for soil structures. Chinese Journal of Geotechnical Engineering, 19(2), 1-7 (in Chinese)

Spencer, E. (1967). A method of analysis of the stability of embankments assuming parallel inter-slice forces. Geotechnique, 17(1), 11-26

Stocker, M. F., Korber, G. W., Gassler, G., and Gudehus, G. (1979). Soil nailing. International Conference on Soil Reinforcement, Paris, 469-474

Stocker, M. F. and Riedinger, G. (1990). The bearing behaviour of nailed retaining structures. Proc. Conf. on Design and Performance of Earth Retaining Structures, Geotechnical Special Publication No. 25, Ithaca, USA, 612-628

Su, L. J. (2006). Laboratory pull-out testing study on soil nails in compacted completely decomposed granite fill. PhD thesis, March 2006, The Hong Kong Polytechnic University

Su, L. J., Chan, T. C. F., Shiu, Y. K., Cheung, T., and Yin, J. H. (2007). Influence of degree of saturation on soil nail pull-out resistance in compacted completely decomposed granite fill. Canadian Geotechnical Journal, 44, 1314-1328

Tabrizi, K. S., Gucunski, N., and Maher, M. H. (1995). 3-D FEM analysis of excavation of a soil-nail wall. Computing in civil engineering: proc. 2nd Congress held in conjunction with A/E/C Systems '95, Atlanta, Georgia, 812-819

Terzaghi, K. and Peck, R. B. (1967). Soil Mechanics in Engineering Practice. John Wiley and Sons, Inc., New York

Thompson, S. R. and Miller, I. R. (1990). Design, construction and performance of a soil nailed wall in Seattle, Washington. Design and Performance of Earth Retaining Structures, ASCE Geotechnical Special Publication No. 25, 629-643

Tsaparas, I., Rahardjo, H., Toll, D. G., and Leong, E. C. (2002). Controlling parameters for rainfall-induced landslides. Computers and Geotechnics, 29, 1-27

Tsui, T. Z. (2007). Physical modelling of 3-D and 2-D soil-nailed slopes in Hong Kong. Final year project report, April 2007, The Hong Kong Polytechnic University

Turnbull, W. J. and Hvorslev, M. J. (1967). Special problems in slope stability. Journal of the Soil Mechanics and Foundation Division, ASCE, 93(SM4), 499-528

Ugai, K. (1985). Three-dimensional stability analysis of vertical cohesive slopes. Soils and Foundations, 25(3), 41-48

Ugai, K. (1988). Three-dimensional slope stability analysis by slice methods. Proceedings of the Sixth International Conference on Numerical Methods in Geomechanics, Innsbruck, 11-15 April, edited by G. Swoboda, 1369-1374

Ugai, K. and Leshchinsky, D. (1995). Three-dimensional limit equilibrium and finite element analysis: a comparison of results. Soils and Foundations, 35(4), 1-7

Unterreiner, P., Benhamida, B., and Schlosser, F. (1997). Finite element modelling of the construction of a full-scale experimental soil-nailed wall. French National

Research Project CLOUTERRE. Journal of Ground Improvement, 1(1), 1-8

Wang, Y. J. (2001). Stability analysis of slopes and footings considering different dilation angles of geomaterial. Ph.D. thesis, The Hong Kong Polytechnic University

Wang, Y. J., Yin, J. H., and Lee, C. F. (2001). The influence of a non-associated flow rule on the calculation of the factor of safety of soil slopes. International Journal for Numerical and Analytical Methods in Geomechanics, 25, 1351-1359

Wang, M. C., Wu, A. H., and Scheessele, D. J. (1979). Stress and deformation in single piles due to lateral movement of surrounding soils. Behavior of Deep Foundations, ASTM 670, Raymond Lunggren, Ed., American Society for Testing and Materials, 578-591

Weibull, W. (1951). A statistical distribution function of wide applicability. Journal of Applied Mechanics, ASME, 18(3), 293-297

Won, J., You, K., Jeong, S., and Kim, S. (2005). Coupled effects in stability analysis of pile-slope systems. Computers and Geotechnics, 32(4), 304-315

Xie, M., Esaki, T., Zhou, G., and Mitani, Y. (2003). Geographic information systems-based three-dimensional critical slope stability analysis and landslide hazard assessment. Journal of Geotechnical and Geoenvironmental Engineering, ASCE, 129(12), 1109-1118

Xie, M., Esaki, T., and Cai, M. (2004a). A GIS-based method for locating the critical 3D slip surface in a slope. Computers and Geotechnics, 31, 267-277

Xie, M., Esaki, T., and Zhou, G. (2004b). GIS-based probabilistic mapping of landslide hazard using a three-dimensional deterministic model. Natural Hazards, 33, 265-282

Xie, M., Esaki, T., and Cai, M. (2006a). GIS-based implementation of three-dimensional limit equilibrium approach of slope stability. Journal of Geotechnical and Geoenvironmental Engineering, ASCE, 132(5), 656-660

Xie, M., Esaki, T., Qiu, C., and Wang, C. (2006b). Geographic information system-based computational implementation and application of spatial three-dimensional slope stability analysis. Computers and Geotechnics, 33, 260-274

Yamagami, T., Jiang, J. C., and Ueno, K. (2000). A limit equilibrium stability analysis of slopes with stabilizing piles. Slope stability 2000: proceeding of sessions of Geo-Denver 2000, August 5-8, 2000, Denver, Colorado, Sponsored by the Geo-Institute of the ASCE, edited by D. V. Griffiths, Gordon A. Fenton, Timothy R. Martin, 343-354

Yang, M. Z. and Drumm, E. C. (2000). Numerical analysis of the load transfer and deformation in a soil nailed slope. Numerical methods in geotechnical engineering – recent developments, Proceedings of sessions of geo-denver 2000, Geotechnical special publication No. 96, August 2000, Denver, Colorado, 102-115

Yuan, J. X., Yang, Y. W., Tham, L. G., Lee, P. K. K., and Tsui, Y. (2003). New approach to limit equilibrium and reliability analysis of soil nailed walls. International Journal of Geomechanics, 3(2), 145-151

Zhang, M. J., Song, E. X., and Chen, Z. Y. (1999). Ground movement analysis of soil nailing construction by three-dimensional (3-D) finite element modeling (FEM). Computers and Geotechnics, 25(4), 191-204

Zhang, L. M., Ng, C. W. W., and Lee, C. J. (2004). Effects of slope and sleeving on the behavior of laterally loaded piles. Soils and Foundations, 44(4), 99-108

Zhang, X. (1988). Three-dimensional stability analysis of concave slopes in plan view. Journal of Geotechnical Engineering, 114(6), 658-671

Zhang, X. (1999). Slope stability analysis based on the rigid finite element method. Geotechnique, 49(5), 585-593

Zheng, H. (2007). A rigorous three-dimensional limit equilibrium method. Chinese Journal of Rock Mechanics and Engineering, 26(8), 1529-1537 (in Chinese)

Zheng, Y. R., Zhao, S. Y., Kong, W. X., and Deng, C. J. (2005). Geotechnical engineering limit analysis using finite element method. Rock and Soil Mechanics, 26(1), 163-168 (in Chinese)

Zhu, D. Y. and Qian, Q. H. (2007). Rigorous and quasi-rigorous limit equilibrium solutions of 3D slope stability and application to engineering. Chinese Journal of Rock Mechanics and Engineering, 26(8), 1513-1528 (in Chinese)

Zhu, D. Y. and Lee, C. F. (2002). Explicit limit equilibrium solution for slope stability. International Journal for Numerical and Analytical Methods in Geomechanics, 26(15), 1573-1590

Zhu, D. Y., Lee, C. F., and Jiang, H. D. (2003). Generalized framework of limit equilibrium methods and numerical procedure for slope stability analysis. Geotechnique, 53(4), 377-395

Zienkiewicz, O. C., Humpheson, C., and Lewis, R. W. (1975). Associated and non-associated visco-plasticity and plasticity in soil mechanics. Geotechnique, 25(4), 671-689